Hyperfine Structure Measurements of Neutral and Singly Ionized Atoms (^{127}I, ^{209}Bi) using Fourier Transform Spectroscopy

By

CHILUKOTI ASHOK

PHYS 01201504011

Bhabha Atomic Research Center

A thesis submitted to the
Board of Studies in Physical Sciences
In partial fulfillment of requirements
for the Degree of

DOCTOR OF PHILOSOPHY
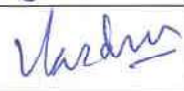
of

HOMI BHABHA NATIONAL INSTITUTE

August, 2019

Homi Bhabha National Institute[1]

Recommendations of the Viva Voce Committee

As members of the Viva Voce Committee, we certify that we have read the dissertation prepared by Mr. Chilukoti Ashok entitled "Hyperfine Structure Measurements of Neutral and Singly Ionized Atoms (^{127}I, ^{209}Bi) using Fourier Transform Spectroscopy" and recommend that it may be accepted as fulfilling the thesis requirement for the award of Degree of Doctor of Philosophy.

S.No.	Name	Designation	Signature	Date
1.	Dr. R.C. Rannot	Chairman		13/08/2019
2.	Dr. M. N. Deo	Guide / Convener		13/08/2019
3.	Dr. Ajay Wasan	External Examiner		13 Aug 2019
4.	Prof. S. Wategaonkar	Member 1		13/8/19
5.	Dr. D. V. Udupa	Member 2		13/8/19
6.	Dr. Vas Dev	Member 3		13/8/19

Final approval and acceptance of this thesis is contingent upon the candidate's submission of the final copies of the thesis to HBNI.

I/We hereby certify that I/we have read this thesis prepared under my/our direction and recommend that it may be accepted as fulfilling the thesis requirement.
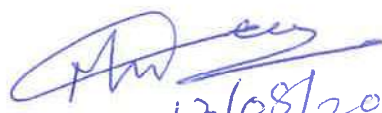
Date: 13/08/19

Place:

Signature

Co-guide (if any)

Signature   13/08/2019

Guide

ii

STATEMENT BY AUTHOR

This dissertation has been submitted in partial fulfillment of requirements for an advanced degree at Homi Bhabha National Institute (HBNI) and is deposited in the Library to be made available to borrowers under rules of the HBNI.

Brief quotations from this dissertation are allowable without special permission, provided that accurate acknowledgement of source is made. Requests for permission for extended quotation from or reproduction of this manuscript in whole or in part may be granted by the Competent Authority of HBNI when in his or her judgment the proposed use of the material is in the interests of scholarship. In all other instances, however, permission must be obtained from the author.

CHILUKOTI ASHOK

DECLARATION

I, hereby declare that the investigation presented in the thesis has been carried out by me. The work is original and has not been submitted earlier as a whole or in part for a degree / diploma at this or any other Institution / University.

CHILUKOTI ASHOK

List of Publications arising from the thesis

Journals

1. "Hyperfine Structure Measurements of Neutral Iodine Atom (^{127}I) using Fourier Transform Spectrometry", <u>Chilukoti Ashok</u>, Vishwakarma SR, Himal B, Ankush BK, Deo MN., JQSRT, **2018**, *205*,19-26.

2. "Hyperfine Structure Measurements of Neutral Atomic Iodine (^{127}I) in Near Infrared and Visible Regions", <u>Chilukoti Ashok</u>. Vishwakarma SR. Deo MN., JQSRT, **2018**;*220*,148-161

3. "Hyperfine Structure Measurements on Singly Ionized Atomic Iodine (I II) using Fourier Transform Spectroscopy", <u>Chilukoti Ashok</u>. Vishwakarma SR. Deo MN., JQSRT, **2018**;*221*,71-79.

4. "Fourier transform spectroscopic investigations of atomic bismuth (^{209}Bi I) in the spectral region from IR to UV (2500-40,000 cm^{-1})", <u>Chilukoti Ashok</u>, Vishwakarma SR, Deo MN., JQSRT, **2019**;*229*,60-70.

5. "Hyperfine structure measurements of neutral atomic iodine (^{127}I) in the infrared region (1800-6000 cm^{-1})", <u>Chilukoti Ashok</u>, Vishwakarma SR, Himal Bhatt, Deo MN., JQSRT, **2019**;*235*,162-179.

Conference paper (related to PhD work)

1. "Measurements and Analysis of Hyperfine Structure of Atomic Iodine using High Resolution Fourier Transform Spectroscopy", <u>Chilukoti Ashok</u>, S. R. Vishwakarma, Himal Bhatt, B. K. Ankush and M. N. Deo, *Light Quanta: Modern Perspectives and Applications (2015) – Allahabad University.*

2. "Hyperfine Structure Analysis of Atomic Bismuth [^{209}Bi (I=9/2)] using High Resolution Fourier Transform Spectroscopy" – (Oral Presentation).
   <u>Chilukoti Ashok</u>, Vishwakarma SR and Deo MN, National Conference on Advances in Spectroscopic Techniques and Materials (ASTM-2018), March 14-16, 2018, ISM Dhanbad, Jharkhand, India.

CHILUKOTI ASHOK

Dedicated

To

My Parents and Brother

ACKNOWLEDGEMENTS

CONTENTS

List of the Figures

11

One Ne line is also present at 19192.7 cm^{-1}.

List of Tables

Homi Bhabha National Institute

SYNOPSIS OF Ph.D. THESIS

1. Name of the Student: Chilukoti Ashok

2. Name of the Constituent Institution: Bhabha Atomic Research Center

3. Enrolment No. :   PHYS 01201504011

4. Title of the Thesis: Hyperfine Structure Measurements of Neutral and Singly Ionized Atoms (^{127}I, ^{209}Bi) using Fourier Transform Spectroscopy

5. Board of Studies: Physical Sciences

SYNOPSIS

Hyperfine Structure Measurements of Neutral and Singly Ionized Atoms (^{127}I, ^{209}Bi) using Fourier Transform Spectroscopy

Atomic emission spectroscopy provides information about atomic parameters such as the center of gravity wavenumber values of spectral transitions, identification of new spectral lines, energy level classifications, fine structure and hyperfine structure (*hfs*) constants, and isotope shift measurements which play a key role in basic physics to understand the atomic structure, chemical properties and astrophysical observations.

The hyperfine coupling constants (magnetic dipole moment constant '*A*' and electric quadrupole moment constant '*B*') determined from optical hyperfine structure measurements, allows calculating the nuclear moments, which are useful to further understand the nuclear structure, nuclear properties to determine the abundances of chemical elements observed in the stellar spectra.

In my Ph.D., I have been worked on the hyperfine structure measurements of neutral and singly ionized atoms iodine and bismuth by using a high resolution Fourier transform

spectrometer. This thesis consists of seven chapters, where Chapter 1 describes the introduction of atomic emission spectroscopy and hyperfine structure along with the properties of interested samples and motivation of the present work. In Chapter 2, theory related to hyperfine structure, selection rules, spectral broadening effects, experimental techniques such as sample preparation, discharge methods, cooling methods, and working principle of Fourier transform spectroscopy and data analysis has been described. Chapter 3 provides the observed spectral transitions and hyperfine structure measurements of neutral iodine (^{127}I) in the spectral range of 1800 − 25000 cm^{-1}. Chapter 4 addresses the hyperfine structure investigations of neutral atomic bismuth (^{209}Bi) in the spectral range of 2500 − 40000 cm^{-1}. Chapter 5 presents the hyperfine structure investigations on singly ionized atoms iodine (I II) and bismuth (Bi II). Chapter 6 provides a detailed discussion on forbidden transitions observed in the spectra of I I, I II, Bi I and Bi II. Finally, Chapter 7 gives a summary of the entire thesis work.

Chapter 1 provides a detailed discussion on atomic emission spectroscopy and hyperfine structure. The interaction of the nuclear spin angular momentum (I) with the total electronic angular momentum (J) produces a further splitting of atomic fine structure levels, called hyperfine splitting. The spectral transition between the hyperfine levels gives the hyperfine structure of a fine structure transition. The atomic properties of the interested samples iodine and bismuth were discussed. Neutral atomic iodine (I I) with electronic configuration [Kr]4d^{10}5s^{2}5p^5 can be ionized (ionization potential is 10.45eV) to singly ionized atomic iodine (I II) with the electronic configuration [Kr]4d^{10}5s^{2}5p^4. The large value of magnetic dipole moment (μ) of +2.81327(8)μ_N (where μ_N is the nuclear magneton) [1] and electric quadrupole moment (Q) of −0.696(12) barn [2], combining with nuclear spin value 5/2, produces very broad hyperfine structure. Atomic Bismuth (Bi I), with atomic number Z = 83, ground state configuration [Xe] 4f^{14} 5d^{10} 6s^2 6p^3, nuclear spin (I) = 9/2, magnetic dipole moment (μ) = +4.1103(15)μ_N and electric quadrupole moment (Q) = -0.516(15) barn[1].

Hfs measurements on spectral transitions and determination of *A* and *B* constants for most of the energy levels are incomplete. As a result, the spectra of iodine and bismuth were not fully understood. This has given a motivation to observe the spectral transitions with an accurate center of gravity wavenumber values and also to derive the *hfs* constants *A* and *B* for the energy

2

levels to get more atomic parameters. The *hfs* database generated from the experimental methods is very useful in various spectroscopic investigations and development applications.

Chapter 2 addresses the theoretical frame work of hyperfine structure, experimental techniques such as sample preparation, discharge methods, sample cooling methods, working principle of Fourier transform spectroscopy and analysis of *hfs* structure.. In this chapter a brief discussion on interaction of magnetic and electric moments to nuclear spin to split the fine structure levels into hyperfine structure [3]. Energy level shift equations were given and explained the hyperfine splitting parameters and the selection rules for the transitions between hyperfine levels were also provided. Various spectral broadening mechanisms were also discussed.

In this chapter, the preparation of Electrodeless Discharge Lamps (EDL) of iodine and bismuth has been discussed in detail. In case of Bi, along with EDL, Hollow Cathode Lamps (HCL) were also prepared. EDL and HCL were operated by means of microwave excited and DC discharge respectively to generate the plasma. The accuracy of *hfs* constants depends upon the width of resolved *hfs* components. In the present case improved resolution achieved, due to (i) the instrumental resolution, i.e. longer path difference in the interferometer and (ii) cooling the EDL. Thus, we could measure much improved values of the hyperfine constants. While high resolution spectra were useful in observing the *hfs* components of intense lines with ease, lowering the resolution was helpful in measuring the relatively less intense lines with good S/N ratio. To minimize power and Doppler broadening effects on spectral lines, the EDL was operated under low microwave power along with reduced temperature. In case of EDL, both the microwave cavity and EDL were cooled with nitrogen gas which was passed through a liquid nitrogen bath. The HCL was operated under low discharge currents and also dipped into the LN_2 bath to reduce the broadening effects.

The entire spectra were recorded by means of a high resolution Fourier transform spectrometer (IFS 125 HR), which works on the basic principle of Michelson interferometer [4]. The instrument was equipped with various beam splitters (KBr /CaF$_2$ /Qrtz Vis /Qrtz UV) and appropriate detectors (InSb/ InGaAs/ Si diode/ PMT-Vis/ PMT-UV) to cover the spectral region from IR to UV. The maximum resolution can be achieved by the instrument is 0.00126 cm^{-1}. The observed spectra were calibrated with standard Ne lines [5].

The analysis of the *hfs* structure to derive *A* and *B* constants was also discussed here. Two programs: HFSAB and WINHFS were utilized for the *hfs* analysis [6]. The shift of each *hfs* component from the center of gravity, *J* values of upper and lower energy levels and the assignment of F transitions have been used by HFSAB to generate *A* and *B* constants. WINHFS simulates the spectrum and refines the *hfs* constants by optimizing the fit parameters such as *hfs* *A* and *B* constants, width and spectral line profile (fitted with Gaussian profiles) for the *J* values in a transition.

Chapter 3 describes the atomic hyperfine structure measurements of neutral Iodine (^{127}I).

Emission spectra of neutral iodine have been observed in the range 1800 to 25000 cm^{-1} and a total of 778 spectral lines of I I were observed in the entire region. This entire data have been divided into three parts: 1800-6000, 6000-10000 and 10000-25000 cm^{-1}. A mixture of iodine vapor and Ne was excited in an EDL driven by a surfatron microwave cavity operated by Opthos microwave power supply (working range 0-140 W). The emitted light was focused to a high resolution Fourier transform spectrometer. The instrument was equipped with a KBr/CaF2 beam splitter and InSb (77K) detector to record the spectra in the 1800 - 6000 cm^{-1} region. The spectra were recorded with a maximum resolution of 0.0026 cm^{-1}. The light transmittance of normal Quartz EDL is quite low, below 3000 cm^{-1}. Therefore, lines appearing in this region are not possible to observe. To avoid this difficulty, an EDL made with CaF$_2$ window which made possible to observe more than 100 new lines below 3000 cm^{-1}. In this region, 355 lines were observed, of which 211 were reported for the first time. Center of gravity wavenumber values for their Line position has been derived for all 355 line and *hfs* measurements were performed on 255 lines. The *hfs* constants *A* and *B* were determined for 102 energy levels (even 53 and odd 49) and are compared to the previous data [7-9].

In the spectral region of 6000 - 10000 cm^{-1}, I I spectra were recorded by exciting the EDL the emitted light emitted was made to fall on the entrance aperture of the FTS. The spectrometer was equipped with a CaF$_2$ beam splitter, InSb (77K) and InGaAs detectors to record the spectra in the 6000 - 10000 cm^{-1} region. A total of 183 spectral lines were identified, which of 53 were reported for the first time. New line positions were derived for all the transitions observed in the present work. The *hfs* constants *A* and *B* derived for 60 energy levels involved in all 30 even and 30 odd parity energy levels involved in the present investigation have been listed While the

4

already known *hfs* values for 25 even and 26 odd levels agree very well with the presently derived *hfs* values, the *hfs* values for 5 even and 4 odd levels have been reported here for the first time.

The same experimental setup has been used in this region (10000-25000 cm^{-1}) also. For this range, the instrument was equipped with various beam splitters (CaF$_2$ in the infrared /Quartz in the visible region) and appropriate detectors (Si diode /Photomultiplier Tube) to observe the spectra in the near infrared and visible spectral regions. Multiple band pass filters (band width: 10, 25 and 50 nm) were used in the spectral region above 12000 cm^{-1} to enhance the S/N. On an average, 50 to 150 scans were co-added depending upon the resolution and S/N. A total of 240 spectral transitions were observed in the range of 10000 - 25000 cm^{-1}. Line position center of gravity wavenumber values were determined. Among all 240 spectral transitions, 149 are newly observed and the remaining 91 were observed again. *Hfs* investigations were performed on 177 spectral lines to derive *A* and *B* constants for 100 energy levels (48 even parity and 52 odd parity levels), from which the constants of 11 even parity and 7 odd parity levels are reported for the first time. Among all 177 spectral lines, the *hfs* of 128 lines was investigated for the first time. *Hfs* constants were derived for 100 energy levels (48 even and 52 odd). Among 100 levels, *A* and *B* constants of 18 levels were reported for the first time. Few spectral lines were identified as blended lines at 10917.682, 11286.828, 11292.256, 13526.657, 13814.546, 22673.834, 12611.489 and 17343.301 cm^{-1}. Among all these transitions, the first six are overlapping iodine - iodine transitions and the remaining two are iodine - Ne transitions.

Chapter 4 addresses the atomic hyperfine structure measurements of neutral Bismuth.

The Bismuth plasma has been generated by two techniques: Microwave discharge of EDL and DC discharge of LN$_2$ cooled HCL. Bismuth Iodide (BiI$_3$) and Bismuth Oxide (Bi$_2$O$_3$) samples were used for the preparation of EDL [10] and HCL [11] respectively. The methods of preparation of EDL and HCL have been discussed. Emission light has been focused onto a High Resolution Fourier Transform Spectrometer, equipped with various beam splitters (CaF$_2$ in the Infrared, Qrtz Vis in the visible and Qrtz UV in the UV region) and appropriate detectors (InSb/ InGaAs/ Si diode/ PMT-Vis/ PMT-UV) to cover the spectral range 2500 - 40000 cm^{-1}. Various instrumental resolutions were applied up to the highest resolution of 0.006 cm^{-1} in the IR region. Several band pass optical filters were used in the visible and UV spectral region to enhance the

S/N ratio as well as to observe the weak transitions. In the present investigations, 107 spectral transitions were observed in the entire spectral region from IR to UV (2500 - 40000 cm^{-1}). The new center of gravity wavenumbers for the observed transitions were determined. *Hfs* investigations were carried out on 76 well resolved transitions. Among 76 lines, 30 were *hfs* analyzed for the first time. *Hfs* constants *A* and *B* were determined for 31 energy levels (14 even and 17 odd) and are compare to previous data [12-14]. *A* constants for 6 levels and *B* constants for 8 levels were derived for the first time. Two blended lines were observed at 6520 and 10359 cm^{-1}. For the line at 6520 cm^{-1}, two Bi I lines corresponds to 6520.313 cm^{-1} and 6520.391 cm^{-1} are overlapping. Another blended line at 10359 cm^{-1}, is a overlap of Bi I line at 10359.866 cm^{-1} and iodine line at 10360.259 cm^{-1}. The importance of EDL and HCL in different operating conditions were explained on the basis of Self-absorption of few observed spectra.

Chapter 5 describes the atomic hyperfine structure measurements of singly ionized Iodine (I II) and Bismuth (Bi II).

Emission spectra of singly ionized iodine have been observed in the range 12000 to 25000 cm^{-1}. EDLs were used as a source of iodine plasma, which were sealed with 1 mg of iodine and 1 mbar of buffer gas (neon). Iodine is available in nature as I_2 molecule but the dissociation energy (1.58 eV) is less than the molecular ionization energy (9.3 eV) [15], so it can be easily dissociated into iodine atoms. The collision of buffer gas with iodine atoms produces the plasma inside EDL. In normal conditions, spectral transitions of I I are dominant and only few strong lines of I II were observed. The source temperature should be brought down below 261 K - 245 K to observe the I II spectral transitions predominantly. To achieve these conditions, both the microwave cavity and EDL were cooled with nitrogen gas which was passed through a liquid nitrogen bath. The temperature of the discharge tube was stabilized by controlling the flow of cooled nitrogen gas by a valve. The spectra were recorded only after achieving a stable discharge condition. In these investigations, 141 spectral lines were observed. *Hfs* measurements were carried out on 73 spectral lines and the *A* and *B* constants were derived for 61 energy levels (29 even parity and 32 odd parity). The derived values were compared to available literature [16]. Further, one blended line at 20611 cm^{-1} were observed.

High resolution emission spectra of singly ionized bismuth (Bi II) [17, 18] spectra have been observed in the spectral region from visible to UV (13000 - 38000 cm^{-1}). EDL and LN_2

cooled HCL were employed by means of a microwave discharge and DC discharge methods respectively. The emitted light has been recorded with the High Resolution Fourier Transform Spectrometer equipped with various beam splitters (Qrtz Vis /Qrtz UV) and appropriate detectors (Si diode/ PMT-Vis/ PMT-UV). In the entire spectral region, 45 spectral lines were observed. Among 45, *hfs* investigations were carried out on 33 lines and *hfs* constants were derived for 40 (for 23 even and 17 odd).

Chapter 6 provides the discussion on forbidden transitions observed in the spectra of I I, I II, Bi I and Bi II.

In the spectra of I I, a transition between two odd parity levels $5s^2 5p^5\,^2P_{1/2}$ (7602.970 cm^{-1}) and $5s^2 5p^5\,^2P_{3/2}$ (0.00 cm^{-1}) at 7602.970 cm^{-1} has been analyzed. In I II spectra, a magnetic dipole transition (M1) at 22414 cm^{-1} between two even parity levels has been detected and analyzed.

Hyperfine structure investigations were of performed on three forbidden transitions at 461.7, 647.5 and 875.7 nm [19-20]. As the magnetic dipole transitions are weak in nature, it is possible to observe them only by strong discharge methods. In the present case, all three lines were observed only with EDL discharge but not in HCL discharge. The line at 461.7 nm is a transition between $6s^2 6p^3\,^2P_{1/2}$ - $6s^2 6p^3\,^4S_{3/2}$, produces six *hfs* components according to $\Delta F = 0, \pm 1$. In the present observations, all the six *hfs* components were observed and analyzed for the first time. *Hfs* constants were derived for both the levels with uncertainty of 0.02 cm^{-1} and reported. The line at 647.5 nm is a transition between $6s^2 6p^3\,^2D_{5/2}$ - $6s^2 6p^3\,^4S_{3/2}$ in visible spectral region. This transition was studied previously and observed 12 *hfs* components of the magnetic dipole ($\Delta F = 0, \pm 1$) and 2 of electric quadrupole ($\Delta F = \pm 2$) transitions. In the present investigations, all 18 *hfs* components (12 components of $\Delta F = 0, \pm 1$ and 6 of $\Delta F = \pm 2$) were observed. All six $\Delta F = \pm 2$ transitions were observed for the first time. *Hfs* investigations were carried out and precise values of *A* and *B* constants were determined. The transition at 875.5 nm (11419.038 cm^{-1}) in the IR region is a magnetic dipole transition between the levels $6p^3\,^2D_{3/2}$ and $6p^3\,^4S_{3/2}$. Out of 10 *hfs* components (J = 3/2 ← J = 3/2), seven were completely resolved. *Hfs* investigations were carried out and precise values of *A* and *B* constants were determined. A magnetic dipole transition at 13325.476 cm^{-1} has been observed and *hfs* measurements were performed for the first time.

7

Chapter 7 summarizes the outcomes of the work done and its usefulness in understanding of basic properties atomic spectra and the applications of *hfs* in determination of nuclear properties and elemental abundance of stellar spectra. In this work, high resolution emission spectra of neutral and singly ionized atoms Iodine as well as Bismuth were reported. The methods of minimizing the broadening effects by cooling the sources and operating at low powers were discussed. Many lines were observed for the first time and for all observed spectral lines, new centre of gravity wavenumber values were provided with improve accuracy. Hyperfine investigations were carried out on many lines and the *hfs* constants were derived for the energy levels. Improved *hfs* constants were derived for the already known levels and for many levels, constants were derived for the time. Few lines were identified as blended lines and forbidden lines, which are important in stellar spectra.

References:

[1] Stone NJ. Table of nuclear magnetic dipole and electric quadrupole moment. Vienna Austria: International Atomic Energy Agency; 2014. p.88. Nuclear data section report no. INDC(NDS)-0658.

[2] Van stralen JNP, Visscher L. Molecular relativistic electric field gradient calculations suggest revision of the value of the nuclear electric quadrupole moment of 127I. Mol Phys 2003;101:2115-24.

[3] Kopfermann H. Nuclear moments. New York: Academy press inc.; 1958.

[4] Matveev AN. Optics. MIR publishers, Moscow, 1988.

[5] Saloman EB, Sansonetti CJ. Wavelengths, energy level classifications and energy levels for the spectrum of neutral neon. J Phys Chem Ref Data 2004;33:1113-58.

[6] Kumar PS, Kumar PVK, Suryanarayana MV. Application development for the calculation of hyperfine structure constants from the atomic hyperfine spectrum under the windows platform. 2002 (BARC Report BARC/2002/ E/ 027).

[7] Luc-Koeng E, Morillon C, Vergès J. Experimental and theoretical studies in atomic iodine: Infrared arc spectrum observations, classification and hyperfine structure. Phys Scrip 1975;12:199.

[8] Deng LH, Li YX, Zhu YY, Chen YQ. Hyperfine structure near infrared spectrum of atomic iodine. JQSRT 2015;161:153.

[9] Mu XL, Deng LH, Huo X, Jia Ye, Windholz L, Wang HL. Hyperfine structure investigations in atomic iodine. JQSRT 2018;217:229.

[10] Bhowmick GK, Verma R, Verma MK, RamanVA, Joshi AR, Deo MN, Gantayet LM, Tiwari AK, Ramakumar KL, Kumar N, Preparation of electrodeless discharge lamps for emission studies of uranium isotopes at trace level. Spectrochim Acta B 2010;65:1047.

[11] Schüler H. Über die Anregung von Spektren zur Untersuchung von Hyperfeinstrukturen. Z Phys 1930;59:149.

[12] George S, Gorbett MJ. Newly observed lines of the first spectrum of bismuth in the lead sulfide region. J Opt Soc Am 1982;72:589.

[13] George S, Munsee JH. Hyperfine-structure measurements in bismuth using a Fourier-transform spectrometer. J Opt Soc Am B 1985;2:1258.

[14] Sobolewski LM, Werbowy S, Kwela J, Hyperfine and Zeeman structure of lines of Bi I. J Opt Soc Am B 2014;31:3038.

[15] Cockett MCR, Donovan RJ, Lawley KP. Zero kinetic energy pulsed field ionization (ZEKE-PFI) spectroscopy of electronically and vibrationally excited states of I2+: The A 2Π3/2,u state and a new electronic state, the a 4σ-u state, J Chem Phys 1996;105:3347.

[16] Martin WC, Corliss CH. The Spectra of Singly Ionized Atomic iodine (I II). J Res Natl Bur Stand 1960;64A:443.

[17] Crawford MF, McLay AB. Spark spectra of bismuth Bi III and Bi II *Proc. R. Soc. Lond.* A 1934;**143**:540.

[18] Fisher RA, Goudsmit S. Hyperfine structure in ionized Bi *Phys. Rev.* 1931;**37**:1057.

[19] Mrozowski S. Forbidden Lines of Bismuth Bi I. Phys Rev 1945;69:169.

[20] Werbowy S, Kwela J. M1−E2 interference in the Zeeman spectra of Bi I. Phys. Rev. A. 2008;77:23410.

Chapter 1

Introduction

1.1 Introduction

"Spectroscopy" is the subject which deals with the interaction of electromagnetic radiation with matter. The electromagnetic radiation contains large range of wavelengths such as gamma rays, X-rays, ultraviolet, visible, infrared, microwave, and radio frequency rays. The electronic transitions of valance electrons of all the elements in the periodic table appear only in relatively limited spectral regions of the electromagnetic spectrum, which are Ultraviolet, Visible and Infrared regions. So a large number of spectral lines are expected in the atomic spectra of elements in these regions.

Atomic spectroscopy is the absorption and emission of light associated with the transitions between the atomic energy levels. Depending upon the origin of spectral transitions, atomic spectroscopy can be divided into three types: atomic emission, atomic absorption and atomic fluorescence spectroscopy, as shown in Fig. 1.1. In atomic absorption spectroscopy, a valance electron from the ground state gets promoted to the excited state by supplying a photon. The photon energy must be equal to the energy difference between the ground and excited states. In atomic emission spectroscopy, valence electrons in the atom are excited from the ground state to the higher energy states by supplying external energy. The atom in the excited state may emit a photon, and deactivate to the ground state. The energy of the emitted photon is equal to the energy difference between the excited and ground states. In atomic fluorescence, the atoms are excited from lower states to higher state by absorbing photon energy and also de-excited by emitting the photon. So this is a combination of atomic absorption and emission processes.
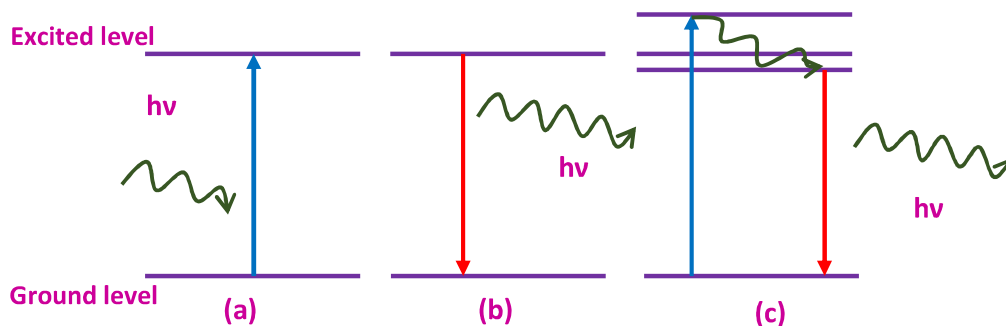
Fig. 1.1 The three basic types of atomic transitions in (a) atomic absorption (b) atomic emission and (c) atomic fluorescence spectroscopy.

Atomic spectroscopy discusses about these emission and absorption transitions between various energy levels of the elements. Each element has a unique set of energy levels and hence a unique spectrum. The study of this spectrum reveals information about the precise frequency/ energy of expected spectral transitions (center of gravity wavenumber values), identification of new spectral lines, energy level classifications, fine structure and hyperfine structure (*hfs*) constants and isotope shift measurements. These studies play an important role in basic physics to understand the atomic structure, chemical properties and provide an aid in astrophysical observations to determine the abundances of chemical elements. Among the various spectroscopic techniques, atomic emission spectroscopy is the most powerful and effective technique used to study the atomic properties of metals and non-metals.

The relation between the atomic energy levels and atomic structure was successfully proposed by Bohr by introducing the concept of circular orbits and the frequency of emission or absorption between these orbits of the electron. Dirac explained the splitting of these Bohr levels into fine structure levels due to relativistic corrections such as i) relativistic correction to kinetic energy, ii) spin-orbit coupling and iii) Darwin term. These fine structure levels are further

24

subjected to Lamb shift. By considering corrections due to atomic nucleus, the fine structure levels are further subjected to perturbations such as isotope shift, volume effects and hyperfine splitting in the atomic spectra, as shown in Fig. 1.2. The isotope shift and volume effects result in shifts of the fine structure levels, whereas hyperfine structure is the further splitting of 'fine' structure levels into several 'hyperfine' levels. This splitting is due to the spin possessed by odd nuclei. Because of the spin angular momentum, the nucleus has the electromagnetic multipole moments. The interaction of these multipoles with the magnetic and electric fields produced by the electrons at the nucleus causes the splitting in fine structure levels. Since the nuclear moments are much smaller than the electron moments, hyperfine splitting are even smaller corrections than those corresponding to the fine structure.
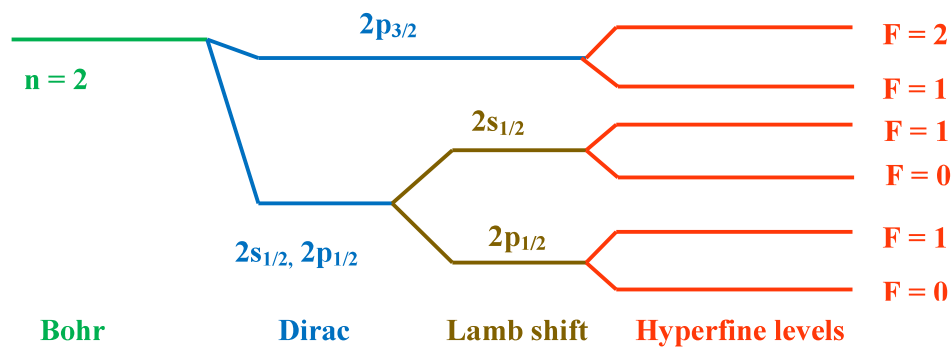
Fig. 1.2

Fig. 1.2 Shifts and splitting in the Bohr levels due to Dirac, Lamb and hyperfine interactions.

1.2 Importance of hyperfine structure

The hyperfine structure of spectral lines results from the splitting of fine structure energy levels. Hence, the study of *hfs* is useful in basic physics to get precise information on the

complete structure of atomic energy levels and understand various coupling mechanisms between them. Nuclear spin can be determined from the well resolved *hfs* structure by applying the methods like interval rule, number of *hfs* components and intensities.

The effect of *hfs* on stellar abundance analysis was discussed by Booth & Blackwell [1]. Andersson et al. [2] and Prochaska et al. [3] have provided the hyperfine dependent elemental abundance values for Mn and Sc. It is shown that if one neglects the *hfs* effect on the observed line profile, the stellar abundance gets overestimated. Hyperfine transitions of heavy alkali atoms like rubidium and cesium are used in atomic clocks [4] owing to a high reproducibility of these transitions frequencies. A 'second' is, in this way, described as "9,192,631,770 periods of the photon emitted in hyperfine transition in the ^{133}Cs atom" [5]. The *hfs* measurements are further useful in the diagnosis for Hall-thrusters by laser induced fluorescence [6,7].

The analysis of hyperfine structures provides the values of *hfs* coupling constants *A* and *B*. '*A*' is the magnetic dipole moment constant, which describes the interaction of electron magnetic field and nuclear magnetic dipole moment; and '*B*' is electric quadrupole moment constant, which describes the interaction of electron electric field and nuclear electric quadrupole moment. Determination of these coupling constants from optical hyperfine structure measurements allows calculating the nuclear moments, which are useful to further understand the nuclear structure and nuclear properties. However, for such analysis, the determination of accurate center of gravities of spectral lines in the resolved hyperfine structure patterns is essential, especially for elements having large nuclear moments.

1.3 Motivation for the present work

In this thesis, detailed investigations on the hyperfine structure measurements and analysis of neutral and singly ionized atoms of iodine and bismuth have been presented. The studies have been carried out using High Resolution Fourier transform spectroscopic technique. The spectroscopic investigations of these elements are very important for the understanding of basic atomic electronic structure, nuclear properties and also for applications in astrophysical and technological developments.

Iodine (Z=53) is the fourth member of halogen group and biologically important heavy element with several medicinal applications. It is one of the low abundance element $0.90(\text{Atoms}/10^6 \text{ Si})$ [8] in solar spectra but has a great significance in meteoritic studies. In the periodic table, it belongs to the few elements which have only one stable isotope (^{127}I). The classification of energy levels and exploration of new lines of ^{127}I in fine and hyperfine structures in a wide spectral range can be useful in the precise determination of its atomic and nuclear structure. Neutral atomic iodine (I I), with ground state electronic configuration $[\text{Kr}]4d^{10}5s^25p^5$, can be ionized (ionization potential is 10.45 eV) to singly ionized atomic iodine (I II) with the electronic configuration $[\text{Kr}]4d^{10}5s^25p^4$. The nuclear magnetic dipole (μ) and electric quadrupole (Q) moments are +2.81327(8) nuclear magneton [9] and -0.696(12) barn [10] respectively. Due to such a large μ and Q values, the spectral lines of ^{127}I, with nuclear spin $I = 5/2$, produce a rich hyperfine structure.

The spectroscopic investigations on I I were performed by many groups in the past [11-13]. The arc and spark spectrum of I I were photographed by McLeod [14] with a vacuum grating spectrograph covering 800 to 1900 Å ($125000 - 52631$ cm^{-1}) region, thus reporting a

total of 250 lines. Using Electrodeless Discharge Lamps (EDL), Kiess and Corliss [15] measured the iodine spectra in a wide spectral region 23070 Å - 1195 Å (4334 – 83682 cm^{-1}), and reported more than 900 spectral lines. Tolansky [16] had measured the fine structures of 42 lines of iodine in the spectral region 4500 – 6600 Å (22000 – 15000 cm^{-1}) by generating the spark spectrum of iodine using a water-cooled hollow cathode discharge. Eshbach et al. [17] recorded the spectrum of iodine in the 0.8 to 2.2 μm (12500 – 4545 cm^{-1}) IR region and measured the positions and the intensities of 31 spectral lines. Humphreys et al. [18, 19] examined the first spectra of iodine in the spectral region 1.8 – 4 μm (5500 – 2400 cm^{-1}) and reported 175 spectral lines. In addition, a CW laser emission from iodine atom was observed and attributed to the eight electronic transitions that fall between 3.0 and 9.0 μm (3300 – 1100 cm^{-1}) [20]. However, *hfs* studies in the spectrum of I I are scarce in the literature due to its high spectral complexity. In all, nearly 190 lines with analyzed *hfs* structure have been reported in a few different papers [21-23] and the precise knowledge of *hfs* constants is thus limited.

In the case of I II, very less number of spectroscopic measurements has been performed in the past [24-26]. The spectra of I II were observed by Martin et al [27] and reported the CG values for 2400 lines in the spectral region IR to UV. *Hfs* investigations were carried out by Murakawa [28] to derive *A* and *B* constants for 8 levels. Later, *hfs* on six fine structure levels was performed by Fowels [29] by using laser in the visible region.

Thus, a survey of literature on spectroscopic investigations conducted on I I and I II reveals that many lines have not been reported in the spectral region from infrared (IR) to Visible. The *hfs* measurements on spectral transitions and determination of *A* and *B* constants for most of the energy levels are therefore incomplete. As a result, the atomic spectrum of iodine is not fully understood. This necessitates detailed studies on the high resolution spectra of I I and I

II, as the accurate determination of the center of gravity wavenumber values of spectral lines obtained from well resolved hyperfine structures are very important to deduce the improved energy levels of atomic spectra and also to derive the *hfs* constants A and B for the energy levels to get more atomic parameters. The *hfs* structure of iodine spreads within the range of 1-2 cm^{-1}. As iodine can produce more *hfs* components in this small range of spectral region, it is difficult to resolve the complete structure of *hfs* pattern due to the domination of Doppler broadening. It is to be noted here that an unresolved *hfs* structure leads to the determination of inaccurate A and B constants. To overcome this difficulty and to get a well resolved *hfs* structure, special techniques need to be applied to cool the source in order to minimize the Doppler broadening.

Unlike iodine, neutral atomic bismuth (Bi I) is a heavy element with 83 electrons and the ground state configuration is [Xe]4f^{14}5d^{10}6s^{2}6p^3. Neutral bismuth can be ionized (ionization potential is 7.289 eV) to singly ionized atomic bismuth (Bi II) with the electronic configuration [Xe]4f^{14}5d^{10}6s^{2}6p^2. With these electronic configurations, bismuth energy level structures follow the intermediate coupling scheme. The large value of magnetic dipole moment $\mu = +4.1103(15)$ μ_N and electric quadrupole moment $Q = -0.516(15)$ barn [9], combined with nuclear spin $I = 9/2$, produces very broad hyperfine structure.

In this relatively large range of *hfs* splitting in bismuth spectra, which spans a range of about 8 cm^{-1}, many well resolved *hfs* components can be easily resolved. However, although the spectroscopic investigations on Bi have been carried out previously by many researchers [30-37], *hfs* measurements for many lines are still incomplete. Many resonance lines also appear in the spectra of Bi which are useful to understand the concept of self-absorption. Also, the accurate determination of line position values can be used to understand the coupling mechanisms between energy levels in bismuth. Another interesting feature of Bi spectra is the appearance of

forbidden transitions among the ground state configurations [38-40]. These transitions are not only important for fundamental understanding of selection rules, but are also vital in astrophysical observations. The detection of Bi abundance in chemically peculiar HgMn stars: χ-Lupi and HR 7775 [41,42] made bismuth an attractive element in the heavy elements group for spectroscopic as well as astrophysical investigations.

The aim of this thesis is to investigate the hyperfine structure of neutral and singly ionized iodine and bismuth atoms i.e, I I, Bi I, I II and Bi II in the spectral region from IR to UV. Various cooling methods were employed to reduce the Doppler broadening, to obtain a well resolved *hfs* structure which increases the accuracy of *hfs* constants.

1.4 Layout of the thesis

This thesis composes of seven chapters, briefly discussed as follows. Chapter 1 is the introduction part.

Chapter 2 provides a detailed discussion on the theory of hyperfine structure and Fourier transform spectroscopy (FTS), experimental techniques and *hfs* data analysis. In hyperfine theory section, a discussion on hyperfine structure splitting, selection rules, intensity rules are provided. In Fourier transform spectroscopy section, details of Michelson interferometer, advantages of FT spectroscopy and various aspects of practical FTS are provided. Different types of spectral broadening effects are also mentioned. In experimental techniques, the preparation of emission sources EDL and Hollow Cathode Lamps (HCL), Microwave and DC discharge methods to excite and generate the plasma in the source is discussed. Comparison between EDL and HCL discharge has also been presented. Details of Fourier transform spectrometer used (Model:

30

Bruker IFS125HR) and calibration methods of spectral lines have also been presented, which has been used for the work presented in the entire thesis. An important part of the present work is the inclusion of cooling to reduce the temperature of EDL and HCL, which has also been described in this chapter. This results the minimization of the Doppler broadening in the spectral lines. The details of software *HFSAB* and *WINHFS*, which were used to analyze the *hfs* data, have been provided.

Chapter 3 presents the observed spectral lines and hyperfine structure measurements of neutral iodine (^{127}I) in the spectral range of $1800 - 25000$ cm^{-1}. We have carried out extensive investigations on this important element to analyze *hfs* structures of more than 450 transition lines in the widest spectral range reported so far. A mixture of iodine vapor and Ne was excited in an EDL driven by a surfatron microwave cavity operated by microwave power supply. A total of 777 spectral lines of I I have been observed. This entire data has been divided into three parts (1800-6000 cm^{-1}, 6000-10000 cm^{-1}, 10000-25000 cm^{-1}) as per the optics and detector ranges. As the light transmittance of normal Quartz EDL is quite low, below 3500 cm^{-1}, an EDL with CaF$_2$ window has been made to observe those lines. Nearly 100 new lines were identified below 3500 cm^{-1}. The effect of source cooling on spectral resolution, calculations of temperature, analysis of unidentified and blended lines has also been discussed in this chapter.

Chapter 4 addresses the *hfs* investigations of neutral atomic bismuth (^{209}Bi) in the spectral range of $2500 - 40000$ cm^{-1}, a total of 107 Bi I lines have been observed. Hyperfine structure measurements were performed on 76 well resolved lines, of which 21 were analyzed for the first time. The *hfs* constants A and B were derived for all the 31 levels (14 even and 17 odd levels) involved in these transitions. Among those, A constants of 6 levels and B constants of 8 levels are reported for the first time. A discussion on spectral line self-absorption and its effect in

systematically destroying *hfs* structure in the case of strong EDL discharge has also been included. These self-absorbed *hfs* structures obtained with EDL have been compared with *hfs* structures observed with HCL. Brief discussions have been presented on the operating conditions of EDL and HCL sources and blended lines.

Chapter 5 presents the hyperfine structure investigations on singly ionized iodine (I II) and bismuth (Bi II). The temperature conditions to observe the spectra of ionized species have been discussed. Emission spectra of singly ionized iodine have been observed in the range 12000 to 25000 cm^{-1} by exciting the microwave discharge of EDLs. For iodine, a total of 141 spectral lines were detected as I II transitions. Among the 141 observed lines, *hfs* measurements were carried out on 73 spectral lines. *Hfs* constants were derived for 61 energy levels of which, 29 were even parity and 32 were odd parity levels. One blended line at 20611 cm^{-1} has been observed and simulated. The emission spectra of Bi II have been observed in the spectral region from visible to UV (13000 - 40000 cm^{-1}) by microwave discharge EDL and DC discharge LN$_2$ cooled HCL methods. In the entire spectral region, 45 spectral lines were detected as Bi II lines, of which *hfs* investigations on 33 lines have been carried out.

Chapter 6 describes the *hfs* of forbidden transitions obtained from I I, I II, Bi I and Bi II spectra. Completely resolved magnetic dipole transitions of I I at 7602 cm^{-1} and I II at 22414 cm^{-1} have been observed. Three forbidden transitions of Bi I at 461.7, 647.5 and 875.7 nm one of Bi II at 750.3 nm have been detected using the EDL discharge. Hyperfine structure investigations were performed on these four forbidden transitions. A line at 647.5 nm (transition between $6s^2 6p^3\ ^2D_{5/2}$ - $6s^2 6p^3\ ^4S_{3/2}$ levels), with 18 *hfs* components (12 for $\Delta F = 0, \pm 1$ and 6 for $\Delta F = \pm 2$) has been discussed, for which all six $\Delta F = \pm 2$ transitions were observed for the first time.

Finally, Chapter 7 gives a summary of the entire thesis work.

Chapter 2

Theory, Experimental Techniques and Data Analysis

2.1 Theory of Hyperfine Structure

Due to the interaction of nuclear moments possessed by the odd nuclei with the electric and magnetic fields produced by the electrons, each fine structure level splits into further levels, which is known as hyperfine structure. The perturbative Hamiltonian H_{hyp}, responsible for the correction factor for the hyperfine splitting of fine structure levels, can be written as [43-48],

$$H_{hyp} = H_{Mag} + H_{Elec} \qquad (1)$$

The first perturbative Hamiltonian term, H_{Mag} is due to the interaction of nuclear magnetic dipole with electron orbital angular momentum (L) and spin angular momentum (S). The second perturbative Hamiltonian term H_{Elec} is due to the interaction of nuclear electric quadrupole moment with electrostatic potential created by the electrons.

2.1.1   Nuclear Multipoles

The atomic nucleus may possess all orders of multipoles i.e, 2^k number of poles (k=1, 2, 3, 4,…) [49]. But, the possible nuclear moments are limited due to the symmetry arguments of parity and time reversal invariance. Thus, only odd k values of magnetic moments namely magnetic dipole (k = 1), magnetic octopole (k = 3) and so on; and even k values of electric moments, namely electric quadrupole (k = 2), electric hexadecapole (k = 4) etc. will be present. Among these, only the magnetic dipole (k = 1) and electric quadrupole (k = 2) moments have significant contribution to the hyperfine interaction.

The nuclear spin (I), is considered as the resultant of the orbital angular momentum and the intrinsic spin angular momentum of the nucleons (protons and neutrons). Similary, the resultant magnetic moments of all the nucleons is considered as nuclear magnetic moment μ_I. The nuclear spin I and magnetic moment μ_I are connected by the following relation [43],

34

$$\mu_I = \frac{e}{2M} \hbar I g_I \qquad (2)$$

where $\hbar = \frac{h}{2\pi}$ and g_I is the nuclear g-factor, Using the proton mass m_P, electron mass m_e and Bohr magnetron μ_B, equation (2) can also be written as

$$\mu_I = \frac{e}{2m} \hbar I g_I \frac{m_e}{m_P} = \mu_B I g_I \frac{m_e}{m_P} = \mu_n I g_I \qquad (3)$$

with $\mu_B = \frac{e}{2m_e} \hbar$ and $\mu_n = \mu_B \frac{m_e}{m_P}$

The quantity μ_n is called nuclear magneton (n.m.). Its values is $\mu_n = 5.0493.10^{-24}$ erg/gauss.

If the nucleus axial symmetry is about z-axis, then the electric quadrupole moment Q can be defined as,

$$Q = \int \rho(3z^2 - r^2)d\tau = \int \rho r^2 (3\cos^2\theta - 1)d\tau \qquad (4)$$

where $r^2 = x^2 + y^2 + z^2$ and $\rho = \frac{Z}{4\pi \frac{r_0^3}{3}}$ is the charge density.

Electric quadrupole moment, Q has the dimensions of an area and is a measure of the deviation of the charge distribution from spherical symmetry. Q is positive for an elongated nucleus and negative for a flattened nucleus.

2.1.2 Magnetic dipole hyperfine structure

The perturbation Hamiltonian term H_{Mag} due to the nuclear magnetic dipole moment has two parts. First part is the interaction energy of the nuclear magnetic dipole moment with the magnetic field produced by the orbital motion of the electrons (H_1) and spin motion of the electrons (H_2). The total magnetic dipole interaction term can be written as,

$$H_{Mag} = H_1 + H_2 \qquad (5)$$

35

The corresponding shift in the energy levels can be written as

$$\Delta E_{Mag} = \Delta E_1 + \Delta E_2 \qquad (6)$$

The interaction energy V_{mag} of the nuclear magnetic moment μ_I and magnetic field produced by the electrons $H(0)$ can be expressed as [43],

$$V_{mag} = -\mu_I . H(0) = -\mu_I H(0) \cos (\mu_I, H(0)) \qquad (7)$$

In order to get the shift of the energy levels from the interaction energy V_{mag}, it is necessary to take the time average over the unperturbed electronic motion. Thus, the magnetic field $H(0)$ is replaced by its average $\overline{H(0)}$ in eq.(7). Then the interaction energy will become,

$$\Delta E_{mag} = -\mu_I \overline{H(0)} \cos (\mu_I, H(0)) \qquad (8)$$

In normal case, $H(0)$ and J are anti-parallel and the nuclear magnetic moment is positive, μ_I has its most stable position in the direction parallel to $H(0)$ so that cos (I,J) has the value -1 and the eq.(8) becomes

$$\Delta E_{mag} = -\mu_I \overline{H(0)} \cos(\mu_I, H(0)) = AIJ \cos (I,J) \qquad (9)$$

where $\qquad A = \dfrac{\mu_I \overline{H(0)}}{IJ} = \dfrac{\mu_n g_I \overline{H(0)}}{J} \qquad (10)$

is called the magnetic dipole hyperfine coupling constant.

The angular momentum vectors I and J are coupled and form the resultant total angular momentum vector F of the atom.

$$\cos(I,J) = \dfrac{F^2 - I^2 - J^2}{2IJ} \qquad (11)$$

From the quantum mechanical treatment, $F^2 = F(F+1)$, $I^2 = I(I+1)$ and $J^2 = J(J+1)$, now

36

$$\Delta E_{Mag} = AIJ \frac{F^2 - I^2 - J^2}{2IJ} \tag{12}$$

$$\Delta E_{Mag} = A \frac{F(F+1) - I(I+1) - J(J+1)}{2} = \frac{AC}{2} \tag{13}$$

where $C = F(F+1)$- $I(I+1)$-$J(J+1)$.

2.1.3 Electric quadrupole hyperfine structure

The energy shift due to the interaction of electric field vector gradient produced by the electrons and the nuclear quadrupole moment can be derived as [43],

$$\Delta E_{Elec} = \frac{B}{4} \left(\frac{3}{2} cos^2(I,J) - \frac{1}{2} \right) \tag{14}$$

with $\quad B = eQ\overline{\varphi_{JJ}(0)}$ $\qquad\qquad$ (15)

is called the electric quadrupole hyperfine coupling constant and $\varphi_{JJ}(0)$ is the vector gradient at the nucleus of the electric field of the orbital electron having cylindrical symmetry about the J axis.

For small values of I, J and F by using Casimir formula [50],

$$\Delta E_{Elec} = \frac{3B}{8} \frac{C(C+1) - 2I(I+1)J(J+1)}{I(2I-1)J(2J-1)} \tag{16}$$

where $C = F(F+1)$- $I(I+1)$-$J(J+1)$.

The atoms with all closed shells and sub-shells having spherical charge distributions do not contribute to ΔE_{Elec}. As, the nuclei with $I = 0$ and $I = 1/2$ possess a spherical charge distribution, therefore non-zero ΔE_{Elec} contributions will only come from nuclear spin greater than 1/2, i.e. $I > 1/2$.

2.1.4 Total hyperfine interaction

The addition of energy shifts due to magnetic dipole and electric quadrupole interactions produces the resultant hyperfine shift for each fine structure level. The total hyperfine energy level shift is using eq.13 & 16,

$$\Delta E_{hfs} = \Delta E_{Mag} + \Delta E_{Elec}$$

$$\Delta E_{hfs} = A\frac{F(F+1)-I(I+1)-J(J+1)}{2} + \frac{3B}{8}\frac{C(C+1)-2I(I+1)J(J+1)}{I(2I-1)J(2J-1)} \tag{17}$$

$$\Delta E_{hfs} = \frac{AC}{2} + \frac{3B}{8}\frac{C(C+1)-2I(I+1)J(J+1)}{I(2I-1)J(2J-1)} \tag{18}$$

with $C = F(F+1)- I(I+1)-J(J+1)$.

2.1.5 Vector model of hyperfine structure splitting

The hyperfine splitting of atomic fine structure levels, i.e. the interaction of the nuclear spin angular momentum (I) with the total electronic angular momentum (J) as discussed above, can be described using the atomic vector model [51]. The resultant angular moment F, shown in Fig. 2.1 represents the total angular moment of the atom.

$$\vec{F} = \vec{J} + \vec{I} \tag{19}$$

Due to the interaction of $\vec{I}$ and $\vec{J}$, the total angular momentum quantum number $\vec{F}$ may takes the values as

$$I - J\ to\ I + J \quad \text{if} \quad I \geq J$$

$$J - I\ to\ J + I \quad \text{if} \quad J \geq I \tag{20}$$
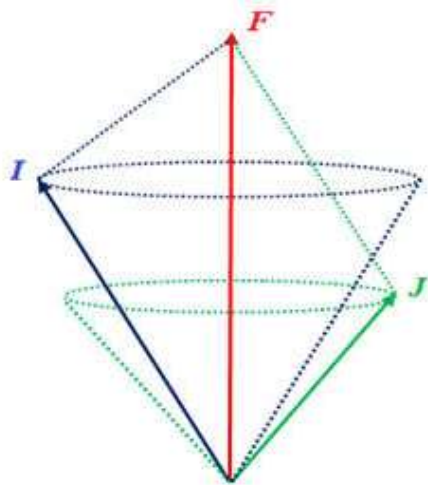
Fig 2.1 Vector diagram for the hyperfine splitting coupling of angular momentum

The hyperfine structure separations also follow the interval rule, as in the case of fine structure multiplets. The separation of two adjacent states is proportional to the largest F of the two states. The hyperfine structure separations also depend upon the coupling of electron angular moments, i.e. (L-S) type (between the extra-nuclear moments) or (j,j) type coupling (found mostly in heavy elements).

The splitting of fine structure levels into hyperfine structure has been shown in Fig. 2.2 by considering a transition between the levels in I II. The fine structure levels 6p $^5P_3$ and 5d $^5D_4$ are further split into hyperfine levels. In case of upper level 6p $^5P_3$, $J = 3$ couples with $I = 5/2$ and the resultant F values are 11/2, 9/2, 7/2, 5/2, 3/2 and 1/2 according to eq. (20). In this case, $J \geq I$, so the total *hfs* levels are $2I+1 = 6$. As shown in Fig. 2.2, in the *hfs* of the upper level, the lower the F value, deeper is the level. This structure is known as *normal hfs* structure. Similarly the lower level 5d $^5D_4$ takes the F values as 3/2, 5/2, 7/2, 9/2, 11/2 and 13/2. For this level, the hyperfine splitting levels follow an opposite trend than in the first case. This is called *inverted hfs* structure. This structure format depends upon the A value of a particular level. If A is

39

positive, then the structure tends to be normal, while inverted structure will be formed if A is negative. These A values are further dependent on g_I values as given in eq. (16).
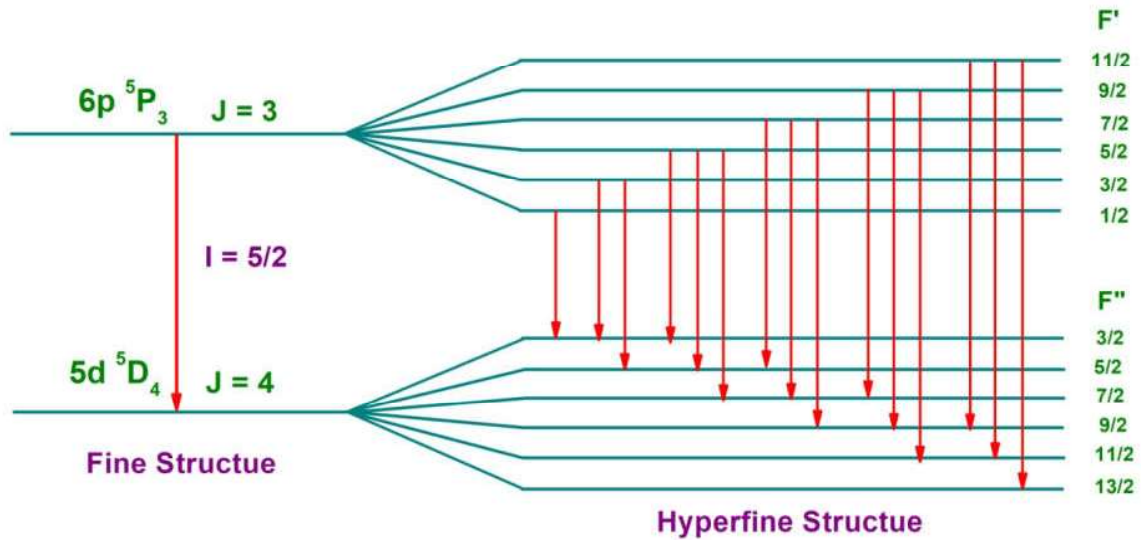
Fig. 2.2 Hyperfine splitting of fine structure levels.

2.1.6 Selection Rules

In the absence of external magnetic field, the selection rules for the all *hfs* transitions for electric and magnetic dipole radiation are as follows,

1. For electric dipole radiation

    i. $\Delta J = 0, \pm 1$ but $J = 0 \rightarrow J = 0$ is forbidden.

    ii. $\Delta L = \pm 1$

    iii. $\Delta S = 0$

    iv. $\Delta F = 0, \pm 1$ but $F = 0 \rightarrow F = 0$ is forbidden.

2. For magnetic dipole radiation

   i. $\Delta J = 0, \pm 1$ but $J = 0 \rightarrow J = 0$ is forbidden.

   ii. $\Delta L = 0, \pm 1, \pm 2$

   iii. $\Delta S \neq 0$

   iv. $\Delta F = 0, \pm 1$ but $F = 0 \rightarrow F = 0$ is forbidden.

2.1.7   Intensity rule

The intensities are functions of I, J and F. Transitions with same ΔJ and ΔF possess highest intensity. Similarly, the transitions with opposite ΔJ and ΔF generate lower intensities. The *hfs* components with $\Delta F = +1$ have a very high relative intensity if the transition involves $\Delta J = +1$. For the cases $\Delta J = -1$ and $\Delta J = 0$, the components $\Delta F = -1$ and $\Delta F = 0$, respectively, have overwhelming intensity. The hyperfine structure of such lines forms a flag pattern [52].

For a transition from J' to J, the relative intensity distribution of the hyperfine components are given by Racah coefficients [53] as follows,

$$S_{FF'} = S(F \rightarrow F') = \frac{(2F+1)(2F'+1)}{2I+1} \begin{Bmatrix} J' & F' & 1 \\ F & J & 1 \end{Bmatrix}^2 \qquad (21)$$

where, the factor $\begin{Bmatrix} J' & F' & 1 \\ F & J & 1 \end{Bmatrix}$ is known as Wigner 6j symbol.

2.2 Spectral Line Shapes and Broadening

The spectral lines arising from absorption or emission processes are infinitely narrow. The observed spectral line intensity is a function of frequency. This distribution arises from a number of different causes.

Natural broadening: Every atomic level, except the ground state, has a finite energy width ΔE. From the uncertainty principle, the uncertainty in the energy can be written as

$$\Delta E \cong \hbar/t \quad \text{or} \quad \Delta \nu \cong 1/t$$

This represents that the more the lifetime of the atom in a state, the less the energy width of that state. This is an inherent property of every energy level. This width will be present in every energy level. But the order of natural line width is considerably low compared to remaining broadening effects. The intensity distribution follows the Lorentzian profile.

Doppler broadening: The observed frequency of light emitted by a moving source is shifted by the Doppler effect. The observed frequency increases if the atoms are moving towards the observer and decreases if the motion is away from the observer. If the source of frequency ν_0 is moving with velocity v, then the frequency measured by the observer is

$$\nu = \nu_0 (1 \pm \frac{v}{c})$$

where c is velocity of light.

At the source temperature T, the Doppler line profile follows the Gaussian distribution.

The Doppler width ($\Delta\sigma$) of the spectral lines in terms of wavenumber is,

$$\Delta\sigma = \sigma_0 (7.16 \times 10^{-7}) \sqrt{\frac{T}{m}} \quad \text{cm}^{-1} \tag{22}$$

where σ_0 is the transition wavenumber in cm^{-1}, 'm' is atomic mass in amu, and 'T' is temperature in Kelvin.

From the above eq. (22) the Doppler width increases with temperature and wavenumber of the line. The width decreases as the atomic mass increases.

Collision broadening: At high pressures, in the gas sources, the life time of a state is reduced by the collisional excitation and de-excitation of atoms with other atoms. This reduction in lifetime of each state causes the broadening of the spectral lines.

Self-absorption: In resonance lines, more number of atoms are involved in the transition. The intensity of such transitions is high compared to non-resonance lines. In such transitions, photons emitted by the atoms may get absorbed by other cooled atoms before the light escapes from the discharge tube. In general, the inner part or middle part of the source is strongly excited compared to the outer portion. In such cases, the cold atoms present at the outer portion absorb the radiation. This results in the loss of this portion of intensity in the original spectral line. In the spectral line profile, as the probability of emission of photons is greatest at the center of the line, the absorption is also high at the centre of the line. This causes a broadening in the spectral line and the line appears as a flat line at the peak position. If the self-absorption is strong, then an intensity minimum develops in the centre of spectral line. This pattern is called self-absorption [54].

2.3 Fourier Transform Spectroscopy

Fourier transform spectroscopy measures all the wavenumbers simultaneously by modulating the incident light in the distance domain by Michelson interferometer [55-57].

2.3.1 Michelson Interferometer

Fourier transform spectrometer works based on the principle of Michelson's interferometer. The schematic of Michelson's interferometer is shown in Fig. 2.3. The interferometer consists of four arms. The beamsplitter is oriented at 45 degrees to the incoming beam of collimated radiation such that 50% of the intensity is reflected and 50% is transmitted.

The reflected beam travels to mirror M1 where it is back reflected to the beamsplitter. In the same way, the transmitted beam travels to mirror M2 and back reflected to the beamsplitter. These two beams interfere, based on their optical path difference. 50% of these beams are again transmitted back towards the source, whereas the rest travel towards the detector.

If the two interfering beams are in phase with each other then they constructively interfere and the resultant beam is more intense than either of the two beams. If the two beams are out of phase with each other, then they destructively interface and the resultant beam intensity is less than either of the two beams. By moving the movable mirror (M2) the two beams will flip alternatively in phase and out of phase with each other, which means that as the mirror continues to move, the resultant beam intensity grows brighter and dimmer. A plot of measured light intensity versus optical path difference is called interferogram which is the fundamental measured quantity in Fourier transform spectroscopy.

Thus, the signal measured from an interferometer is called an interferogram, which is the intensity distribution as a function of the change in optical path difference (δ) between two beams [58].

$$I(\delta) = \int_{-\infty}^{\infty} B(\sigma)e^{2\pi i \sigma \delta} d\sigma \qquad (23)$$

where $I(\delta)$ is the measured interferogram and $B(\sigma)$ is the power spectrum of the source in terms of the wavenumber σ,

By applying inverse Fourier transform, the interferogram can be converted into the spectrum which is a function of wavenumber (σ).

$$B(\sigma) = \int_{-\infty}^{\infty} I(\delta)e^{-2\pi i \sigma \delta} d\delta \qquad (24)$$
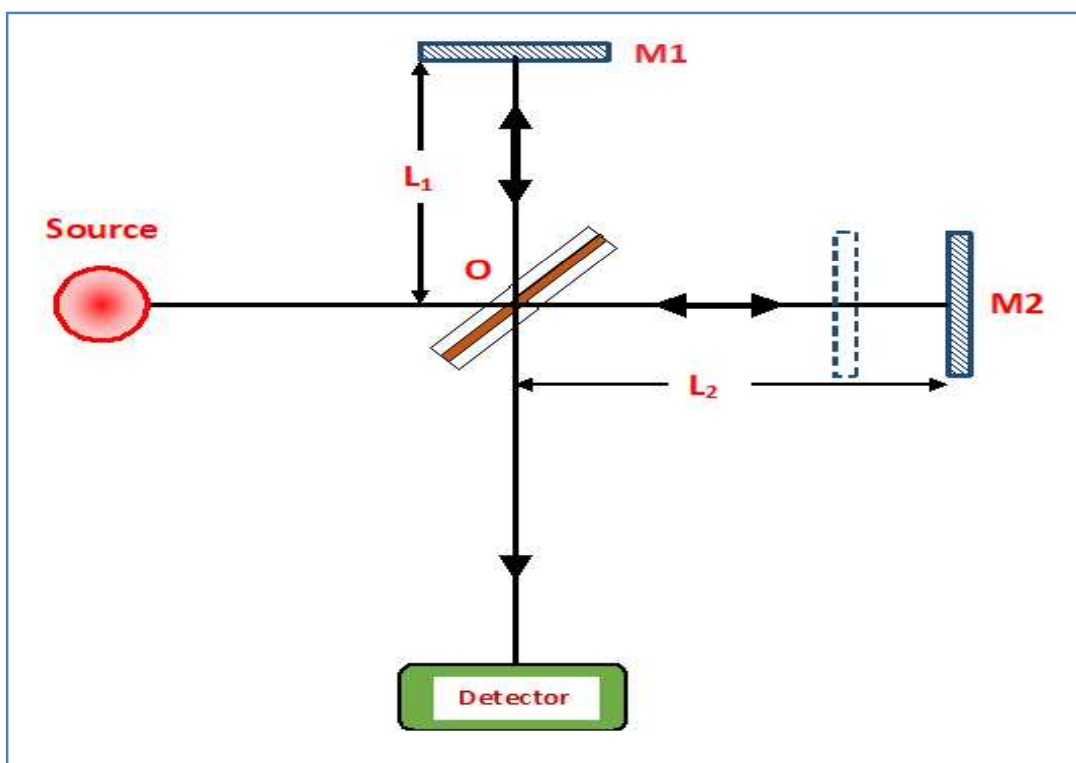
Fig. 2.3 Schematic of the Michelson interferometer

2.3.2 Advantages of Fourier Transform Spectroscopy

a. Jacquinot (Throughput) advantage

Throughput is a measure of the amount of light from source that hits the detector. In dispersive spectrometers the beam passes through slits, prisms and gratings which reduce the intensity of beam reaching to detector. But in FT spectrometer no such slits, prisms and gratings are present. So a large amount of light impinges on the detector increasing the signal level. This phenomenon is called the (Jacquinot) throughput advantage.

b. Fellgett (Multiplexing) advantage

In a dispersive spectrometer, wavenumbers are observed sequentially, as the grating is scanned. But in FT spectrometers all wavelengths from the source impinge simultaneously on the detector. This leads to the multiplex or Fellgett advantage. Under identical conditions, the signal-

to-noise ratio (S/N) of the spectrum recorded from the FTS will be greater than that of the dispersive spectrum by a factor of $\sqrt{M}$. Here M is the number of spectral elements in a spectrum and is defined as

$$M = \frac{\sigma_1 - \sigma_2}{\Delta\sigma_{res}}$$

Where σ_1 and σ_2 are the upper and lower wavenumbers of the observed spectral region and $\Delta\sigma_{res}$ is the resolution. Though recent developments of array detector coupled with echelle spectrometer have reported better signal to noise ratio and multiplexing advantage than FTS [59], the commercially available echelle spectrometers still offer lower resolution than FTS

c. Stray Light advantage

The detector is sensitive to only the modulated frequency. In FTS, the interferometer modulates each wavelength at a different frequency. The modulated frequency is

$$f_m = 2\upsilon\sigma$$

where υ is the velocity of moving mirror and σ is the wavenumber. So, there is no presence of stray light at the detector.

d. Connes advantage

In FT spectrometers, a reference laser (He-Ne) has been used to obtain the frequency scale of the spectrum. Thus, there is no requirement for any further calibration of the spectrum measured by these spectrometers. This advantage is known as Connes advantage.

2.3.3 Important aspects of Fourier transform spectroscopy

a. Apodization

From eq.(24), the basic Fourier transform integration has infinite limits from $-\infty$ to $+\infty$ for the optical path difference. But the optical path difference of practical instrument is finite.

The finite limits in the integration lead to the generation of false side-lobes in the transformed spectrum. To remove these false side-lobes, the interferogram is multiplied by a suitable mathematical function called 'apodization function'. Depending upon the sample (gas, solid or liquid) and resolution required, various apodization functions can be applied. Triangular, Box-car, Norton-Beer, Four Point and Blackmann-Harris are frequently used few apodization functions. Although the apodization function suppresses the side-lobes, it degrades the resolution of the spectrum.

b. High Resolution

The resolution of a spectrometer is defined as the ability of an instrument to distinguish the closely spaced spectral lines. For interferometers, the solution can be written as

$$Resolution \propto \frac{1}{\delta}$$

Where δ is maximum optical path difference for a scan. Hence, the resolution of an interferometer varies inversely as the maximum optical path difference i.e, maximum mirror displacement. Even though the resolution will improve by large distances of mirror displacement, the S/N reduces and the mirror alignment has to be carefully maintained.

c. Phase Correction

The FT measured interferogram is generally a complex spectrum which is the sum of real and imaginary parts. This complex spectrum is equivalent to amplitude multiplied by complex exponential. The aim of the phase correction is to extract the amplitude spectrum from the complex output. This can be done by multiplication of an inverse phase exponential to the complex spectra. The reason for getting a complex spectrum in FT is due to i) imperfection in beamsplitter which may not send equal energy to both the arms, ii) The two arms may not be identical and iii) recording a single-sided interferogram. These errors can make the interferogram

47

to be asymmetric. These errors modify the $e^{-2\pi i \sigma \delta}$ factor in the computation of the spectrum by a multiplicative factor $e^{-i\varphi}$ and hence are known as phase factors. Recording a double-sided interferogram reduces the phase errors.

All the above aspects can be summarized in terms of the advantages of FTS technique over dispersive technique, as follows:

1. High signal to noise ratio.

2. Very high resolution.

3. High wavenumber accuracy.

4. Fast scanning time.

5. Large wavenumber range per scan.

6. Vastly reduced stray or unwanted flux problems.

2.4 Experimental Techniques

In this section, a detailed discussion on experimental setup which includes the preparation of atomic emission sources to generate the atomic spectral lines, the methods of discharging, cooling setup to reduce the Doppler width of the spectral lines, a high resolution spectrometer to observe the well resolved *hfs* pattern of emitted lines and spectral calibration procedures have been given. A method of analysis of hyperfine structure to obtain the *hfs* constants has been described. Lastly, the determinations of uncertainties of *hfs* constants are discussed.

To obtain a well resolved *hfs* pattern, suitable light sources are required, which can produce sharp spectral lines. Those lines can be observed by using a high resolution instrument. In the present investigations, we have used two light sources. One is microwave discharge of an

electrodeless discharge lamp (EDL) and another is DC discharge of a liquid nitrogen (LN$_2$) cooled hollow cathode lamp (HCL) to produce a large number of atomic emission lines in a wide spectral range of 1800 - 40000 cm^{-1}, i.e. from infrared to ultra-violet. These lines were observed by the high resolution Fourier transform interferometer.

2.4.1 Atomic Emission Sources

Atomic plasma has been generated by two basic types of light sources EDL [60-61] and HCL [62]. EDLs may excite by using radiofrequency or microwave discharge methods. As the emission light intensity from the microwave excitation is more than radiofrequency excitation, in the present work, the EDL were excited by microwave discharge method. HCL were excited by DC discharge method. The intensity of spectral lines produced by EDL is stronger than HCL discharge. Only microwave excited EDL were prepared to generate the iodine plasma, whereas both the microwave excited EDL and DC discharge of HCL were prepared for bismuth plasma. The methods of preparation of EDL of iodine, bismuth iodide and HCL of bismuth oxide have been discussed below.

a. Preparation of EDL with I$_2$

A quartz tube comprising of two sections, as shown in Fig. 2.4 has been prepared for the fabrication of an EDL. Section A is a glass vacuum stop cock of 10 mm OD, fused to a quartz tube of 10 mm OD by a glass to quartz graded seal at point 2, shown in Fig. 2.4. Section B is a quartz tube having two segments (segment 1: length of 8 cm and OD of 10 mm, segment 2: length of 4 to7 cm and OD of 6 mm) and is used for the fabrication of EDL. The glass tube (prior to any construction) was cleaned with nitric acid, acetone and then by distilled water to clean it from any contamination. The inner surface of section B was degassed by heating at 800 °C for about 3 hour. The system was evacuated 1.0 × 10^{-3} Torr, subjected to a repeated microwave

discharge cleaning with pure neon gas until a persistent color of Ne discharge was obtained and re-evacuated to 1.0×10^{-5} Torr. After proper cleaning, about 1 mg of pure Iodine (I_2) (99.9% spec grade) and about 1 Torr of neon (as a buffer gas) was filled into the tube without breaking the vacuum. Sealing the segment 2 at 'a' completes the preparation of the I_2 EDL.
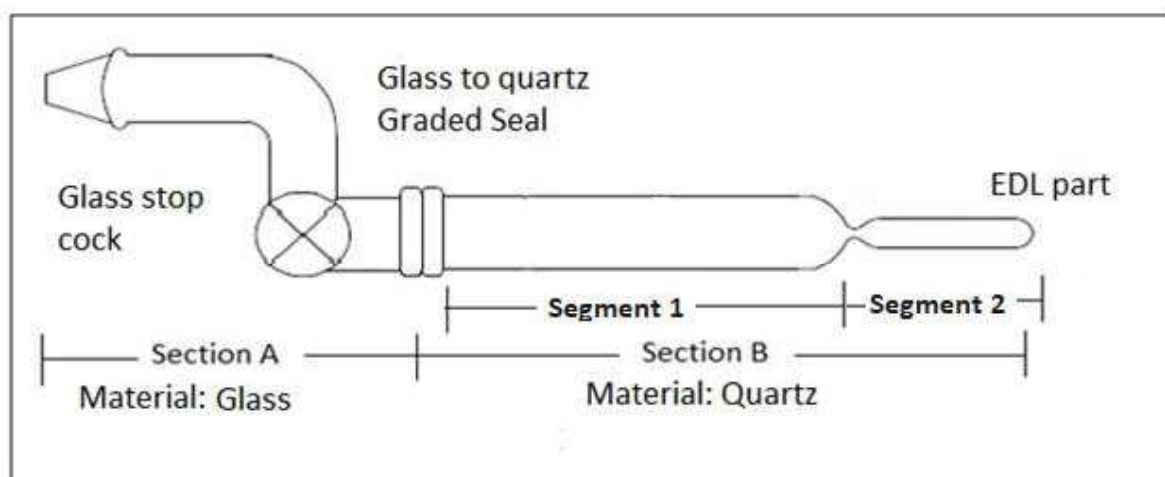
Fig. 2.4 Sectional view of the tube used for the fabrication of iodine EDL. 1) Glass stop cock, 2) Glass to quartz graded seal, 3) EDL part.

b. Preparation of EDL with BiI₃

For the preparation of bismuth iodide EDL, a similar procedure was followed as described by Bhowmick et al. [63]. A quartz tube of length 5 cm and outer diameter (OD) of 7 mm was used to make a reaction tube for the synthesis of BiI_3. Using glassblowing, one end of the tube was made as a thin capillary, while the other end was fused to a glass vacuum stop cock with a graded seal. The glass tube (prior to any construction) was cleaned with nitric acid, acetone and then by distilled water to remove any contamination. The system was evacuated 1.0 $\times 10^{-3}$ Torr, subjected to a microwave discharge cleaning with pure neon gas for several times until a persistent color of Ne discharge was obtained and evacuated to 1.0×10^{-5} Torr. After proper cleaning, about 2 mg of pure bismuth metal (99.9% spec grade) and 4 mg of iodine (I_2)

were placed into the reaction tube without breaking the vacuum, after which the tube was sealed. For the synthesis of BiI_3, the sealed tube was strongly heated in a furnace for 4 hours.

A second tube was prepared for the fabrication of an EDL that contained two sections as shown in Fig. 2.5. Section A is a glass vacuum stop cock of 10 mm OD, fused to a quartz tube of 10 mm OD by a glass to quartz graded seal at point 2, shown in Fig. 2.5. Section B is a quartz tube having two segments (segment 1: length of 8 cm and OD of 10 mm, segment 2: length of 4 cm and OD of 7 mm) and is used for the fabrication of EDL. This entire tube was cleaned by the same procedure as described above. Now, the sealed reaction tube was inserted into segment 1 of section B and fused with the stop cock at point 'a' as shown in Fig. 2.5. The entire assembly is then connected to a vacuum system, evacuated to 1.0×10^{-3} Torr. The inner surface of Section B was degassed by heating at 800 °C for about 3 hour. Subsequently, it was filled with neon at about 2 Torr pressure and subjected to a microwave discharge for another 3 hours. This procedure was repeated several times to clean Section B from any contamination. After the tube was evacuated to 1.0×10^{-5} Torr, it was filled with neon (as a buffer gas) at about 1 Torr, and sealed off at 'a' by glass blowing. Then, the capillary of the reaction tube was broken by gently shaking the tube. A simultaneous, heating of segment 1 to 300 °C and cooling of segment 2 with cooled water was used to transfer some amount of BiI_3 into segment 2. Sealing the segment 2 at 'b' completes the preparation of the BiI_3 EDL.
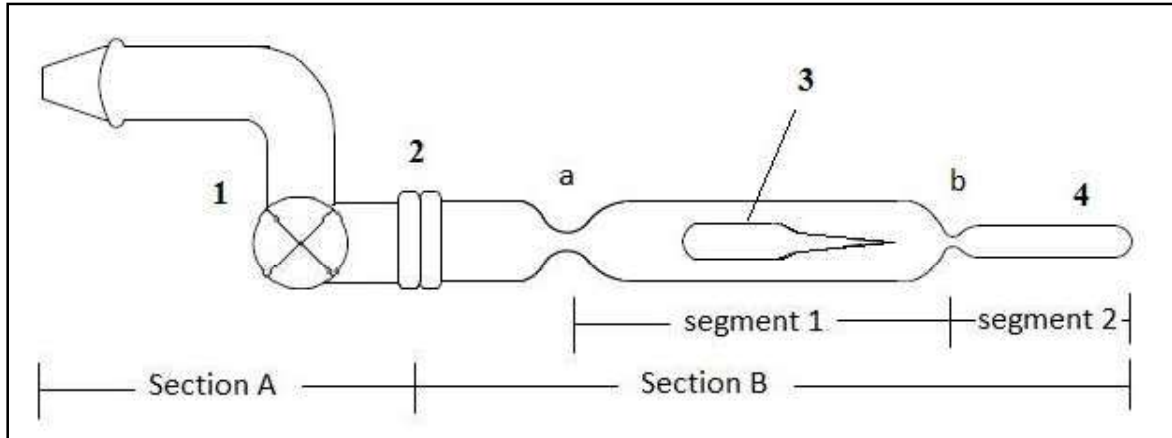
Fig. 2.5: Sectional view of the second tube used for the fabrication of a BiI_3 EDL. The reaction tube is shown inside the segment 1. 1) Glass stop cock, 2) Glass to quartz graded seal, 3) BiI_3 reaction tube and 4) EDL part.

c. Detachable hollow cathode lamp with Bi_2O_3

HCL containing bismuth oxide (Bi_2O_3) was another source, used to generate the Bi plasma. The schematic of detachable hollow cathode lamp has been shown in Fig. 2.6. This is a similar kind of lamp as described in ref. [62]. The HCL consists of three detachable parts: cathode, anode and glass tube. The cathode was fabricated with oxygen free copper. One end of the cathode was shaped as B29 socket for vacuum sealing. A 4 mm diameter and 20 mm deep bore was prepared in the cathode to insert a small replaceable copper tube (sample holder) of 18 mm length and 3 mm dia. The anode part is a hollow tube of aluminum metal with adjustable height and graded diameter towards the cathode. A glass tube of having B29 cone at one end was used to assemble the HCL. The B29 cone end of the glass tube was attached to the cathode by using low temperature N-type grease, while the other end was attached to the anode. A stop cock was fused to the glass tube for evacuation and gas filling.

Commercially available bismuth oxide (Bi_2O_3) powder of 99.9% purity has been used. The powder was mixed with distilled water to make a paste and was coated in the inner surface

52

of the cylindrical copper sample holder. Then the tube was kept under IR lamp for several hours to remove the water content from the sample and the sample sticks to the inner wall of the copper tube. This sample tube was then inserted in the bore hole of the cathode. After loading sample, a quartz window as view port was mounted on the top of the anode and the assembly was evacuated to 1×10^{-4} torr. Subsequently, the HCL was filled with carrier gas (present case: Ne) of about 2 torr pressure and subjected to a DC discharge. The life of the prepared HCL was found to be nearly 12 hours. In order to reduce the full width at half maximum (FWHM) of the *hfs* components, HCL were dipped vertically in a liquid nitrogen bath. This method of operation significantly reduces the Doppler width (as $\Delta\sigma \propto T^{1/2}$) of the spectral lines, which results in well resolved *hfs* components in the spectra.
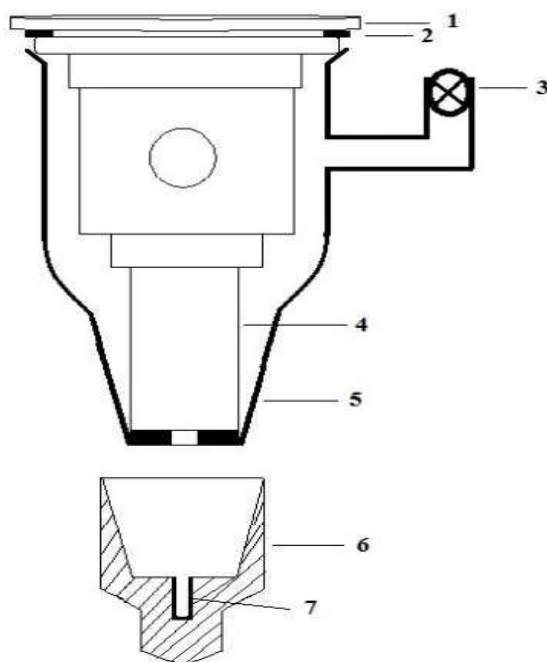
Fig. 2.6 Schematic of detachable hollow cathode lamp. 1) Quartz window, 2) O-ring, 3) Stop cock, 4) Aluminum anode, 5) B29 shape Glass tube, 6) Copper cathode 7) Removable copper tube (sample holder).

d. Comparison between EDL and HCL

In general, the intensity of the EDL discharge is much stronger than that of HCL. A comparison between the EDL and HCL discharges has been given in the Table 2.1 highlighting all the major differences. Further, chapter 4 of this thesis describes the importance of the two discharge sources taking aid from a few representative examples.

Table 2.1 Comparison between the EDL and HCL discharges

EDL	HCL
It is operated by microwave discharge method	It is operated by DC discharge method
Discharge occurs through collisional excitation process	Discharge occurs through Sputtering process
A brief spark from a high frequency coil is required to initiate the discharge.	No such coils are required
It is a strong discharge	It is not a strong discharge
Instabilities are occur while discharging	Stable discharge condition
Difficult to operate at low powers	Can operate at low currents
Spectral lines are usually broader	Spectral lines are narrow
Weak lines can be observe	Weak lines cannot be observe
Original *hfs* pattern get destroys in resonance lines due to spectral self reversal	Good *hfs* patterns can observe for resonance lines
Long life time : few months	Maximum of 12 hours of life time
Difficult to prepare	Easy to prepare

2.4.2 Discharge methods and Cooling setup

a. Discharge methods

EDL and HCL were operated by means of microwave and DC discharge methods respectively. Table 2.2 represents the discharge conditions of iodine and bismuth lamps, which were adopted in present investigations.

Table 2.2 Discharge methods to excite EDL and HCL

SOURCE	TYPE OF DISCHARGE	CONDITION
EDL (Electrodeless Discharge Lamp)	Microwave Discharge	With Cooling (I_2) Without Cooling (BiI_3)
HCL (Hollow Cathode Lamp)	DC Discharge	LN_2Cooling (Bi_2O_3)

EDL were excited by means of microwave discharge method. Two different types of microwave cavities (cylindrical cavity and surtatron cavity), operating frequency at 2.4 GHz were utilized. Cavities are connected to a microwave power supply by a coaxial cable. After supplying the power, the discharge is initiated by a brief spark from a high frequency Tesla coil. The cavity is then tuned to optimum operating conditions. The bismuth EDL was excited by cylindrical cavity, whereas iodine by surfatron [64] cavity.

Fig. 2.7(a) shows the Bi discharge from the cylindrical cavity. This is a vertical discharge. Fig. 2.7(b) presents the horizontal iodine discharge from surfatron cavity. Compared to vertical discharge, more light can be collected in the case of horizontal discharge. Surfatron cavity also has the facility to cool the EDL with air or LN_2 to reduce the Doppler width of the spectral lines.
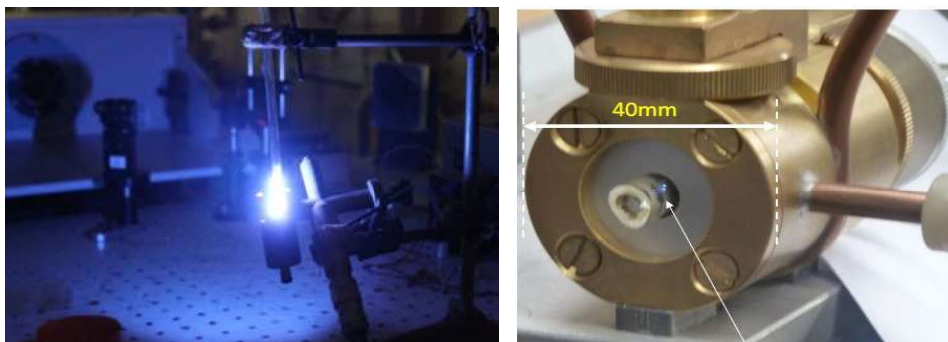
Fig. 2.7 (a) Emission light of Bi from the EDL. (b) Surfatron cavity with EDL

Fig. 2.8(a) shows the DC discharge setup of bismuth HCL. The emission light from view port is also shown in Fig. 2.8(b). The connection of positive power supply to anode and negative supply to cathode produces the plasma. There is no need to initiate the discharge by brief Tesla spark, as like in EDL. A HCL can be operated continuously only for a maximum of 12 hours because of the Bi_2O_3 powder coating getting sputtered out leading to reduction in emission light intensity. Operating at high currents also causes the sample loss. Therefore the sample must be replaced and a fresh HCL has to be prepared in each experiment. These HC Lamps were operated at minimum discharge current of 4 mA and maximum of 20 mA.
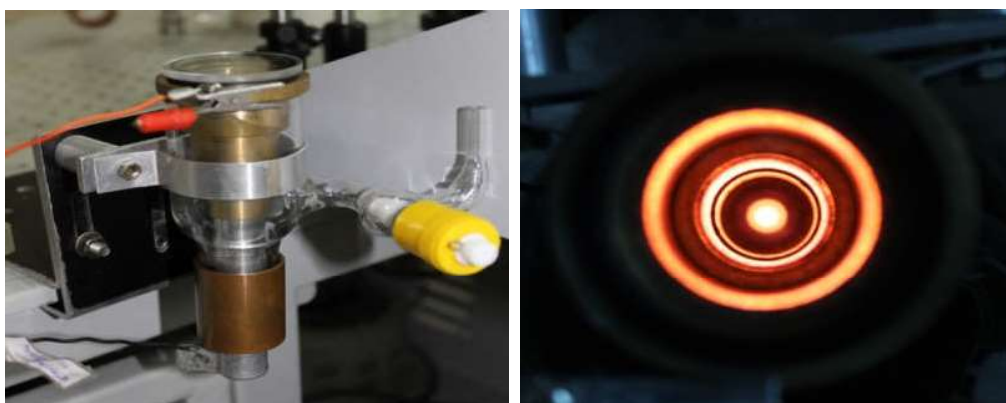
Fig. 2.8 (a) Represents the discharge set up of HCL by DC currents. (b) shows the emission light from the HCL discharge.

b. Cooling Setup to minimize the Doppler broadening

The *A* and *B* constants can be derived more accurately for a completely resolved *hfs* structure than for a partially or unresolved structure. The spectral resolution depends on the instrumental resolving power and broadening effects such as natural broadening (very small in the present case), Doppler broadening, collision broadening etc. Even using a high resolution spectrometer, it is not possible to resolve the *hfs* of the spectral lines when broadening effects are dominant. Since in the plasma the temperature is usually high, Doppler broadening (eq. 22) is the major contribution to the spectral broadening of the emission spectra.

As the width of a spectral line (Doppler width) is directly proportional to the square root of temperature (eq.29), in an attempt to reduce the FWHM of the spectral lines to resolve the *hfs* components, an experimental setup was designed to operate the EDL at low temperatures. The EDL was mounted on the 'surfatron' microwave cavity. The surfatron was operated at low powers, i.e. below 10 W to reduce the contributions from power broadening in the FWHM of spectral lines. The schematic of the experimental arrangement has been shown in Fig. 2.9. As air/ water cooling had not much effect on the FWHM of the recorded peaks, we used nitrogen gas as the coolant which was cooled by passing it through a liquid nitrogen bath as shown in the schematic. Thus, the cooled gas interacts with the outer surface of the EDL which results in the decrease of temperature. This method, in fact, enabled clear identification of many spectral lines with good resolution, which were not observed without cooling. A photograph of the EDL discharge under cooling condition and the light emitting from the EDL is shown in Fig. 2.10(a).
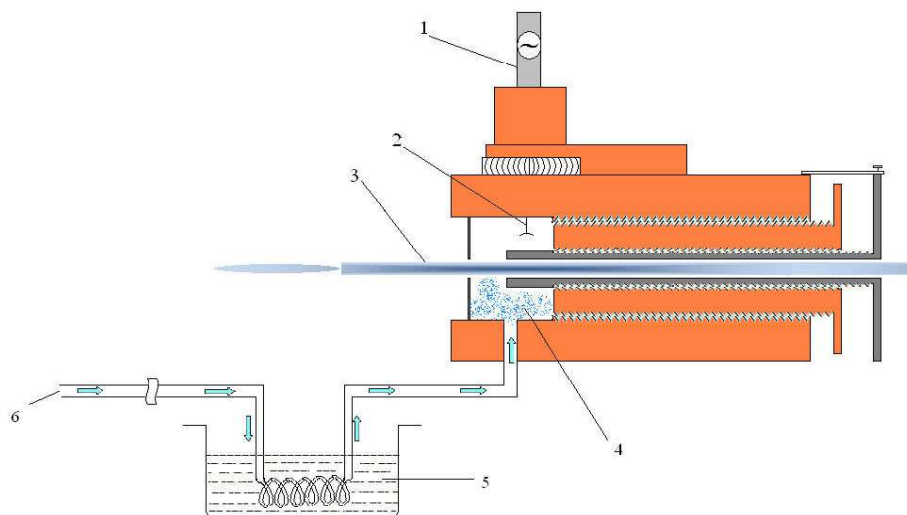
Fig. 2.9 Schematics of the experimental arrangement. (1) Microwave power supply connector, (2) Antenna disk, (3) EDL, (4) Cooled nitrogen vapors, (5) Liquid nitrogen bath, and (6) Inlet for nitrogen gas.

Similarly, HCL were also operated under cooling condition using LN_2. The bottom part of the HCL was dipped vertically in a liquid nitrogen bath. A photograph of the HCL discharge under cooling condition is shown in Fig. 2.10(b).
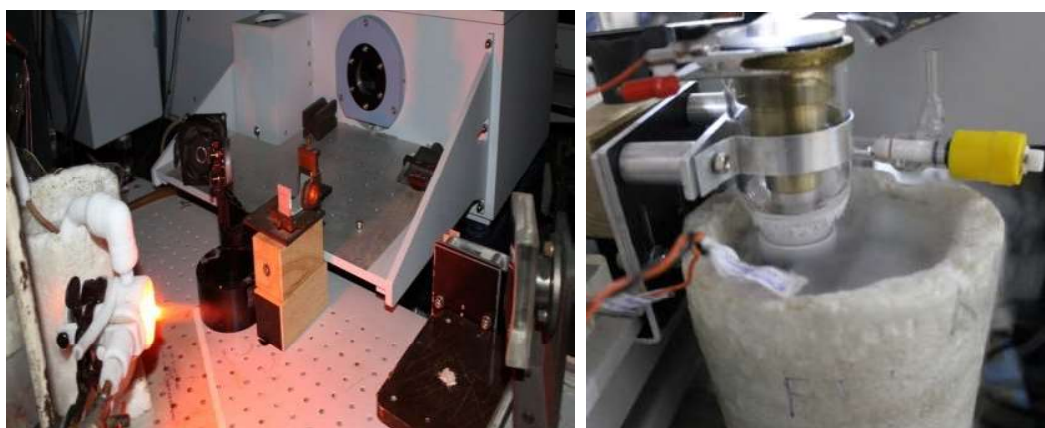
Fig. 2.10(a) Cooling setup of EDL discharge (b) HCL cooling setup

2.4.3 Fourier Transform Spectrometer : Bruker IFS 125 HR

The emission spectra were recorded by using a high resolution Fourier transform spectrometer (FTS) (model: Bruker IFS 125 HR). This instrument has the capability to cover the spectral region from IR to UV using a range of beamsplitters and detectors. The schematic diagram of the optical path of the instrument Bruker IFS 125 HR has been shown in Fig. 2.11. In addition to the interferometer, FTS has many components such as sources, beamsplitters, detectors, optical filters, optical windows and computer processing unit.

a. Sources

Fourier Transform Spectrometer can be used with internal as well as external sources. The internal source chamber consists of Globar, UV and Tungsten lamps. These sources are utilized in the molecular absorption studies. The emission light from external sources such as EDL and HCL can be directed to FTS using elliptical and parabolic mirrors. The experiments in this thesis have been performed using the external sources.

b. Beamsplitters

Beamsplitter is the heart of the interferometer. This is an optical component oriented at 45 degrees to the incoming beam of collimated radiation such that the beam can be divided as 50% of the intensity is reflected and 50% is transmitted. These are made up of dielectric materials of large indices of refraction. Depending upon the spectral region of interest, the material gets changed to transparent in that region. Table 2.3 describes the spectral ranges and materials used for various beam splitters.

59

Table 2.3 Various beamsplitters used in the present work and their operating spectral regions

Beamsplitter	Spectral range
KBr	400 cm^{-1} - 5000 cm^{-1}
CaF$_2$	1800 cm^{-1} - 14000 cm^{-1}
Qrtz Vis	9500 cm^{-1} - 25000 cm^{-1}
Qrtz UV	20000 cm^{-1} - 50000 cm^{-1}
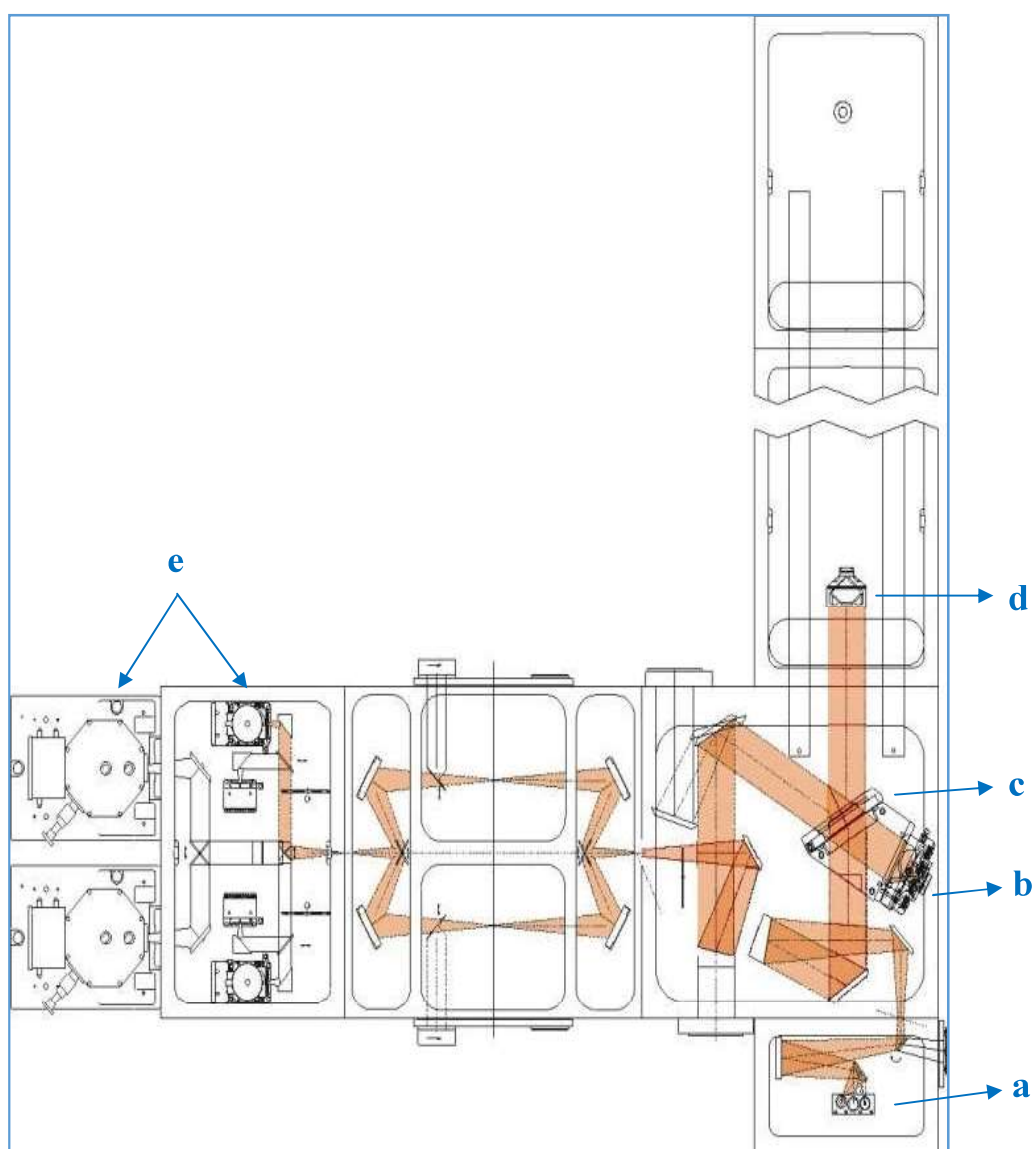
Fig. 2.11 The optical path of the high resoltion fourier transform spectrometer Bruker IFS 125 HR. (a) Sources, (b) Fixed mirror, (c) Beam splitter (d) Moveble mirror (e) Detector chambers

c. Detectors

FTS can be equipped with various detectors depending upon the spectral region of interest. Table 2.4 provides the details of the detectors used in present investigations.

Table 2.4 Various detectors used in the present measurements and their operating spectral regions

Detector	Spectral region	Operating Temperature
InSb	1800 cm^{-1} - 9600 cm^{-1}	77 K
InGaAs	5800 cm^{-1} - 12800 cm^{-1}	Room temperature
Si diode	9000 cm^{-1} - 25000 cm^{-1}	Room temperature
PMT-Vis	12000 cm^{-1} - 28000 cm^{-1}	Room temperature
PMT-UV	25000 cm^{-1} - 40000 cm^{-1}	Room temperature

d. He-Ne Laser

In FTS, He-Ne laser is conveniently used to determine the frequency of the modulated light. Laser interferogram provide the moving mirror position with a high accuracy. The red laser light is quite useful to consider the light path especially for optical alignment. He-Ne laser is also used as an internal wavelength calibration standard.

e. Optical Filters

Several band pass optical filters of band width 10, 25 and 50 nm were used in the visible and UV spectral regions to enhance the S/N ratio of the region of interest and avoid the unwanted signals. This helps in observing the weak transitions.

2.5 Spectral Calibration

As the FTS is a well calibrated instrument, the high resolution data obtained from this, provides high wavenumber accuracy. When FTS is operated with external emission sources to record the data, the spectral calibration of the measured spectra is necessary with respect to standard lines to remove the minute deviations arising from source fluctuations. In the present investigations, we co-added a large number of scans at each resolution and spectral region. Separate calibration constants (1+K) were derived for each co-added spectrum with respect to standard Ne lines [65] using the formula:

$$1 + K = \frac{\sigma_{std}}{\sigma_{obs}}$$

(25)

where σ_{std} and σ_{obs} are the wavenumbers of standard and experimentally observed Ne lines respectively, K is the wavenumber correction factor.

Many spectra were recorded in a given spectral region. The center of gravity wavenumber values have been derived for a specific *hfs* structure in each such measurement separately. The mean of these values have been considered as the C.G. and corresponding standard deviation value as the uncertainty of a particular *hfs* structure. The reproducibility of our measurements was within 3rd decimal.

2.6 Hyperfine Structure Analysis

For the analysis of one *hfs* transition, the corresponding part of the spectrum was extracted from the calibrated observed spectrum. The *hfs* analysis was carried out by iterative least-squares fitting programs (*HFSAB* and *WINHFS*), developed by Kumar et al. [66]. The shift of each *hfs* component from the center of gravity, *J* values of upper and lower energy levels and

the assignment of F transitions based on the relative intensity distribution to each *hfs* component have been used by a program called *HFSAB* to generate A and B constants for upper and lower energy levels. Another program *WINHFS*, simulates the spectrum and refines the *hfs* constants by optimizing the fit parameters such as *hfs* A and B constants, width and spectral line profile (Gaussian /Lorentzian) for the J values in a transition. The emission spectra is limited by Doppler broadening, so the relativistic correction factors (C_{++}) 1.08604 for iodine and 1.27797 for Bi [67] due to 2nd order effects such as quadrupole coupling do not considerably influence the derived parameters. However, these relativistic corrections may play an important role in the case of Doppler-free, two-photon and atomic-beam spectroscopy. Hence, in the present case, Eq.18 suffices for the expected contributions to fit the observed *hfs*. The A *and* B constants are presented in milli Kaysers (mK = 10^{-3} cm^{-1}) units.

The analysis of the *hfs* structure to derive A and B constants is discussed here on the calibrated line at 32588.210 cm^{-1}, corresponding to the transition ($^{3}P_0$)7s[0]1/2 - 6p^{3} $^{4}S_{3/2}$ of bismuth. This transition produces six *hfs* components. Each *hfs* component was assigned to a transition F″ ← F′ according to their relative intensity distributions. The shift of each *hfs* component from the center of gravity value was derived as shown in Fig. 2.12.
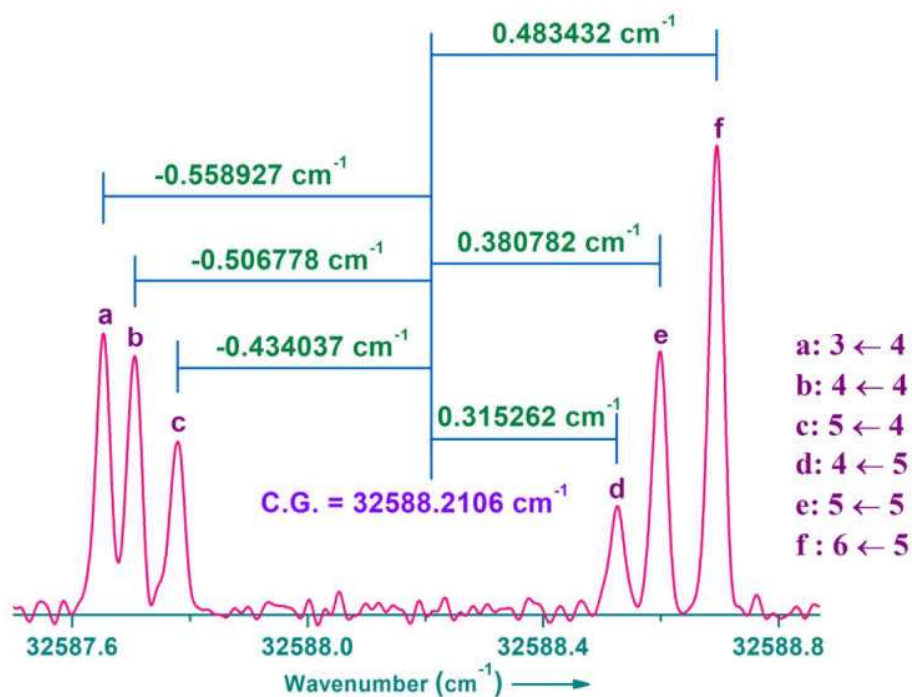
Fig. 2.12 Assigned F″- F′ transitions, and shift values of the *hfs* components from the center of gravity in the observed spectrum at 32588 cm⁻¹.

Fig. 2.13 represents the assigning of *F* transitions based on the relative intensity distribution to each *hfs* component in the program *HFSAB* and the generated *A* and *B* constants for both lower and upper energy levels involved in a transition.
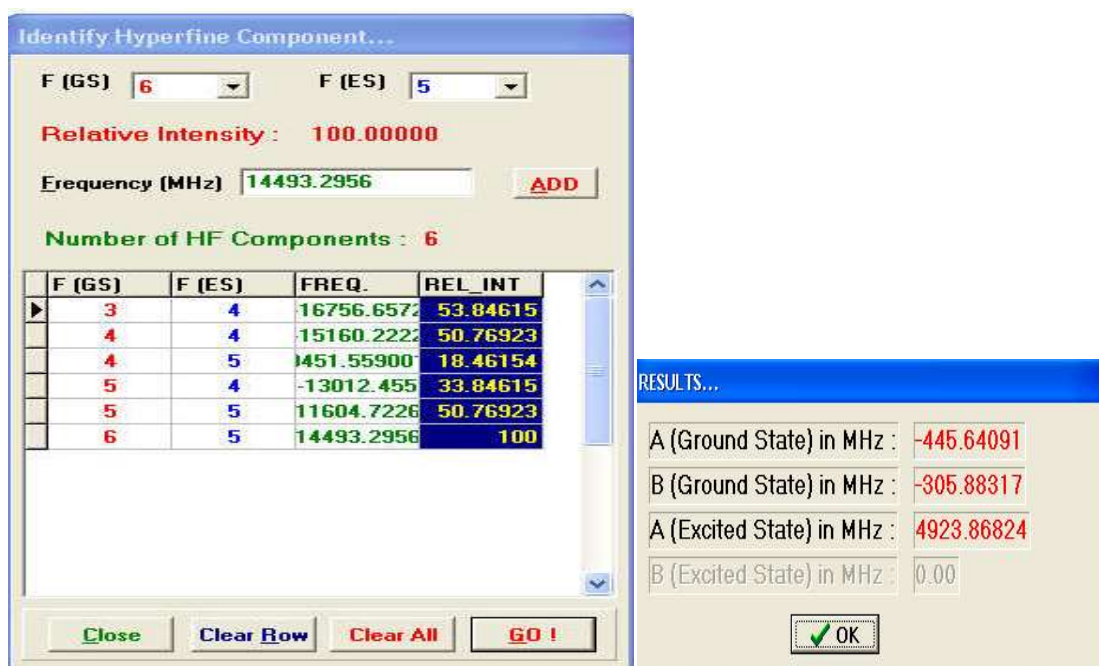
Fig. 2.13 Assigning of *F* transition in the program *HFSAB* and the generated *A* and *B* values.

Fig. 2.14 presents the generated spectrum using *WINHFS* program and the parameters used. The *A* and *B* constants were refined until the simulated spectrum matches the observed spectrum. In the present case, all six *hfs* components were completely resolved, therefore accurate *A* and *B* constants could be derived from the fitting data. The derived constants (without refining) were used to simulate the spectrum. The simulated and observed spectra were compared in Fig. 2.15 both the spectra match well with each other. Similar procedure has been applied for all the *hfs* measurements.

65
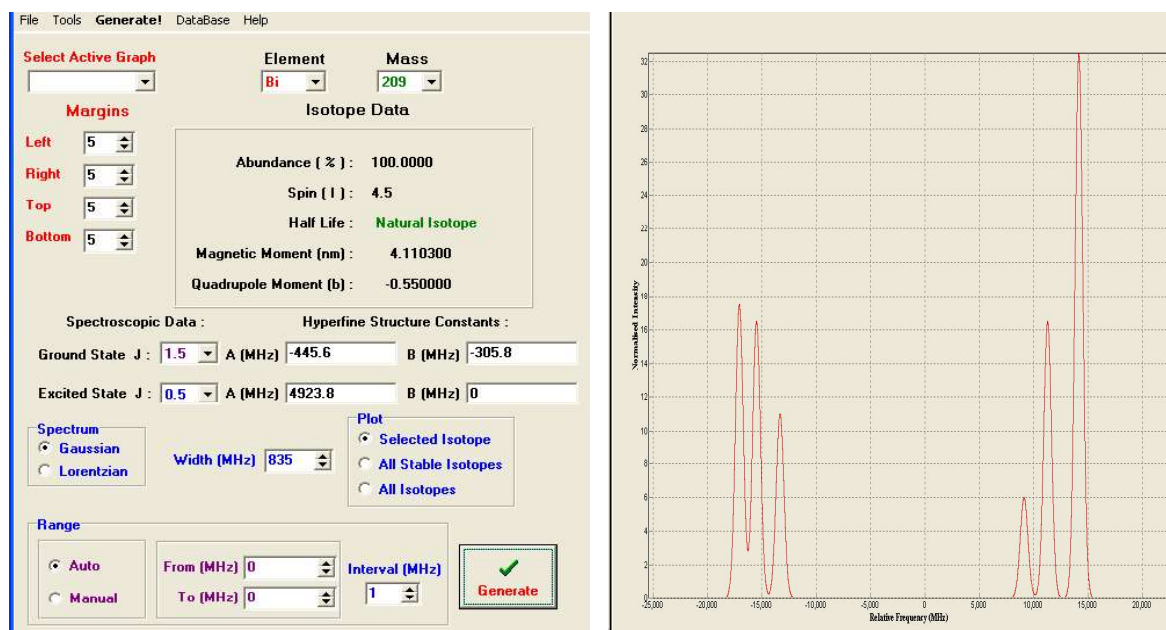
Fig. 2.14 shows the spectrum generated using *WINHFS* program and the used parameters.
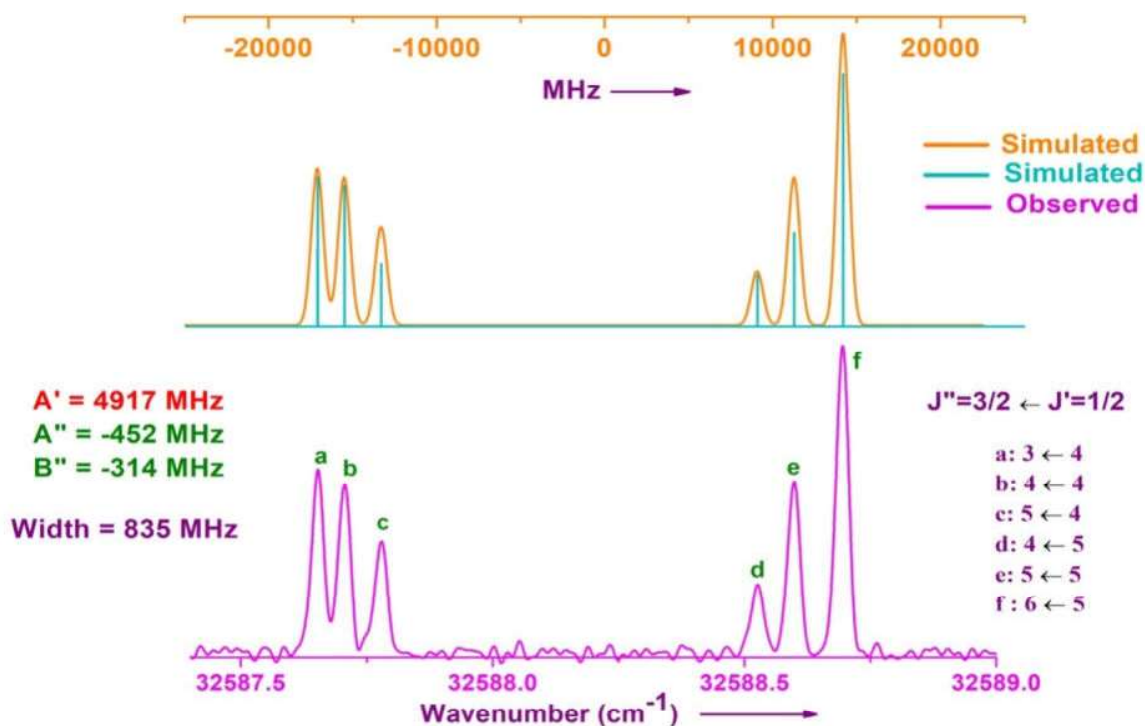
Fig. 2.15 Comparison of observed and simulated spectrum, width and *A* and *B* values of both upper and lower levels as determined from the experimental recording.

Uncertainties of A and B were derived as follows. For the levels involved in more than one transitions, A and B values were derived independently and the mean values are given as obtained A and B. For the levels involved in a single transition, repeated measurements were carried out to derive A and B constants and the mean values were given for each level. In both the cases, standard deviations obtained were considered as their uncertainties. The same procedure was applied for all the measurements. An example is provided for the derivation of A and B constants and their uncertainties for an energy level at 70151.201 cm^{-1}. This level is involved in various transitions as mentioned in the first column of Table 2.5. The A and B constants obtained for each transition are also presented.

Table 2.5: A and B constants obtained for a level at 70151.201 cm^{-1} involved in various measurements.

Line position (cm^{-1})	A in mK	B in mK
2903.396	15.177	5.337
3089.079	15.744	3.369
4481.221	15.477	3.436
4506.734	15.678	4.436
4814.437	15.010	6.004
4898.317	14.944	6.438
5040.139	15.444	5.404
5042.860	15411	5.404
5161.212	15.477	4.637
5244.920	15.744	4.236
5470.233	15.577	4.837
Mean (Std. Dev.)	**15.426 (0.276)**	**4.867(0.974)**

Chapter 3

Hyperfine structure measurements of neutral atomic Iodine (^{127}I)

3.1 Introduction

In 1917, Wood and Kimura [68] measured the spark spectra of iodine from a Geissler tube. Tolansky [12,16,69-70] examined the fine structures in the arc and spark spectrum of iodine to determine the nuclear spin as 5/2. McLeod [14], photographed the arc and spark spectrum of I I in the ultraviolet spectral region, thus reporting many new lines. In 1954, Electrodeless Discharge Lamps (EDL) was excited by Eshbach et al. [17] to measure the positions and the intensities of 31 spectral lines in the IR region. Subsequently, in 1959, Kiess and Corliss [15] carried out an extensive survey of the iodine spectra in the spectral region from 23070 Å (4334 cm^{-1}) in the IR to 1195 Å (83682 cm^{-1}) in the extreme UV region (EUV), which led to a list of more than 900 spectral lines. Zeeman patterns had been observed in many lines and the ionization potential (10.45 eV) of iodine was also measured and reported [15]. The first spectra of halogens, viz. chlorine, bromine and iodine in the spectral region 1.8 − 4 μm was reported by Humphreys et al. [18, 19]. In a further survey in EUV regions, three strong auto-ionized resonances were identified by Pettini et al. [71] in the absorption spectrum of iodine and assigned to a collective excitation of the 4d- inner shell. Dual laser- produced plasma technique was employed to observe trends in 4d- photo absorption phenomena along the iodine isonuclear sequence of I, I^+, and I^{2+} [72]. Recently, multiphoton ionization was carried out to observe two well developed Rydberg series of I (6s $^2P_{3/2}$) built on $5s^25p^4\,^3P_1$ ion core, which were assigned to 'nd' and 'ns' Rydberg states, with very high (up to n = 47) principal quantum number [73].

In 1954, Jaccarino et al. [74] had studied the *hfs* in $^2P_{3/2}$ ground state of stable ^{127}I using atomic beam magnetic resonance (ABMR) method. In this study, the measured intervals could not be explained by dipole and quadrupole like interactions alone due to significant contribution from nuclear magnetic octupole interaction. The majority of iodine *hfs* data in the infrared (3000

- 11500 cm^{-1}) region was measured by Luc-Koenig et al. [21] by means of Fourier transform spectroscopy and *hfs* in 130 spectral lines has been analyzed to obtain magnetic dipole and electric quadrupole coupling *hfs* constants, *A* and *B* respectively for 37 even and 42 odd energy levels. Also, the theoretical parametric studies have been performed to obtain the *hfs* monoelectronic constants '*a' (nl)* and '*b' (nl)*. Hfs of ^{127}I at 612 nm and 640 nm transitions has been observed by saturated absorption in a gas cell placed within a He- Ne modified cavity laser [75]. Using FTS and EDL discharge, *hfs* and isotope shift in the 1.3 μm transition of ^{129}I has been measured and analyzed by Engleman et al. [76]. In 2015, Lun hua Deng et al. [22] had investigated *hfs* in 45 atomic spectral lines of ^{127}I in the spectral range of 11300- 13000 cm^{-1} using optical heterodyne concentration modulation spectroscopy with a tunable single-mode CW Ti: Sapphire laser and *hfs* constants *A* and *B* in 18 even and 28 odd levels have been reported. Recently, this group presented further *hfs* investigations [23].

However, precise knowledge of atomic spectral lines, energy levels and their *hfs* constants of for iodine is still not completely available. *Hfs* of many lines was not analyzed and the *hfs* constants were unknown for many levels. Key objectives of the present investigation are to gather the *hfs* data in as large number of lines as possible in a wide spectral range and to derive the accurate *hfs A* and *B* constants of the levels involved in the studies.

3.2 Experimental Details

A mixture of iodine vapor and Ne was excited in an EDL driven by a surfatron [64] microwave cavity operated by Opthos microwave power supply. The preparation of EDL with I$_2$ and the microwave discharge have been described in chapter 2. Emission spectra of neutral iodine have been recorded using a high resolution Fourier transform spectrometer in the spectral range from 1800 to 25000 cm^{-1}. This entire data has been divided into three parts: 1800 - 6000

cm^{-1}, 6000-10000 cm^{-1} and 10000-25000 cm^{-1} depending upon the experimental arrangements such as working range of beamsplitter, detectors and optical windows. Table 3.1 provides the various beamsplitters and corresponding detectors equipped in FTS to observe the spectra in all the above three regions.

In all these three regions, various instrumental resolutions like 0.04, 0.02, 0.018, 0.012, 0.01, 0.008 and 0.006 cm^{-1} were applied to identify weak as well as strong lines. The cooling setup (described in chapter 2) has been applied in all regions to reduce the Doppler broadening of the spectral lines.

. **Table 3.1:** Beamsplitters and detectors utilized in the spectral range of 1800-25000 cm^{-1}

Spectral range (cm^{-1})	Beamsplitter	Detector
1800 - 6000	KBr / CaF$_2$	InSb
6000 - 10000	CaF$_2$	InSb/ InGaAs
1000 - 25000	Qrtz Vis /Qrtz UV	Si diode / PMT-vis /PMT-UV

3.3 Hyperfine Structure Investigations

3.3.1 In the spectral region: 1800-6000 cm^{-1}

In general, the EDLs used for emission experiments are made up of quartz tube of 6 mm outer diameter (OD) and 5 cm length. However, the optical transmission below 3500 cm^{-1} is very poor with the quartz EDL. This results in the blocking of emission lines to be observed in the low energy infrared region. To overcome this difficulty, a CaF$_2$ window of 2 mm thickness and 8

mm diameter was sealed to the EDL to get high optical transmission below 3500 cm^{-1}. Here additional care has to be taken so that the sealant should not be present inside the EDL. The tube is then cleaned and evacuated to 1.0 X 10^{-3} Torr. It was further subjected to a microwave discharge cleaning with pure Ne gas for several times till we get a persistent color of Ne discharge and evacuated to 1.0 X 10^{-5} Torr. If the tube is not cleaned well, small contamination in the EDL may generate the emission spectra of CO molecule which overlap with our substance spectra. If sealant passes inside EDL again, few more bands appear in the spectra. Another important consideration is that the operating power should be as low as possible, because the heat generated during the discharge can melt the sealant and break the EDL vacuum. Thus, in this case the microwave power was limited to maximum 6 W. The instrument was equipped with KBr, CaF$_2$ beam splitters and InSb (77K) detector to record the spectra in the 1800 - 6000 cm^{-1} region. The spectra were recorded with a maximum resolution of 0.0026 cm^{-1}.

Fig. 3.1 shows the comparison of observed spectra between the normal quartz EDL and the one with CaF$_2$ window. Nearly 100 extra lines were observed in case of CaF$_2$ window discharge. Fig. 3.2 is an illustrative example to compare the high resolution spectra recorded with EDL of CaF$_2$ window and the normal quartz EDL for an *hfs* structure of a line at 2256.658 cm^{-1}. As can be observed in Fig. 3.2, an intense line at 2256.658 cm^{-1} was observed with a well resolved *hfs* pattern in the case of CaF$_2$ window, which otherwise could not be studied. In this *hfs* structure, not only strong *hfs* components, weak components (marked as i, j, and k) are also detected.
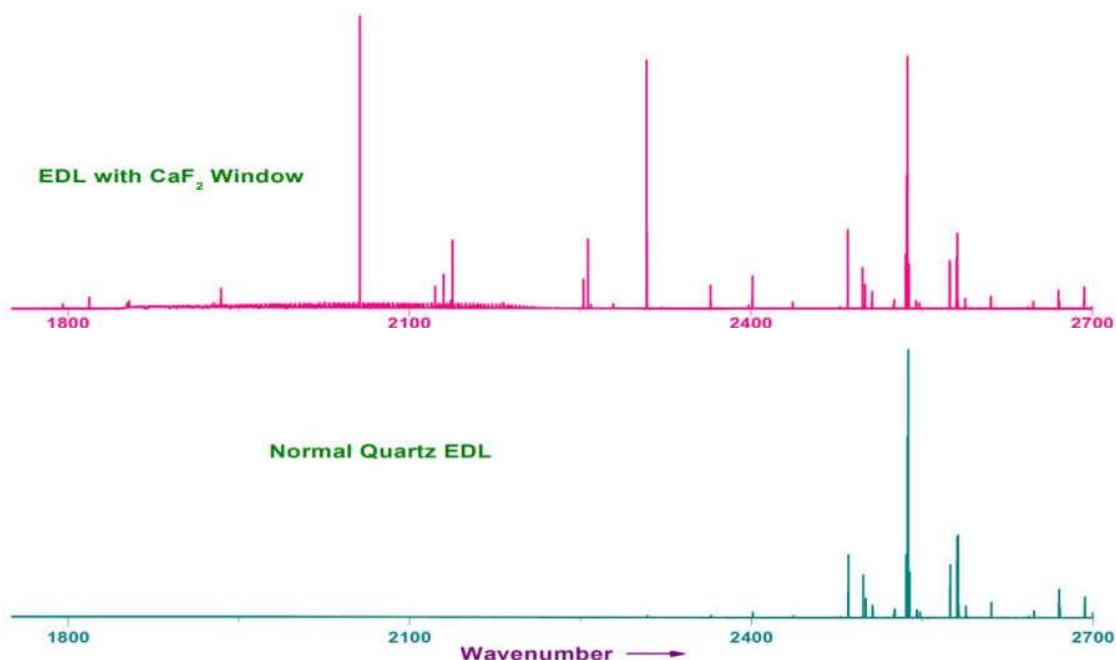
Fig. 3.1 Shows the comparison of observed spectra between the EDL with quartz and CaF_2 windows. Nearly 100 lines were observed with EDL of CaF_2 window which were absent in quartz EDL.
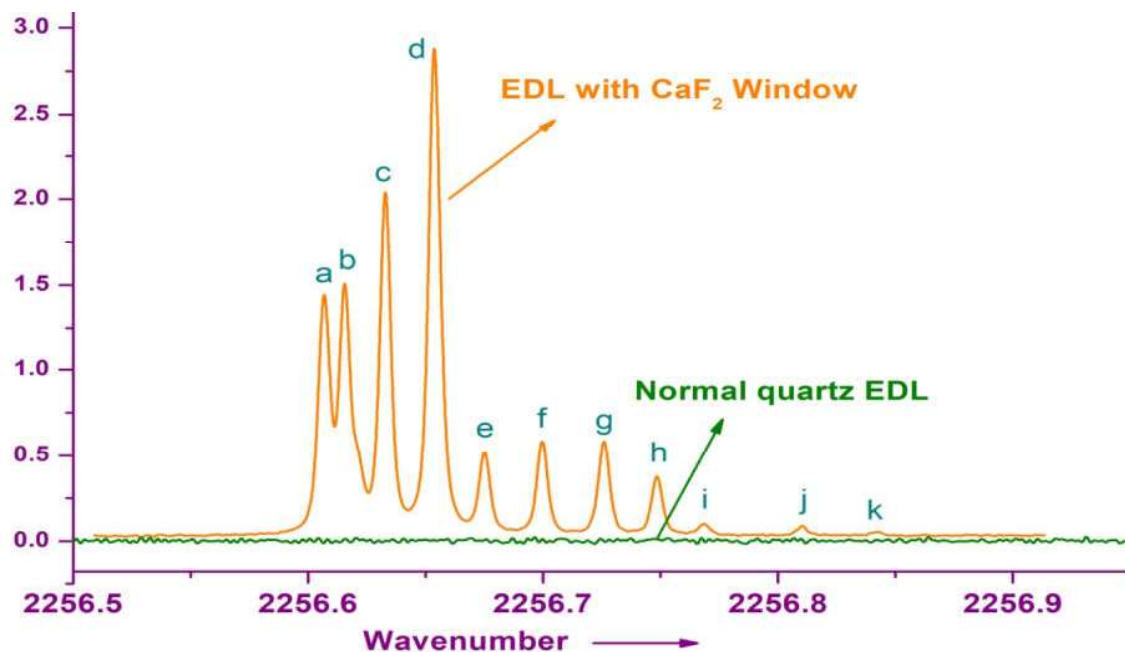
Fig. 3.2 A comparison of high resolution well resolved *hfs* structure of the line at 2256.658 cm^{-1} observed with EDL of CaF_2 window. The line is completely absent in normal EDL discharge.

An example of the importance of proper cleaning and evacuation of EDLs in such experiments has been shown in Fig. 3.3(a), which indicates the appearance of CO molecular band nearly at 2100 cm^{-1}. These rotational lines overlap with the emission lines of I I, which may hinder the unambiguous identification of *hfs* components. By considering the proper precautions while preparing the EDL as discussed in the previous section, the molecular band intensity has been reduced considerably as shown in Fig. 3.3(b).
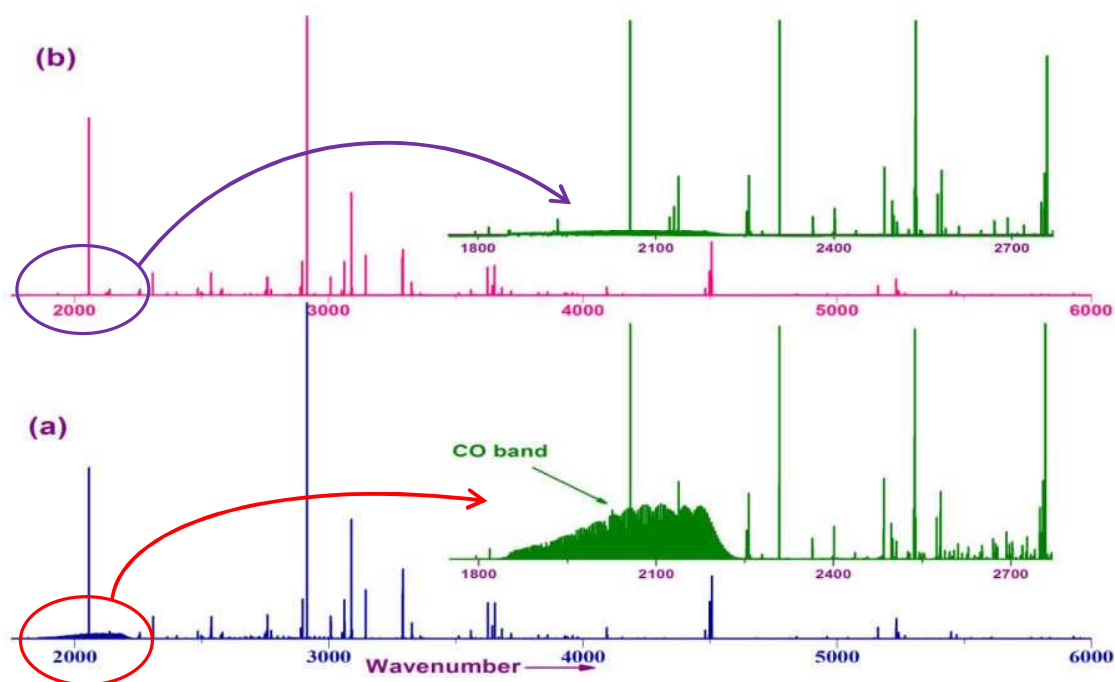
Fig. 3.3 a) Appearance of CO molecular band nearly at 2100 cm^{-1} which is overlapping with the emission lines of I I. **b)** The band intensity is considerably reduced by properly cleaning the EDL.

Fig. 3.3 also presents the complete observed spectra of I I in the entire spectral region of 1800 - 6000 cm^{-1}. In this entire spectral range, a total of 354 spectral lines were identified as I I transitions. Along with I I lines, Ne lines are also present in the same spectra (Ne is used as

buffer gas). These Ne lines are used for the spectral calibration. The entire spectra were calibrated as described in chapter 2. Table 3.2 (Appendix I) represents the list of observed spectral lines and their corresponding energy levels. First column lists the derived line position center of gravity wavenumber values of all the 354 observed lines. The energy levels were classified using NIST data base [77]. Few of the observed and simulated spectra for a few lines in this region are shown in Figs. 3.4 - 3.10. The hyperfine structure for all these lines is observed for the first time. The observed spectra were compared with the simulated ones for all the structures and are matching well. Figs. 3.4, 3.5, 3.6 and 3.7 represents the well resolved *hfs* structures, whereas Fig. 3.8 and 3.9 are unresolved structures. Fig. 3.10 shows a transition at 5956.290 cm^{-1} with a flag pattern structure. The center of gravity values were derived with 3rd decimal accuracy. The spectral designation of few observed lines could not be identified. Those lines were listed as unclassified lines in Table 3.2.
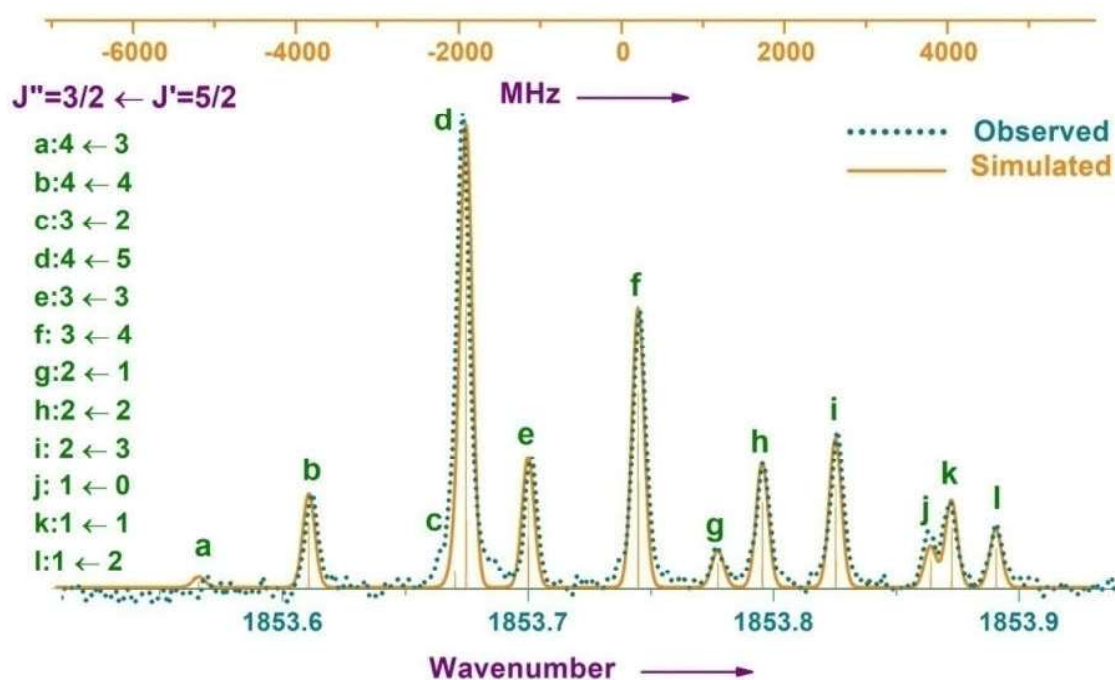
Fig. 3.4 A well resolved *hfs* splitting observed at 1853.746 cm^{-1} with 0.002 cm^{-1} resolution. This line was generated with EDL discharge of 6W power. Out of 12 *hfs* components 10 were identified.

75
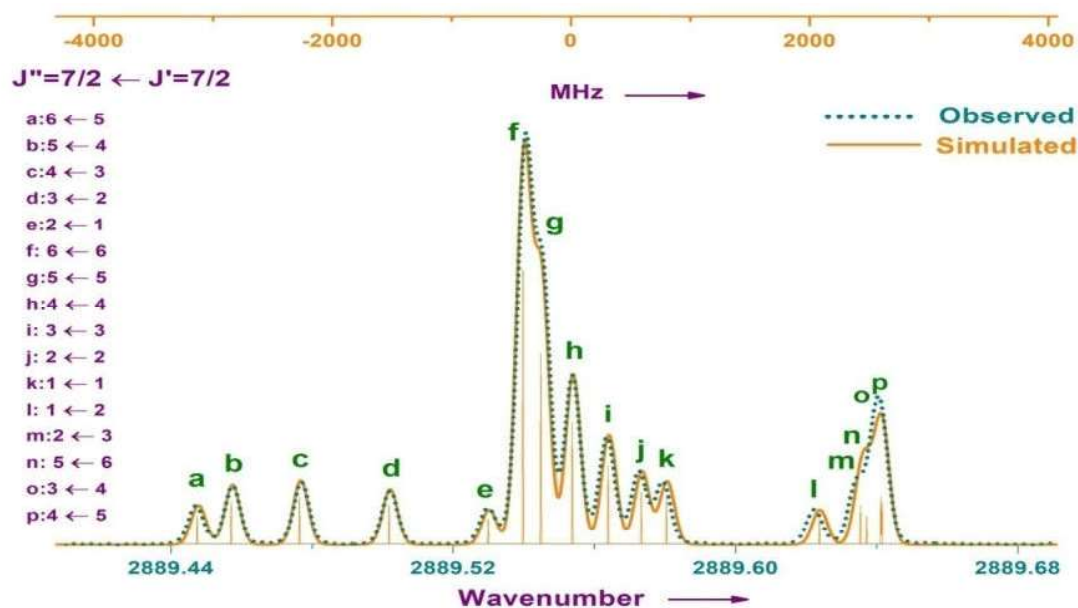
Fig. 3.5 A well resolved *hfs* splitting observed at 2889.554 cm^{-1} with 0.002 cm^{-1} resolution. This line was generated with EDL discharge of 6W power. Out of 16 *hfs* components 12 were clearly resolved.
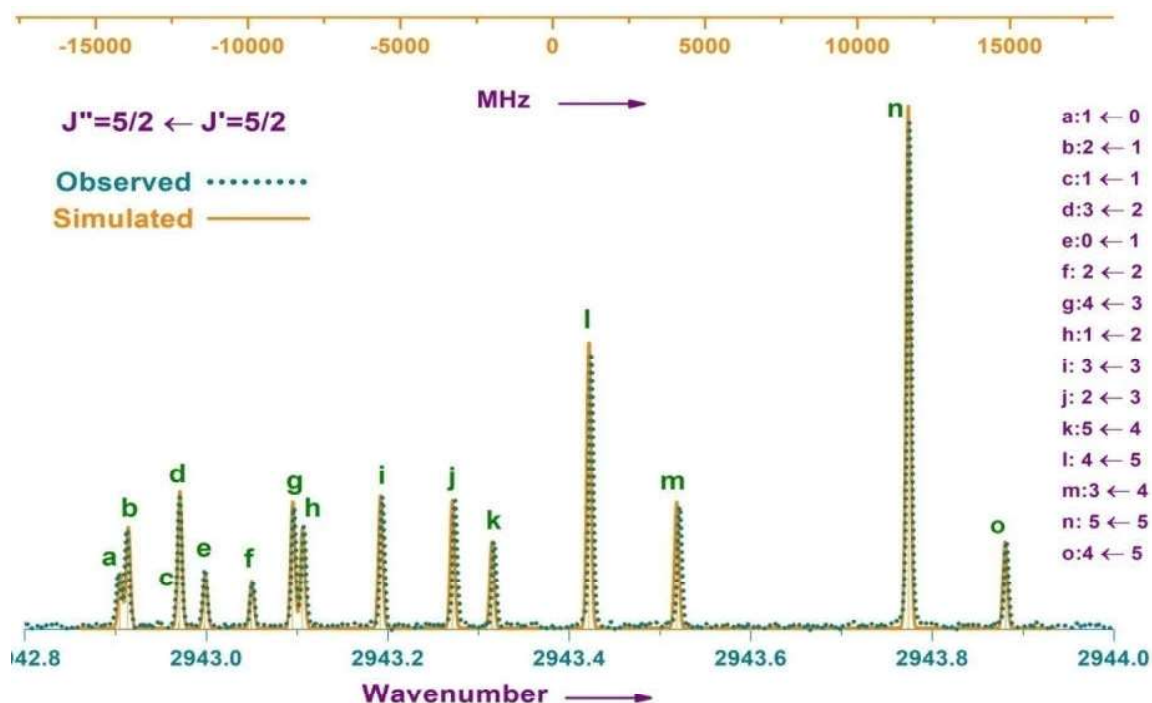
Fig. 3.6 A well resolved *hfs* structure for the line at 2943.387 cm^{-1} recorded with 0.002 cm^{-1} resolution in the EDL discharge of 6W power. Out of 15 *hfs* components 14 were clearly identified. Only one week component at 'c' was not resolved.

76
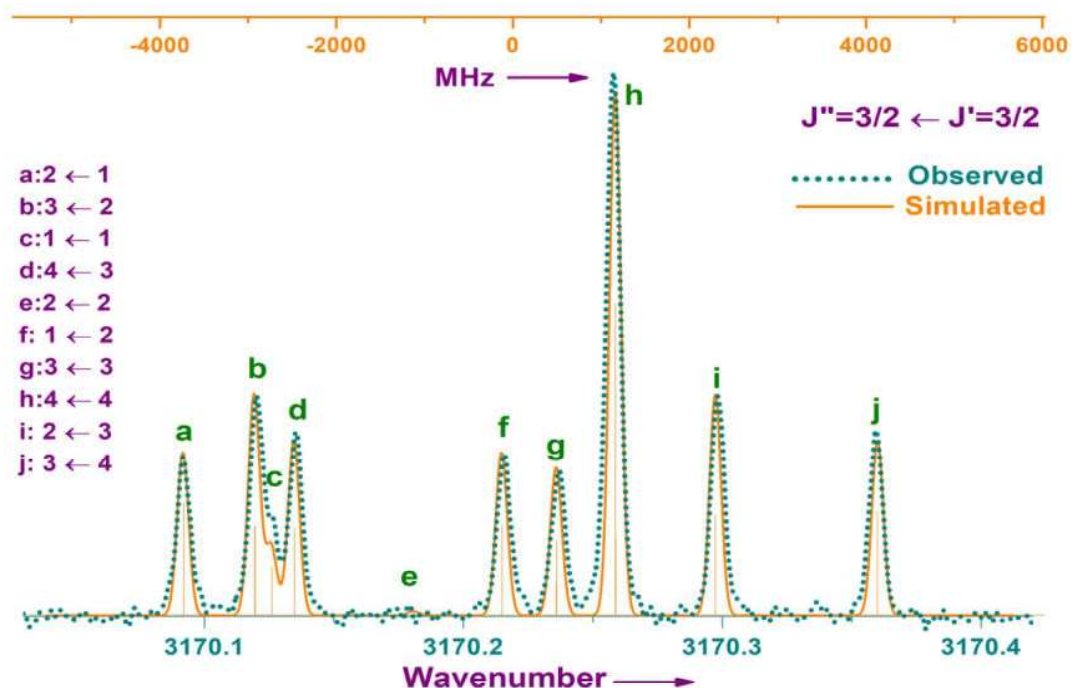
Fig. 3.7 A well resolved *hfs* structure for the line at 3170.219 cm^{-1} recorded with 0.002 cm^{-1} resolution in the EDL discharge of 6W power. Except a week transition at 'e', all 9 components were identified.
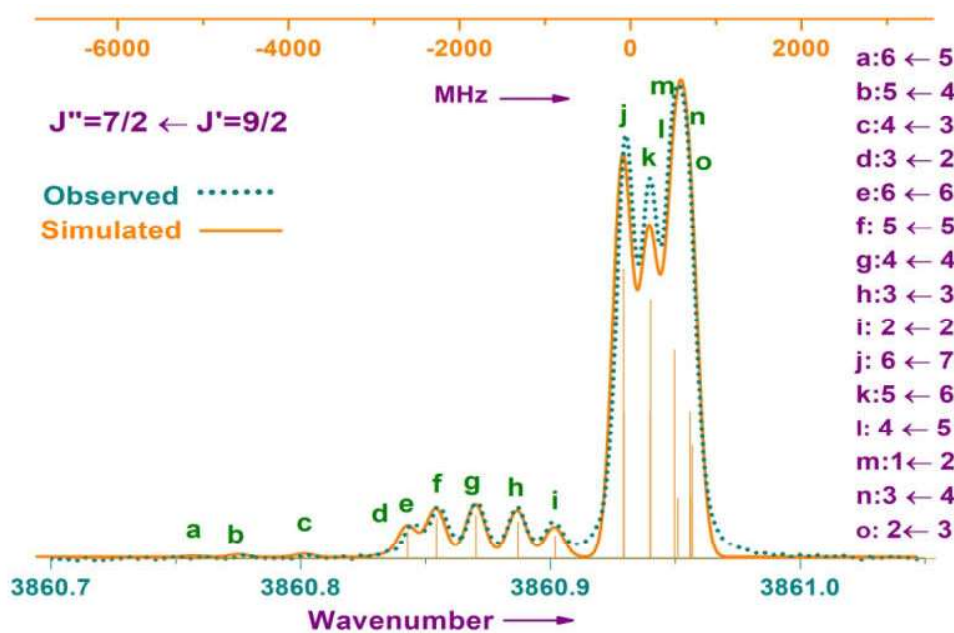
Fig. 3.8 An unresolved *hfs* structure for the line at 3860.932 cm^{-1} recorded with 0.002 cm^{-1} resolution in the EDL discharge of 6W power.
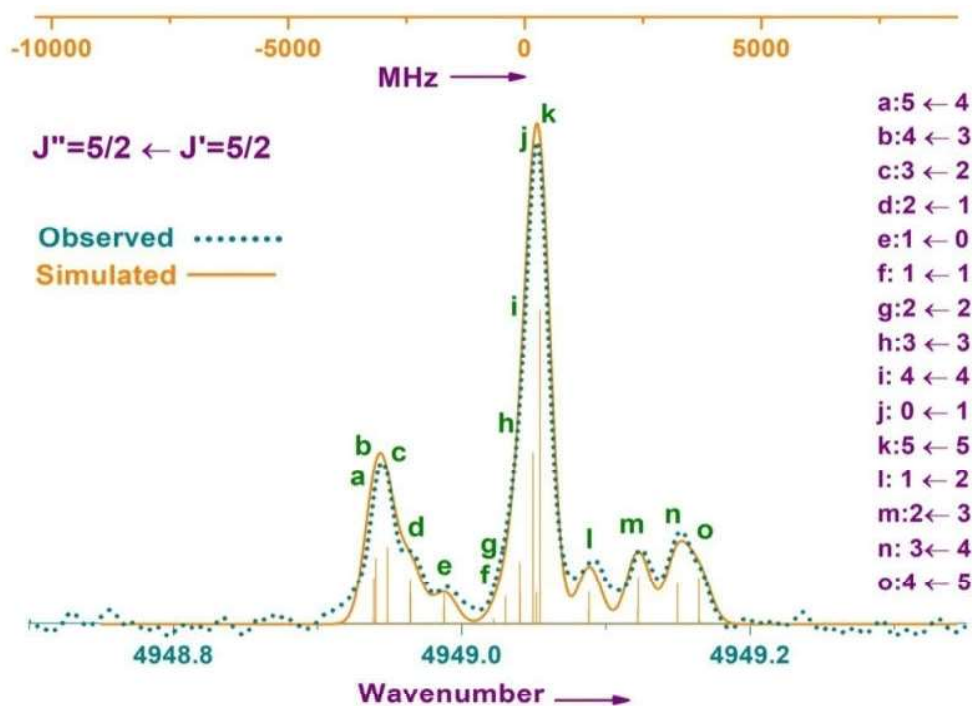
Fig. 3.9 An unresolved *hfs* structure for the line at 4949.045 cm⁻¹ recorded with 0.01 cm⁻¹ resolution in the EDL discharge of 14W power.
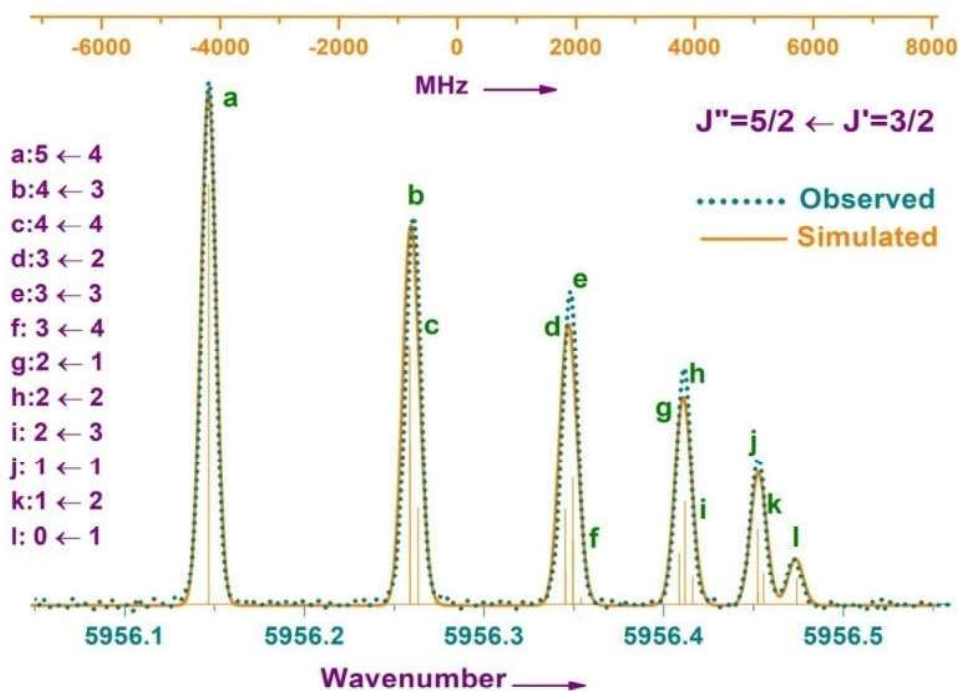
Fig. 3.10 A partially resolved *hfs* structure for the line 5956.290 cm⁻¹ recorded with 0.004 cm⁻¹ resolution in the EDL discharge of 8W power.

The procedure of hyperfine structure analysis and derivation of *A* and *B* constants using the program [66] have been described in chapter 2. The same methodology has been applied here. Among 354 observed lines, *hfs* investigations were performed on 224 spectral lines which have well resolved *hfs* structure and good S/N. Only center of gravity wavenumber values were derived for the remaining lines. *Hfs* analysis on 172 lines is carried out for the first time. Those lines for which *hfs* are analyzed in this work are mentioned in the last column of Table 3.2. A total of 97 energy levels (53 even and 44 odd) were involved in these 224 transitions. *Hfs* constants were derived for all 97 energy levels, out of which the constants of 18 levels are reported for the first time. The derived *A* and *B* values of even and odd parity levels are given in Table 3.3 and Table 3.4 (Appendix I) respectively, along with previously reported [21-23] values. *Hfs* constants were derived for 53 even parity levels. Among these levels, 41 levels were previously reported [21-23] and the remaining 12 were obtained for the first time. In case of odd levels, *Hfs* constants were obtained for 44 levels of which, 38 levels were previously reported [21-23] and the remaining six levels were treated for the first time.

Uncertainties of *A* and *B* values given in Table 3.3 and Table 3.4 were derived, as described in chapter 2.

3.3.2 In the spectral region: 6000 - 10000 cm^{-1}

In the spectral region of 6000 - 10000 cm^{-1}, I I spectra were recorded by exciting the normal quartz EDL. The preparation of EDL with I_2 done as described in chapter 2. In this case, the spectrometer was equipped with a CaF_2 beam splitter, InSb (77K) and InGaAs detectors to record the spectra. The full range of spectrum recorded from 6000 to 10000 cm^{-1} is shown in Fig. 3.11. Observed and simulated *hfs* splitting of a fully resolved transition at 9827.401 cm^{-1} is depicted in the expanded region of 9827- 9828 cm^{-1}.
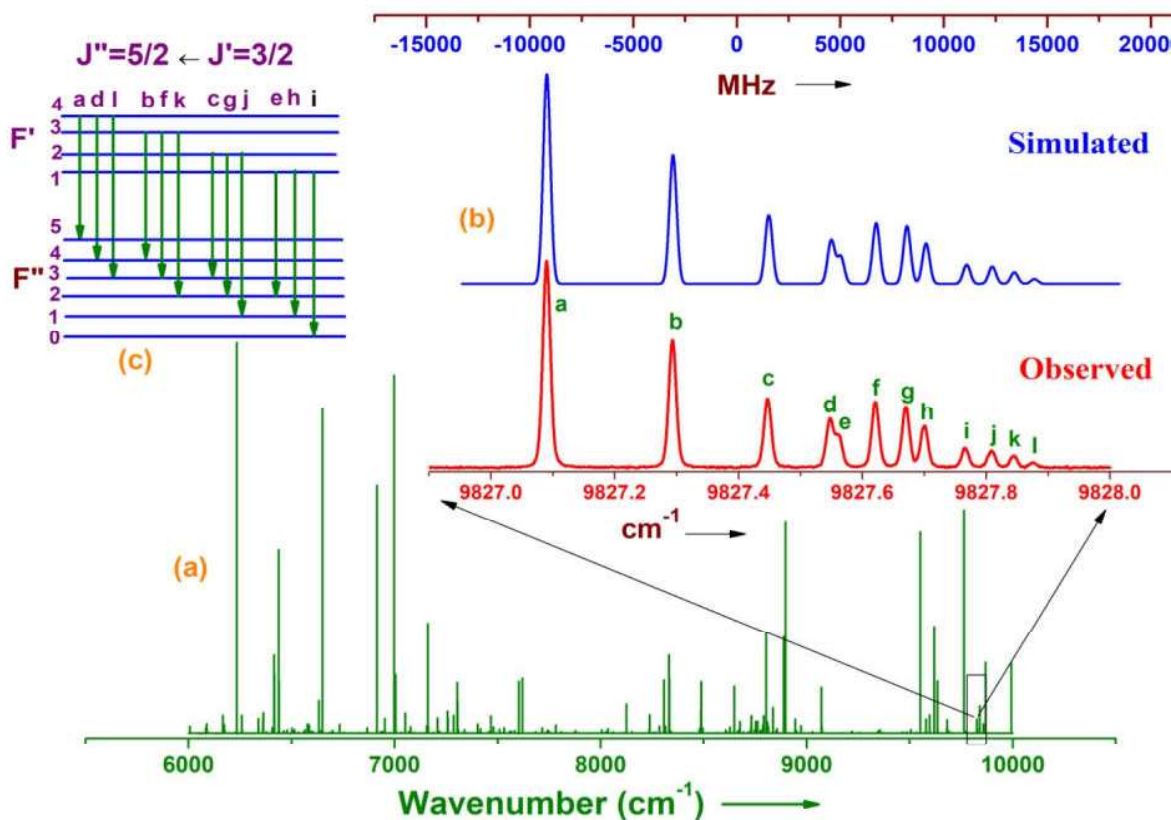
Fig 3.11 (a) The I I spectra recorded in the 6000-10000 cm⁻¹ wave number region. **(b)** Observed and simulated *hfs* splitting observed in the transition at 9827.401 cm⁻¹ depicted in the expanded region of 9827- 9828 cm⁻¹, which shows well resolved 12 components except the partially resolved 'd' and 'e' components. **(c)** Possible *hfs* transitions.

In this spectral region, 183 spectral lines were detected as I I transitions. Among these lines 53 are reported for the first time. Out of 53 newly reported lines, 34 lines are coming from the spectral region 9000 - 10000 cm⁻¹. Table 3.5 (Appendix I) represents the list of observed transitions and their energy level classifications. The new center of gravity wavenumber values derived for all the observed transitions are given in first column. The last column indicates the new lines observed in the present work. Few of the well resolved *hfs* structures are presented in Figs. 3.12 – 3.15. All observed lines are compared with the simulated structures. For the line at 6174.095 cm⁻¹ shown in Fig. 3.12, except for one component marked as 'l', all the other

80

remaining components are clearly resolved. *Hfs* structures for the lines at 7005.695, 8425.243 and 9681.130 cm^{-1} are shown in Figs. 3.13, 3.14 and 3.15 respectively. *Hfs* structures of these lines were analyzed for the first time. Completely resolved structures were obtained for the lines at 7005.695 and 8425.243 cm^{-1} whereas partially resolved structure was observed for 9681.130 cm^{-1} line.
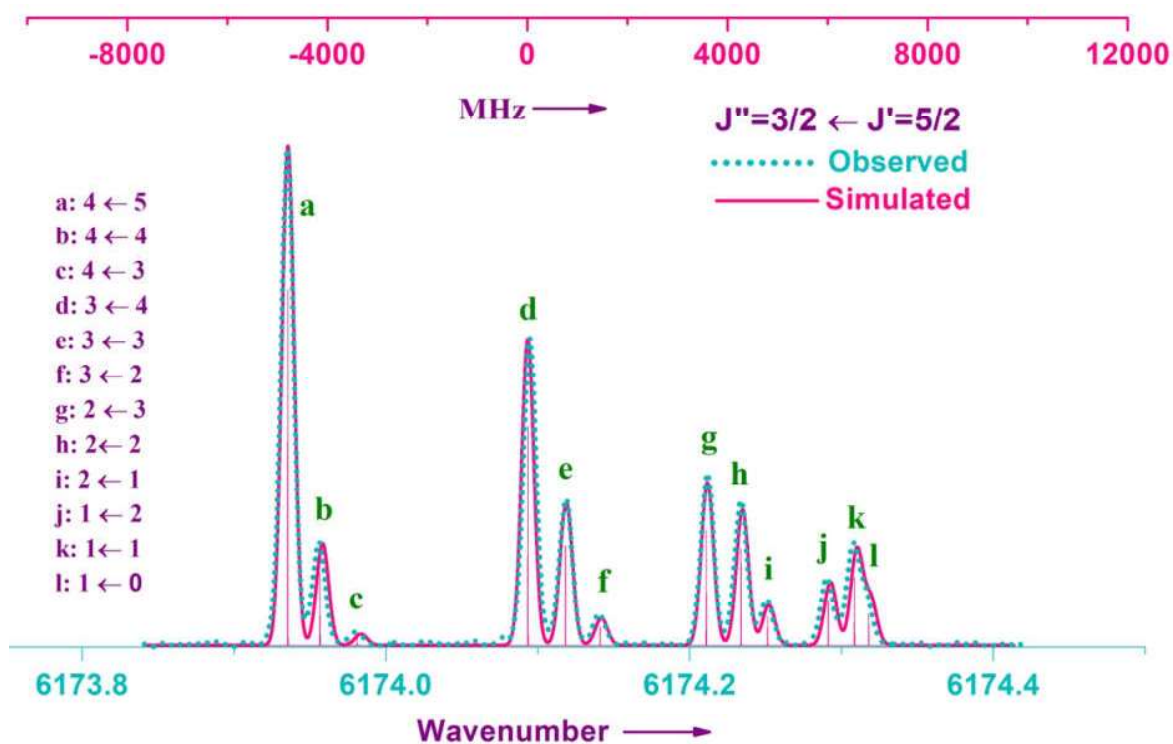
Fig. 3.12 A well resolved *hfs* structure of the line at 6174.095 cm^{-1} observed in EDL discharge of 8W, with a resolution of 0.004 cm^{-1}. Out of 12 components 11 are completely resolved and a shoulder peak is observed for the remaining one.
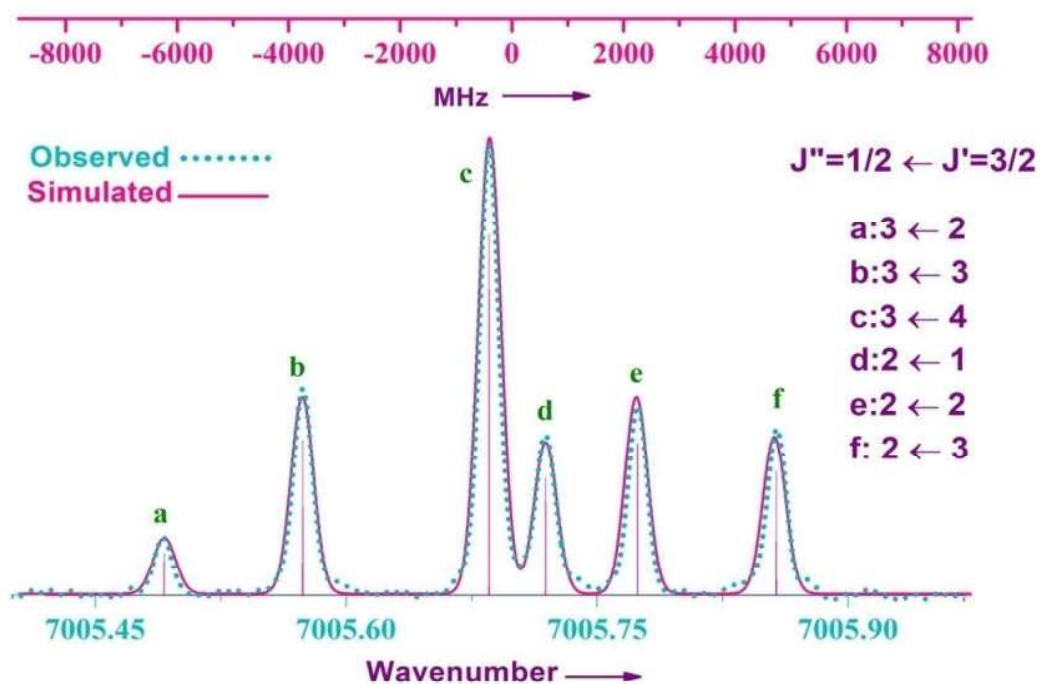
Fig. 3.13 A fully resolved *hfs* structure of the line at 7005.695 cm^{-1} observed in EDL discharge of 10 W, with a resolution of 0.008 cm^{-1}.
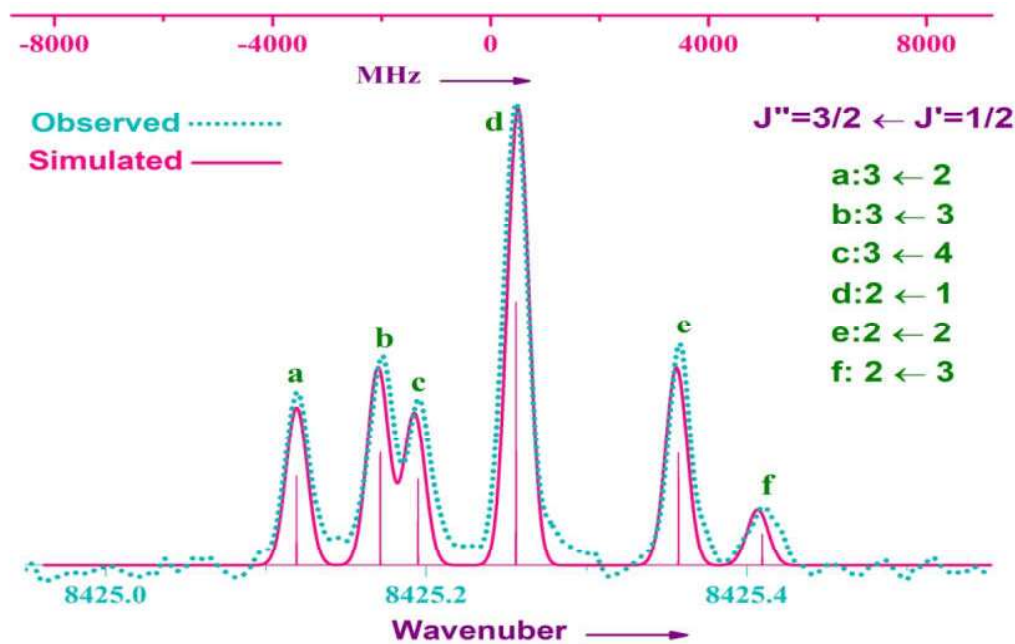
Fig. 3.14 A fully resolved *hfs* structure of the line at 8425.243 cm^{-1} observed in EDL discharge of 10 W, with a resolution of 0.008 cm^{-1}.
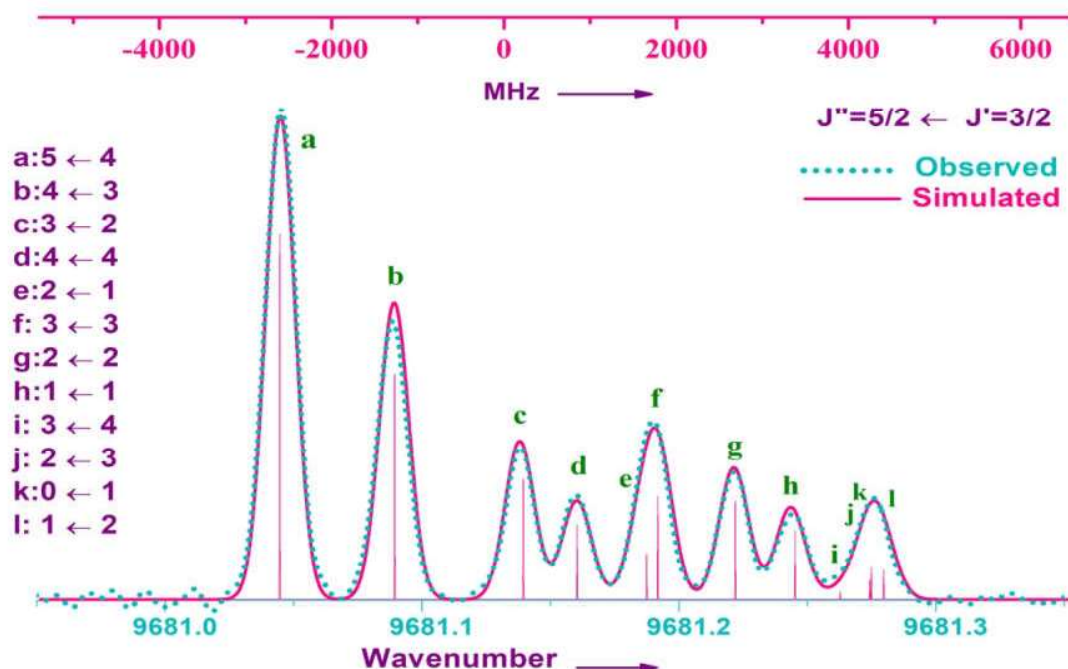
Fig. 3.15 A partially resolved *hfs* structure of the line at 9681.130 cm^{-1} observed in EDL discharge of 9 W, with a resolution of 0.0035 cm^{-1}.

The *hfs* constants *A* and *B* derived for 60 energy levels of which 30 levels are even and 30 are odd parity energy levels. Table 3.6 (Appendix I) represents the derived *A* and *B* constants for 30 even levels and Table 3.7 (Appendix I) for 30 odd parity levels. In both the cases the derived *hfs* constants have been compared with the previous work. While the already known *hfs* values for 25 even and 26 odd levels agree very well with the presently derived *hfs* values, the *hfs* values for 5 even and 4 odd levels have been reported here for the first time. The uncertainties given in Table 3.6 and 3.7 for the *hfs* constant *A* and *B* are derived as mentioned in chapter 2.

3.3.3 In the spectral region: 10000 - 25000 cm^{-1}

In the spectral region of 10000- 25000 cm^{-1}, the instrument was equipped with beam splitter (CaF$_2$ in the near infrared / Quartz in the visible region) and appropriate detector (Si

diode / Photomultiplier Tube) to observe the spectra in the near infrared and visible spectral regions. Multiple band pass filters (band width: 10, 25 and 50nm) were used in the spectral region above 12000 cm^{-1} to enhance the S/N. On average, 50 to 150 scans were co-added depending upon the resolution and S/N.

A total of 240 spectral transitions were observed in the entire spectral region of which, 149 are newly observed. Newly derived line position center of gravity wavenumber values and corresponding energy levels are listed in Table 3.8 (Appendix I).

Figs. 3.16-3.18, correspond to well resolved, partially resolved and unresolved hyperfine structures, respectively. In each Figure, the corresponding fitting residual is plotted below the spectrum.
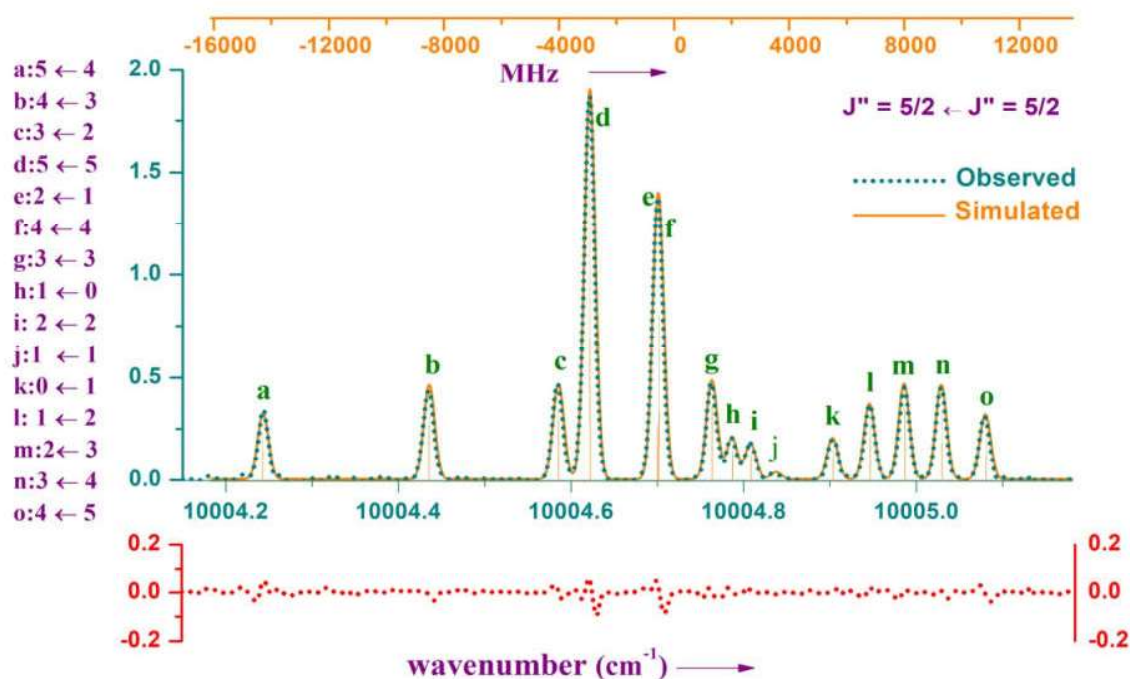
Fig. 3.16 The transition at 10004.717 cm^{-1} shows a well resolved *hfs* splitting. The observed spectrum was compared to a simulated spectrum using theoretical intensity ratios and is matching well. The fitting residual is shown in the lower trace.
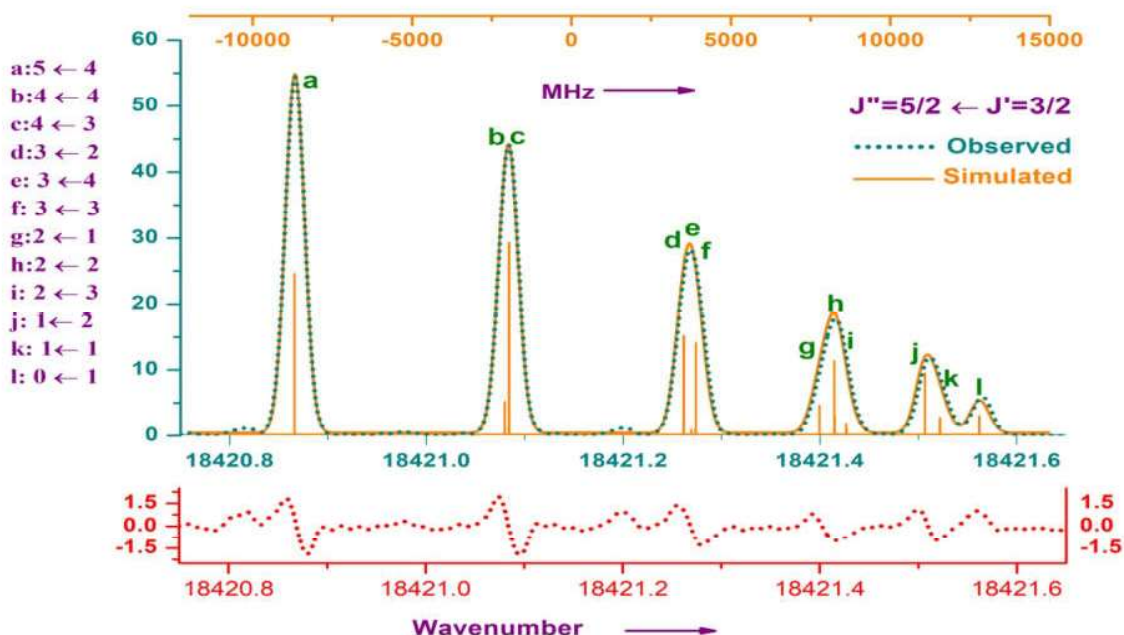
Fig. 3.17 A partially resolved *hfs* splitting is observed at the transition at 18421.149 cm^{-1}. The observed and simulated spectra are compared. The fitting residual is shown in the lower trace.
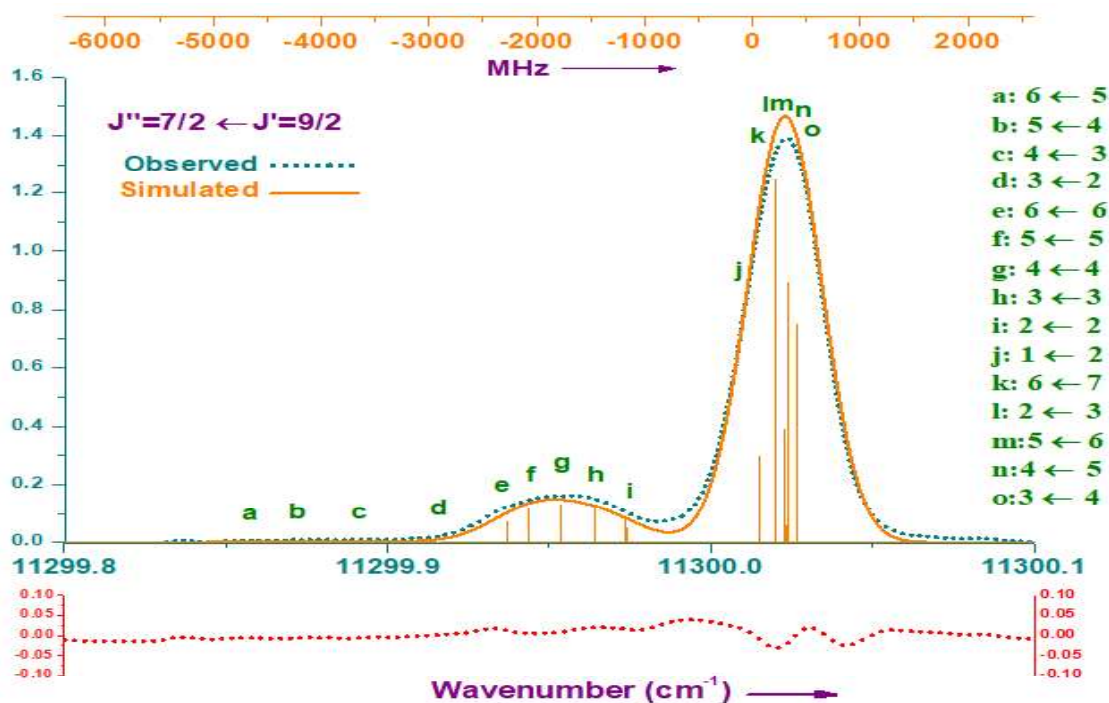
Fig. 3.18 An unresolved *hfs* splitting is observed at the transition at 11300.013 cm^{-1}. The recorded and simulated spectra are compared and the fitting residual is shown below the spectrum.

Hfs investigations were performed on 177 spectral lines to derive *A* and *B* constants for 100 energy levels (48 even parity and 52 odd parity levels), from which the constants of 14 even parity and 10 odd parity levels are reported for the first time. Among the total 177 spectral lines the *hfs* of 128 lines was investigated for the first time. The last column in Table 3.8, indicates the *hfs* analyzed lines in the present work and literature [21-23]. Table 3.9 and Table 3.10 (Appendix I) present the *A* and *B* constants of even and odd parity energy levels respectively, along with previously reported [21-23] values. The uncertainties given in Table 3.9 and 3.10 are derived as mentioned in chapter 2.

In the case of even levels, *hfs* constants were derived for 48 levels. *A* and *B* constants for 37 levels were previously reported [21-23] and the remaining 14 levels were analyzed for the first time. Each of these 11 levels was involved only in one transition, therefore repeated measurements were carried out to derive *A* and *B* constants and the mean values are given for each level.

Hfs constants were obtained for 52 odd levels. Among these 52 levels, *A* and *B* constants of 45 levels were previously reported [21-23] and the remaining 10 levels were analyzed for the first time. Six of these levels were involved in only one transition but the level at 79844.469 cm^{-1} was involved in three transitions having wave numbers of 11294.735, 13489.382 and 13824.011 cm^{-1}. In this case, all three transitions were analyzed and constants were derived independently. The mean value of all three transitions is given in Table 3.10.

3.4 Cooling Effect on Spectral Lines

To minimize the Doppler broadening effects on spectral lines, EDL was operated under low microwave power along with reduced temperature. Surfatron cavity and EDL were cooled with nitrogen gas, which is passed through a LN_2 bath. Consequently, the FWHM of the spectral lines drastically reduced and well resolved *hfs* patterns were observed. A detailed experimental setup was discussed in chapter 2. Here few illustrative examples are provided to see the spectral improvements upon cooling the EDL and cavity.

Figs. 3.19(a) to 3.19(c) have been presented here as the representative examples showing the effect of lowering the temperature on spectral lines, which establish the importance of temperature reduction for unambiguous analysis of *hfs* data of iodine. All three lines were observed at same instrumental resolution (0.0035 cm^{-1}) and EDL operating power (9W) both under cooling and without cooling conditions. Simulated spectra are given for the spectra observed under cooled condition. Many peaks get resolved under cooled conditions.

Further details of cooling effects like FWHM of spectral lines and temperature calculations are illustrated in Fig. 3.20 and 3.21. Fig. 3.20 shows the well resolved *hfs* structure of a line at 2056 cm^{-1}, which is the strongest in the spectral region below 3000 cm^{-1}. This was recorded at the instrumental resolution of 0.002 cm^{-1} and the EDL was operated at 6 W microwave power. A table is also included in Fig. 3.19, to present the line positions (in cm^{-1}) and their respective FWHM values (in MHz). A minimum FWHM value of 93 MHz has been achieved for the *hfs* component at 2056.462 cm^{-1}. Most of the *hfs* components are have the FWHM values less than 120 MHz.
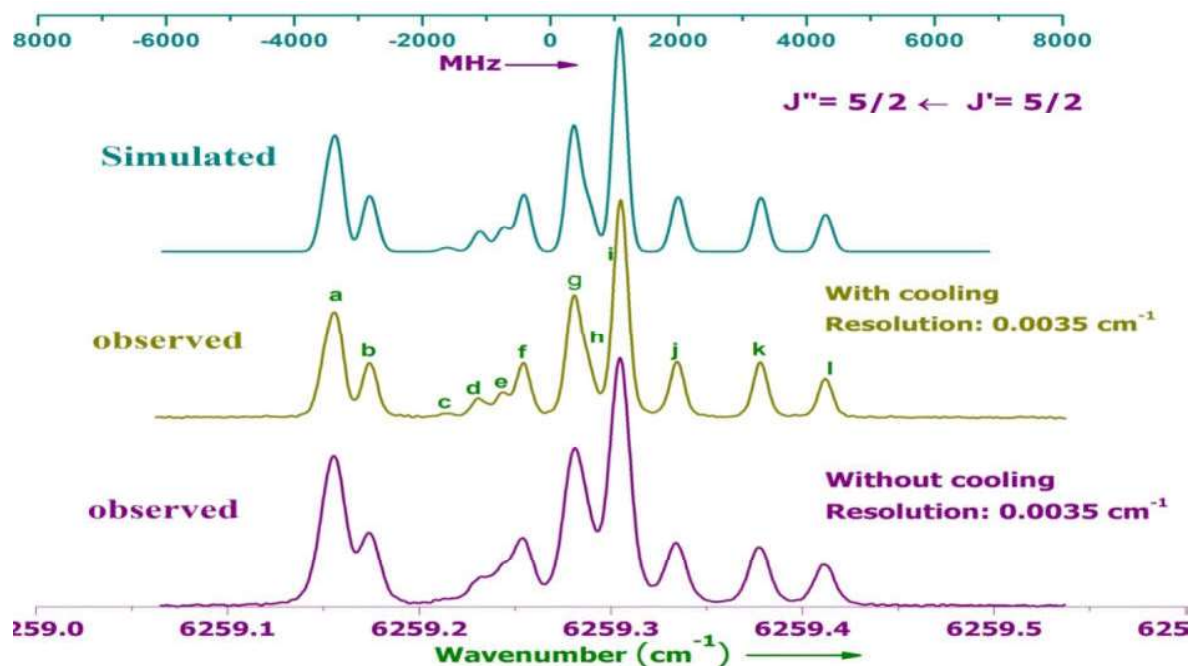
Fig. 3.19(a) Comparison of spectral resolution with cooling and without cooling conditions for a line at 6259.267 cm⁻¹ observed at same resolution (0.0035 cm⁻¹) and operating power (9 W) are shown. *Hfs* components at c, d, e and f are resolved under cooled condition.
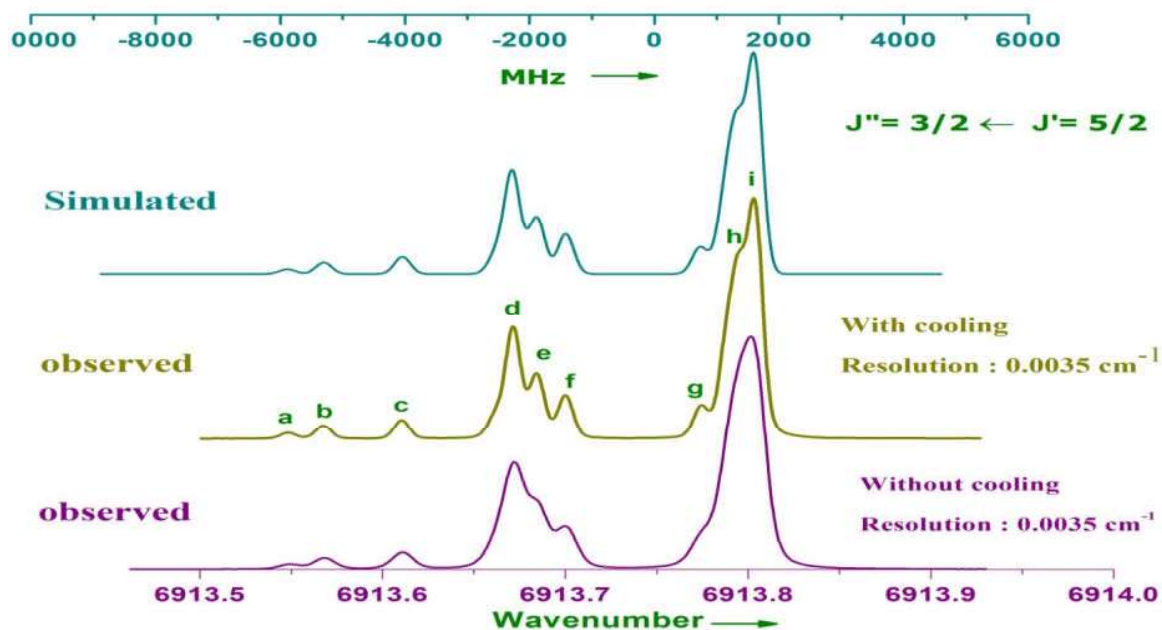
Fig. 3.19(b) The line at 6913.746 cm⁻¹ shows improvements of the spectral features upon cooling the EDL. *Hfs* components at e, f, g and h are resolved clearly under cooled condition.
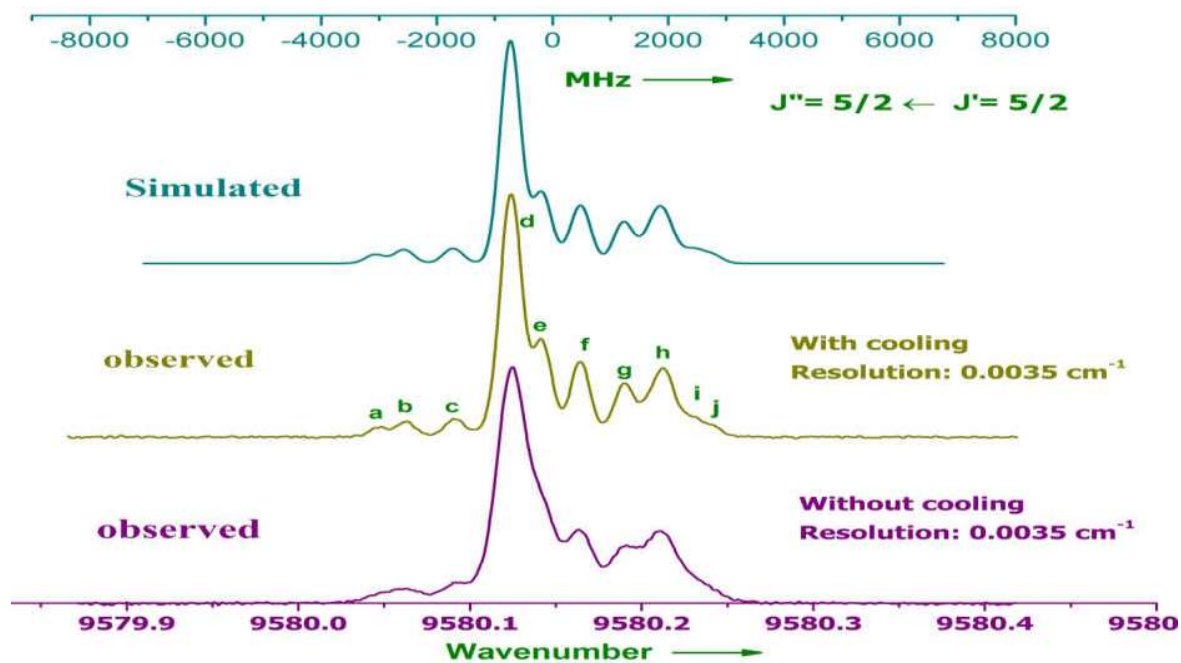
Fig. 3.19(c) The line at 9580.143 cm^{-1} shows improvements of the spectral features upon cooling the EDL. *Hfs* components at a, b, e and g are resolved clearly under cooled condition.

	Line position (cm-1)	FWHM (MHz)
a	2056.255	–
b	2056.28	138
c	2056.311	114
d	2056.334	117
e	2056.353	117
f	2056.375	117
g	2056.38	114
h	2056.414	120
i	2056.432	114
j	2056.449	117
k	2056.462	93
l	2056.468	132
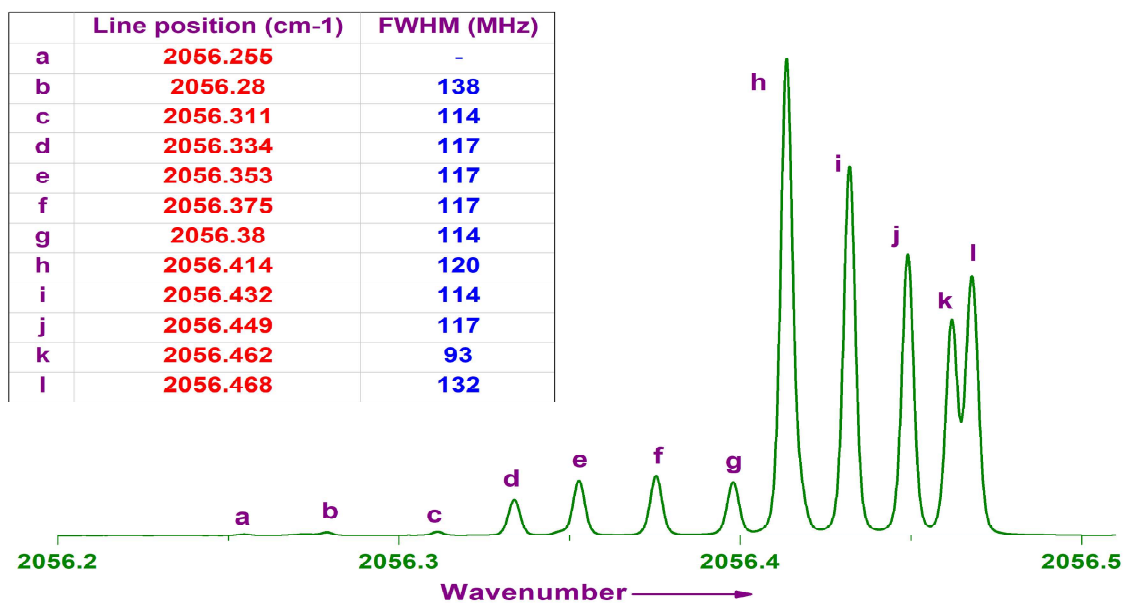
Fig. 3.20 Shows a well resolved *hfs* structure of 2056 cm^{-1} line and it also includes a table presenting the line positions in cm^{-1} and their respective FWHM values in MHz.

To assess the role of lowering of temperature, we also estimated the change in temperature as well as Doppler width of the spectral lines. On the outer EDL surface, a temperature difference of ~ 285 K was found using a temperature sensor upon cooling the EDL at a typical microwave power of 4W. The corresponding change in the plasma temperature upon cooling was estimated using the line widths of several spectral lines. The Fig. 3.21 shows the *hfs* structure of the line at 7602.6 cm^{-1}. Table 3.11 given below represents the comparison of change in the spectral width of all the six *hfs* components with and without cooling. The FWHM calculated using *OPUS* software for the data corresponding to cooling and without cooling conditions yielded the temperatures of ~ 395 K and ~ 680 K respectively using Doppler width equation (2.31), which is reasonably close to the estimated temperature measurements. A Pt-100 sensor has been used to measure the temperature of the source and the same is substantiated from the Doppler width of the Ne lines [65].
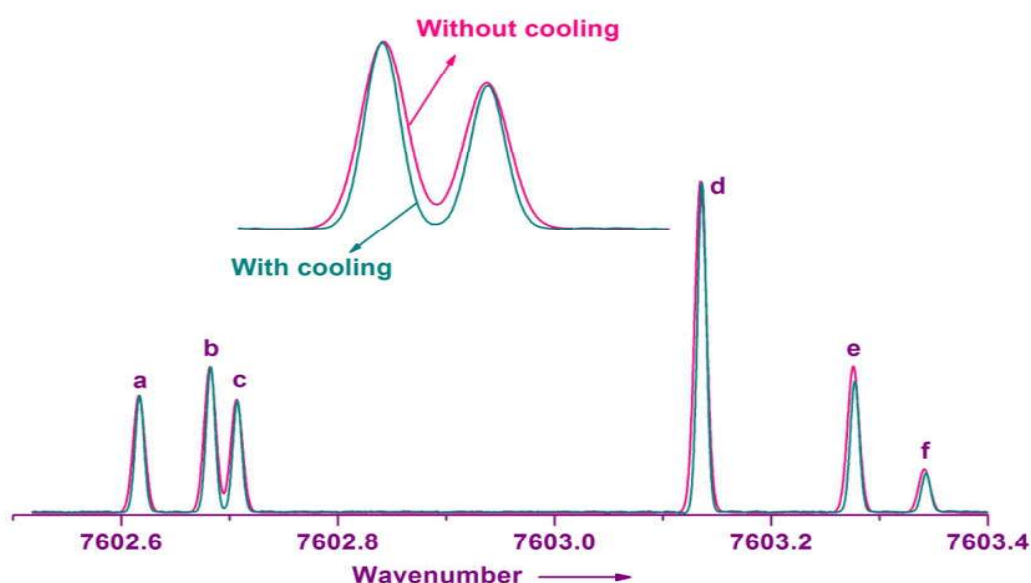
Fig. 3.21 Fully resolved *hfs* structure of a line at 7602 cm^{-1} with cooling and without cooling conditions to compare the FWHM.

Table 3.11 A comparison of FWHM of *hfs* components of 7602 cm^{-1} line in normal and cooling conditions.

Transition F″← F′	FWHM (Without Cooling) cm^{-1}	MHz	FWHM (With Cooling) cm^{-1}	MHz
3 ← 2	0.0126 ~	377.74	0.0096 ~	287.80
2 ← 2	0.0126 ~	377.74	0.0097 ~	290.80
1 ← 2	0.0111 ~	332.77	0.0094 ~	281.81
4 ← 3	0.0126 ~	377.74	0.0097 ~	290.80
3 ← 3	0.0126 ~	377.74	0.0097 ~	290.80
2 ← 3	0.0125 ~	374.74	0.0097 ~	290.80

Another example to illustrate the improvements in spectral resolution upon cooling the EDL is shown in Fig. 3.22. The line at 10969.250 cm^{-1} consists of 10 *hfs* components since it is a J″ = 3/2 to J′ = 3/2 transition. At normal plasma condition, four partially resolved *hfs* components and one shoulder peak were observed, whereas seven well resolved components were identified while operating the EDL under cooled conditions. The instrumental resolution was fixed at 0.006 cm^{-1} for both the cases. Spectral width was reduced by about 250 MHz due to the change from normal to cooled conditions.
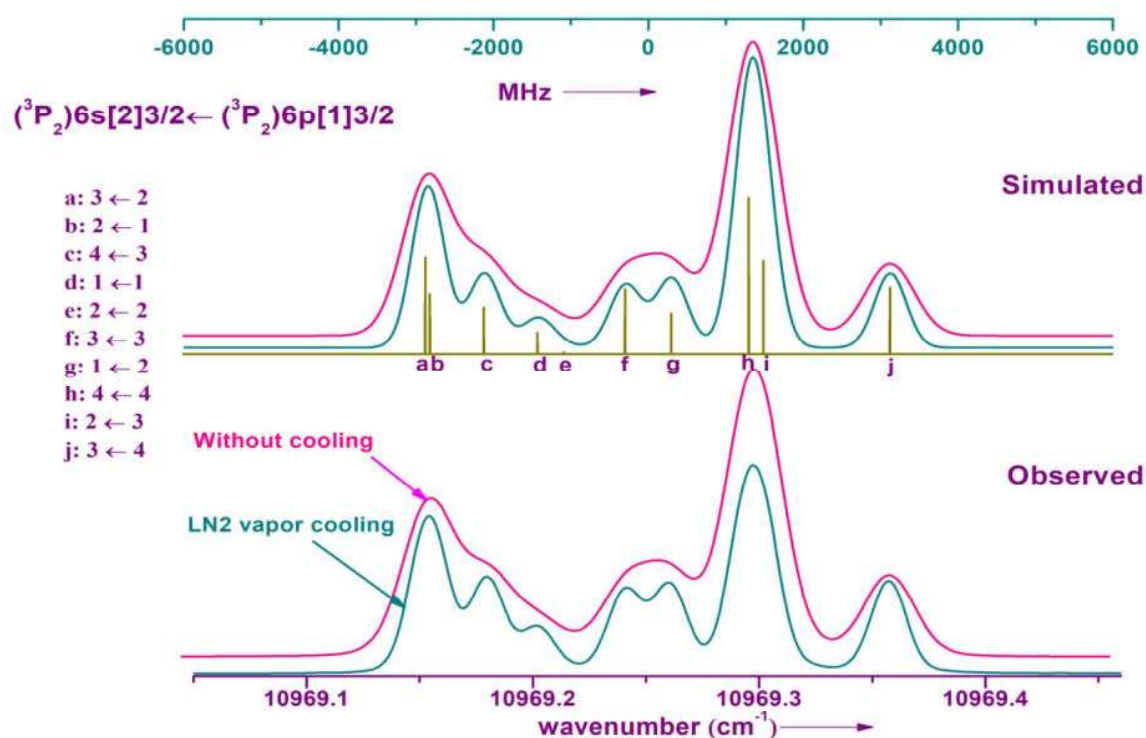
Fig. 3.22 A drastic spectral improvement is shown for a line at 10969.250 cm^{-1} under cooled condition. *Hfs* components at c, d, f and g are clearly resolved.

3.5 Unidentified Lines and Blended Lines

Few lines have been identified as unclassified transitions. For these transitions center of gravity wavenumber values have been determined and listed in Table 3.2. Fig. 3.23 represents some of the unclassified lines observed at 2500, 2548, 2574, 2580, 2719 and 3668 cm^{-1}. Since, the spectra of I II are starting to appear above 12000 cm^{-1}, the present undefined lines are belongs to I I spectra. The lines shown in Fig 3.23 (a) & (b) are seem to show a well resolved *hfs* structures, however their classification is not known. In contrast, for the lines shown in Figs. 3.23(c) & (d), the *hfs* structure is completely lost. Yet another example is shown in Figs 3.23(e) & (f), where only one transition has been identified for the highly complex and populated

structure. Thus, the examples in Figs. 3.23 (c) to 3.23(f) represent the cases of unclassified blended lines.
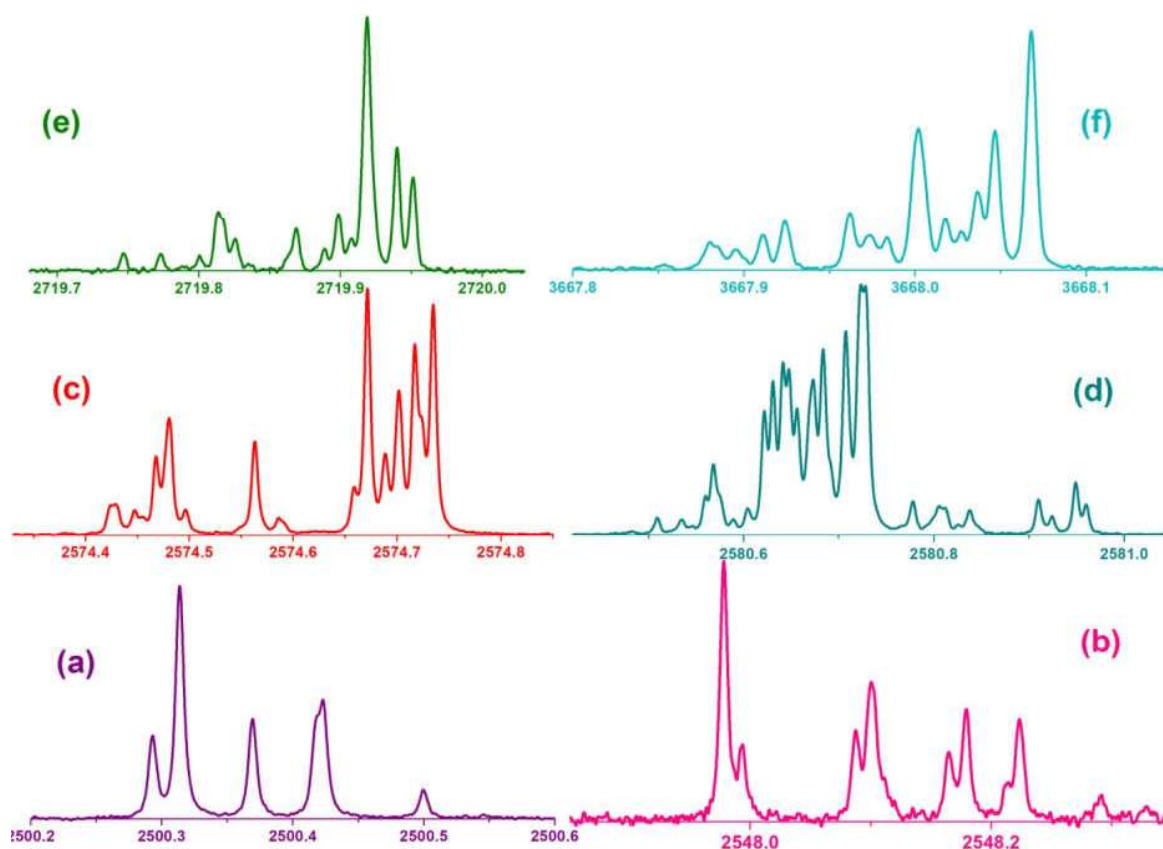
Fig. 3.23 Unidentified lines observed in the I I spectra. (a) and (b) represents well resolved *hfs* structure for the lines. (c), (d), (e) and (f) present blended lines.

Lines at 6331, 6415, 8719, 8787 and 9684 cm^{-1} are identified as blended lines. The observed blended line at 9684 cm^{-1} is shown in Fig. 3.24(a).This is an overlapping of two iodine lines at 9684.848 and 9684.945 cm^{-1}. The simulated spectra for both the lines were generated individually and combined as shown in Fig. 3.24 (b). The two simulated *hfs* structures have been plotted along with the observed spectrum in Fig. 3.25 to show extent of overlap structure. The simulated and observed *hfs* structures are matching very well.
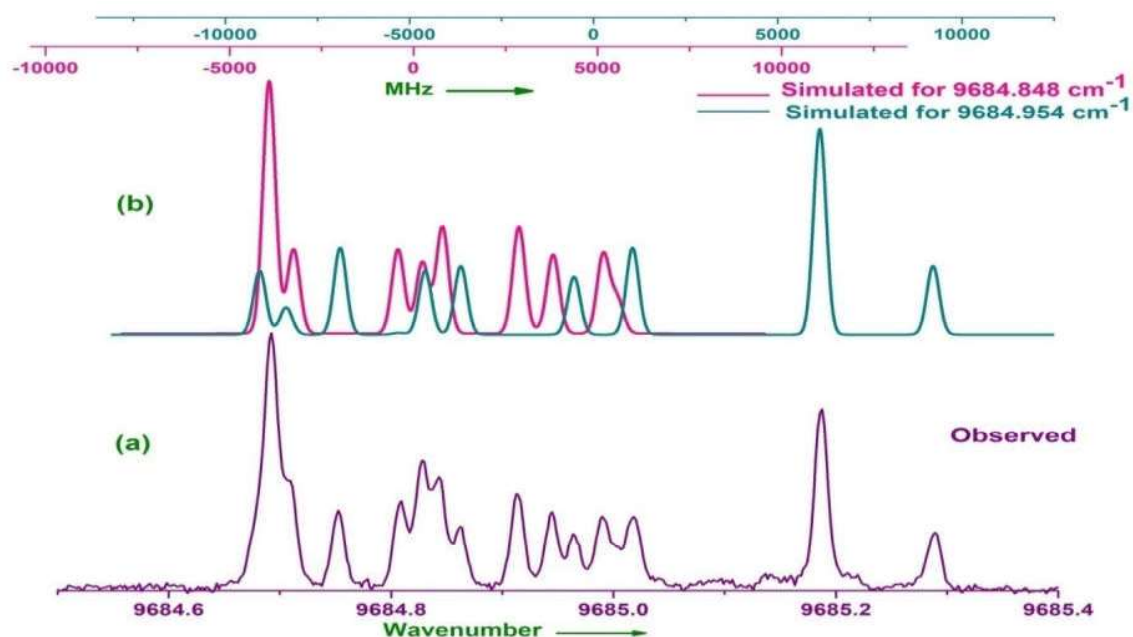
Fig. 3.24 (a) An observed blended line at 9684 cm^{-1} (b) Simulated spectra of 9684.848 and 9684.945 cm^{-1} transition.
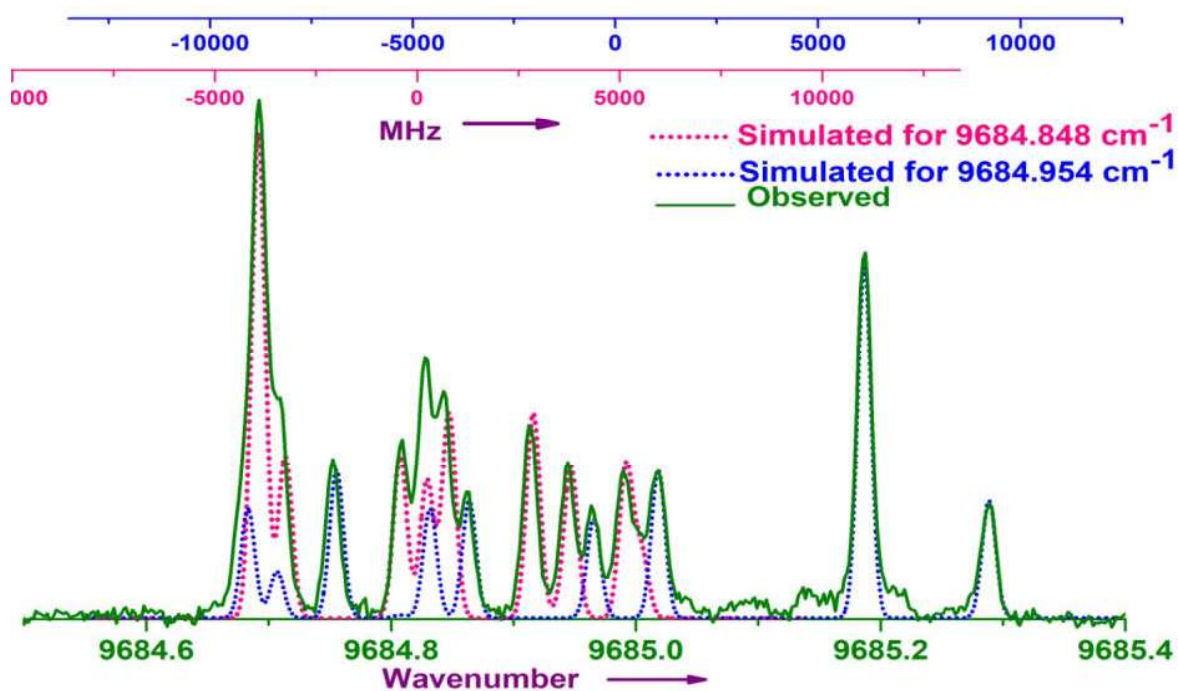
Fig. 3.25 Comparison of observed blended line and simulated spectra of the transitions at 9684.848 and 9684.945 cm^{-1}.

Few more lines were also identified as blended lines at 10917.682, 11286.828, 11292.256, 13526.657, 13814.546, 22673.834, 12611.489 and 17343.301 cm^{-1}. Among all these transitions, the first six are overlapping iodine − iodine transitions and the remaining two are iodine − Ne transitions [65]. Common centre of gravity values are given for the blended lines in Table 3.8.

An illustration of a blended line corresponding to two I I transitions at 10917.619 cm^{-1} and 10917.715 cm^{-1} is depicted in Fig. 3.26. The simulated spectrum matches well with the observed spectrum. The center of gravity wavenumber differences (10917.715 - 10917.619 cm^{-1} = 0.096 cm^{-1}) of the two transitions is identical with center of gravity differences of their simulated spectra (2878 MHz).
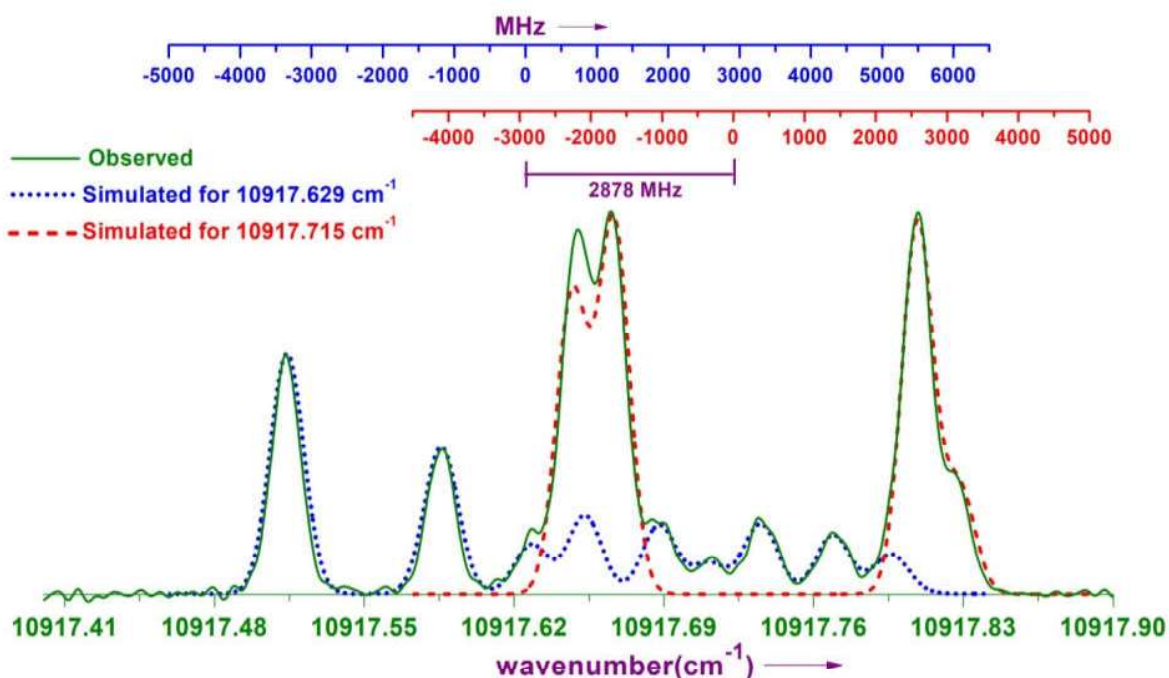
Fig. 3.26 An observed blended line and the simulated spectra of two iodine lines having nearly the same wavenumbers (at 10917.619 cm^{-1} and 10917.715 cm^{-1}). The center of gravity MHz difference of 2878 MHz fits well with the wavenumber difference.

3.6 Conclusion

High resolution spectroscopic investigations were performed on neutral atomic iodine in the spectral region from 1800 to 25000 cm^{-1}. Electrodeless discharge lamps of I_2 were prepared and excited by using a surfatron microwave cavity to generate the plasma. Emission spectra were recorded in the spectral region $1800 - 25000\ cm^{-1}$ employing a high resolution Fourier transform spectrometer, equipped with various beam splitters and appropriate detectors depending upon the spectral region. A total of 777 spectral lines were observed in the entire spectral region. Center of gravity wavenumber values were determined for all observed lines. An experimental set up has been applied to minimize the Doppler broadening of the spectral lines. Minimum FWHM of 93 MHz has been achieved for a *hfs* component for 2056 cm^{-1} line. With reduced Doppler width, well resolved *hfs* structures were observed in the entire spectral region. *Hfs* investigations were performed on nearly 454 spectral lines and *hfs* constants were derived for nearly 117 energy levels. For 19 even parity and 13 odd parity (total 32) levels *A* and *B* constants are reported for the first time. Apart from *hfs* investigations, few lines were identified as unclassified and blended lines.

Chapter 4

Hyperfine structure measurements of neutral atomic Bismuth (^{209}Bi)

4.1 Introduction

The atomic spectra of neutral Bismuth (^{209}Bi) have been extensively studied by many researchers in the past. In 1930, Zeeman et al. [30] studied the bismuth spectrum to report hyperfine structure and Zeeman effects of few spectral lines. Mrozowski [31] prepared EDL containing mixture of bismuth metal and few mm of He gas. The generated arc spectra were observed employing a 30-foot grating spectrograph, which increased the number of known energy levels to 45. The hyperfine structure measurements were performed on 55 lines. Clearman [32] reported a large number of Bi I lines and energy levels along with their configuration by studying the arc spectra in the range 1200 − 2000 Å. Atomic beam magnetic resonance technique has been employed by Title and Smith [78], Hull and Brink [79] and Landman and Lurio [80] to perform the hyperfine structure investigations on the ground state configuration ($6p^3$) of Bi I. Further, *hfs* analysis of ground configuration as well as some excited levels was carried out by Dickie and Kelly [34, 80], Guern et al. [81] and Dembczyński et al. [82-83] utilizing Fabry-Perot interferometric technique. Holmgren and Svanberg [84] obtained the *hfs* magnetic dipole constant (A) and electric quadrupole constants (B) for the levels ($^3P_0$)6d $^2D_{3/2}$ and ($^3P_1$)7s $^4P_{3/2}$ using the level crossing method. Poulsen and Hall [85] also worked on *hfs* of Bi I lines, energy levels and determined the lifetimes by combining tunable CW-dye laser spectroscopy of an atomic beam sample with interferometric wavelength measurements. George and co-workers employed various spectroscopic techniques such as Ebert plane grating spectrograph [86], Fabry-Perot interferometer [87], 1-m plane-grating Czerny-Turner scanning spectrometer [35] and Fourier transform spectroscopy [36-37,88] to investigate the *hfs* structure of atomic Bi I in more detail and reported several new spectral lines as well as *hfs* constants for many levels. Rosen [89] performed theoretical work on the magnetic and electric hyperfine

structure analysis on the ground configuration of ^{209}Bi by using an effective Hamiltonian formalism. To calculate the Bi abundance, Wahlgren et al. [41] detected the spectral lines of Bi I, Bi II and Bi III in the high resolution spectra of chemically peculiar HgMn stars: χ- Lupi and HR 7775, obtained using the Goddard high resolution spectrograph onboard the Hubble telescope. Most recently, Sobolewski et al. [90] derived the *hfs* A constant for 10 levels by measuring the hyperfine structure and Zeeman splitting of 10 lines.

In spite of such detailed investigations reported for Bi, the knowledge of complete *hfs* structure requires further studies. In addition, the spectrum of Bi comprises some peculiar line shape effects, which may emerge due to effects such as self absorption, blending of lines etc. Thus, we have used two light sources: One is an Electrodeless Discharge Lamp (EDL) and another is a liquid nitrogen (LN$_2$) cooled Hollow Cathode Lamp (HCL) to produce a large number of Bi lines in the spectral range of 2500 - 40000 cm^{-1}. These lines were observed by a high resolution Fourier transform interferometer with improved precision for measurement of center-of-gravity wavenumbers. *Hfs* measurements were also carried out to obtain the accurate *hfs* constants for many new energy levels and line shape analysis for various lines have been performed.

4.2 Experimental Details

Atomic spectra of Bi I were generated from bismuth plasma by two discharge techniques: a microwave discharge in an EDL containing BiI$_3$/Ne and a DC discharge in a LN$_2$-cooled HCL containing Bi$_2$O$_3$/Ne. The preparation of EDL and HCL has been described in Chapter 2. The light emitted from the source was focused onto the input port of high resolution Fourier transform spectrometer (FTS). The instrument was equipped with various beam splitters (CaF$_2$ in

the Infrared, Qrtz Vis in the visible and Qrtz UV in the UV region) and appropriate detectors (InSb, InGaAs, Si diode, PMT-Vis, and PMT-UV) to cover the spectral range from 2500 to 40000 cm^{-1} (IR to UV). The spectra were recorded in this spectral range at various instrumental resolutions from 0.006 cm^{-1} to 0.025 cm^{-1} depending upon the spectral region. To enhance the S/N ratio, as well as to observe weak transitions, several band pass optical filters were used in the visible and UV spectral regions.

Fig. 4.1 shows the typical *hfs* structures of three observed spectral lines in the IR, visible and UV regions with their energy levels. The three energy levels $6p^{34}S_{3/2}$, $6p^{32}D_{3/2}$ and $6p^2\ 7s$ $^4P_{1/2}$ are involved in three transitions at 32588.210 (UV region), 21169.201 (visible region) and 11419.038 cm^{-1} (IR region). Each level is common for two transitions.

The line at 32588.210 cm^{-1} in UV region corresponds to a resonance transition $6p^2\ 7s$ $^4P_{1/2}$ - $6p^{34}S_{3/2}$. A well resolved *hfs* structure of such resonance line can be obtained with hollow cathode discharge operated at low currents. If we observe with EDL discharge, a strong self absorption may destroy the original *hfs* pattern. The self-absorption phenomenon of few spectral lines is discussed in more details in a further section. A completely resolved *hfs* structure was observed for the transition using a LN_2-cooled HCL with 4 mA discharge current, shown in Fig. 4.1(a).
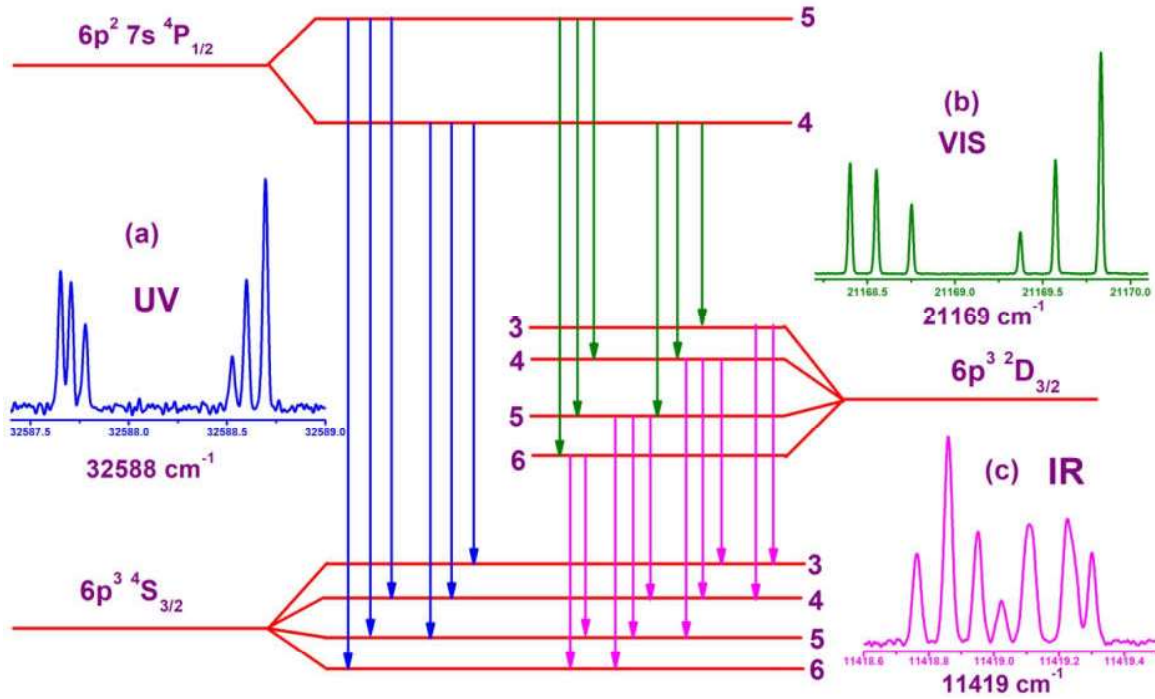
Fig. 4.1 Observed spectral transitions of Bi I in three different spectral regions: IR, Vis and UV. a) A completely resolved *hfs* structure of a line at 32588.210 cm^{-1} in the UV region was observed with a HCL at a 4 mA discharge current and 0.02 cm^{-1} resolution. b) The line at 21169.201 cm^{-1} in the visible region, recorded with a HCL at a 20 mA discharge current and 0.016 cm^{-1} resolution. c) The line at 11419.038 cm^{-1} in the IR region, observed with EDL at 15 W microwave power and 0.01 cm^{-1} resolution.

The line at 21169.201 cm^{-1} is a transition between the levels 6p^2 7s ^{4}P$_{1/2}$ and 6p^{3}^{2}D$_{3/2}$ appearing in visible region. As this transition involves a ground configuration, this leads to a strong emission line observed with a HCL at a 20 mA discharge current. A well separated *hfs* structure was obtained with six *hfs* components as shown in Fig. 4.1(b).

Another line at 11419.038 cm^{-1} (875.5 nm), in the IR region, is a forbidden transition between the two odd parity levels 6p^3 ^{2}D$_{3/2}$ and 6p^3 ^{4}S$_{3/2}$ [38,91-92]. As the magnetic dipole transitions are weak in nature, we could observe them only in the strongest discharge conditions.

101

This line was observed in EDL discharge with good S/N. Out of 10 *hfs* components ($J = 3/2 \leftarrow J = 3/2$), seven are completely resolved, as shown in Fig. 4.1(c).

4.3 Hyperfine Structure Investigations

In this work, we have measured and identified 107 spectral lines of Bi I in the entire spectral range from IR to UV. All the observed spectra were calibrated with standard Ne lines [65] as described in Chapter 2. Line position center of gravity wavenumber values of the observed transitions were determined for all the 107 lines and presented in Table 4.1 (Appendix I) along with their energy levels and designations [93]. The uncertainties given for the C.G. values include statistical and systematic uncertainties. Here, systematic uncertainties were obtained from the uncertainty of the calibration. The *hfs* investigations were performed on 76 well resolved lines, of which 21 were analyzed for the first time and are indicated in the last column of Table 4.1.

A few representative examples of observed *hfs* structures along with the simulated spectra are depicted in Figs. 4.2 − 4.11. Fig. 4.2 represents a completely resolved line at 2787.390 cm^{-1} observed with the EDL discharge at 18 W power and 0.006 cm^{-1} resolution, in the mid-IR region. Fig. 4.3 represents the line at 4432.953 cm^{-1} in the mid-IR region recorded with an EDL discharge at 16 W power and 0.008 cm^{-1} resolution. The *hfs* is analyzed on this line for the first time. Fig. 4.4 shows well-separated *hfs* components for a line at 8536.766 cm^{-1}, recorded with the LN$_2$-cooled HCL dicharge at a 5 mA current and 0.012 cm^{-1} resolution. The FWHM of all *hfs* components was reduced dractically and reached an estimated minimum value of 315 MHz. Fig. 4.5 shows the line at 15325.061 cm^{-1} in the visible region recorded with the EDL discharge at 18 W power and 0.02 cm^{-1} resolution. An optical filter centered at 650 nm was used

in this observation. Out of 12 *hfs* components, 11 were completely resolved, and one shoulder peak has been observed. The *hfs* investigations were carried out on this line for the first time. Fig. 4.6 shows a line at 16296.121 cm^{-1} in the visible region. The *hfs* structure is observed for this line with the EDL discharge at 6 W power and 0.018 cm^{-1} resolution. Out of 10 *hfs* components, 9 were completely resolved. Figs. 4.7 and 4.8 present the lines at 17409.611 and 25712.568 cm^{-1} respectivly, observed in the visible region. The *hfs* measurements were carried out on these lines for the first time. One well resolved and two completely resolved *hfs* structures for the lines in the UV region at 33052.382, 37070.837 and 38041.881 cm^{-1} are depicted in Figs. 4.9, 4.10 and 4.11 respectively.
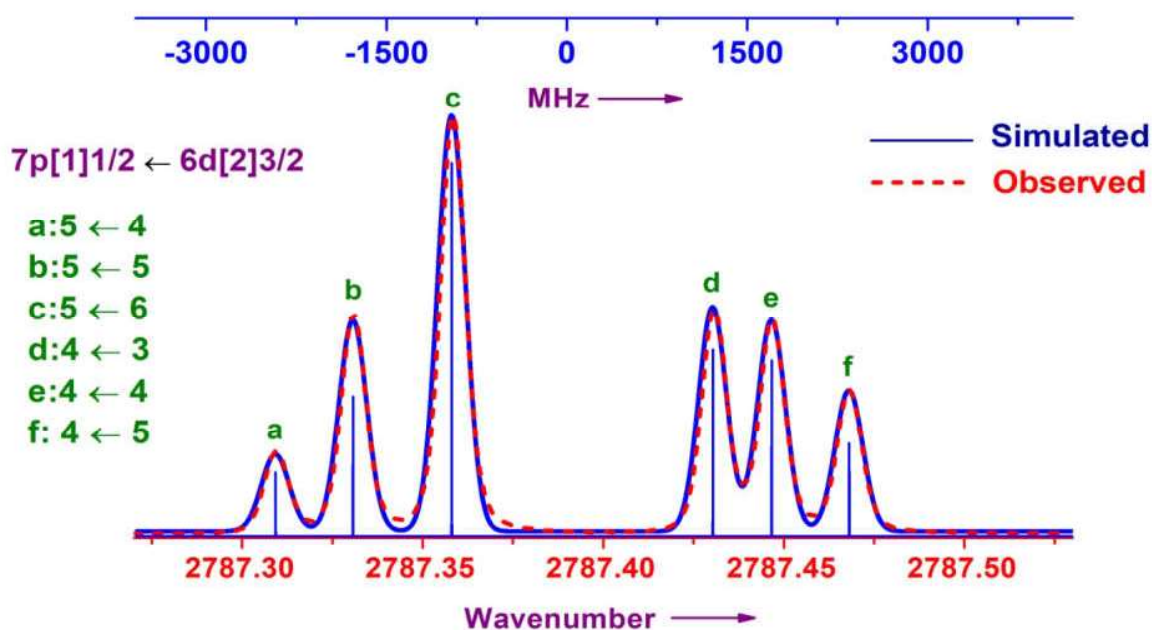
Fig. 4.2 The *hfs* structure observed for the line at 2787.390 cm^{-1} in the mid-IR region recorded with an EDL discharge at 18 W power and 0.006 cm^{-1} resolution. All six *hfs* components were completely resolved and are indicated with a,b,c,d,e and f. The simulated and observed spectra are matching well.
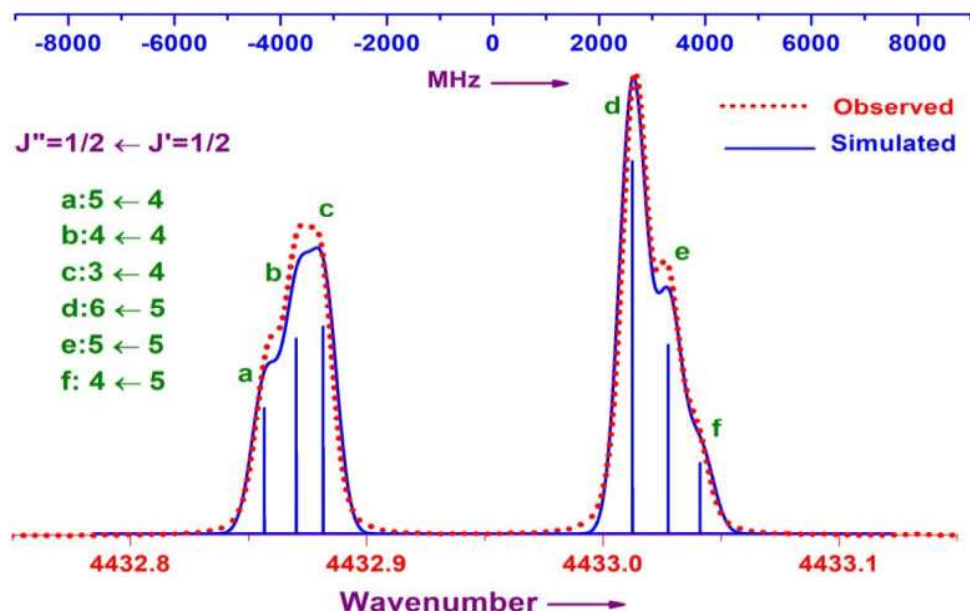
Fig. 4.3 The *hfs* structure observed for the line at 4432.953 cm^{-1} in the mid-IR region recorded with an EDL discharge at 16 W power and 0.008 cm^{-1} resolution. The simulated and observed spectra are matching well.
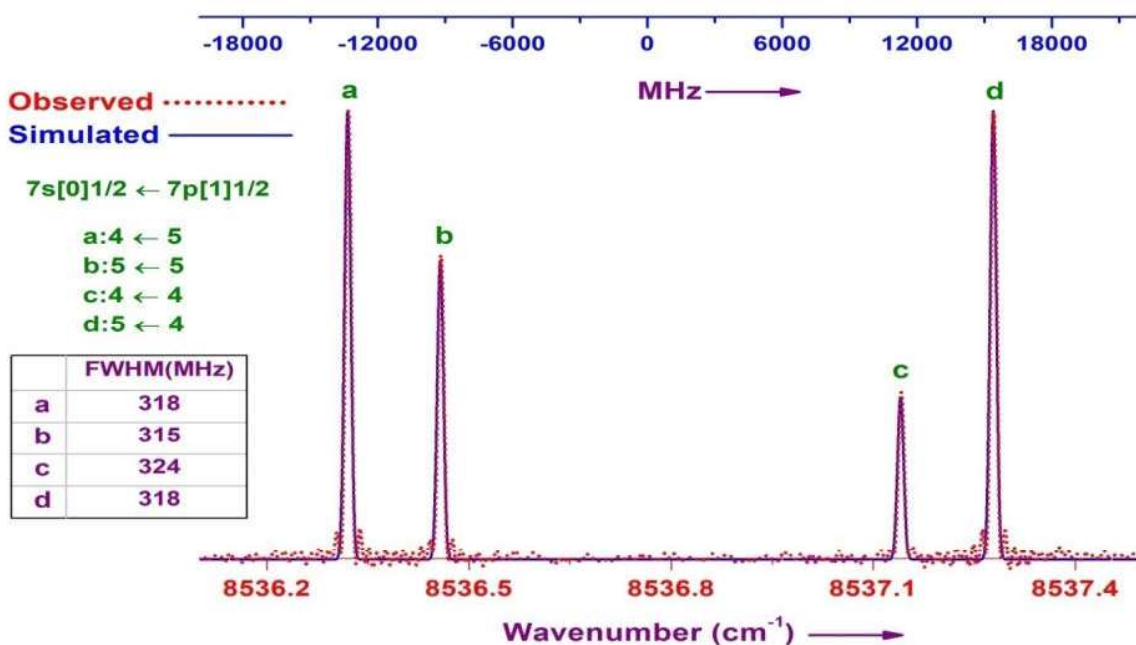
Fig. 4.4 Fully resolved and well seperated *hfs* components for the line at 8536.766 cm^{-1} observed with the LN$_2$-cooled HCL discharge at 5 mA discharge current and 0.012 cm^{-1} resolution. The FWHM of each *hfs* component is given in MHz. The simulated spectrum is matching well with the observed one.
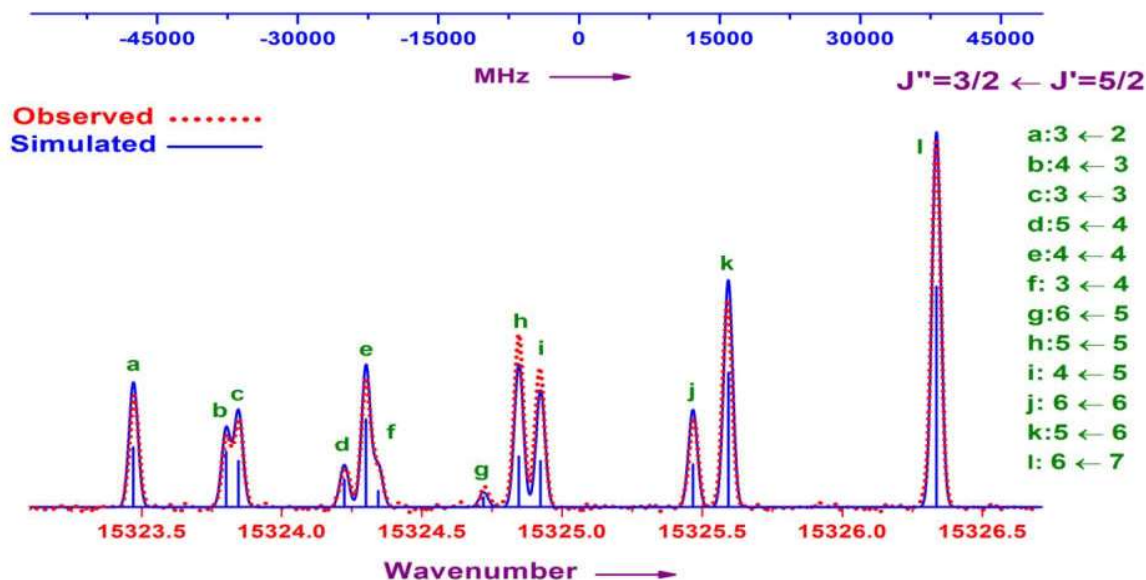
Fig. 4.5 The *hfs* structure observed for the line at 15325.061cm^{-1} in the visible region recorded for the first time with the EDL discharge at 18 W power and 0.02 cm^{-1} resolution. Out of 12 *hfs*components, 11 were completely resolved, and one shoulder peak is indicated by 'f'. An optical filter centered at 650 nm was used in this observation.The simulated spectrum is matchingwell with the observed one.
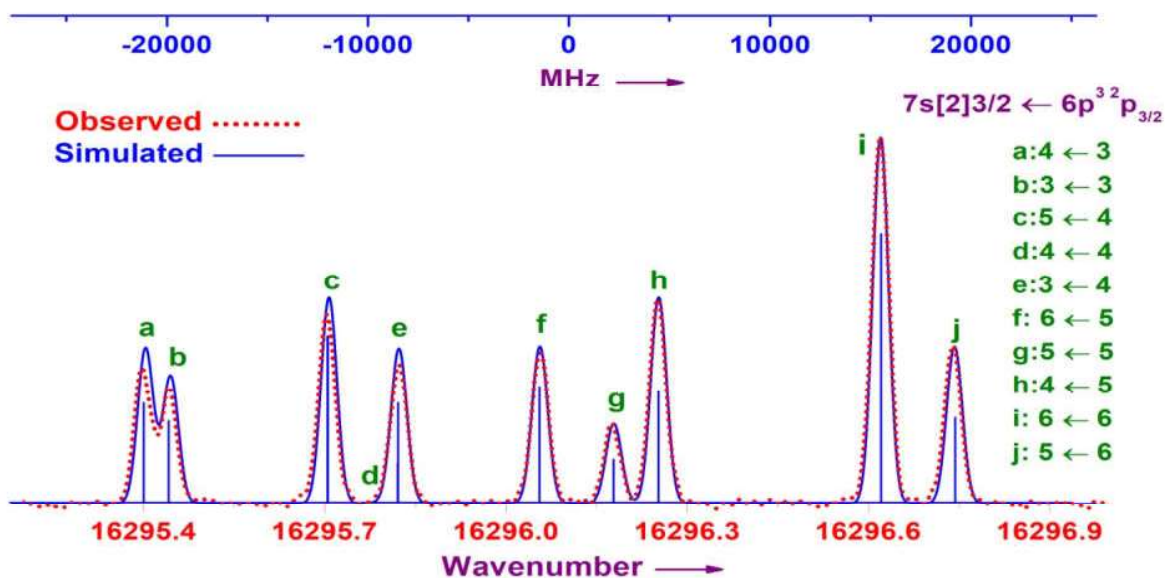
Fig. 4.6 The *hfs* structure observed for the line at 16296.121 cm^{-1} in the visible region with the EDL discharge at 6 W power and 0.018 cm^{-1} resolution. Out of 10*hfs* components, 9 were completely resolved. An optical filter centered at 625 nm was used in this observation.The simulated spectrum is matchingwell with the observed one.
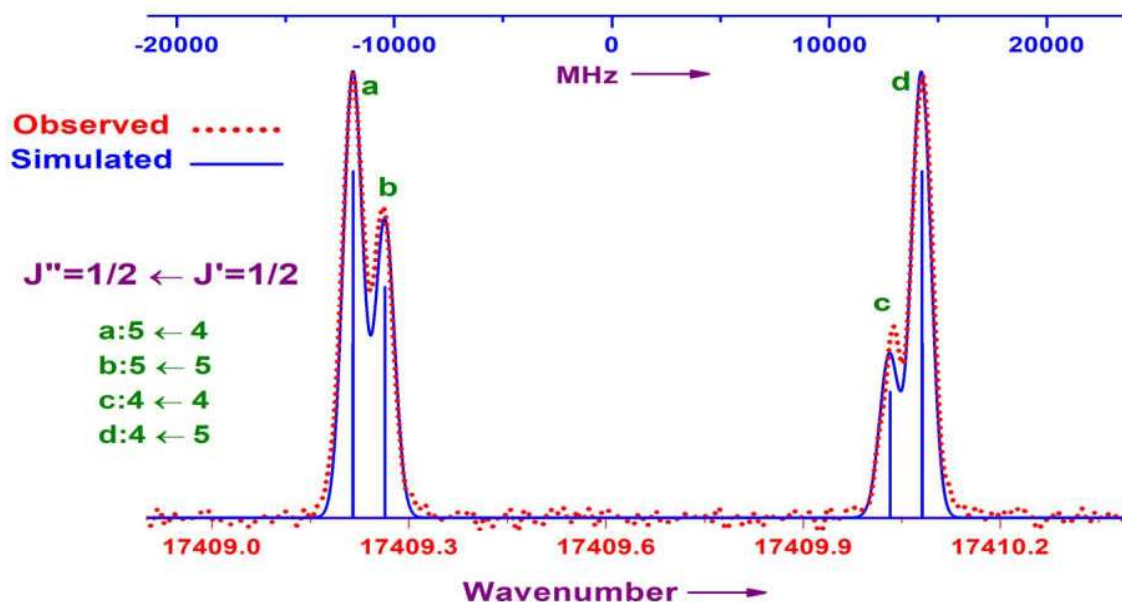
Fig. 4.7 The *hfs* structure observed for the line at 17409.611 cm⁻¹ in the visible region recorded for the first time with the EDL discharge at 5 W power and 0.016 cm⁻¹ resolution. All four *hfs* components were resolved and are indicated with a,b,c and d. An optical filter centerd at 575 nm was used in this observation. The simulated and observed spectra are matching well.
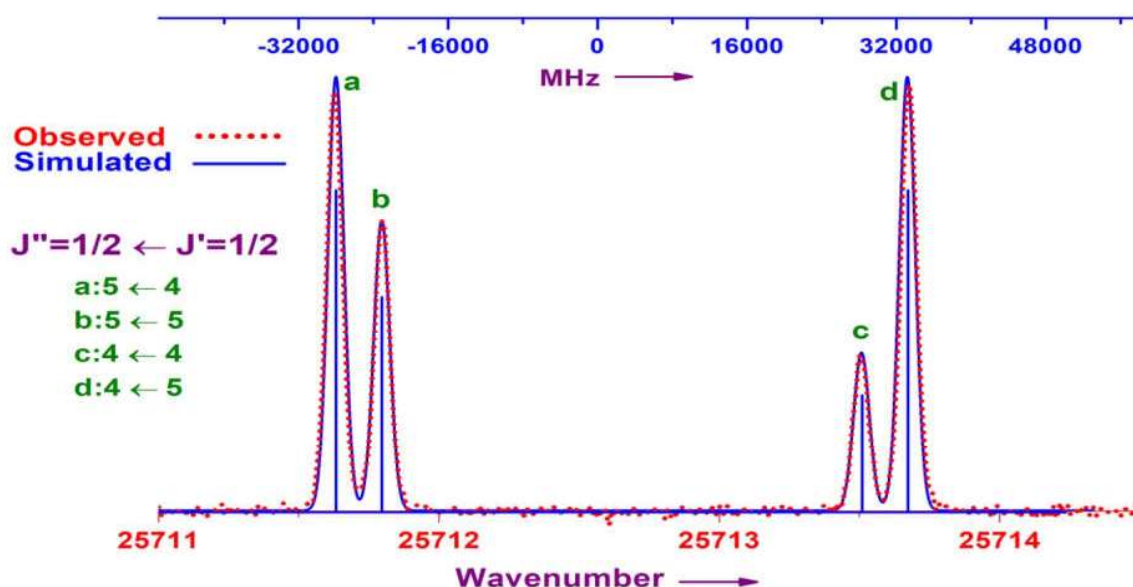
Fig. 4.8 The *hfs* structure observed for the line at 25712.568 cm⁻¹ in the visible region recorded for the first time with the EDL discharge at 7 W power and 0.02 cm⁻¹ resolution. All four *hfs* components were completely resolved and are indicated with a,b,c and d. The simulated and observed spectra are matching well.
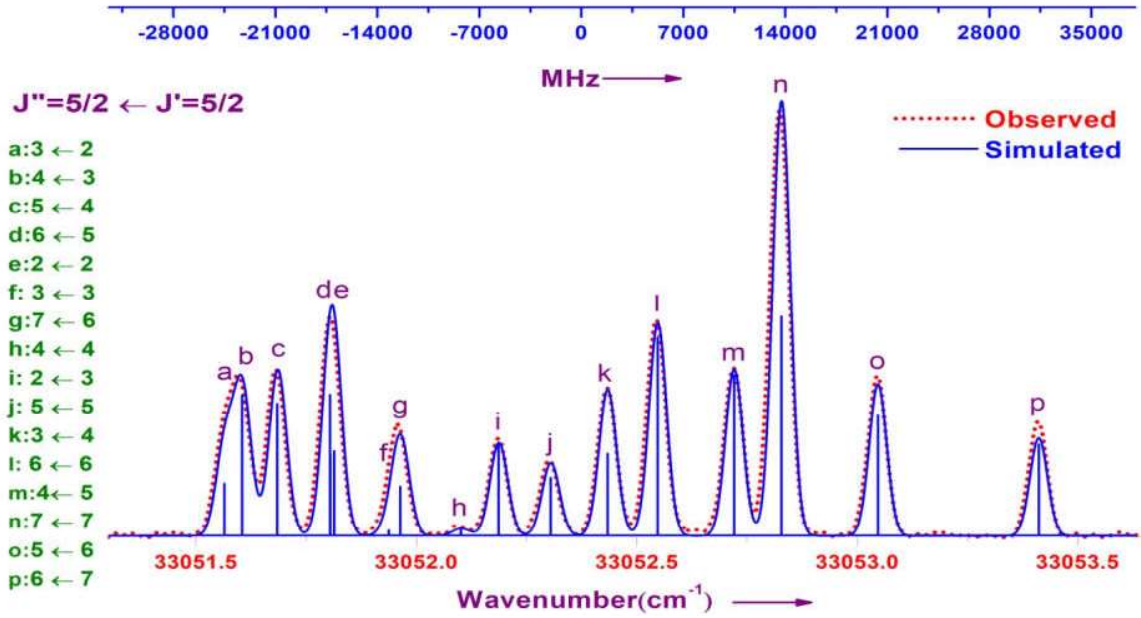
Fig. 4.9 The *hfs* structure observed for the line at 33052.382cm⁻¹ in the visible region recorded for the first time with the HCL discharge at 20 mAcurrent and 0.025 cm⁻¹ resolution. Out of 16 *hfs* components 13 were observed. The simulated and observed spectra are matching well.
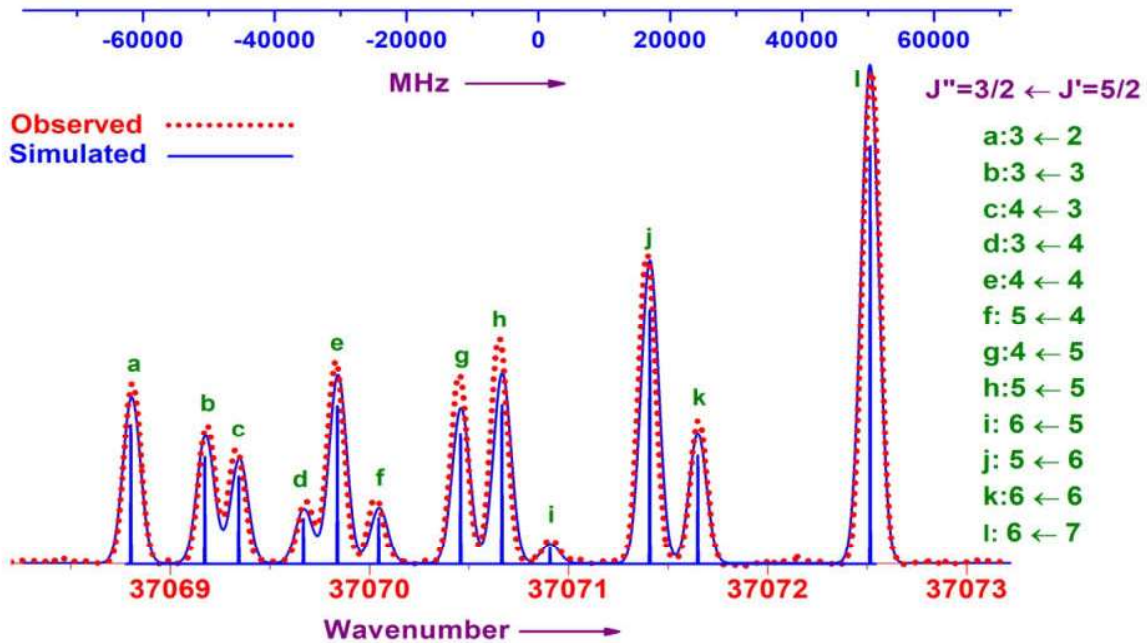
Fig. 4.10: The *hfs* structure observed for the line at 37070.837 cm⁻¹ in the UV region recorded with the EDL discharge at 15 W power and 0.025 cm⁻¹ resolution. All 12 *hfs* components were completely resolved and are indicated with a,b,c,d and so on. An optical filter centered at 275 nm was used in this observation.The simulated and observed spectra are matching well.
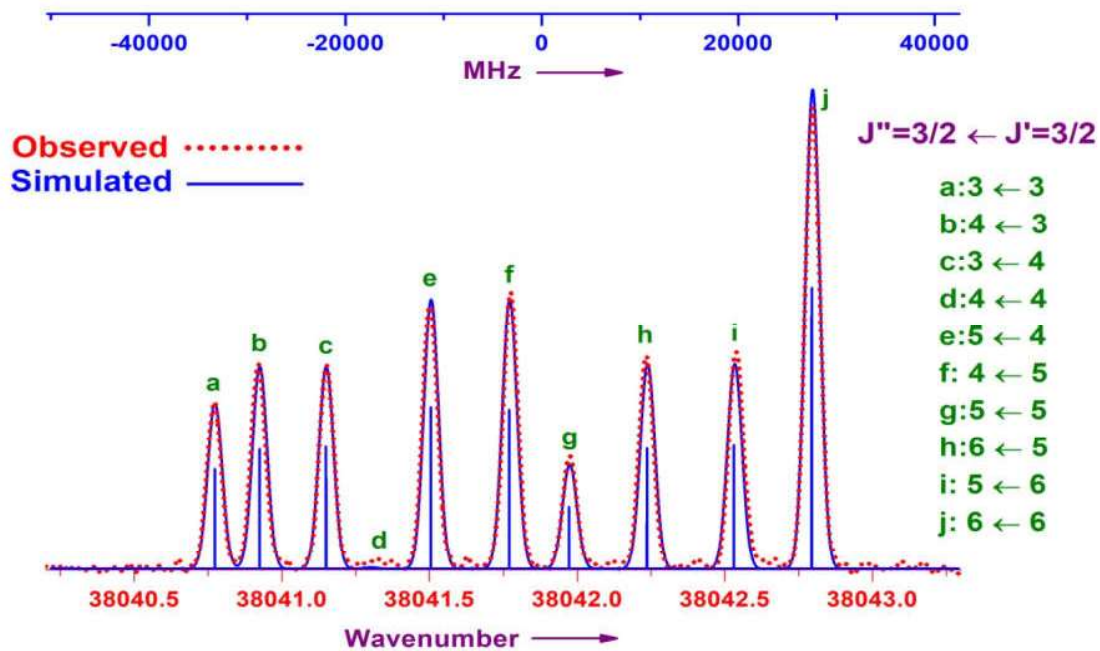
Fig. 4.11 The *hfs* structure observed for the line at 38041.881 cm^{-1} in the UV region recorded with the EDL discharge at 15 W power and 0.025 cm^{-1} resolution. All 10 *hfs* components were completely resolved and are indicated with a,b,c,d and so on. An optical filter centered at 275 nm was used in this observation. The simulated and observed spectra are matching well.

Hfs measurements were performed on 76 well resolved spectral lines by using the programs *HFSAB* and *WINHFS* [66]. A total of 31 energy levels were involved in these *hfs* investigations. *Hfs* constants *A* and *B* were derived for 31 energy levels of which 14 are even parity and 17 are odd parity. The *hfs* constants of even and odd levels are presented in Table 4.2 and Table 4.3 (Appendix I) respectively along with their energy level values and configurations. Out of 31 energy levels, *A* and *B* constants of 12 even and 13 odd levels are matching well with the previously reported values. Measurements of *hfs* for the remaining two even levels, viz. [($^3P_0$)8d[2]3/2 and ($^3P_0$)10d[2]3/2)] and four odd levels [($^3P_0$)8p[1]3/2, ($^3P_0$)9p[1]3/2, ($^3P_0$)5f[3]5/2 and ($^3P_0$)6f[3]5/2)] are presented for the first time. The *B* constants have been derived for the even ($^3P_0$)9d[2]3/2 and odd ($^3P_0$)7p[1]3/2 levels for the first time. Uncertainties

for A and B values, given in Tables 4.2 and 4.3, have been determined using the procedure described in Chapter 2.

4.4 Spectral Line Broadening and Self-absorption

The entire Bi I spectra have been measured using two discharge sources, EDL and HCL. Each discharge method has its own importance. A comparision is given between EDL and HCL sources in Chapter 2. As the intensity of an EDL discharge is much stronger than that of HCL, the weak lines appear in the EDL discharge and the strong lines in HCL. Although, lines generated in EDL are broader due to Doppler broadening, this method is very efficient to record weak transitions with a reasonable S/N. However, in case of resonance lines or very intense lines, hfs structure deforms from its original pattern due to the strong self-absorption of spectral peaks, even when operated with lower microwave powers. In such cases, the HCL discharge provides a well resolved hfs structure. Further, the HCL was cooled to minimize the Doppler width.

Among the few examples on the above effects, we now discuss a line at 34496 cm^{-1}, which corresponds to the transition ($^3P_1$)7s[1]1/2 - 6s^{2}6p^3 $^2D_{3/2}$. A strong self- absorption deforms its original hfs pattern when recorded using the EDL discharge source. A comparision is shown between EDL and HCL dicharges for this transition in Fig. 4.12. All six hfs componets of this transition ($J = 1/2 \leftarrow J = 3/2$) get completely resolved in the LN$_2$-cooled HCL at 10 mA discharge current, as shown in Fig 4.12 (a). In Fig. 4.12 (b), the spectra observed with the EDL discharge at 6 W microwave power has been shown. In this case, the hfs components were broader than in the HCL discharge, and self-absorption was noticeable. After a further increase in the microwave power to 22 W, the original hfs pattren was completely destroyed due to

strong self-absorption of spectral peaks as shown in Fig 4.12 (c). A comparision of the width of each *hfs* component is given for HCL discharge at 10 mA and EDL discharge at 6 W power.

a: 4 ← 5
b: 5 ← 5
c: 6 ← 5
d: 3 ← 4
e: 3 ← 3
f: 4 ← 4

	EDL(MHz)	HCL(MHz)
a	2467	1343
b	2803	1310
c	6029	1367
d	1442	1328
e	2491	1322
f	2701	1355
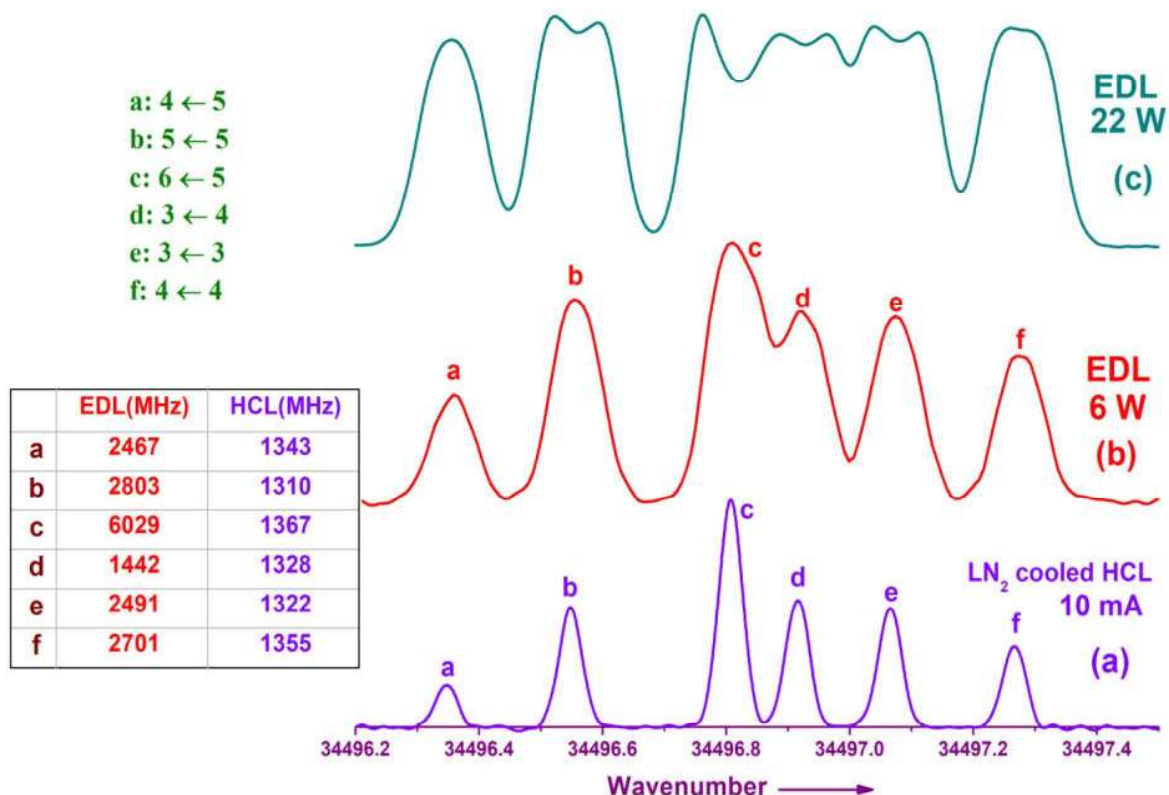
Fig. 4.12 An illustrative example of self-absorption of spectral peaks has been shown for the line at 34496.851 cm^{-1}. a) Completely resolved *hfs* components observed in a LN$_2$-cooled HCL source with 10 mA discharge current. b) Increased spectral broadening and initiaition of self-absorption at 6 W microwave power in an EDL source. c) Complete self-absorbed spectral peaks observed with an EDL source at 22 W microwave power. The width values are also given for each *hfs* transitions. Here a,b,c,d,e and f represents the corresponding *hfs* transitions.

Second example of self-absorption peaks can be observed for a resonance line at 32588.201 cm^{-1} in the UV region. This is a transition between the levels ($^3P_0$)7s[0]1/2 - 6s^{2}6p^3 $^4S_{3/2}$ and leads to six *hfs* components in its original *hfs* pattern. As this transition is a resonance transition, even small discharge power may cause a strong self-absorption thereby destroying its

110

hfs structure. The transformation of the spectral features from the original *hfs* structure to a strong self-absorption structure, observed under various discharge conditions has been illustrated in Fig.4.13. Fig.4.13 (a) presents a completely resolved *hfs* structure, observed with LN_2-cooled HCL discharge at 4 mA DC current. This is the original *hfs* pattern for this transition with fully resolved structure. If HCL is not cooled and is operated at a DC current of 20 mA, few peaks get broadened, as shown in Fig.4.13 (b). Upon further increasing the DC current upto 45 mA, all peaks show the self-absorption pattern (Fig.4.13 (c)). The same transition was also observed in the EDL discharge of 8 W microwave power. Although, the operating power is low, the *hfs* structure was completely lost due to the strong self-absorption of all *hfs* components, as depicted in Fig. 4.13(d). At 17 W of microwave power, the *hfs* components get suppressed, as can be seen in Fig.4.13 (e), showing complete deformation from its original pattern.

Another example of self-absorption is shown in Fig.4.14 for a line at 34023.412 cm^{-1}. The spectra recorded with 6 W of microwave power in the EDL discharge shows a deformation from its original *hfs* pattren observed in the HCL discharge of 10 mA DC current. *Hfs* structure has been analyzed for the spectrum observed in HCL discharge and compared with the simulated spectra in Fig. 4.14..
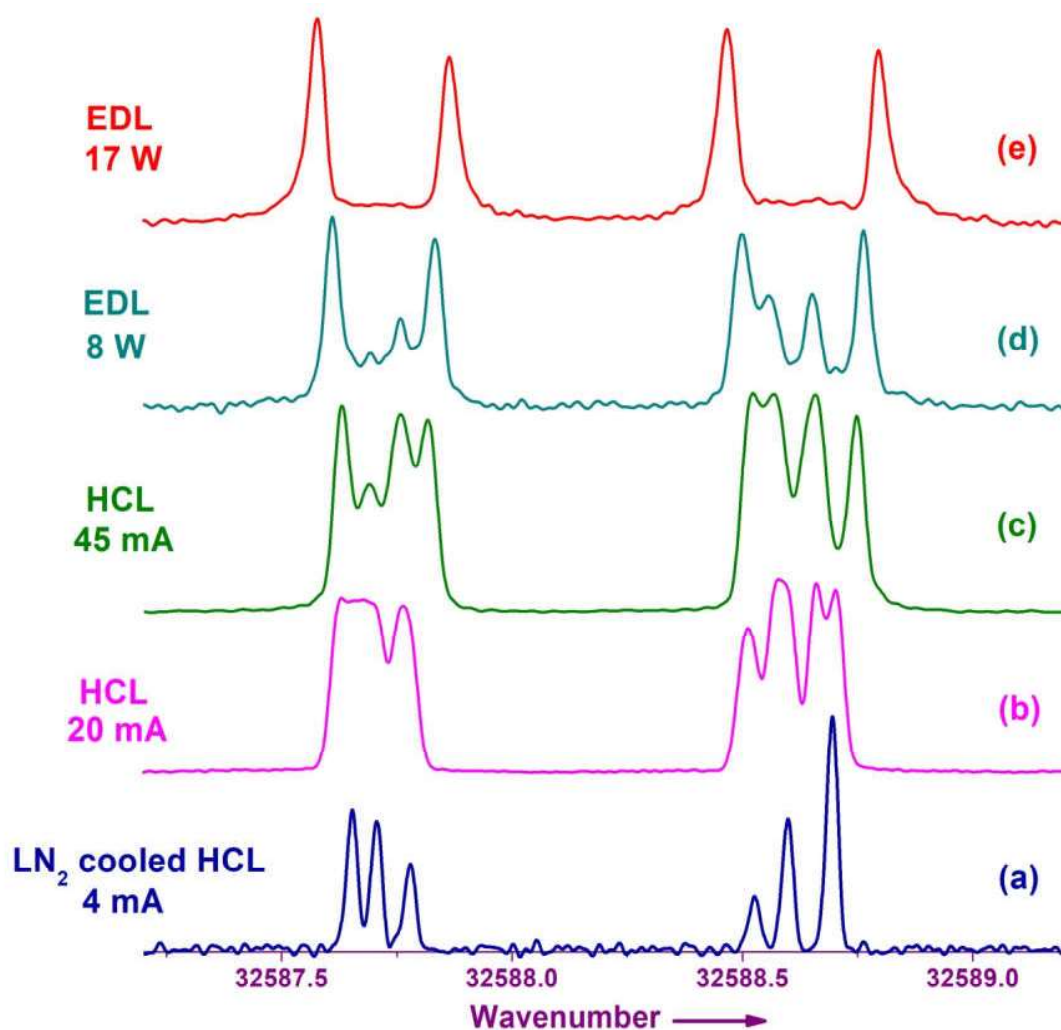
Fig. 4.13 Transformation of *hfs* structure from its original hfs structure to a strong self-absorption peaks for the line at 32588 cm^{-1}. a) Fully resolved *hfs* components observed in a LN$_2$-cooled HCL source with 4 mA discharge current. b) Broadening of few peaks and initiaition of self-absorption at 20 mA discharge current in without cooling HCL. c) All peaks were showing the self-absorption observed at 45 mA discharge current in without cooling HCL. d) Self-absorption of spectral peaks with an EDL source at 8 W microwave power. e) Complete deformation of *hfs* structure due to strong self-absorption with an EDL source at 17 W microwave power.

112
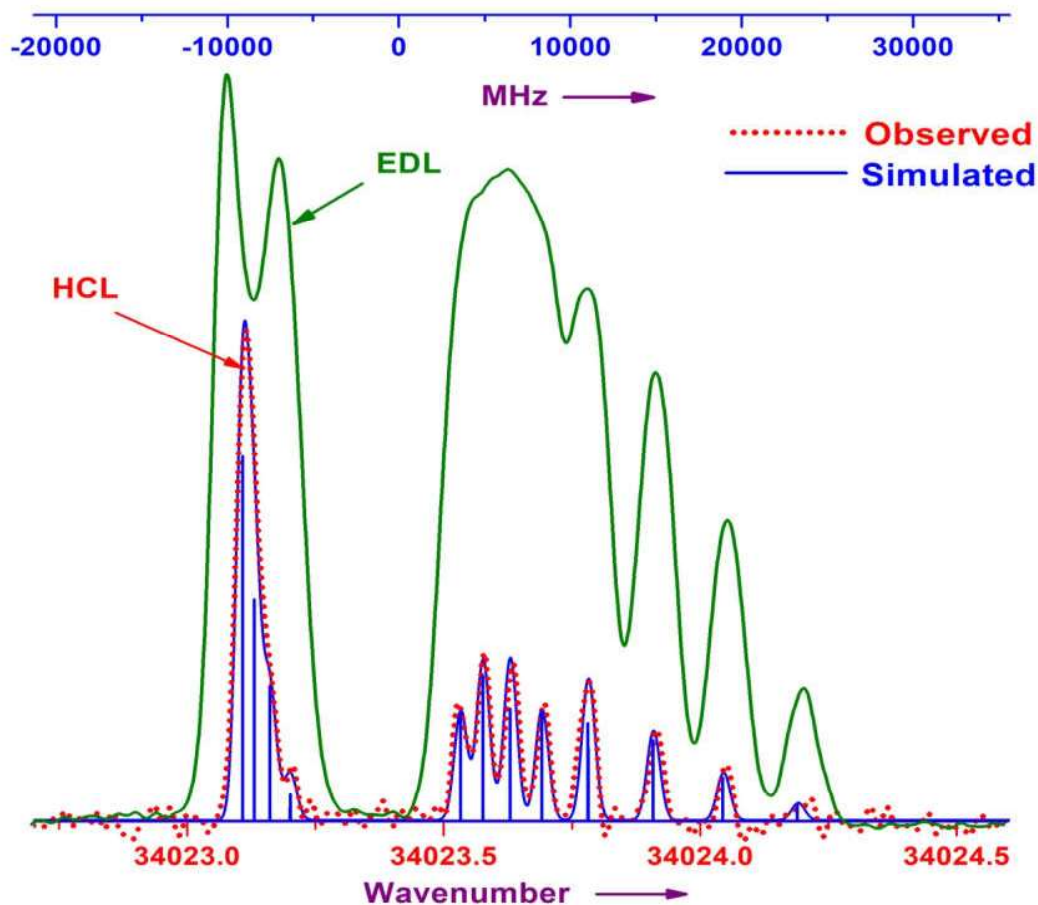
Fig. 4.14 Self-absorption spectral peaks observed for the line at 34023.412 cm^{-1} with an EDL discharge of 6 W power. Clearly resolved *hfs* pattren has been observed in a HCL discharge with 10 mA current. The simulated spectrum is matching well with the observed one using HCL discharge.

4.5 Blended Lines

Two blended lines have been identified at 6520 and 10359 cm^{-1}. For the line at 6520 cm^{-1}, the $F'' = 4 - F' = 5$ *hfs* component at 6520.313 cm^{-1} is completely overlapped by $F'' = 5 - F' = 5$ *hfs* component of 6520.391 cm^{-1}. The simulated and observed spectra of both transitions are depicted in Fig.4.15. The seperation between the two transitions (6520.391 - 6520.313 = 0.078 cm^{-1} = 2338 MHz) is in close agrement with the center of gravity difference 2198 MHz

113

calculated from the simulated spectra shown in Fig. 4.15. A common centre-of-gravity value 6520.383 cm^{-1} is given for both these transitions in Table 4.1.
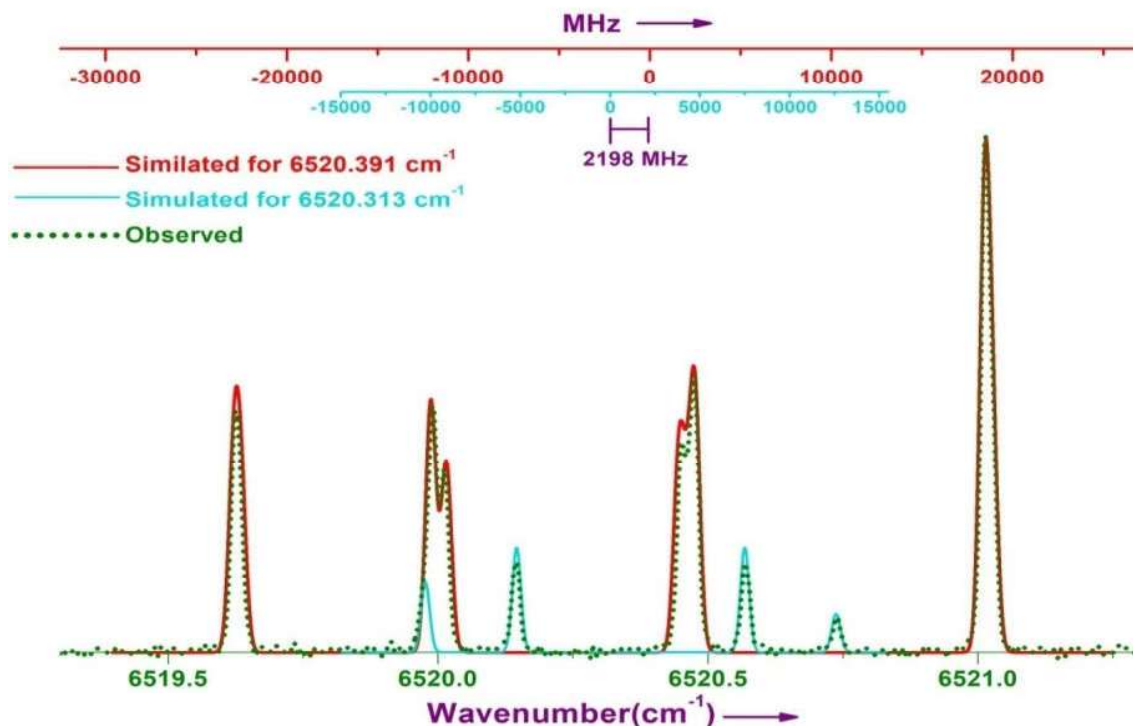
Fig. 4.15 A blend of two bismuth lines at nearly the same center of gravity wavenumbers (at 6520.391 cm^{-1} and 6520.313 cm^{-1}) has been observed. The individual lines are simulated and compared with the observed structure. The center of gravity difference of 2198 MHz between the two transitions is also shown.

As discussed in the previous section, BiI$_3$ was used for the EDL preparation, therefore a few iodine lines are present in the observed spectra. A blended line is identified near 10359 cm^{-1}, where iodine (I I) line (10360.259 cm^{-1}) [94] is found to appear inside the hfs structure of the Bi I line which is expected at 10359.866 cm^{-1}. The entire *hfs* structure of I I was contained between two successive *hfs* components of Bi I as shown in Fig.4.16. Both the transitions were simulated and compared with the observed spectrum. In this case also, the center of gravity difference

(11853 MHz) (shown in Fig.4.16) of the simulated spectra is mathching with the separation between the two transition (10360.259 - 10359.866 = 0.393 cm^{-1} = 11782 MHz) shown in Fig. 4.16. Both Bi I and I I transitions were included in the calculation of the centre-of-gravity value 10360.848 cm^{-1}, given in Table 4.1.
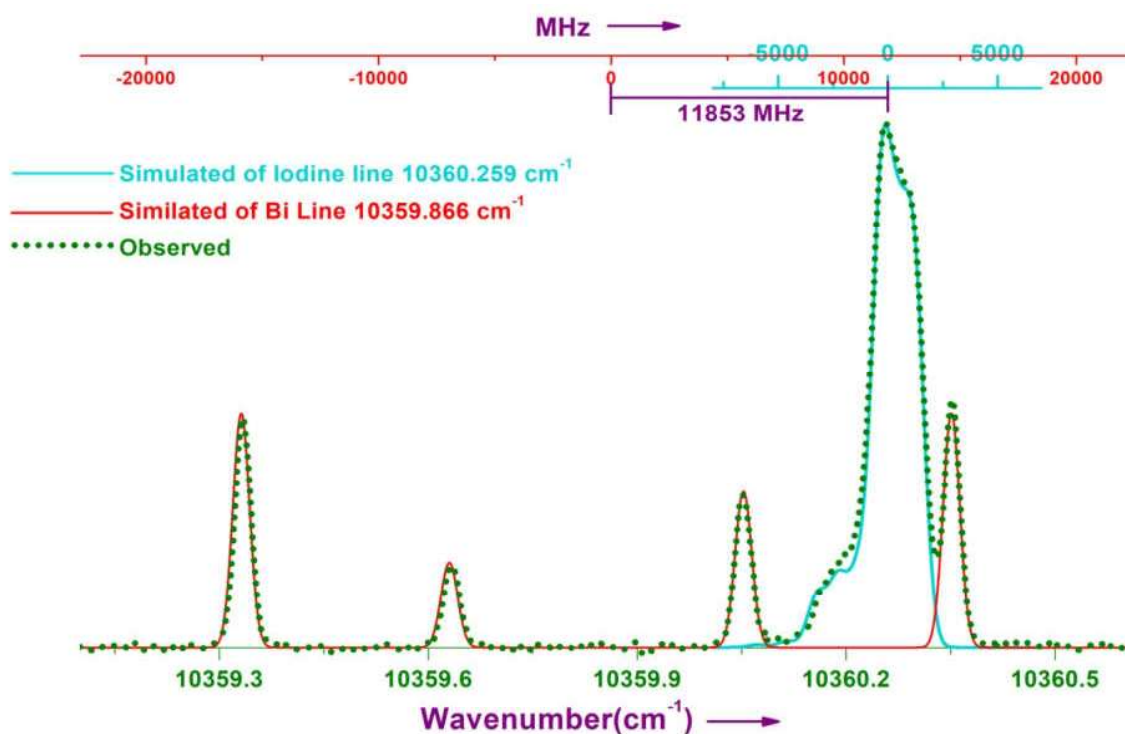
Fig. 4.16 A blended line formed by transitions in Bi I at 10359.86 cm^{-1} and I I at 10360.259 cm^{-1} is depicted along with simulated spectra. The center of gravity differences of 11853 MHz between the two transitions is also shown.

4.6 Conclusion

Emission spectra of atomic bismuth have been recorded in the spectral range from 2500 to 40000 cm^{-1}(IR to UV) using a Fourier transform spectrometer. EDL and HCL were utilized to generate the Bi plasma. A total of 107 spectral lines were observed in the entire spectral region. Hyperfine structure measurements have been performed on 76 lines, of which 21 have been

analyzed for the first time. The *hfs* constants A and B are derived for 14 even and 17 odd levels. Among those, A constants of 6 levels and B constants of 8 levels are reported for the first time. A brief discussion has been presented for the spectral line self-absorption in various operating conditions of EDL and HCL sources. In addition two blended lines were also identified at 6520 and 10360 cm^{-1}.

116

Chapter 5

Hyperfine structure measurements of singly ionized Iodine (I II) and Bismuth (Bi II)

5.1 Hyperfine structure measurements of singly ionized Iodine (I II)

Lacroute [24] and Murakawa [25,95] studied the strong lines of I II spectrum and classified the *hfs* spectral transitions for the ground $5s^2 5p^4$ configuration and excited levels belonging to the $5s^2 5p^3(^4S)nl$, $5s^2 5p^3(^2D)nl$, and $5s^2 5p^3(^2P)nl$ configurations and also determined the nuclear spin value 5/2. Murakawa [28] evaluated the *hfs* constants for 5 odd parity and 3 even parity energy levels. To determine the nuclear spin value as 5/2, Fry & Fisher [26] carried out, Zeeman Effect experiments in the hyperfine structure of I II. In the *hfs* measurements on six fine structure transitions in visible region using laser technique, Fowles et al. [29,96] reported that only one *hfs* component in each fine structure transition is sufficiently strong enough to be used for laser application. Willet and Heavens [97] observed a laser transition at 651.6 nm, corresponding to the intercombination $((2D^0)6p\ ^3F_2 - 5p^5\ ^1P_1)$ transition. Martin et al. [27] used electrodeless discharge lamps to observe the emission spectra of I II and reported 2400 fine structure transitions within 120 even and 190 odd parity levels. Labat et al. [98] measured Stark broadening effects for I^+ as well as I^{++} in pulsed linear arc plasma and derived the Stark broadening parameters for three spectral lines of each. Kono et al. [99] reported radiative lifetime measurements for I I and I II. A Global Model of iodine plasma was developed by Katsonis et.al. [100] and Grondeinet et.al. [101]. These authors have generated the spectra of I I by IDGM model and have drawn a comparison with the experimental data, for applications in electric thrusters. They have also generated the I II spectra from 450 to 700 nm spectral region. But, due to lack of sufficient experimental data, they could not compare the generated spectra of I II. Thus, as also emphasized by Katsonis et. al.[100], detailed experimental investigations on I II spectra are required for fundamental as well as technological applications.

We have observed the atomic emission spectra of I II in the spectral region 12000 −
24000 cm^{-1} with well resolved *hfs* structures, using the Fourier transform spectroscopy technique
and is discussed in this chapter. The *hfs* constants *A* and *B* for the energy levels are deduced to
get more atomic parameters of I II spectra. The *hfs* database generated from the experimental
methods is very useful in various spectroscopic investigations and development applications.

5.1.1 Experimental conditions for observing I II spectra

Fourier transform spectroscopy coupled with microwave discharge method was
employed in the present work to record the singly ionized iodine spectra. EDLs were used as a
source of iodine plasma, which were sealed with 1 mg of iodine and 1 mbar of buffer gas (Ne).
Iodine is naturally available as I_2 molecule but the dissociation energy (1.58 eV) is less than the
molecular ionization energy (9.3 eV) [102], because of which it can be easily dissociated into
iodine atoms. The collision of buffer gas with iodine atoms produces the plasma inside EDL. In
normal conditions, spectral transitions of I I are dominant and only few strong lines of I II were
observed. As discussed by Martin et al. [27] and Hargus et al. [6], the source temperature should
be brought down below 261 K - 245 K to observe the I II spectral transitions predominantly. To
achieve this condition, we have made an experimental arrangement as described in Chapter 2,
where, both the microwave cavity and EDL were cooled with nitrogen gas which was passed
through a liquid nitrogen bath. The temperature of the discharge tube was stabilized by
controlling the flow of cooled nitrogen gas by a valve. The spectra were recorded only after
achieving a stable discharge condition. A Pt-100 temperature sensor was used to measure the
temperature of the source and the same is substantiated from the Doppler width of the Ne lines.

The emission light from the EDL was focused onto the 1 mm entrance aperture of the FTS by using elliptical and parabolic mirrors. To record the spectra in the region 12000 to 24000 cm^{-1}, CaF$_2$ and quartz-visible beam splitters were used. Silicon diode and photo multiplier tube (PMT) detectors were employed to cover the complete wavelength range. Depending upon the spectral region, several band pass filters have been used to enhance the S/N ratio by avoiding neighboring intense lines from the spectrum, so as to detect the lines with weak intensity. The complete experimental details used for the data acquisition such as spectral region, resolution, no. of scans and optics are given in Table 5.1 (Appendix I). Although various instrumental resolutions were applied to check the appearance of I II and their intensities, the spectral analysis was carried out using only the high resolution spectrum with good S/N ratio.

5.1.2 Hyperfine structure investigations

A total of 141 spectral lines of I II have been observed in the entire spectral range of 12000 to 24000 cm^{-1}. Out of these 141 spectral lines, 73 lines have good S/N and have fully or partially resolved hyperfine structure and these have been used to derive *hfs* constants. Center of gravity wavenumbers have been calculated for the remaining 74 lines. The spectral classification has been done by identifying the lines referring Martin et al. [27]. The recorded spectra were averaged for specific filtered spectral region and calibrated with standard Ne lines [65]. The calibration procedure has been discussed in Chapter 2. The derived calibration constants are given in Table 5.1 for each spectral region and resolution. The *hfs* analysis was carried out by iterative least-squares fitting programs, developed by Kumar et al. [66]. The method of derivation of *hfs* constants has been discussed in Chapter 2.

120

The accuracy of *hfs* constants depends upon the width of resolved *hfs* components. Therefore, the measurements have been repeated several times by choosing various resolutions to obtain well resolved *hfs* components. While high resolution spectra were useful in observing the *hfs* components of intense lines with ease, lowering the resolution was helpful in measuring the relatively less intense lines with good S/N ratio. The noise levels increase as we go to high resolution measurements, which lead to noisy spectra for low intense lines, hindering the identification of *hfs* components. Therefore, relatively lower resolution spectra are recorded when the S/N ratio levels are poor in high resolution spectra. Hence, to get accurate *hfs* constants from the observed 141 transitions, analysis has been performed only on 73 selected transitions, which were fully or partially resolved and also having good S/N ratio.

Hfs structures of few observed transitions at 17506, 18186, 18294 and 19245 cm^{-1} were depicted along with simulated spectrum in Figs. 5.1- 5.4.
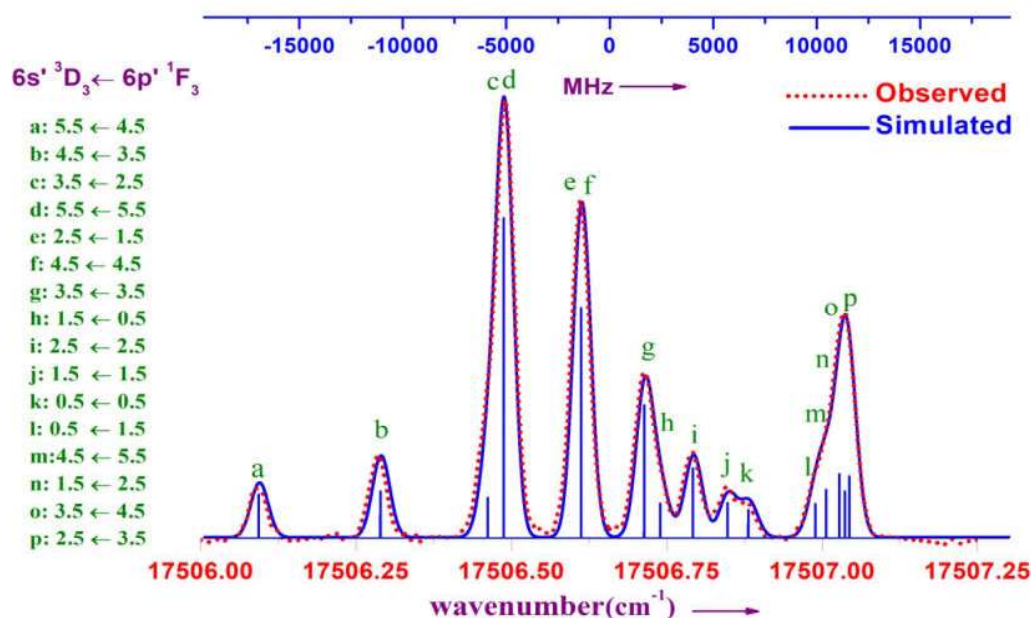
Fig. 5.1 Spectral transition of I II showing the *hfs* splitting at 17506 cm^{-1}. The observed and simulated spectra were compared to each other and are matching well. F″←F′ transitions are indicated by a,b,c,d,…. (a:F″←F′).
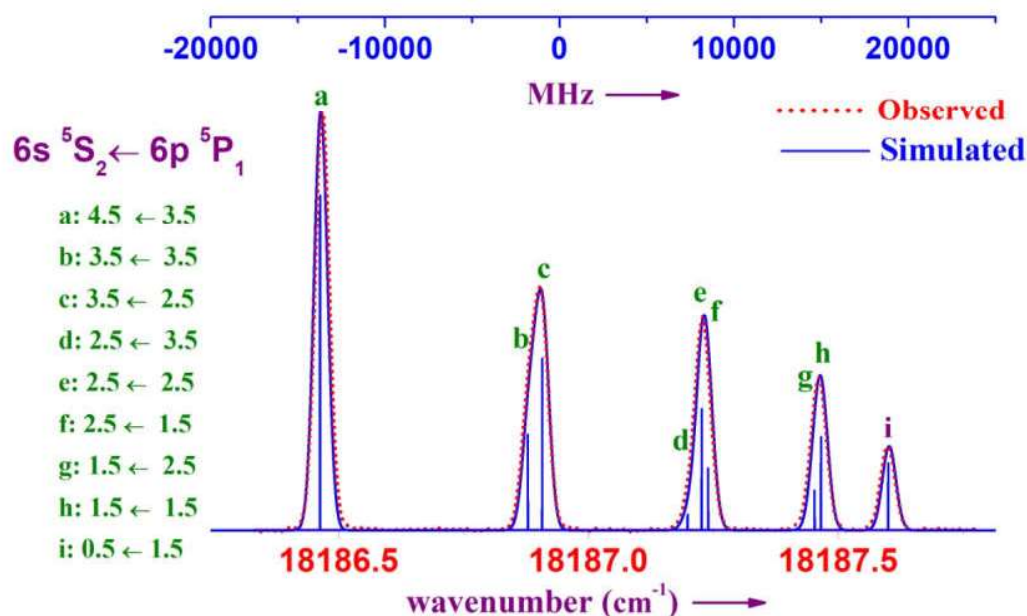
Fig. 5.2 Spectral transition of I II showing the *hfs* splitting at 18186 cm^{-1}. The observed and simulated spectra were compared to each other and are matching well. F″←F′ transitions are indicated by a,b,c,d,…. (a:F″←F′).
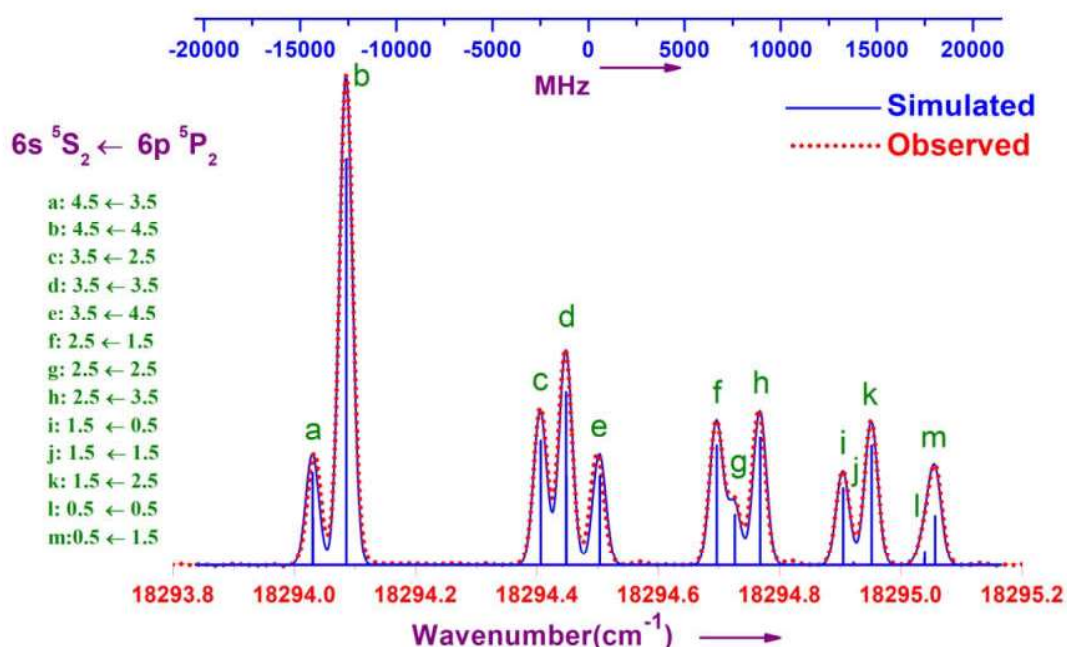
Fig. 5.3 Spectral transition of I II showing the *hfs* splitting at 18924 cm^{-1}. The observed and simulated spectra were compared to each other and are matching well. F″←F′ transitions are indicated by a,b,c,d,…. (a:F″←F′).
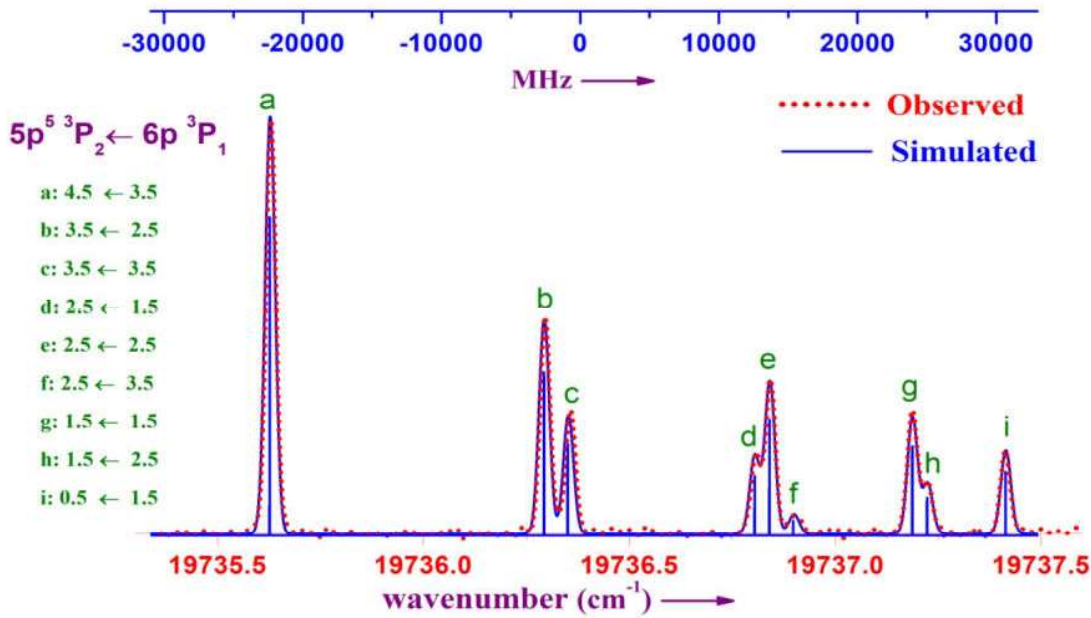
Fig. 5.4 Spectral transition of I II showing the *hfs* splitting at 19736 cm^{-1}. The observed and simulated spectra were compared to each other and are matching well. F″←F′ transitions are indicated by a,b,c,d,…. (a:F″←F′). All *hfs* components were resolved in the observed spectrum.

The newly derived center of gravity wavenumber values of 141 observed spectral transitions and their corresponding fine structure energy levels with electronic configurations have been tabulated in Table 5.2 (Appendix I). Center of gravity values given in Table 5.2 are the averages of center of gravity derived in various measurements given Table 5.1. Since FTS is a well calibrated instrument, the wavenumbers are obtained with 3rd as well as 4th decimal accuracy. The uncertainties are derived from the standard deviation of center of gravity wavelengths. Few unclassified lines of I II observed by Martin et al. [27] have also been observed in the present investigations, which confirm their presence in the I II spectra. These lines are indicated by * in Table 5.2.

Hfs measurements were performed on 73 spectral lines to derive the *A* and *B* constants for 61 energy levels (29 even parity and 32 odd parity). All these *hfs* constants *A* and *B* of even

and odd parity levels are listed in Table 5.3 and Table 5.4 (Appendix I) respectively. The previously reported [97] *hfs* constants for eight levels are compared with the present work in Table 5.3 and Table 5.4. Uncertainties of A and B constants were derived as discussed in Chapter 2. In the current investigations, many of the levels are present in more than one transition. For those levels, standard deviations are reported as uncertainties. For the levels present in only one transition, repeated measurements were carried out on that single transition at different instrumental resolutions and *hfs* analysis were examined in each case. The derived A and B constants were slightly different in each measurement. The uncertainties in A and B constants were estimated from these differences of a single transition.

5.1.3 Blended line at 20611 cm^{-1}

One blended line has been observed in the emission spectra of iodine at 20611 cm^{-1}, which is due to the overlap of neutral iodine and singly ionized iodine lines at nearly the same wavenumber position. These lines are at 20611.51 cm^{-1} for I II transition belonging to $J'' =1$ and $J' =1$ levels (9 *hfs* components) and at 20611.37 cm^{-1} for of I I transition belonging to $J'' =1.5$ and $J' =1.5$ levels (10 *hfs* components). The center of gravity wavenumber value is compulsory to derive the calculated profile, which is not possible in the present case for individual I II and I I transitions. So, the A and B values used for I II transition were derived from the other transitions having these energy levels (101644 and 81032 cm^{-1}). The constants were refined to derive the calculated profile until it matches the observed profile. The same procedure was applied for I I transition also. A common center of gravity value 20611.51 cm^{-1} has been assigned for both the transitions. *Hfs* constants A and B used to derive the calculated profile for these transitions of I II and I I are given in Table 5.5 (Appendix I).

Fig. 5.4 represents the observed blend line and simulated spectra of I II and I I. The difference in center of gravity wavenumbers of I II and I I has been calculated from the simulated spectra as 4197 MHz, matching with the difference in their center of gravity values derived from their energy levels difference (20611.51 cm^{-1} − 20611.37 cm^{-1} = 0.14 cm^{-1} = 4197.1 MHz).
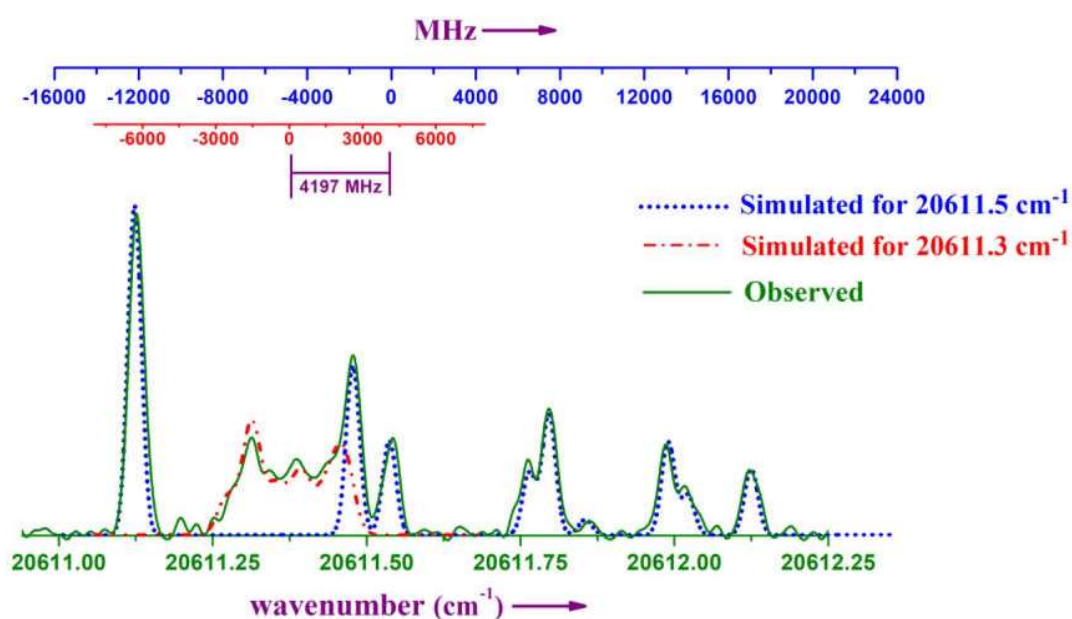
Fig. 5.5: An observed blend line belonging to I II at 20611.5 cm^{-1} and I I at 20611.3 cm^{-1} is depicted along with simulated spectra. The center of gravity differences of 4197 MHz between the two transitions are also shown.

5.1.4 I II Transition at 695.8 nm and its importance

One of the major applications of iodine is in space communication as electrostatic spacecraft propellant. In general, xenon (Xe) is the most preferred propellant due to its high atomic mass (131 amu), relatively low ionization potential (12.1 eV) [6] and inert nature. But, the low concentration of Xe in the atmosphere makes it necessary to search for alternatives spacecraft propellants. Among all the considerable elements (Kr, Bi, I etc.), iodine is the best choice as its mass (126.9 amu) is close to Xe and is having a low ionization potential (10.45 eV).

Hargus et al. [6] worked on the iodine electrostatic propulsion diagnostics development and identified the Laser induced fluorescence (LIF) transitions of singly ionized iodine to examine the plasma acceleration within an electrostatic plasma propulsion thruster. In their search for identification of suitable LIF transition from the meta-stable state $5d^5D_4$, it was found that the transition at 695.8 nm is a suitable choice for this application.

The transition at 695.8 nm (14366.3cm^{-1}) has been observed and analyzed in the present work. The *hfs* constants A and B were derived for both upper and lower levels. As predicted by Hargus et al. [6], these A values were positive and the energy levels were non- inverted. But the *hfs A* constant for lower state has been obtained as negative ($A'' = - 47$ MHz), whereas it is found to be positive ($A' = 134$ MHz) for the excited state. So, the energy levels were inverted for lower level and non-inverted for higher level. The observed and simulated spectra of the transition at 14366 cm^{-1} is shown in Fig. 5.6(a) and the corresponding energy level diagram is shown in Fig. 5.6(b).
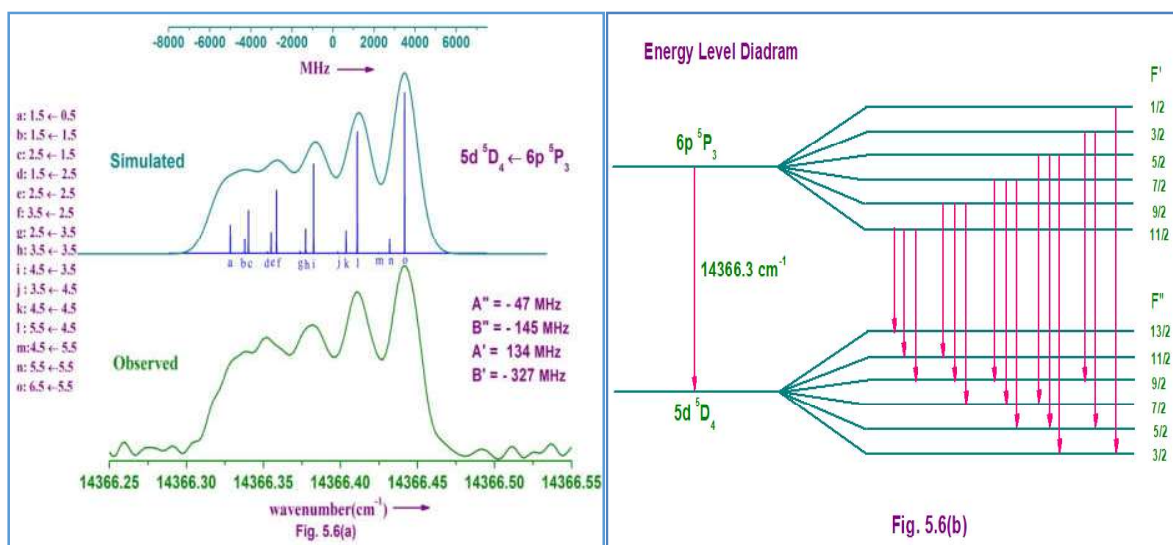
Fig. 5.6 (a) Partially resolved *hfs* structure of a line at 14366 cm^{-1} is shown. **(b)** Corresponding energy level diagram and *hfs* transitions for 14366 cm^{-1} line.

127

5.2 Hyperfine structure measurements of singly ionized Bismuth (Bi II)

In 1930, the first spark spectrum of bismuth was observed by McLennan et al [103] in the spectral range of 705.0 to 134.0 nm, which identified the evidence of hyperfine structure in Bi II and Bi III spectra. Fishar and Goudsmith, in 1931 [104], made experimental and theoretical measurements of hyperfine structures on 21 lines of Bi II spectra. The term schemes for the energy levels and energy level separations were also reported and compared with the values obtained using theoretical relation given by Goudsmith [46]. In 1933, Crawford et al [105] reported extended investigations of the spark spectrum of Bi II in the spectral region of 100.0 to 1000.0 nm. The hyperfine structures in five multipole lines of ground configuration of Bi II were reported by Cole [106], by exciting high frequency electrodeless discharge lamps. *Hfs* investigations were carried out on a pure electric quadrupole transition at 587.0 nm between the two ground configuration levels by Arcimowicz [107]. Subsequently, Photo-absorption spectrum of atomic bismuth was obtained in the spectral region 40.0 to 200.0 nm using a 3 meter normal incidence spectrograph [108]. In this work, the identification of an extended series $6s^2 6p^2$ $^3P_0$ - $6s^2 6pn$d $^3D_1$ (n = 6→14) in Bi II spectra was noticed and a new value of the ionization potential of Bi II as 134720 ± 30 cm^{-1} (16.7 eV) was reported. In 1987, Stachowska [109] performed the *hfs* measurements on nine spectral lines of Bi II and also investigated the hyperfine structure for the ground configuration levels. During the same period, the *hfs* of low-lying levels of Bi II were studied by Bouazza [110], by observing the Far UV lines of Bi II spectra using HCL discharge. In 1996, Grabowski [111] analyzed the *hfs* and Zeeman splitting of nine lines from the array 6p7p → 6p7s and two lines at 496.9, 581.8 nm of Bi II spectra.

The theoretical nuclear magnetic moment and electric quadrupole moment from the sl - configurations of Bi II were derived by Crooker and Shipley [112] in 1970, also reporting three new A - factors. In another theoretical work, Holmgren [113] reported the relativistic analysis of magnetic dipole and electric quadrupole interaction in the 6p7s configuration of Bi II, where hyperfine interaction constants were derived using Hartree-Fock (HF) wavefunctions. In 2001, A detailed analysis of Bi II transition probabilities has been presented by Palmeri [114], using the Hartree-Fock method with relativistic corrections and the multi-configuration Dirac-Fock fully relativistic approach.

The spectroscopic investigations of Bi II obtained from the laboratory analysis are not only of interest for technical applications, such as diagnosis for Hall-thrusters [7,115] as discussed earlier, but have also found importance in astrophysical observations. While investigating the astrophysical relevance of bismuth, Wahlgren et al. [41] had detected Bi I, Bi II and Bi III transitions in the high resolution spectra of chemically peculiar HgMn stars: χ- Lupi and HR777, obtained using the Goddard high resolution spectrograph onboard the Hubble telescope to calculate the Bi abundance. In 2002, Dolk [42] determined the *hfs* constants A and B for 56 Bi II levels by analyzing the 104 Bi II lines observed from the emission spectra of bismuth using Fourier Transform Spectrometer. From the laboratory measurements, it has been established that bismuth is present in HR 7775 at an enhancement level of nearly 5 orders of magnitude relative to the meteoritic abundance. Astrophysical *gf* values were also reported for a number of Bi II lines.

However, most recently in 2013, Andrzejewska [116] presented the spectra of Bi II in a wide wavelength range of 74 - 620 nm. In this work, further new levels (total 10) were observed and 91 new lines were classified, whereas six new *hfs* A constants were also determined, thus

highlighting the need for thorough re-investigations on the spectra of ionized bismuth species in well optimized experimental conditions to improve the precision of *hfs* constants and search for the missing lines, if any. Thus, we have measured the high resolution emission spectra of Bi II in the spectral range 13000 - 40000 cm^{-1} with optimized experimental conditions as described below.

5.2.1 Experimental details

The spectra were recorded using two discharge methods, i.e. using EDL as well as HCL. The advantages and limitations of these two techniques have been discussed in Chapter 4 of this thesis. EDL containing BiI$_3$ and HCL containing Bi$_2$O$_3$ were excited by microwave discharge and DC discharge respectively. The emitted light has been observed by FTS, which was equipped with different beam splitters (Qrtz Vis and Qrtz UV) and appropriate detectors (Si diode, PMT-Vis, PMT-UV) to cover the spectral range 13000 - 40000 cm^{-1}. Various instrumental resolutions were applied up to the highest resolution of 0.016 cm^{-1}. Several band pass optical filters were used in the visible and UV spectral regions to enhance the S/N ratio as well as to observe the weak transitions. As described in Chapter 2, HCL was operated at low temperature condition using liquid nitrogen to minimize the Doppler broadening of *hfs* components.

5.2.2 Hyperfine structure investigations

A total of 45 spectral lines have been detected in the emission spectra of Bi II in the spectral range 13000 - 40000 cm^{-1}. Table 5.6 (Appendix I) represents the newly derived center-of-gravity wavenumber values of the spectral lines and their corresponding energy level designations. Among these 45 observed spectral lines, 33 lines were chosen to perform the *hfs*

measurements, which are having well separated *hfs* components and good S/N. The corresponding lines are indicated in the last column of Table 5.6. Few observed and simulated spectra of Bi II have been depicted in Figs.5.7-5.11.

Fig. 5.7 shows a completely resolved structure of a line at 17678.046 cm^{-1} between the levels 6p5f (1/2,5/2)2 and 6p7s (3/2,1/2)2. The observed and simulated spectra have been compared in Fig 5.7 and are matching well with each other. Fig. 5.8 illustrates the *hfs* structure of the line at 19191.008 cm^{-1} between the levels 6p7p (1/2,3/2)2 and 6p7s (1/2,1/2)1. This line is also completely resolved and spans a range of 4 cm^{-1}. Since, the source contains Ne as a buffer gas, one line of Ne at 19192 cm^{-1} appeared as a blended line with one *hfs* component of Bi II, indicated in Fig. 5.8. The simulated spectra have also been shown in the same figure, which shows a good match. The fully resolved *hfs* structure of the line observed at 20020.313 cm^{-1} corresponding to the transition 6p7p (3/2,3/2)2 - 6p7s (3/2,1/2)1, along with its simulated pattern, has been presented in Fig.5.9. Transition between the levels 6p7p (3/2,1/2)2 - 6p6d (1/2,3/2)1 results in a line at 24508.468 cm^{-1}. Few *hfs* components of this transition could not be fully resolved (Fig.5.10). The simulated and observed *hfs* structures were matching well, as depicted in Fig.5.10. A partially resolved *hfs* structure for a line at 35637.300 cm^{-1} corresponding to the transition 6p6f (1/2,5/2)2 - 6p6d (1/2,3/2)1 in the UV region, has been observed. The simulated and observed structure is shown in Fig.5.11. In this case, out of nine *hfs* ($J = 2 - J = 1$) components, seven were observed.
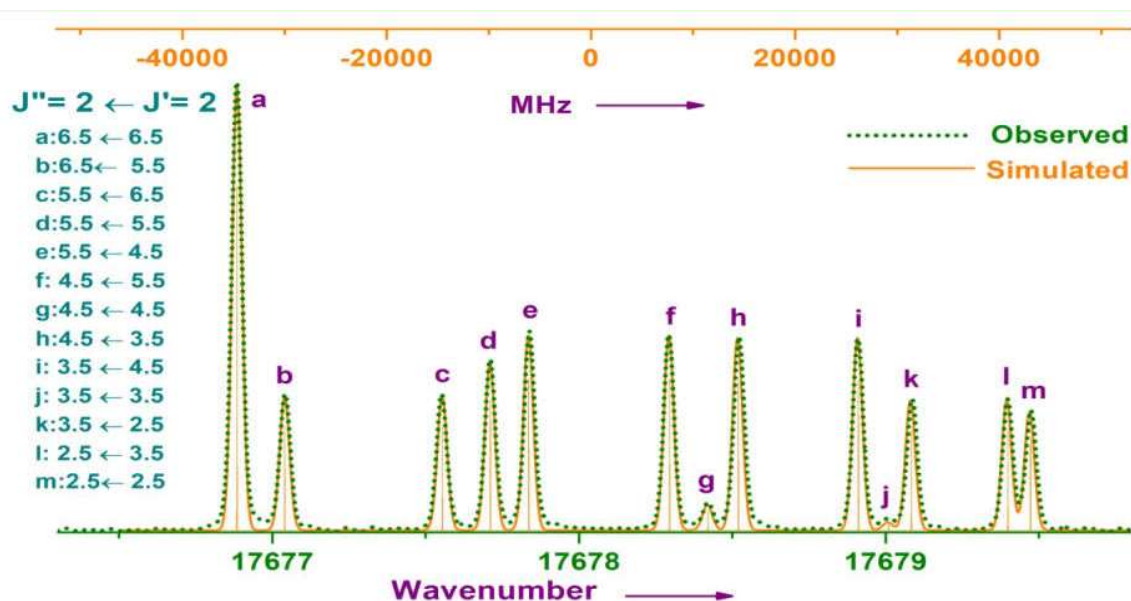
Fig. 5.7 Shows a line at 17678.046 cm^{-1} between the levels 6p5f (1/2,5/2)2 and 6p7s (3/2,1/2)2. All 13 *hfs* components are fully resolved. The observed and simulated spectra are matching well.
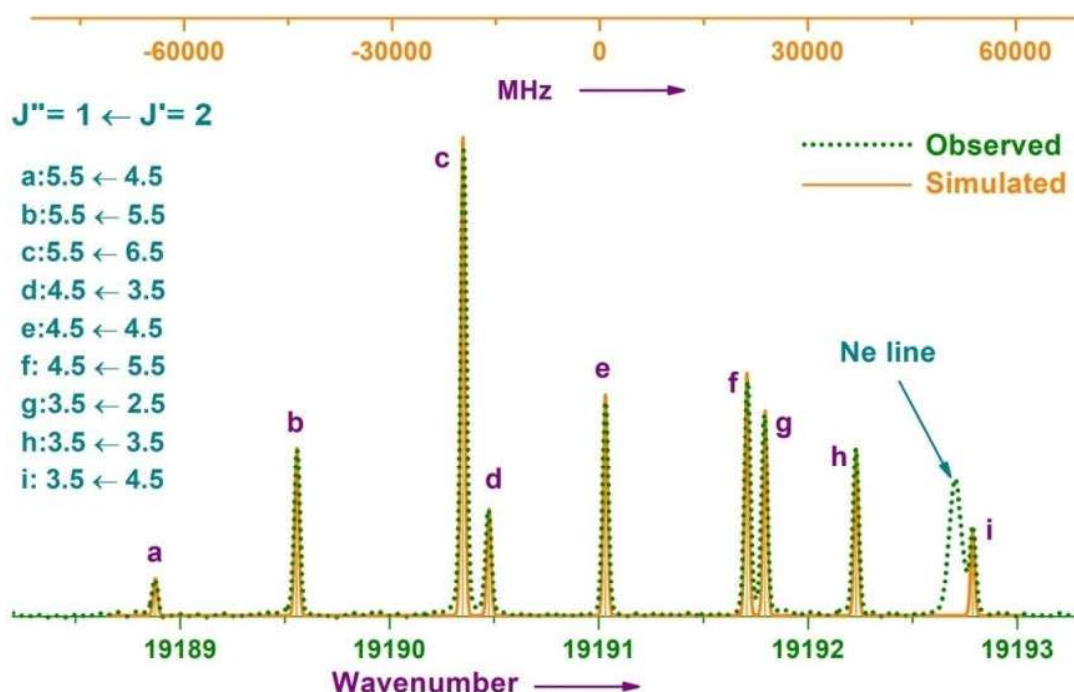
Fig. 5.8 Illustrates the *hfs* structure of the line at 19191.008 cm^{-1} between the levels 6p7p (1/2,3/2)2 and 6p7s (1/2,1/2)1. All nine *hfs* components are observed. One Ne line is also present at 19192.7 cm^{-1}.
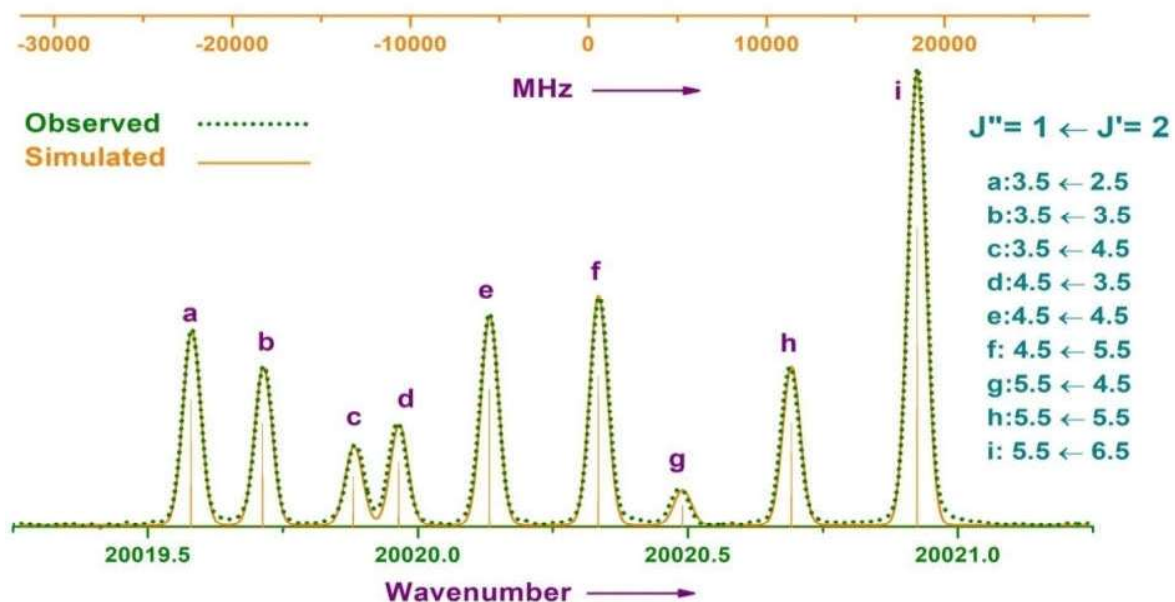
Fig. 5.9 A completely resolved *hfs* structure of the line at 20020.313 cm^{-1} corresponding to the transition 6p7p (3/2,3/2)2 - 6p7s (3/2,1/2)1.
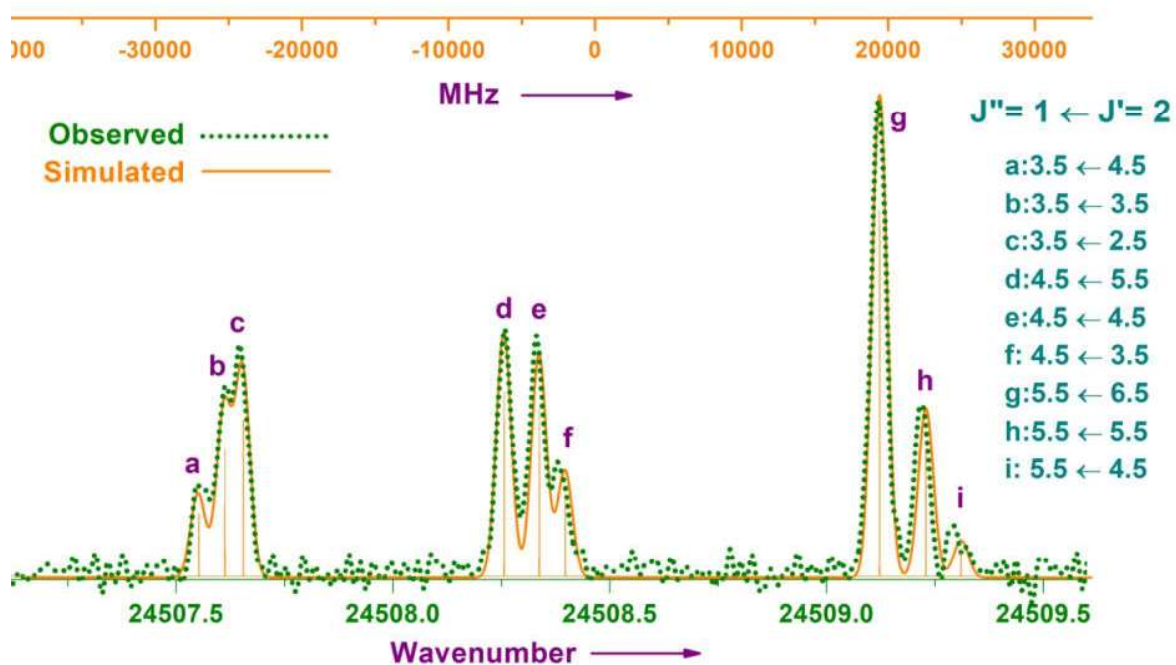
Fig. 5.10 Shows the simulated and observed *hfs* structures of the line at 24508.468 cm^{-1} between the levels 6p7p (3/2,1/2)2 - 6p6d (1/2,3/2)1.
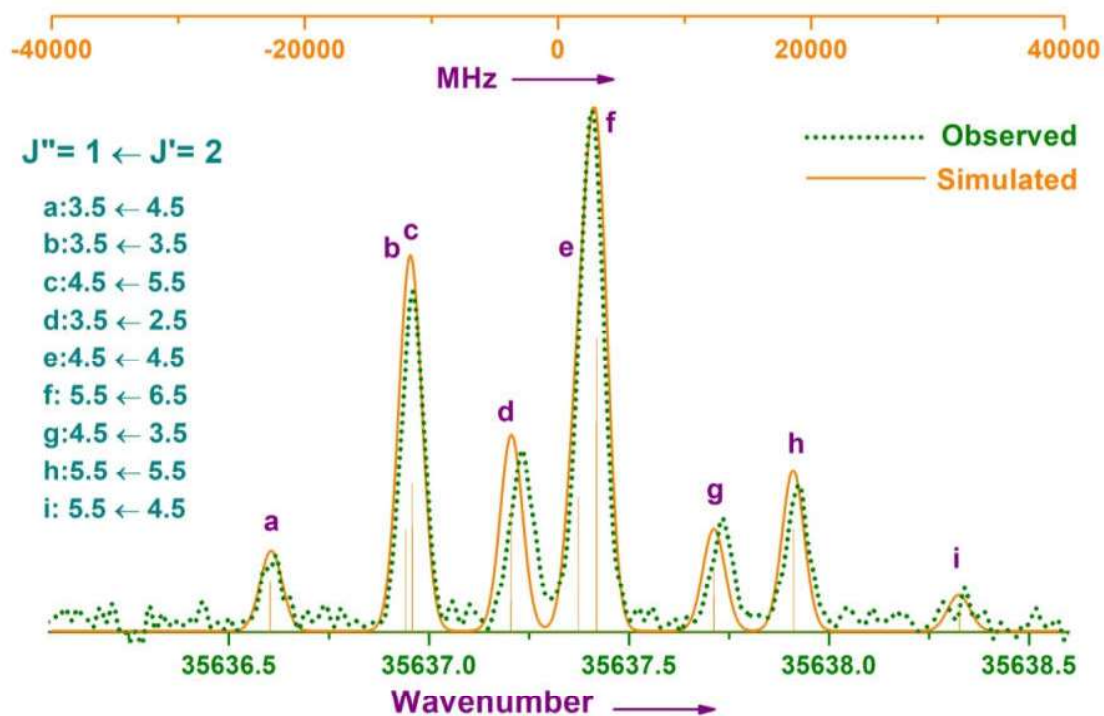
Fig. 5.11 A partially resolved *hfs* structure of a line at 35637.300 cm^{-1} corresponds to the transition 6p6f (1/2,5/2)2 - 6p6d (1/2,3/2)1. The simulated structure is also given along with the observed spectrum.

Hfs investigations were carried out on 40 energy levels, which are involved in 33 spectral transitions. *Hfs* constants were determined for all 40 energy levels. Among these 40 levels, 23 correspond to the even parity and 17 to the odd parity levels. The derived *A* and *B* constants for 23 even parity levels have been presented in Table 5.7 (Appendix I) along with their energy level designation. For 17 odd parity levels, Table 5.8 (Appendix I) represents the energy levels and their corresponding derived *hfs* constants. Along with the *hfs* constants determined in this work, previously reported values are also given in Table 5.7 and Table 5.8.

5.3 Conclusion

A total of 141 spectral lines were observed from the emission spectra of I II, using high resolution Fourier transform spectrometer in the spectral region 12000 - 24000 cm^{-1}. Microwave discharge method was employed to generate iodine plasma in the EDL. The center of gravity wavenumber values of all the observed lines have been reported. Hyperfine structure investigations were performed on 73 transitions and the corresponding *hfs* constants were derived for 61 energy levels (29 even parity and 32 odd parity). One blended line at 20611 cm^{-1} has been observed and analyzed. *Hfs* was analyzed for a line at 695.8 nm, which is useful for the Laser induced fluorescence transition for technological applications.

Emission spectra of singly ionized atomic Bismuth (Bi II) have been re-visited using Fourier transform spectrometer in the spectral range of 13000 - 40000 cm^{-1} (Near IR to UV). Electrodeless discharge lamps and LN$_2$ cooled Hollow Cathode Lamps were utilized to generate the Bi plasma by means of microwave and DC discharge methods, respectively. In the present investigations, 45 spectral lines were observed. Hyperfine structure measurements were carried out on 33 lines to determine the *hfs* constants *A* and *B* for 40 energy levels.

Chapter 6

Forbidden Transitions

Introduction

The selection rules and transition probabilities for atomic radiation have been formulated for the electric dipole radiation which is significantly more intense than the higher order multipole radiation emitted. Forbidden transitions are those transitions which do not follow these rules. Thus, some lines detected in the spectra of terrestrial objects remain un-classified. Mrozowski [38] classified the forbidden lines as those with extremely small transition probabilities compared to the highest transition probabilities between levels of approximately the same total quantum numbers in an atom.

In 1928, while Bowen [118] described such lines in terms of the transitions among low-lying metastable states and ground states of the neutral and highly ionized atomic configurations, Rubinowicz [119] utilized second order radiation theory for electric quadrupole radiation and calculated selection rules for multipole radiation, which are different, not only from those for electric dipole radiation, but also for different order multipoles. In 1932, Brinkrnan [120] showed that the first order term corresponding to a radiation of a magnetic dipole also contributes to the forbidden transitions. Since then, there have been many reports on the theory of forbidden lines and substantial experimental work has been carried out [121-123].

For most neutral atoms and ions, the energy levels of ground configuration lie below all the levels of excited configurations and hence are meta-stable. For most of the forbidden transitions, the upper energy level is meta-stable state. Most observed forbidden lines are therefore produced by transitions within ground configuration. These are 'forbidden', as such transitions from meta-stable states to lower levels are not allowed by electric dipole radiation.

The concentration of the atoms in the meta-stable states is proportional to the intensity of the forbidden lines. Also the intensity of these forbidden lines provides the information on the

density, temperature, chemical composition, and other important properties of various extra-terrestrial bodies. Forbidden lines are also important in nuclear spectroscopy and these forbidden lines in gamma spectra are generally more intense than the allowed lines.

Thus, the exact line position identification and analyzing the forbidden lines from the laboratory data is very much useful in the astrophysical observations. In general, these lines are easily observable in the spectra of low density sources of highly ionized atoms present in the interstellar regions. In the present work, an attempt has been made to observe the forbidden transitions of I I, I II, Bi I and Bi II using EDL source. As these forbidden transitions are weak in nature, we could observe them only in strong discharge sources during our experiments. EDL, being a strong discharge source, could be utilized to observe and study the forbidden transition lines with significant intensity. Hyperfine structure investigations were performed on these lines to determine the *hfs* constants.

6.1 Forbidden transitions in I I and I II spectra

The ground configuration of neutral iodine$5s^2 5p^5$ has two fine structure terms $^2P_{3/2}$ and $^2P_{1/2}$. Only one forbidden transition can be observed between these ground configuration terms at 7602.970 cm^{-1}.

In 1954, Eshbach and Fisher [17] reported the line at 13149.19 nm (7602.9 cm^{-1}) by observing the iodine spectra using electrodeless discharge lamp with high resolution spectrograph. But they were not able to classify this transition. Later in 1959, Kiess and Corlis [15] designated the line as a forbidden transition between the levels and calculated the corresponding wavenumber as 7603.15 cm^{-1}. The Zeeman Effect on this transition was observed by Verges by using SISAM spectrometer [124]. In 1973, Luc-Koeng et.al [125] performed the hyperfine structure measurements on this line by means of Fourier transform spectrometer and determined the *hfs* constants for both the levels. Further in 1980, Engleman et al [76] reported the high-resolution Fourier transform spectra of ^{127}I and ^{129}I by exciting electrodeless discharge lamps.

Singly ionized iodine has the ground state configuration $5s^2 5p^4$ with five fine structure levels$^3P_2$, $^3P_0$, $^3P_1$, $^1D_2$ and $^1S_0$.Transitions among these meta-stable states may cause the appearance of forbidden lines in I II spectra.

In 1960, Martin and Corlis [27] observed the two forbidden transitions at 728.2 nm (13727 cm^{-1}) and 446.0 (22414 cm^{-1}) nm in the electrodeless discharge of I II spectra. Both the lines were classified to be the transitions between the ground configurations terms. The Zeeman pattern was also observed for these transitions. Later in 1975, Morillon and Verges [126]

reported the hyperfine structure of the line at 7086.88 cm^{-1} corresponding to the $^3P_1$ - $^3P_2$ transition between the ground configuration terms.

6.1.1 Experimental details

A similar experimental set up has been employed as described in Chapter 3. Microwave excited Electrodeless Discharge Lamps (EDL) were utilized to generate the iodine plasma and the emitted light has been directed to Fourier transform spectrometer. The complete experimental details such as beamsplitter, detector, resolution, number of scans, optical filters and applied power has been given in Table 6.1.

Two magnetic dipole transitions at 1314.919 and 446.018 nm have been observed corresponding to I I and I II in the spectra respectively. New center-of-gravity wavenumber values were determined for these observed transitions and presented in Table 6.2 along with their energy level classifications.

Table 6.1 Experimental details for the observed forbidden transitions of I I and I II

Wavenumber	Beamsplitter	Detector	Resolution	No. of Scans	Filter	Power
7602 cm^{-1}	CaF$_2$	InGaAs	0.0035cm^{-1}	80	-	9W
22414 cm^{-1}	Qrtz UV	PMT Vis	0.02cm^{-1}	192	450 nm	16 W

Table 6.2 Centre of gravity wavenumber values and their corresponding energy levels for observed forbidden transitions of I I and I II.

Element	Wavenumber	E upper	E lower	Classification
I I	7602.968(3)	7602.970	0	$5s^25p^5\,^2P_{1/2}$ - $5s^25p^5\,^2S_{3/2}$
I II	22414.372(2)	29501.30	7087.00	$5s^25p^4\,^1S_0$ - $5s^25p^4\,^3P_1$

6.1.2 Forbidden transition of I I at 7602 cm^{-1}

The transition at 7602.968 cm^{-1} is identified as a strong magnetic dipole transition of I I in the infrared region. This transition is classified between two odd levels $5s^2 5p^5 {}^2P_{1/2}$ (7602.970 cm^{-1}) and $5s^2 5p^5 {}^2P_{3/2}$ (0.00 cm^{-1}) with six *hfs* components ($J = 3/2 \leftarrow J = 1/2$). As the ground state is also involved in this transition this can also be called as a resonance line. Although the hyperfine structure of this line was studied previously [125,76], the hyperfine components were not fully resolved. In the present observation, all components are completely resolved. A comparison made is shown in Fig. 6.1 between the observed and simulated spectra and is matching well with each other. *Hfs* constants were derived and are compared with previous literature in Table 6.3. The *A* value of P$_{3/2}$ is different from the previous value [125,76] by more than 3 sigma is due to the more resolved the spectral lines observed than previous spectra.
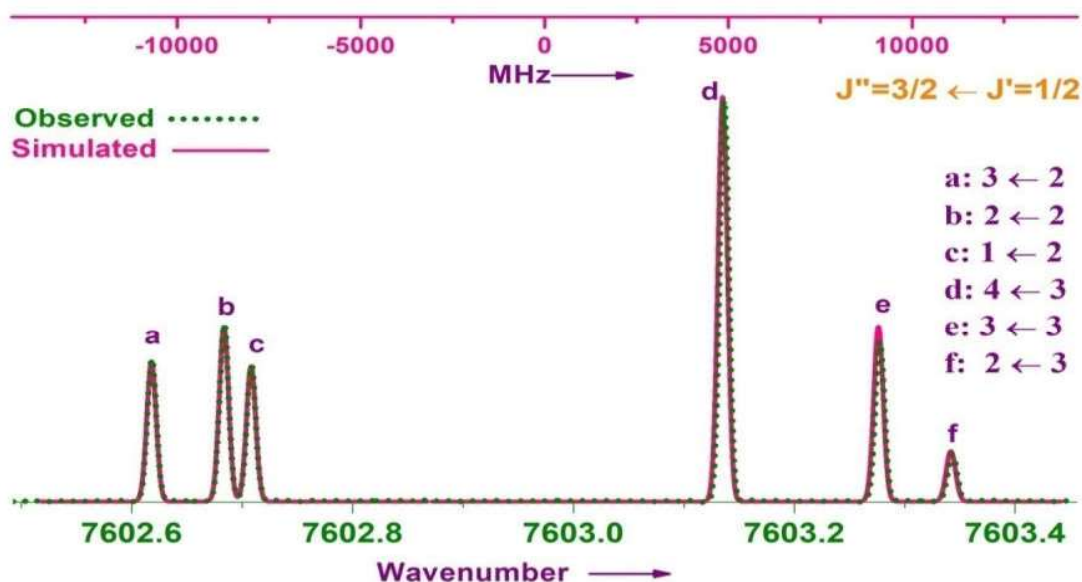
Fig. 6.1 A completely resolved *hfs* structure of a line at 7602.968 cm^{-1}. Observed and simulated spectra are matching well.

Table 6.3 *Hfs* constants for the ground and excited states with previous values for the line at 7602.968 cm^{-1} of I I.

Term	Present Work		Previous Work	
	A (mK)	B (mK)	A (mK)	B (mK)
Ground state $5s^2\,5p^5\,{}^2S_{3/2}$	26.46(18)	37.65(22)	27.59(05)[a] 27.59(01)[b]	38.18(10)[a] 38.13(06)[b]
Excited State $5s^2\,5p^5\,{}^2P_{1/2}$	223.61(15)		219.75(10)[a] 219.73(03)[b]	

[a][125] and [b][76]

6.1.3 Forbidden transition of I II at 22414 cm^{-1}

The ground state of I II, $5s^2\,5p^4$ has five fine structure levels ${}^3P_2$, ${}^3P_0$, ${}^3P_1$, ${}^1D_2$ and ${}^1S_0$ as shown in Fig.6.2. A strong line has been observed at 22414.372 cm^{-1} corresponding to a transition between the levels $5p^4\,{}^1S_0$ (29501.3 cm^{-1}) and $5p^4\,{}^3P_1$ (7087 cm^{-1}). The transition corresponding to the line at 22414.372 cm^{-1} is also indicated in Fig.6.2. This is a magnetic dipole (M1) transition between a singlet and triplet state of even parity levels. Zeeman pattern of this line was observed by Martin et al. [27]. In the present study, three *hfs* components (1.5,2.5), (2.5,2.5) and (3.5,2.5) permitted by the transition from $J = 0$ to $J = 1$ were resolved completely. *Hfs* constants A and B values for the lower and excited state were derived and presented in Table 6.4. Previous data is not available for these levels to compare the present work. The observed and simulated spectra are depicted in Fig.6.3.

Table 6.4 *Hfs* constants for the ground and excited states for the line at 22414.372 cm^{-1} of I II.

Term	Present Work	
	A (mK)	B (mK)
Ground state $5s^2\,5p^4\,{}^3P_1$	-20.78(10)	17.87(24)
Excited State $5s^2\,5p^4\,{}^1S_0$	0	0
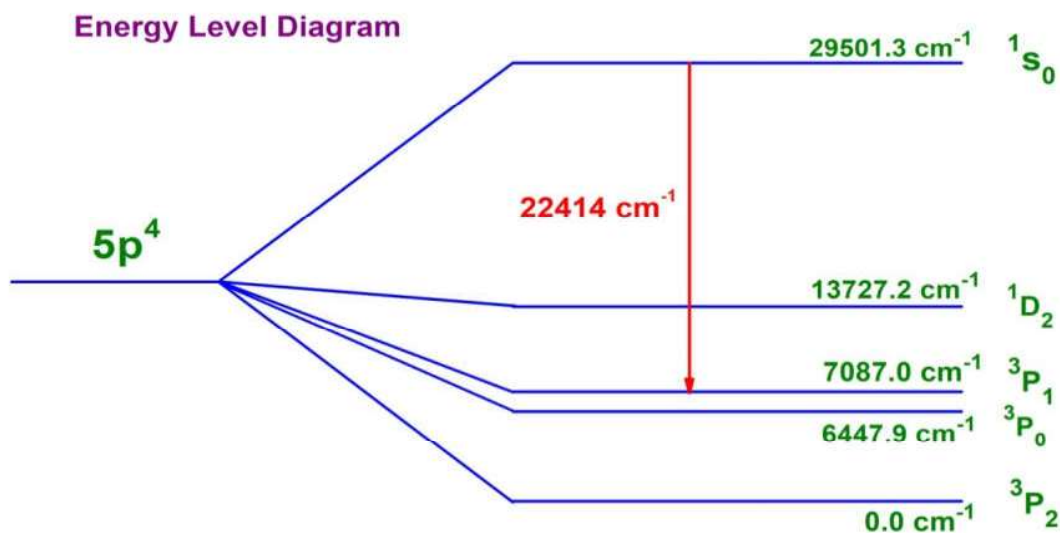
Fig. 6.2 Energy level diagram of five fine structure levels of I II ground configuration. The M1 transition corresponds to transition at 22414 cm^{-1} is also depicting.
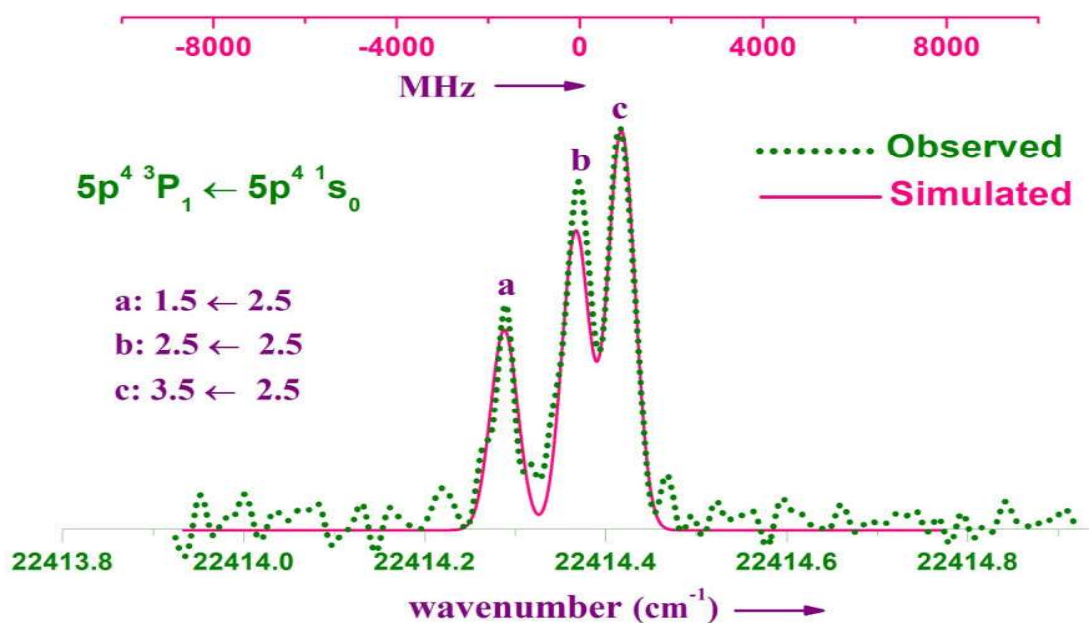
Fig. 6.3 A fully resolved magnetic dipole (M1) transition at 22414 cm^{-1} of I II.

143

6.2 Forbidden transitions in Bi I and Bi II spectra

The ground configuration of neutral bismuth $6s^2 6p^3$ has five fine structure terms $^4S_{3/2}$, $^2P_{3/2,1/2}$, $^2D_{5/2,3/2}$. As the ground configuration of Bi I levels are strongly split, few transitions were observed between them as mixed type and pure quadrupole transitions as well.

Three strong intensity forbidden lines were observed by Toshniwal [127] in the spectrum of Bi I. Later in 1945, Mrozowski [138] investigated the hyperfine structure of six forbidden transitions at 875.5, 647.6, 564.0, 461.5, 459.7 and 301.4 nm using a high resolving power spectrograph. Garstang [128] determined the contribution of the electric quadrupole radiation for the forbidden lines 459.7, 461.5, 564.0 and 647.6 nm as approximately 4, 10, 30 and 20% respectively. Heldt [39] in 1968 reinvestigated the four forbidden lines of Bi I at 647.6, 564.0, 461.5 and 459.7 nm by means of a steinheil GS glass spectrograph and silver coated Febry-Perot etalons. Further, $\Delta F = \pm 2$ components were also detected for the line at 461.5 nm. In 1969, Heldt [129] observed the interference between the magnetic dipole and the electric quadrupole radiation for the first time in a hyperfine structure by studying the Zeeman Effect in the two strongest mixed multipole lines of Bi I with apparatus of high resolving power and magnetic fields up to 6400 G. In 1984, the hyperfine structure of the forbidden transition at 647.5 nm in Bi I has been observed and analyzed employing a FT spectrometer by George [130]. Besides the 12 components corresponding to selection rules $\Delta F = 0, \pm 1$, two components corresponding to $\Delta F = \pm 2$ have also been detected. In 1985, KMJ Trgidgo [91] reported the *hfs* constants for $^2D_{3/2}$ state by studying the forbidden transition at 876 nm by laser spectroscopy. The relative strengths of the electric quadrupole (E2) and magnetic dipole (Ml) contributions for this forbidden transition have been derived. In 1994, Lucas [131] studied the multipole transition in Bi I at 648 nm by Faraday spectroscopy and determined the *hfs* constants for the upper state $^2D_{5/2}$. In 1995,

Bibmont [132] calculated the energy levels and radiative transition probabilities for states within the $6p^k$ (k = 1-5) configurations for the atoms thallium, lead, bismuth, polonium and actinium. Magnetic dipole (Ml) and electric quadrupole (E2) transition probabilities have also been determined. In 2007, The hyperfine structures of two multipole lines at 461.5 nm and 647.6 nm of atomic bismuth have been reported by Wasowicz [133]. Werbowy [92,134-136] calculated the electric quadrupole admixtures in the mixed multipole transitions at 461.5, 459.7, 564.0, 647.6 and 875.5 nm of Bi I using a computer program, on the basis of M1-E2 interference effects in the Zeeman structure of the fitted and recorded lines.

The singly ionized bismuth that has the ground configuration $6s^2 6p^2$ has five fine structure terms $^3P_{0,1,2}$, $^1D_2$ and $^1S_0$. Similar to the Bi I, these levels are also strongly split, so mixed type transitions between these five meta-stable states can be possible to observe.

In 1954, Cole and Mrozowski [137] observed the five forbidden transition among the ground configuration terms. In 1963, Cole [106] photographed the hyperfine structure of five multipole lines at 3240.7, 3683.2, 4850.2, 5913.5 and 7503.2 Å of ground configuration of Bi II by exciting high frequency electrodeless discharge lamps. Hults and Mrozowski [138] re-measured the accurate wavelengths for these five forbidden transitions. In1983, the intensity ratios of the multipole lines corresponding to transitions between the ground configurations $6s^2 6p^2$ of Bi II were worked out by Kwela [139]. Czerwinska [140] reported the hyperfine structure and Zeeman pattern for a forbidden line at 485.0 nm in 1987. Augustyniak and Werel [141] performed the hyperfine structure investigations on the pure electric quadrupole line at λ = 587.0 nm corresponding to the transition between the levels $^3P_2$ and $^1S_0$ of the ground configuration of Bi II. In addition, a comparison has been made between experimental and theoretical relative intensities of the multipole transitions at 485.0, 587.0 and 591.3 nm [141].

6.2.1 Experimental Details

Bismuth plasma has been generated by exciting the EDL containing BiI_3 utilizing microwave discharge method. The generated emission light has been observed by means of a Fourier Transform Spectrometer. The instrument was equipped with Qrtz Vis/ Qrtz UV beam splitter and Si diode/PMT detector. The complete experimental details such as beamsplitter, detector, resolution, number of scans, optical filters and applied power are given in Table 6.5.

In the present work, three multipole lines of Bi I at 461.7, 647.5 and 875.7 nm and one multipole line of Bi II at 750.3 nm have been observed in the emission spectra of Bi. Center-of-gravity wavenumber values were determined for all observed transitions and presented in Table 6.6 along with their energy level classifications.

Table 6.5 Experimental details for observed forbidden transitions of Bi I and Bi II

Wavelength	Beamsplitter	Detector	Resolution	No. of Scans	Filter	Power
Bi I- 875.7 nm	Qrtz-UV	Si Diode	$0.01 cm^{-1}$	242	-	15 W
Bi I- 647.5 nm	Qrtz-UV	PMT-Vis	$0.02 cm^{-1}$	396	650 nm	18 W
Bi I- 461.7 nm	Qrtz-Vis	PMT-Vis	$0.03 cm^{-1}$	100	450 nm	20 W
Bi II- 750.3 nm	Qrtz-Vis	PMT-Vis	$0.02 cm^{-1}$	144	820 nm	14 W

Table 6.6 Centre of gravity wavenumber values and their corresponding energy levels for observed forbidden transitions of Bi I and Bi II

Element	Wavenumber	E upper	E lower	Classification
Bi I	11419.038(5)	11419.039	0	$6s^2 6p^{3\,2}D_{3/2}$ - $6s^2 6p^{3\,4}S_{3/2}$
Bi I	15437.500(3)	15437.501	0	$6s^2 6p^{3\,2}D_{5/2}$ - $6s^2 6p^{3\,4}S_{3/2}$
Bi I	21660.945(7)	21660.914	0	$6s^2 6p^{3\,2}P_{1/2}$ - $6s^2 6p^{3\,4}S_{3/2}$
Bi II	13325.476(4)	13325.401	0	$6s^2 6p^{2\,3}P_1$ - $6s^2 6p^{2\,3}P_0$

6.2.2   Forbidden transitions of Bi I

Fig. 6.4 represents the energy level diagram of the five fine structure levels of the ground configuration of Bi I. All three transitions appear between the three low-lying ground state configurations. The three observed forbidden transitions among these levels are also indicated in Fig. 6.4. Hyperfine structure investigations were carried out on three forbidden transitions. *Hfs* constants A and B are derived for the energy levels involved in each transition. For all the three transitions the lower level is common.
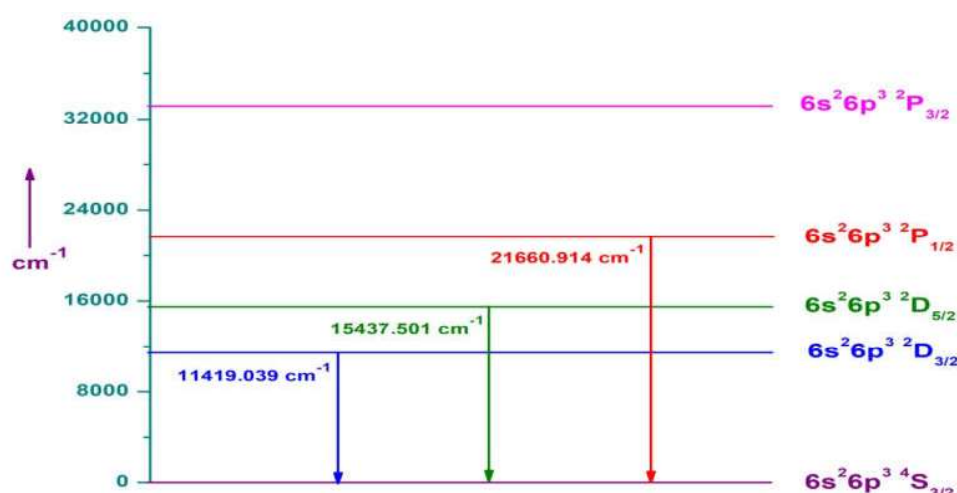
Fig. 6.4 Energy level diagram of the five fine structure levels of Bi I ground configuration. The three observed forbidden transitions among these levels are also indicated.

Line at 875.7 nm (11419.038 cm^{-1}):

The line at 11419.038 cm^{-1} in the IR region is a magnetic dipole transition between the two lowest levels $6p^3$ $^4S_{3/2}$ and $6p^3$ $^2D_{3/2}$ of ground configuration as shown in Fig. 6.4. The transition is from D - S violating the parity symmetry rule. This transition is also an intercombination transition as the selection rule $\Delta S = 0$ is not obeyed. A well resolved hyperfine structure has been observed for this line. Out of 10 *hfs* components ($J = 3/2 \leftarrow J = 3/2$), seven

were completely resolved. *Hfs* measurements were performed to derive *A* and *B* constants. The present *hfs* constants were compared to the previous literature in Table 6.7. Comparisons of observed and simulated spectra are depicted in Fig. 6.5.

Table 6.7 *Hfs* constants for the ground and excited states along with previous values for the line at 11419.038 cm^{-1} of Bi I.

Term	Present	Work	Previous	Work
	A	B	A	B
Ground state $6s^2 6p^3\,^4S_{3/2}$	-15.21(6)	-10.34(15)	-14.9(3)[a] -14.91(3)[b]	-9.1(2.7)[a] -10.16(6)[b]
Excited State $6s^2 6p^3\,^2D_{3/2}$	-41.36(7)	-21.35(18)	-40.92(4)[b]	-20.58(33)[b]

[a][130], [b][91],
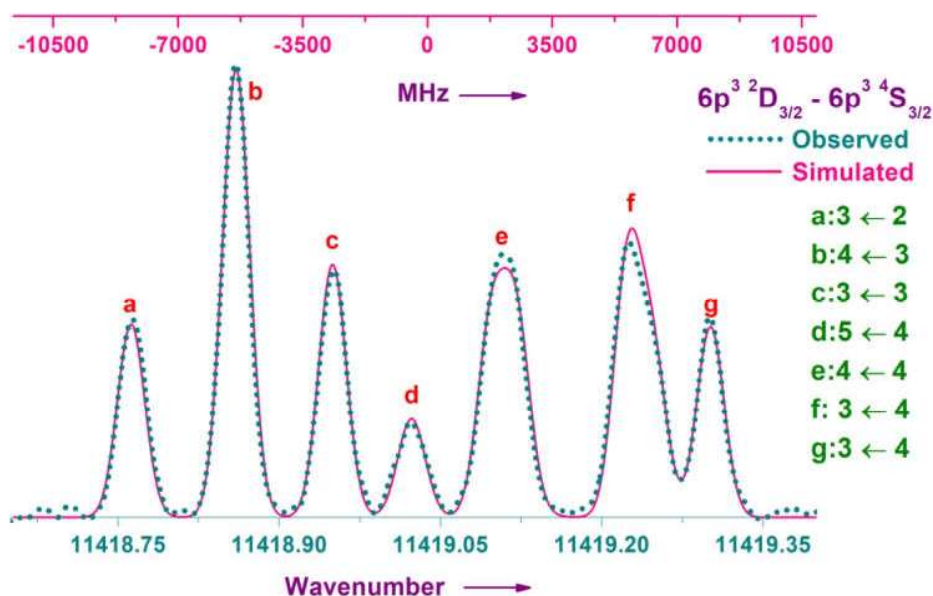
Fig. 6.5 A well resolved *hfs* structure for the transition at 11419.038 cm^{-1} of the Bi I. The simulated spectrum is in good agreement with observed one.

Line at 647.5 nm (15437.501 cm^{-1}):

The transition between the two levels $6p^{34}S_{3/2}$ and $6p^{32}D_{5/2}$ of ground configuration at 15437.501 cm^{-1} is in the visible region. This transition is also violating the parity symmetry and $\Delta S = 0$ selection rules. This transition ($J = 3/2 \leftarrow J = 5/2$), consists 12 components of the magnetic dipole ($\Delta F = 0, \pm 1$) and 6 components of the electric quadrupole ($\Delta F = \pm 2$) transitions. The *hfs* of this line was studied previously by George [20] and observed 12 components of the magnetic dipole ($\Delta F = 0, \pm 1$) and 2 components of electric quadrupole ($\Delta F = \pm 2$) transitions. In the present investigations, all 12 components of the magnetic dipole ($\Delta F = 0, \pm 1$) and also all 6 components of the electric quadrupole ($\Delta F = \pm 2$) transitions have been observed. These six components of pure electric quadrupole transitions have been observed for the first time. The energy level diagram for the line at 647.5 nm along with the possible *hfs* transitions has been shown in Fig. 6.6. Solid lines represent the $\Delta F = 0, \pm 1$ transitions whereas dotted lines represent $\Delta F = \pm 2$ transitions.
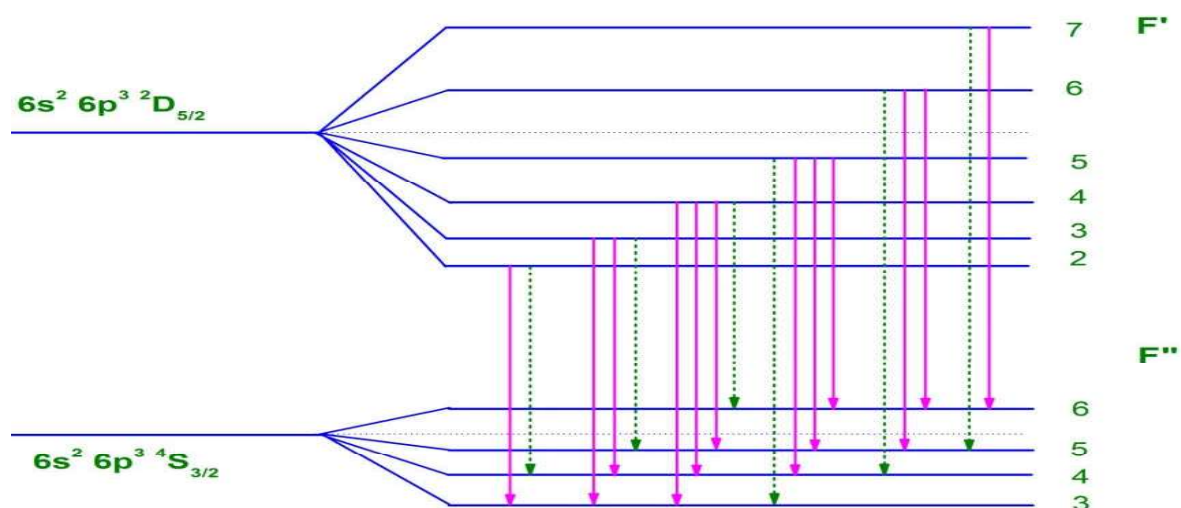
Fig. 6.6 The energy level diagram of the 15437.501 cm^{-1} line along with possible *hfs* transitions according to the selection rules $\Delta F = 0, \pm 1$(solid lines) and $\Delta F = \pm 2$ (dotted lines).

The observed and simulated spectra are presented in Fig.6.7. All 18 *hfs* components were clearly resolved and observed with good S/N. The six components of $\Delta F = \pm 2$ transitions are indicated in Fig.6.7. The simulation program *WINHFS* supports only for $\Delta F = 0, \pm 1$ transitions but not $\Delta F = \pm 2$. Because of this reason, $\Delta F = \pm 2$ peaks are appearing in the residual spectra.

Hfs structure measurements were performed for $\Delta F = 0, \pm 1$ transitions and *hfs* constants were derived for the upper and lower levels, reported in Table 6.8 and compared with the previous values.
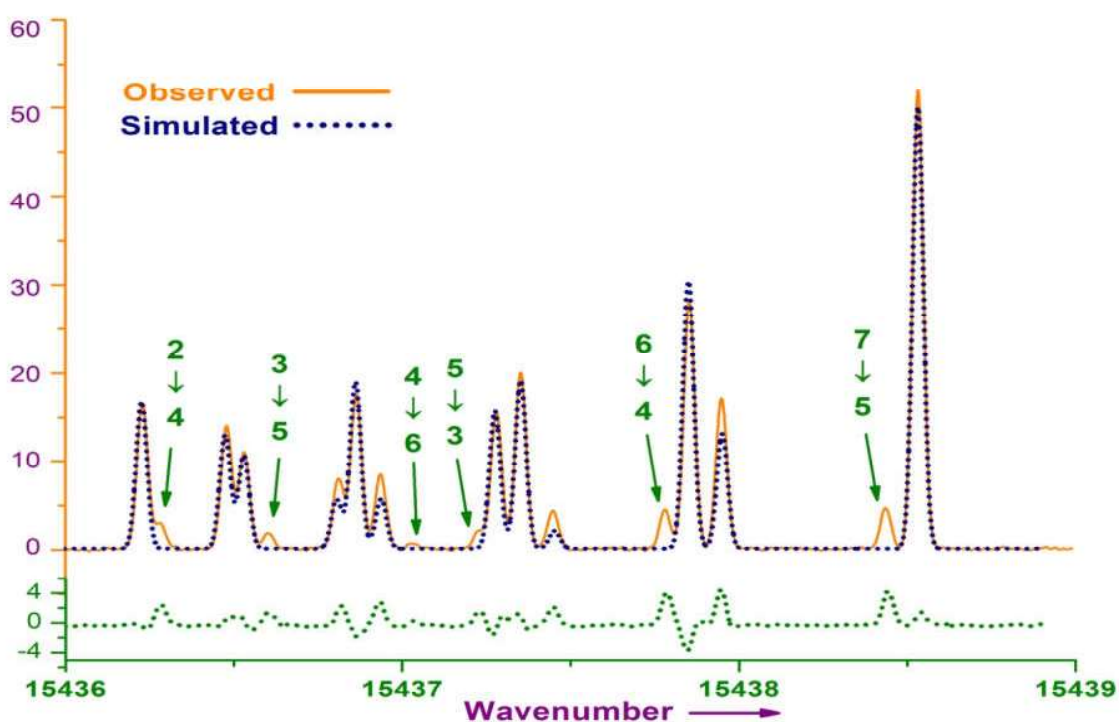
Fig. 6.7 The observed and simulated spectra of the line at 647.5 nm. All the 18 *hfs* components corresponding to $\Delta F = 0, \pm 1$ and $\Delta F = \pm 2$ transitions were observed. Only $\Delta F = 0, \pm 1$ transitions are present in simulated spectrum.

From the *hfs* measurements, the *hfs* splitting of F levels for the ground $6s^2 6p^3$ $^4S_{3/2}$ and excited $6s^2 6p^3$ $^2D_{5/2}$ states were obtained in MHz and given in Table 6.9. From these values, the

line positions of *hfs* components were derived and compared to the observed spectrum. The positions are matching well with observed ones.

Table 6.8 *Hfs* constants for the ground and excited states along with previous values were given the line at 15437.501 cm^{-1}.

Term	Present Work		Previous Work	
	A	B	A	B
Ground state $6s^26p^3\,^4S_{3/2}$	-15.68(9)	-10.14(17)	-14.9(3)[a] -14.91(3)[b]	-9.1(2.7)[a] -10.16(6)[b]
Excited State $6s^26p^3\,^2D_{5/2}$	83.06(13)	1.67(24)	83.5(3)[a] 83.69(27)[c]	0.5(5.5)[a] 1.9(55)[c]

[a][130], [b][91], and [c][82]

Table 6.9 Hyperfine energy level positions for the ground and excited states of the line at 15437.501 cm^{-1} obtained from the simulation program.

Hyperfine Levels of Ground state		Hyperfine Levels Of Excited state	
F''	**Frequency (MHz)**	**F'**	**Frequency (MHz)**
3	3738.1667	2	-34214.5833
4	2060.8333	3	-26759.5833
5	-225.8333	4	-16813.75
6	-3248.5	5	-4372.0833
		6	10571.6667
		7	28025

A comparison has been made for the peak positions of all observed and simulated *hfs* components in Table 6.10. In the first column, the absolute intensities observed in FTS have been given. Second column indicates the various F transitions. The line position values are derived for each *hfs* component is presented in third column. Line positions derived by using energy levels obtained in Table 6.9 are given in fourth column. The difference between the line

151

positions between observed and simulated spectra have been mentioned in fifth column. Selection rule for each transition is given in the sixth column. The last column indicates the FWHM values observed in cm^{-1} for each *hfs* component.

Table 6.10 A comparison of the peak positions of observed and simulated *hfs* components.

Abs. Intensity	$F'' \rightarrow F'$	Observed Wavenumber (cm^{-1})	Simulated Wavenumber (cm^{-1})	o-s	ΔF	Width (cm^{-1})
16.648	$3 \rightarrow 2$	15436.2293	15436.22999	-0.00069	-1	0.0386
3.0567	$4 \rightarrow 2$	15436.2810	15436.28594*	-0.00494	-2	-
14.056	$3 \rightarrow 3$	15436.4799	15436.47866	0.00124	0	0.0418
11.057	$4 \rightarrow 3$	15436.5320	15436.53461	-0.00261	-1	0.0258
1.888	$5 \rightarrow 3$	15436.6033	15436.61089*	-0.00759	-2	0.0314
8.024	$3 \rightarrow 4$	15436.8138	15436.81042	0.00338	1	0.0249
17.632	$4 \rightarrow 4$	15436.8667	15436.86637	0.00033	0	0.0402
8.544	$5 \rightarrow 4$	15436.9385	15436.94265	-0.00415	-1	0.0328
0.718	$6 \rightarrow 4$	15437.0280	15437.04347*	-0.01547	-2	0.0421
2.0385	$3 \rightarrow 5$	15437.2241	15437.22543*	-0.00133	2	-
15.659	$4 \rightarrow 5$	15437.2836	15437.28138	0.00222	1	0.0345
20.076	$5 \rightarrow 5$	15437.3563	15437.35766	-0.00136	0	0.0383
4.409	$6 \rightarrow 5$	15437.4523	15437.45848	-0.00618	-1	0.0371
4.564	$4 \rightarrow 6$	15437.7856	15437.77985*	0.00575	2	0.0312
28.177	$5 \rightarrow 6$	15437.8577	15437.85613	0.00157	1	0.0382
17.179	$6 \rightarrow 6$	15437.9539	15437.95695	-0.00305	0	0.0374
4.722	$5 \rightarrow 7$	15438.4418	15438.43831*	0.00349	2	0.0368
51.979	$6 \rightarrow 7$	15438.5392	15438.53913	0.00007	1	0.0381

Line at 461.7 nm (21660.914 cm^{-1}):

The transition $6s^2 6p^3\,^2P_{1/2}$ - $6s^2 6p^3\,^4S_{3/2}$ produces a line at 21660.914 cm^{-1}. Although, this transition is following parity symmetry selection rule, violation of $\Delta S = 0$ selection rule results in an intercombination transition. In the present observation, all six *hfs* components according to ΔF

152

= 0, ±1, were observed and analyzed for the first time. *Hfs* constants were derived for both the levels with uncertainty of 0.02 cm^{-1} and reported in Table 6.11. The simulated and observed spectra were depicted in Fig.6.8 Here a, b, c, d, e and f denotes the various *hfs* components. Two *hfs* components ('a' and 'b') are partially resolved, whereas the remaining components are well resolved. The simulated and observed spectra show a good matching.

Table 6.11 *Hfs* constants for the ground and excited states along with previous values for the line at 21660.914 cm^{-1}.

Term	Present Work		Previous Work	
	A	B	A	B
Ground state $6s^2 6p^3\,^4S_{3/2}$	-15.51(3)	-8.81(17)	-14.9(3)[a] -14.91(3)[b]	-9.1(2.7)[a] -10.16(6)[b]
Excited State $6s^2 6p^3\,^2P_{1/2}$	375.26(5)		375.9(2)[c] 375.68(44)[d]	

[a][130], [b][91], [c][87] and [d][37]
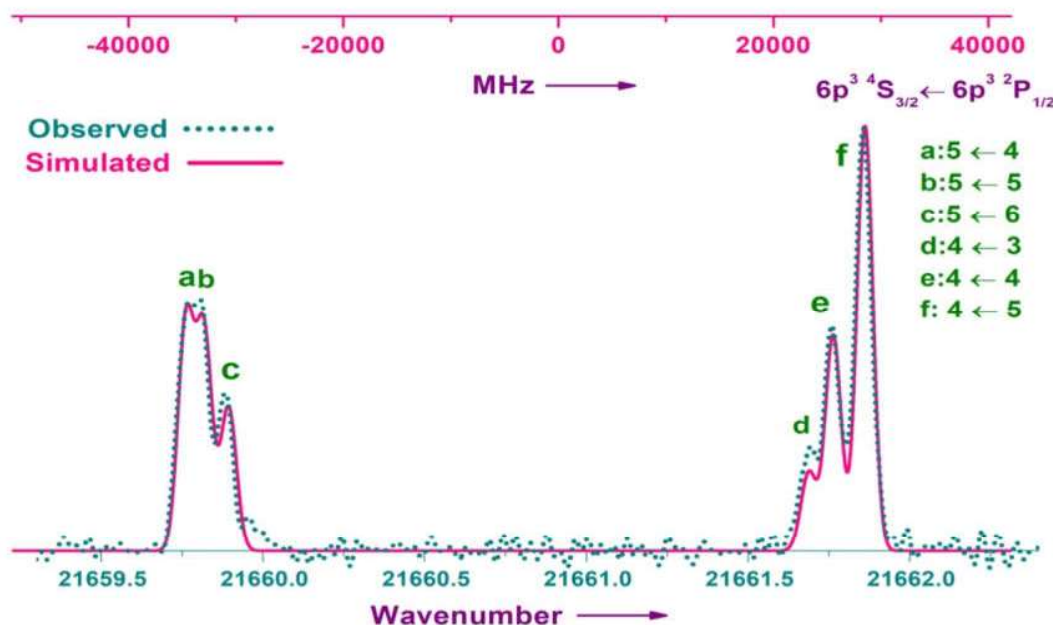
Fig. 6.8 A well resolved *hfs* structure for the transition at 21660.914 cm^{-1} of Bi I. The simulated spectrum is in good agreement with observed one.

6.2.3 Forbidden transition of Bi II at 13325 cm^{-1}

A magnetic dipole transition has been observed between the two low-lying ground configuration levels $6p^{23}P_1$ and $6p^{23}P_0$. This transition produces three *hfs* components ($J = 1 - J = 0$). All three well separated *hfs* components were observed. The *hfs* of this line has been analyzed for the first time in this work. Fig.6.9 illustrates the observed and simulated *hfs* structure of the line at 13325 cm^{-1}. As the ground state J value is zero, only the excited state has non-zero *hfs* constants. The derived *hfs* constants in this work along with previous data for both the levels are presented in Table 6.12.
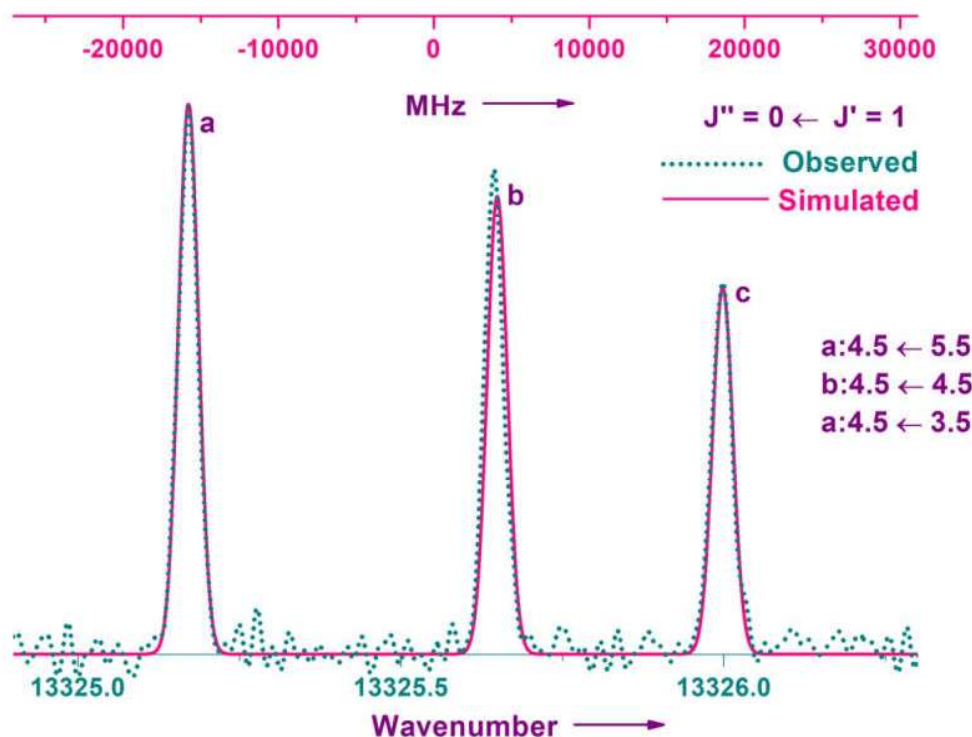
Fig. 6.9 A well resolved *hfs* structure for the transition at 13325 cm^{-1} of Bi II. The simulated spectrum is in good agreement with observed one.

154

Table 6.12 *Hfs* constants for the ground and excited states along with previous values for the line at 13325 cm^{-1}.

Term	Present Work		Previous Work	
	A	B	A	B
Ground state $6s^2 6p^2\, {}^3P_0$	0	0		
Excited State $6s^2 6p^2\, {}^3P_1$	-82.65(5)	-16.71(10)	-82.9(1)[a] -82.5(7)[b]	-16.5(1)[a] -15.5(3.5)[b]

[a][110], [b][111]

6.3 Conclusion

Hyperfine structure investigations were performed on six forbidden transitions. Among these six transitions, two transitions at 1314.919 and 446.018 nm have been observed in I I and I II spectra respectively. From the remaining four transitions, three lines of Bi I at 461.7, 647.5 and 875.7 nm and one line of Bi II at 13325 cm^{-1} have been observed in the emission spectra of Bi. Microwave excited electrodeless discharge lamps were employed to observe these transitions. New center-of-gravity wavenumber values were determined for all six transitions. For the transition at 647.5 nm of Bi I spectra, all 6 components of the electric quadrupole ($\Delta F = \pm 2$) transitions were also observed along with all the 12 components of the magnetic dipole ($\Delta F = 0, \pm 1$) transitions.

Chapter 7

Summary and conclusions

In this thesis, we have presented high resolution spectroscopic investigations of neutral and singly ionized atomic species I I, Bi I, I II and Bi II using Fourier transform spectroscopy technique.

To carry out these investigations, EDL of Iodine, BiI_3 and HCL of Bi_2O_3 were prepared to serve as source of light. While EDL were excited by the microwave discharge, HCL were excited by DC discharge.

In the emission spectra of I I, a total of 777 atomic lines have been identified in the spectral region from 1800 to 25000 cm^{-1} [142-144] and, 141 spectral lines of I II were observed in the spectral region 12000 - 24000 cm^{-1} [145]. These studies were carried out employing electrodeless discharge lamps of I_2 which were prepared and excited using a surfatron microwave cavity.

High resolution emission spectra of atomic bismuth have been recorded in the spectral range from 2500 to 40000 cm^{-1} (IR to UV) and a total of 107 spectral lines were observed [146]. Spectra of singly ionized atomic Bismuth (Bi II) have been examined in the spectral range of 13000 - 40000 cm^{-1} (Near IR to UV) and 45 spectral lines were identified. Electrodeless discharge lamps and LN_2 cooled HCL were utilized to generate the Bi plasma by means of microwave and DC discharge methods, respectively.

New center of gravity wavenumber values were determined for all the 1070 observed lines of the above species investigated. The experimental set up to record I I and I II spectral lines has been designed with liquid nitrogen based cooling set up to minimize the Doppler broadening of the spectral lines and provide optimum conditions for generation of I II. With reduced Doppler width, well resolved *hfs* structures were observed in the entire spectral region.

As a result, minimum FWHM of 93 MHz has been achieved for a *hfs* component of I I at 2056 cm^{-1}. Similarly in the case of Bismuth, the Doppler width has been reduced by operating the HCL under cooled condition using liquid nitrogen.

Out of the 1070 observed spectral lines, *hfs* investigations were performed on nearly 630 lines. *Hfs* constants were derived for 249 energy levels of which 99 are reported for the first time.

Apart from *hfs* investigations, few lines were identified as unclassified lines, blended lines and forbidden lines. Also, a brief discussion has been presented for the spectral line self-absorption in various operating conditions of EDL and HCL sources. Hyperfine structure investigations were performed on six forbidden transitions. For the forbidden transition at 647.5 nm of Bi I spectra, all the 18 components corresponding to the magnetic dipole ($\Delta F = 0, \pm1$) and electric quadrupole ($\Delta F = \pm2$) transitions were observed.

While spectroscopic studies on atomic fine structure is a well established and mature field, exhaustive knowledge on the atomic hyperfine spectra of all the elements is still far from being a completely attained domain. We hope that the investigations presented in this thesis pave the way towards more detailed investigations on hyperfine structure of various species, which may be useful in advancing our understanding on fundamentals of atomic spectra and energy levels; and would be of immense help in various technological and astrophysical applications.

References

1. Booth AJ, Blackwell DE. The effect of hyperfine structure on stellar abundance analysis. MNRAS 1982;204:777.

2. Andersson M, Grumer J, Ryde N, Blackwell-Whitehead R, Hutton R, Zou Y, Jonsson P, Brage T, Hyperfine dependent *gf-* values of Mn I lines in the 1.49-1.80 μm *H* band. ApJS 2015;216:2.

3. Prochaska JX, McWilliam A. On the Perils of Hyperfine Splitting: A Reanalysis of Mn and Sc Abundance Trends. ApJS 2000;537:L57.

4. Karshenboim SG, Flambaum V, Peik E. Atomic Clocks and Constraints on Variations of Fundamental Constants. Springer Handbook of Atomic, Molecular, and Optical Physics 2006.

5. Beehler RE, Mockler RC, Richrdson JM. Cesium Beam atomic Time and Frequency Standards. Nat Bur Sta 1965;1:115.

6. Hargus Jr. WA, Lubkeman JS, Remy KE. Gonzales AE. 48th AIAA/ASME/SAE/ASEE Joint propulsion Conference & Exhibit and 10th International Energy Conversion Engineering Conference, Atlanta, GA, 29 July – 2 August 2012.

7. Scharfe DB, Capelli MA. Stationary reference Bi discharge cell for optical diagnostics of a Bismuth Hall thruster IEPC'05: Proc. 29th Int Electric Propulsion Conf (Princeton, NJ) IEPC-2005-058.

8. Anders E, Grevesse N. Abundances of the elements: Meteoritic and solar. GCA 1988;53:197.

9. Stone NJ. Table of nuclear magnetic dipole and electric quadrupole moment. Vienna Austria: International Atomic Energy Agency; 2014. p. 88. Nuclear data section report no. INDC(NDS)-0658.

10. Van stralen JNP, Visscher L. Molecular relativistic electric field gradient calculations suggest revision of the value of the nuclear electric quadrupole moment of 127I. Mol Phys 2003;101:2115-24.

11. Wood RW, Kimura M. Band and Line Spectra of Iodine. Astrophysical journal 1917;46:182.

12. Tolansky S. Fine structure in the Arc spectra of bromine and Iodine. Proc Roy Soc Lon 1932;136:585.

13. Murakawa K. Anomalies in the Fine Structure of the First Spark Spectrum of Iodine. Nature 1936;137:1030.

14. McLeod JH. New lines in the ultraviolet spectrum of atomic iodine. Phys Rev 1936; 49: 804.

15. Kiess CC, Corliss CH. Description and analysis of the first spectrum of iodine. J radiation research national bureau of standards- a Phys and chem 1959; 63: 4

16. Tolansky S. Nuclear spin of Iodine. Nature 1934;134:851.

17. Eshbach FE, Fisher RA. The first spectrum of Iodine in the region between 0.8 and 2.2 μm. JOSA 1954; 44: 868.

18. Humphreys J, Edward Paul, JR. First spectra of Chlorine, Bromine, and Iodine in the 4-μm Region. JOSA 1971;61:110.

19. Humphreys J, Edward Paul, JR. First spectra of Chlorine, Bromine, and Iodine in the 1.8-4.0 -μm Region, JOSA 1972;62:432.

20. Hongsuk HK, Roy AP, Philip LH, Thomas FD. T-5 Iodine infrared laser. IEEE J Quant Elect 1968; 11: 908.

21. Luc-Koeng E, Morillon C, Vergès J. Experimental and theoretical studies in atomic iodine: Infrared arc spectrum observations, classification and hyperfine structure. Phys Scrip 1975; 12: 199.

22. Deng LH, Li YX, Zhu YY, Chen YQ. Hyperfine structure near infrared spectrum of atomic iodine. JQSRT 2015; 161: 153- 156.

23. Mu XL, Deng LH, Huo X, Jia Ye, Windholz L, Wang HL. Hyperfine structure investigations in atomic iodine. JQSRT 2018;217:229.

24. Lacroute P. Effet zeeman du brome et de l'iode Ann Physique 1935;3:5.

25. Murakawa K. über die Spektren J II, J I und Cl II. Z Physik 1938;109:162.

26. Fry AS, Fisher RA. Zeeman effect in the Hyperfine Structure of Iodine II. Phys Rev 1939;56:669.

27. Martin WC, Corliss CH. The Spectra of Singly Ionized Atomic iodine (I II). J Res Natl Bur Stand 1960;64A:443.

28. Murakawa K. Quadrupole Coupling in the Hyperfine Structure of the Spectrum of I II. J Phys Soc Jpn 1964;19:1539.

29. Fowles GR, Jensen RC. Visible Laser Transition in Ionized Iodine. Applied Optics 1964;3:1191.

30. Zeeman P, Back E, Goudsmit S. Zur Hyperfeinstrukur des Wismuts. Z Phys 1930;66:1.

31. Mrozowski S. Arc spectrum of bismuth Bi I. Phys Rev 1942;62:526.

32. Clearman HE. On the arc spectrum of boron, indium, thallium, lead and bismuth. J Opt Soc Am 1952;42:373.

33. Landman DA, Lurio A. Hyperfine structure of the 6p3 configuration of Bi^{209}. Phys Rev A 1970;1:1330.

34. Dickie LO, Kelly FM. Hyperfine structure in the ground configuration of bismuth. Can J Phys 1967;45:2249.

35. George S, Gorbett MJ. Newly observed lines of the first spectrum of bismuth in the lead sulfide region. J Opt Soc Am 1982;72:589.

36. George S, Munsee JH, Verges J. Newly observed 5f–ng transitions in Bi I spectrum. J Opt Soc Am B 1985;2:1264.

37. George S, Munsee JH. Hyperfine-structure measurements in bismuth using a Fourier-transform spectrometer. J Opt Soc Am B 1985;2:1258.

38. Mrozowski S. Forbidden Lines of Bismuth Bi I. Phys Rev 1946;69:169.

39. Heldt J. Hyperfine Structure of the Multipole lines of Bismuth (Bi I). J Opt Soc Am 1968;58:1516.

40. George S, Munsee JH, Verges J. Hyperfine structure measurements of the line 613.4 nm in bismuth using Fourier-transform spectrometer. J Opt Soc Am B 1985;2:568.

41. Wahlgren GM, Brage T, Brandt JC, Fleming J, Johansson S, Leckrone DS, Proffitt CR, Reader J, Sansonetti CJ. The Bismuth abundance in the HgMn stars χ Lupi and HR 7775 and improved atomic data for selected transitions of Bi I, Bi II, and Bi III. The Astrophysical journal 2001;551:520.

42. Dolk L, Litzen U, Wahlgren GM. The laboratory analysis of Bi II and its application to the Bi-rich HgMn star HR 7775. Astron Astrophys. 2002;388:692.

43. Kopfermann H. Nuclear moments. New York: Academy press inc.; 1958.

44. Bransden BH, Joachain CJ. Physics of Atoms and Molecules. Longman Scientific and Technical 1983.

45. Condon EU, Shortley GH. Theory of Atomic Spectra. Cambridge University Press 1959.

46. Goudsmith S, Bacher RF. Separations in Hyperfine Structure. Phys Rev 1929;34:1501.

47. Goudsmith S. Theory of Hyperfine Structure Separations. Phys Rev 1931;37:663

48. Schwartz C. Theory of Hyperfine Structure. Phys Rev 1955;97:380.

49. Sobelman II. Atomic Spectra and Radiative Transitions. Springer Series on Atoms and Plasmas 1992.

50. Casimir HBG. The Early History of Hyperfine Structure. Hyperfine Interactions 1983;15:1.

51. Candler AC. Atomic Spectra and the Vector model. Cambridge University Press 1937.

52. White H. E. Introduction to Atomic Spectra. McGraw-Hill Inc 1934.

53. Drake GWF. Springer Handbook of Atomic, Molecular, and Optical physics. Springer 2006.

54. Cowan RD, Dieke GH. Self-absorption of Spectrum Lines. Rev Mod Phys 1948;20:418.

55. Smith BR. Fourier Transform Infrared Spectroscopy. Academic Press 1972.

56. Theophenides T (Ed). Fourier Transform Infrared Spectroscopy. Reidel Publishing C., Dordercht, Holland.

57. Hariharan P. Optical Interferometry. Academic Press 2003.

58. Bracewell RN. The Fourier Transform and its Applications. McGraw-Hill Higher Education 2000.

59. Daniel J. Schroeder. Astronomical Optics. Academic Press 1999.

60. Mansfield JM, Bratzel MP, Norgordon HO, Knapp DO, Zacha KE, Winefordner JD. Experimental Investigation of Electrodeless discharge lamps as excitation sources for atomic fluorescence flame spectrometry. Spectrochimica Acta 1968;23B:389.

61. Církva V, Vlková L, Relich S, Hájek M. Microwave photochemistry IV: Preparation of the electrodeless discharge lamps for photochemical applications. Journal of Photochemistry and Photobiology A: Chemistry 2006;179:229.

62. Schüler H. Über die Anregung von Spektren zur Untersuchung von Hyperfeinstrukturen. Z Phys 1930;59:149.

63. Bhowmick GK, Verma R, Verma MK, Raman VA, Joshi AR, Deo MN, Gantayet LM, Tiwari AK, Ramakumar KL, Kumar N, Preparation of electrodeless discharge lamps for emission studies of uranium isotopes at trace level. Spectrochim Acta B 2010;65:1047.

64. Moisan M, Zakrzewski Z, Pantel R. The theory and characteristics of an efficient surface Wave Launcher (surfatron) Producing Long plasma columns. J Phys D: Appl Phys 1979;12:219-237.

65. Saloman EB, Sansonetti CJ. Wavelengths, energy level classifications and energy levels for the spectrum of neutral neon J Phys Chem Ref Data 2004; 33: 1113- 58.

66. Kumar PS, Kumar PVK, Suryanarayana MV. Application development for the calculation of hyperfine structure constants from the atomic hyperfine spectrum under the windows platform. 2002 (BARC Report BARC/2002/ E/ 027).

67. Pekka Pyykko, Micheal Seth. Relativistic effects in nuclear quadrupole coupling. Theor Chem Acc 1977;96:92.

68. Wood RW, Kimura M. Band and Line Spectra of Iodine. Astrophysical journal 1917;46:182.

69. Tolansky S. Fine structure in the Arc spectra of bromine and Iodine. Nature 1931;127:855.

70. Tolansky S. The nuclear spin of Iodine I- fine structure in the first spark spectrum. Proc Roy Soc Lon 1935;149:269.

71. Pettini M, Mazzoni M, Tozzi GP. Excitation of the inner 4d shell of neutral iodine. Phys Lett 1981; 82A: 168.

72. Sullivan OG, McGuinness C, Costello JT, Kennedy ET, Weinmann B. Trends in 4d-subshell photoabsorption along the iodine isonuclear sequence: I, I^+, and I^{2+}. Phys Rev A 1996; 55: 3211.

73. Gu YY, Chojnacki AM, Zietkiewicz CJ, Senin AA, Eden JG. Autoionization in I and I_2 observed by multiphoton ionization and photoelectron spectroscopy: Two atomic iodine Rydberg series built on the … $5s^2 5p^4 {}^3P_1$ ion core and revised value for the I^+ ($^3P_1$) limit. J Chem Phys 2003; 119: 12342.

74. Jaccarino V, King JG, Satten RA, Stroke HH. Hyperfine structure of I^{127} nuclear magnetic moment. Phys Rev 1954; 94: 1798.

75. Bennett SJ, Cerez P. Hyperfine structure in Iodine at the 612 nm and 640 nm helium neon laser wavelengths. Opt. Communications 1978; 25: 343.

76. Engleman R, Keller RA Jr, Palmer BA. Hyperfine structure and isotope shift of the 1.3 µm transition of I^{129}. Apl. Opt 1980; 19:2767.

77. Kramida A, Ralchenko Yu, Reader J. NIST Atomic Spectra Database (ver. 5.2) [online]. National Institute of Standards and Technology, Gaitherburg, MD. 2014.

78. Title RS, Smith KF. The hyperfine structure of ^{209}Bi. Philos Mag 1960;5:1281.

79. Hull RJ, Brink GO. Hyperfine structure of Bi^{209}. Phys Rev 1970;1:685.

80. Dickie LO, Kelly FM. Hyperfine structure in excited levels of the arc spectrum of bismuth. Can J Phys 1971;49:2376.

81. Guern Y, Bideau-Mehu A, Abjean R, Johannin-Gilles A. Interferometric determination of the magnetic hyperfine splitting factors for some excited configurations of Bi I. J Phys B 1980;13:47.

82. Dembczyński J, Arcimowicz B, Wiśniowski K. Investigation of the hyperfine structure of ^{209}Bi in some levels of Bi I spectrum. J Phys B 1977;10:2951.

83. Dembczyński J, Frackowiak J. Hyperfine structure in intermediate coupling of the first excited electron configuration $6p^2 7s$ of ^{209}Bi (I=9/2). Acta Phys Pol A 1975;48:139.

84. Holmgren L, Svanberg S. Level crossing investigation of the hyperfine structure of Bi^{209} in the $6p^2(^3P_0)6d\ ^2D_{3/2}$ and $6p^2(^3P_1)7s\ ^4P_{3/2}$ levels of the Bi I spectrum. Phys Scrip 1974;9:211.

85. Poulsen O, Hall J. Spectroscopic investigations in ^{209}Bi I using tunable-cw-dye-laser spectroscopy. Phys Rev A 1978;18:1089.

86. George S. Hyperfine structure in bismuth-an experiment. Am J Phys 1968;36:27.

87. George S, Klingberg RA. Interferometric measurements of the hyperfine structure in bismuth. J Opt Soc Am 1970;60:869.

88. George S, Munsee JH, Verges J. Hyperfine structure measurements of the line 613.4 nm in bismuth using Fourier-transform spectrometer. J Opt Soc Am B 1985;2:568.

89. Rosén A. Hyperfine structure analysis for the ground configuration of bismuth. Phys Scr 1972;6:37.

90. Sobolewski ŁM, Werbowy S, Kwela J. Hyperfine and Zeeman structure of lines of Bi I. J Opt Soc Am B 2014;31:3038.

91. Tregidgo KMJ, Baird PEG, Macpherson MJD, Palmer CWP, Sandars PGH, Stacey DN, Thompson RC, Absorption and Faraday spectroscopy of the 876 nm line in Bi I. J Phys B 1986;19:1143.

92. Werbowy S, Kwela J. M1−E2 interference in the Zeeman spectra of Bi I. Phys. Rev. A. 2008;77:023410.

93. Kramida, A., Ralchenko, Yu., Reader, J. *NIST Atomic Spectra Database* (ver. 5.6.1), [Online]. Available: https://physics.nist.gov/asd [2018, December 24]. National Institute of Standards and Technology, Gaithersburg, MD.

94. Chilukoti A, Vishwakarma SR, Deo MN. Hyperfine structure measurements of neutral atomic iodine (^{127}I) in near infrared and visible regions. JQSRT. 2018;220:148.

95. Murakawa K. über das elektrische Quadrupolmoment des Jodkerns. Z Physik 1939;112:234.

96. Fowles GR, Jensen RC. Laser Oscillation on A Single Hyperfine Transition in Iodine. Phys Rev Lett 1965;14:347.

97. Willet CS, Heavens OS. Laser Transition at 651.6nm in Ionized Iodine. Optica Acta 1966;13:271.

98. Labat O, Denize S, Labat J, Puric J, Sreckovic A. Stark Broadening of Singly and Doubly Ionized Iodine Spectral lines. Phys Lett A 1990;143:455.

99. Kono A, Hattori S. Radiative-lifetime measurements for I I and I II. J Opt Soc Am 1979;69:253.

100. Katsonis K, Berenguer C. A Detailed Global Model of Iodine Plasma for Optimization and Diagnostics of Electric Thrusters. Imp J Interdisciplinary Res 2016;2:1093.

101. Grondein P, Lafleur T, Chabert P, Aanesland A. Global model of an iodine gridded plasma thruster. Phys of Plasmas 2016;23;033514.

102. Cockett MCR, Donovan RJ, Lawley KP. Zero kinetic energy pulsed field ionization (ZEKE-PFI) spectroscopy of electronically and vibrationally excited states of I2+: The A 2Π3/2,u state and a new electronic state, the a 4σ-u state, J Chem Phys 1996;105:3347.

103. McLennan JC, McLay AB, Crawford MF. Spark spectra of Bismuth, Bi II and Bi III. Evidence of hyperfine structure. Proc Roy Soc A 1930;129:579.

104. Fishar RA, Goudsmith S. Hyperfine structure in ionized Bismuth. Phys Rev 1931;37:1057.

105. Crawford MF, McLay AB, McLennan JC. Spark spectra of Bismuth, Bi III and Bi II 1933;143:540.

106. Cole CD. Multipole lines in the spectra of Bi II and Pb II. J Opt Soc Am 1964;54:859.

107. Arcimowicz B, Dembczynski J. Relativistic effects in the hyperfine structure of the second spectrum of the Bi II ion. Acta Phys Pol A 1979;56:661.

108. Joshi YN, Mazzoni M. The $6s^2 6p^2 \, ^3P_0 - 6s^2 6pnd \, ^3D_1$ series in photo-absorption of Bi II. Phys Lett A 1986;118:237.

109. Stachowska E, Dembczyński J, Arcimowicz B, Kajoch A. Configuration interaction effect on the hyperfine structure of the levels of the 6s6p3 configuration in Bi II. Z Phys D 1987;7:177.

110. Bouazza S, Bauche J. Hyperfine structure in low-lying levels of Pt II, Au II and Bi II. Z Phys D 1988;10:1

111. Grabowski D, Drozdowski R, Kwela J, Heldt J. Hyperfine structure and Zeeman effect studies in the 6p7p-6p7s transitions in Bi II. Z Phys D 1996;38:289.

112. Crooker AM, Shipley G. Spectroscopic determination of the nuclear moments of Bismuth. Can J Phys 1970;48:730.

113. Holmgren L, Rosén A Hyperfine Structure Analysis in the *6p7s* Configuration of Singly Ionized Bi. Phys Scr 1974;10:171.

114. Palmeri P, Quinet P, Biemont E. Atomic transition probabilities in Bi II. Phys Scr 2001;63:468.

115. Scharfe DB, Capelli MA. Bismuth Hall thruster: II. Simulated diagnostics J Tech Phys 2008;49:349.

116. Andrzejewska M, Meijer FG, Stachowska E. On the level system of Bi II. J Phys B 2013;46:1.

117. Kramida A, Ralchenko Yu, Reader J. NIST Atomic Spectra Database (ver. 5.5.6), [Online]. Available: https://physics.nist.gov/asd [2018, June 28]. National Institute of Standards and Technology, Gaithersburg, MD.

118. Bowen IS. The origin of the nebular lines and the structure of the planetary nebulae. The Astrophysical Journal. 1928;67:1.

119. Rubinowicz A. Zeits f Physik 1930;61:338.

120. Brinkrnan HC. Die Multiplettaufspaltung in den Spektren von Atomen mit zwei Leuchtelektronen. Zeitschrift für Physik 1932;79:753.

121. Rubinowicz A. Multipole radiation in atomic spectra. Rep Prog in Phys 1949;12:233.

122. Joseph C, Boyce DH. Menzel, Cecilia HP. Forbidden lines in astrophysical sources. Pro. of the Nat Aca of Scie of the United States of America 1933;19:581.

123. Sortly GH, Aller LH, Baker JG, Menzel DH. Physical Processes in Gaseous Nebulae. Astrophysical journal 1941;93:178.

124. Verges J. Etude des specters d'emission dans l'infrarouge par l'emploi d'un SISAM-I. Spectre de l'iode entre 1.31μ et 2.2μ et l'effet Zeeman de la raie interdite $5s^2\, 5p^5\, ^2P_{3/2} - 5s^2\, 5p^5\, ^2P_{1/2}$ a 7603 K. Spectrochimica Acta 1969;22B:177.

125. Luc-Koeng E, Morillon C and Verges J. Etude de la transition "Interdite" 2P1/2 − 2P3/2 de la configuration np5 dans le brome et l'iode par spectrometerie de Fourier. Physica 1973;70:175.

126. Morillon C and Verges J. Etude des Configurations Fondamentales 5s25p4 de Te I et I II par l'Observation des Raies Multipolaires Infrarouges. Phys Scr. 1975;12:145.

127. Toshniwal GR. On the arc spectrum of Bismuth. The London, Edinburgh, and Dublin Philosophical Magazine and Journal of Science. 1926;4:23:774.

128. Garstang RH. Transition probabilities of forbidden lines. J Res Nat Bur Stand Sect A 1964;68:61.

129. Heldt J, Mrozowski S. Interference effect in mixed multipole lines of Bi I. J Opt Soc Am 1969;60:467.

130. George S, Munsee JH, Verges J. Hyperfine structure in the $6p^3\, ^4S_{3/2}$ - $6p^3\, ^2D_{5/2}$, 647.5 nm forbidden transition in Bi I. J Opt Soc Am B 1984;1:320.

131. Lucas DM, Warrington RB, Thompson CD, Stacey DN. Hyperfine structure, pressure shift and pressure broadening in the 648 nm transition of atomic bismuth by Faraday spectroscopy. J Phys B 1994;27:5497.

132. Biémont E, Quinet P. Forbidden lines in $6p^k$ (k = 1–5) configurations. Phys Scr 1996;54:36.

133. Wasowicz TJ. The E2 admixtures in mixed forbidden lines of Bi I and Pb I. Phys Scr 2007;76:294.

134. Werbowy S, Kwela J, Drozdowski R, Heldt J. M1-E2 interference in the Zeeman effect of the 461.5 nm line of Bi I. Eur Phys J D 2006;39:5.

135. Werbowy and J. Kwela. The E2 admixtures in mixed multipole lines 459.7 nm and 461.5 nm in the spectrum of Bi I. Eur Phys J Special Topics. 2007;144:179.

136. Werbowy S, Kwela J. The E2 admixtures in mixed multipole lines 459.7 and 564.0 nm of Bi I. Can J Phys 2009;87:851.

137. Cole CD, Mrozowski S. Phys Rev 1954;93: 933.

138. Hults M, Mrozowski S. Multipole lines in spectra of elements from the fifth group. J Opt Soc Am 1964;54:855.

139. Kwela J, Stanislaw Z. Intensity ratios of multipole lines of Bi II. J Opt Soc Am 1983;73:1074.

140. Czerwinska J. Computer simulation of experimental Zeeman-effect patterns of forbidden lines of Bi I and Bi II and estimation of electric-quadrupole admixture in mixed-type radiation. J Opt Soc Am B 1987;4:1357.

141. Augustyniak L, Werel K. Pure electric quadrupole line $\lambda = 587.0$ nm in the spectrum of B II. Phys Scr 1984;30:119.

142. Chilukoti Ashok, Vishwakarma SR, Himal Bhatt, Deo MN. Hyperfine structure measurements of neutral atomic iodine (^{127}I) in the infrared region (1800-6000 cm^{-1}). JQSRT 2019;235:162.

143. Chilukoti Ashok, Vishwakarma SR, Himal B, Ankush BK, Deo MN. Hyperfine Structure Measurements of Neutral Iodine Atom (^{127}I) using Fourier Transform Spectrometry , JQSRT 2018;205:19

144. Chilukoti Ashok. Vishwakarma SR, Deo MN. Hyperfine Structure Measurements of Neutral Atomic Iodine (^{127}I) in Near Infrared and Visible Regions. JQSRT 2018;220:148.

145. Chilukoti Ashok. Vishwakarma SR. Deo MN. Hyperfine Structure Measurements on Singly Ionized Atomic Iodine (I II) using Fourier Transform Spectroscopy. JQSRT 2018;221:71.

146. Chilukoti Ashok, Vishwakarma SR, Deo MN. Fourier transform spectroscopic investigations of atomic bismuth (^{209}Bi I) in the spectral region from IR to UV (2500-40,000 cm^{-1}). JQSRT 2019;229:60.

Appendix I

Table 3.2 Center of gravity wavenumber list of **354** observed spectral transitions of I I in the IR spectral region along with their classifications. The even and odd energy levels are taken from the NIST data base [64]. Here σ_{obs} is the center of gravity wavenumber of the observed spectral lines. The value in parentheses represents the uncertainty. σ_{cal} is the wavenumber calculated using the level energies given in the NIST database [64]. Asterisk (*) denotes blended lines, which also includes those lines for which only one transition is known, but the structure appears to be blended.

σ_{obs} (cm^{-1})	σ_{cal} (cm^{-1})	Even Level E_{e} (cm^{-1})	J_{e}	Odd Level E_{o} (cm^{-1})	J_{o}	*hfs* done
1818.575(3)	1818.552	73795.327	5/2	71976.775	3/2	
1851.658(3)	1851.672	75511.130	7/2	77362.802	9/2	
1853.746(2)	1853.755	76903.269	5/2	75049.514	3/2	a
1878.454(4)	1878.489	79285.273	½	77406.784	3/2	
1880.892(3)	1880.911	79285.273	½	77404.362	1/2	
1928.043(4)	1928.037	80772.340	9/2	78844.303	7/2	
1934.380(4)	1934.397	77555.824	3/2	75621.427	3/2	a
1934.733(3)	1934.707	73114.807	½	75049.514	3/2	a
1937.615(2)	1937.634	76903.269	5/2	74965.635	5/2	
1943.932(4)	1943.939	80676.170	7/2	78732.231	5/2	
1947.870(3)	1947.889	80680.120	5/2	78732.231	5/2	
1982.125(5)	1982.127	73639.300	3/2	75621.427	3/2	a
2014.387(5)	2014.413	80869.160	7/2	78854.747	5/2	
2033.125(3)	2033.129	76746.978	3/2	78780.107	1/2	a
2056.430(2)	2056.427	67726.415	9/2	65669.988	7/2	a
2100.294(5)	2100.327	76903.269	5/2	79003.596	7/2	
2105.032(4)	2105.030	79418.489	5/2	77313.459	7/2	a
2122.635(4)	2122.637	75177.235	5/2	73054.598	3/2	a
2130.057(3)*	2130.045	75177.235	5/2	77307.280	7/2	
2130.057(3)*	2130.098	75177.235	5/2	77307.333	5/2	
2136.226(4)	2136.224	75177.235	5/2	77313.459	7/2	
2137.827(3)	2137.820	73639.300	3/2	71501.480	1/2	a
2145.777(4)	2145.767	77555.824	3/2	79701.591	1/2	a
2179.408(5)	2179.401	75177.235	5/2	77356.636	3/2	
2182.368(5)	2182.350	75177.235	5/2	77359.585	5/2	a
2188.255(4)	2188.258	73114.807	½	75303.065	1/2	a
2252.745(3)	2252.759	77555.824	3/2	75303.065	1/2	a
2256.658(2)	2256.653	77450.709	5/2	75194.056	7/2	a
2259.379(2)	2259.372	77450.709	5/2	75191.337	5/2	a
2278.826(3)	2278.844	76136.403	3/2	78415.247	3/2	a
2308.335(2)	2308.334	67298.328	½	64989.994	3/2	a
2364.490(5)	2364.487	77555.824	3/2	75191.337	5/2	a

σ_{obs} (cm^{-1})	σ_{cal} (cm^{-1})	Even Level E_e (cm^{-1})	J_e	Odd Level E_o (cm^{-1})	J_o	hfs done
2397.610(5)	2397.657	76417.783	½	78815.440	3/2	a
2401.191(4)	2401.195	77450.709	5/2	75049.514	3/2	a
2408.104(5)	2408.147	81252.450	5/2	78844.303	7/2	
2436.725(5)	2436.725	75823.909	3/2	73387.184	1/2	a
2477.658(2)	2477.678	76746.978	3/2	79224.656	3/2	
2485.072(4)	2485.074	77450.709	5/2	74965.635	5/2	a
2498.073(3)		Unclassified				
2500.372(2)		Unclassified				
2506.300(2)	2506.310	77555.824	3/2	75049.514	3/2	a
2525.237(3)		Unclassified				
2525.899(4)	2525.860	82385.430	9/2	79859.570	9/2	
2535.913(2)		Unclassified				
2537.047(2)		Unclassified				
2537.723(5)	2537.747	82385.430	9/2	79847.683	7/2	
2539.006(2)		Unclassified				
2545.278(5)	2545.267	82426.650	3/2	79881.383	3/2	
2548.057(4)		Unclassified				
2574.637(4)*		Unclassified				
2580.694(3)*		Unclassified				
2581.467(4)		Unclassified				
2582.042(4)	2582.181	82426.650	3/2	79844.469	5/2	
2588.288(5)		Unclassified				
2610.663(3)	2610.640	74587.415	3/2	71976.775	3/2	a
2643.667(2)	2643.704	76136.403	3/2	78780.107	1/2	a
2648.051(3)	2648.053	75177.235	5/2	72529.182	5/2	a
2670.200(4)	2670.202	63186.758	½	65856.960	1/2	a
2670.749(4)	2670.754	72294.881	3/2	74965.635	5/2	a
2692.774(3)	2692.783	68549.743	3/2	65856.960	1/2	a
2699.775(3)	2699.764	70354.834	3/2	73054.598	3/2	a
2700.795(4)	2700.824	75714.423	½	78415.247	3/2	a
2708.869(4)	2708.892	76106.548	5/2	78815.440	3/2	a
2719.887(5)*	2719.918	74587.415	3/2	77307.333	5/2	
2727.505(3)	2727.500	76004.731	7/2	78732.231	5/2	
2737.758(2)	2737.755	76106.548	5/2	78844.303	7/2	
2749.234(5)	2749.219	76136.403	3/2	73387.184	1/2	a
2754.630(5)	2754.633	72294.881	3/2	75049.514	3/2	a
2758.777(2)	2758.774	68615.734	½	65856.960	1/2	a
2769.235(3)	2769.221	74587.415	3/2	77356.636	3/2	
2773.459(4)	2773.457	74587.415	3/2	71813.958	1/2	a
2794.242(4)	2794.243	78415.670	½	75621.427	3/2	a
2806.889(3)	2806.873	76417.783	½	79224.656	3/2	a
2816.953(4)	2816.947	74587.415	3/2	77404.362	1/2	a
2818.040(4)	2818.043	79395.897	3/2	82213.940	5/2	
2819.385(2)	2819.369	74587.415	3/2	77406.784	3/2	
2844.293(2)	2844.295	75898.893	5/2	73054.598	3/2	
2850.025(4)	2850.016	76004.731	7/2	78854.747	5/2	a
2885.737(2)	2885.746	68615.734	½	71501.480	1/2	a

170

σ_{obs} (cm^{-1})	σ_{cal} (cm^{-1})	Even Level E_e (cm^{-1})	J_e	Odd Level E_o (cm^{-1})	J_o	*hfs* done
2889.554(3)	2889.552	68559.540	7/2	65669.988	7/2	a
2896.457(4)	2896.456	72294.881	3/2	75191.337	5/2	a
2903.396(4)	2903.397	70151.201	5/2	73054.598	3/2	a
2905.277(3)	2905.267	68549.743	3/2	65644.476	5/2	a
2907.266(2)	2907.259	75714.423	½	72807.164	3/2	a
2908.320(5)	2908.322	75823.909	3/2	78732.231	5/2	a
2915.064(5)	2915.064	68559.540	7/2	65644.476	5/2	a
2916.514(4)	2916.547	75898.893	5/2	78815.440	3/2	a
2917.853(3)	2917.871	68587.859	5/2	65669.988	7/2	a
2929.701(5)	2929.686	76903.269	5/2	79832.955	7/2	
2936.903(4)	2936.883	76903.269	5/2	79840.152	5/2	
2943.387(5)	2943.383	68587.859	5/2	65644.476	5/2	a
2944.434(5)	2944.414	76903.269	5/2	79847.683	7/2	
2945.419(3)	2945.410	75898.893	5/2	78844.303	7/2	a
2955.827(3)	2955.854	75898.893	5/2	78854.747	5/2	
2981.953(4)	2981.948	75511.130	7/2	72529.182	5/2	a
2991.519(5)	2991.531	75823.909	3/2	78815.440	3/2	a
3008.182(3)	3008.184	72294.881	3/2	75303.065	1/2	a
3016.746(2)	3016.745	75823.909	3/2	72807.164	3/2	a
3030.619(4)	3030.599	76417.783	½	73387.184	1/2	a
3030.877(3)	3030.838	75823.909	3/2	78854.747	5/2	
3032.336(2)	3032.350	70354.834	3/2	73387.184	1/2	a
3051.952(5)	3051.950	76106.548	5/2	73054.598	3/2	a
3061.901(4)	3061.899	71903.736	5/2	74965.635	5/2	a,b
3065.658(4)	3065.684	75714.423	½	78780.107	1/2	a
3081.806(5)	3081.805	76136.403	3/2	73054.598	3/2	
3085.940(3)	3085.935	74587.415	3/2	71501.480	1/2	a
3086.512(4)	3086.511	61819.779	3/2	64906.290	5/2	a
3089.079(2)	3089.071	70151.201	5/2	67062.130	3/2	a,b
3091.167(3)	3091.130	78415.670	½	81506.800	1/2	a
3091.727(5)	3091.729	75898.893	5/2	72807.164	3/2	a
3093.213(4)	3093.174	76746.978	3/2	79840.152	5/2	
3097.523(2)	3097.491	76746.978	3/2	79844.469	5/2	
3100.986(4)	3101.017	75714.423	½	78815.440	3/2	a
3103.266(5)	3103.206	77555.824	3/2	80659.030	5/2	
3104.699(2)	3104.703	75898.893	5/2	79003.596	7/2	a
3112.608(2)	3112.605	78415.670	½	75303.065	1/2	a
3140.216(3)	3140.163	75704.140	9/2	78844.303	7/2	a
3145.776(5)	3145.778	71903.736	5/2	75049.514	3/2	a
3170.219(2)	3170.215	61819.779	3/2	64989.994	3/2	a
3173.637(5)	3173.611	77450.709	5/2	80624.320	5/2	
3182.963(3)	3182.948	79030.992	3/2	82213.940	5/2	
3189.162(2)	3189.16	78415.670	½	81604.830	1/2	
3200.479(4)	3200.460	75177.235	5/2	71976.775	3/2	a
3210.598(3)	3210.551	77450.709	5/2	80661.260	7/2	
3221.104(2)	3221.101	75511.130	7/2	78732.231	5/2	a
3241.971(4)	3241.956	77555.824	3/2	80797.780	3/2	

σ_{obs} (cm^{-1})	σ_{cal} (cm^{-1})	Even Level E_e (cm^{-1})	J_e	Odd Level E_o (cm^{-1})	J_o	hfs done
3264.214(5)	3264.215	68549.743	3/2	71813.958	1/2	a
3269.759(2)	3269.760	78891.187	3/2	75621.427	3/2	a
3287.608(3)	3287.601	71903.736	5/2	75191.337	5/2	a
3290.323(3)	3290.320	71903.736	5/2	75194.056	7/2	a,b
3292.706(3)	3292.704	70354.834	3/2	67062.130	3/2	a,b
3299.396(5)*	3299.384	76106.548	5/2	72807.164	3/2	
3299.396(5)*	3299.456	75704.140	9/2	79003.596	7/2	
3307.236(2)	3307.230	78415.670	½	81722.900	3/2	a
3321.914(5)	3321.914	78943.341	5/2	75621.427	3/2	
3322.764(5)	3322.753	78891.187	3/2	82213.940	5/2	a
3325.778(4)	3325.763	75898.893	5/2	79224.656	3/2	a
3326.547(3)	3326.546	72294.881	3/2	75621.427	3/2	a,b
3328.845(3)	3328.844	73977.715	7/2	77306.559	9/2	a,b
3329.245(4)	3329.239	76136.403	3/2	72807.164	3/2	
3329.571(4)*	3329.565	73977.715	7/2	77307.280	7/2	
3329.571(4)*	3329.618	73977.715	7/2	77307.333	5/2	
3333.182(2)	3333.173	75511.130	7/2	78844.303	7/2	a
3335.750(3)	3335.744	73977.715	7/2	77313.459	7/2	a
3359.770(5)	3359.794	76746.978	3/2	73387.184	1/2	a
3361.015(4)	3361.041	68615.734	½	71976.775	3/2	a
3363.182(4)	3363.185	76417.783	½	73054.598	3/2	a
3366.159(4)	3366.156	78415.670	½	75049.514	3/2	a
3369.706(3)	3369.711	75898.893	5/2	72529.182	5/2	a
3378.492(4)	3378.472	76746.978	3/2	80125.45	5/2	
3381.879(5)	3381.870	73977.715	7/2	77359.585	5/2	
3385.064(2)	3385.087	73977.715	7/2	77362.802	9/2	a
3400.741(3)	3400.747	75823.909	3/2	79224.656	3/2	
3409.556(4)	3409.565	79030.992	3/2	75621.427	3/2	a
3410.247(5)	3410.212	80772.340	9/2	77362.128	11/2	
3427.010(2)	3427.032	68549.743	3/2	71976.775	3/2	
3463.897(5)*	3463.600	76417.783	½	79881.383	3/2	a
3463.897(5)*	3463.950	76417.783	½	79881.733	1/2	
3511.964(4)*	3511.953	73795.327	5/2	77307.280	7/2	b
3511.964(4)*	3512.006	73795.327	5/2	77307.333	5/2	b
3559.745(4)	3559.749	68549.743	3/2	64989.994	3/2	a
3561.314(5)	3561.309	73795.327	5/2	77356.636	3/2	
3564.269(4)	3564.258	73795.327	5/2	77359.585	5/2	
3577.373(2)	3577.366	76106.548	5/2	72529.182	5/2	a
3597.818(3)	3597.865	68587.859	5/2	64989.994	3/2	a
3611.465(4)	3611.457	73795.327	5/2	77406.784	3/2	
3625.742(5)	3625.740	68615.734	½	64989.994	3/2	a,b
3643.467(2)	3643.453	68549.743	3/2	64906.290	5/2	a,b
3653.251(2)	3653.250	68559.540	7/2	64906.290	5/2	a,b
3663.829(3)	3663.846	79285.273	½	75621.427	3/2	a
3668.008(5)*	3668.033	73639.300	3/2	77307.333	5/2	
3681.573(2)	3681.569	68587.859	5/2	64906.290	5/2	a,b
3692.345(4)	3692.380	76746.978	3/2	73054.598	3/2	

σ_{obs} (cm^{-1})	σ_{cal} (cm^{-1})	Even Level E_e (cm^{-1})	J_e	Odd Level E_o (cm^{-1})	J_o	hfs done
3703.751(5)	3703.749	76136.403	3/2	79840.152	5/2	
3709.970(5)	3710.005	78904.061	7/2	75194.056	7/2	a
3712.712(4)	3712.724	78904.061	7/2	75191.337	5/2	
3717.338(4)	3717.336	73639.300	3/2	77356.636	3/2	b
3717.696(5)	3717.691	71903.736	5/2	75621.427	3/2	a,b
3727.936(4)	3727.927	79030.992	3/2	75303.065	1/2	a
3765.063(3)	3765.062	73639.300	3/2	77404.362	1/2	a
3771.766(5)	3771.778	79393.205	½	75621.427	3/2	a
3774.478(5)	3774.470	79395.897	3/2	75621.427	3/2	a
3797.080(4)	3797.062	79418.489	5/2	75621.427	3/2	a
3824.702(4)	3824.697	61819.779	3/2	65644.476	5/2	a,b
3826.166(5)	3826.361	75177.235	5/2	79003.596	7/2	
3828.227(3)	3828.224	76004.731	7/2	79832.955	7/2	
3841.678(3)	3841.673	78891.187	3/2	75049.514	3/2	a
3842.975(4)	3842.952	76004.731	7/2	79847.683	7/2	
3847.159(5)	3847.134	75823.909	3/2	71976.775	3/2	a
3848.653(4)	3848.671	76903.269	5/2	73054.598	3/2	a
3854.827(5)	3854.839	76004.731	7/2	79859.570	9/2	
3860.932(3)	3860.929	79054.985	9/2	75194.056	7/2	a
3875.367(3)	3875.372	63186.758	½	67062.130	3/2	a
3893.839(2)	3893.827	78943.341	5/2	75049.514	3/2	a
3900.475(5)	3900.465	75714.423	½	71813.958	1/2	a
3903.378(3)	3903.376	76136.403	3/2	80039.779	3/2	a
3922.142(2)	3922.118	75898.893	5/2	71976.775	3/2	a
3925.567(3)	3925.552	78891.187	3/2	74965.635	5/2	
3926.553(4)	3926.528	73477.834	½	77404.362	1/2	a
3928.976(4)	3928.950	73477.834	½	77406.784	3/2	
3938.405(2)	3938.426	78904.061	7/2	74965.635	5/2	a
3939.783(5)	3939.814	76746.978	3/2	72807.164	3/2	a
3941.313(5)	3941.323	68587.859	5/2	72529.182	5/2	a
3945.583(4)	3945.576	75898.893	5/2	79844.469	5/2	
3948.796(4)	3948.790	75898.893	5/2	79847.683	7/2	
3959.238(3)	3959.213	79150.550	7/2	75191.337	5/2	a
3969.654(3)	3969.642	68559.540	7/2	72529.182	5/2	
3977.709(5)	3977.706	78943.341	5/2	74965.635	5/2	a,b
3979.440(4)	3979.439	68549.743	3/2	72529.182	5/2	a
3981.483(5)	3981.478	79030.992	3/2	75049.514	3/2	a,b
3982.201(5)	3982.208	79285.273	½	75303.065	1/2	a,b
4005.177(4)	4005.157	74587.415	3/2	78592.572	5/2	a
4009.950(3)	4009.951	75823.909	3/2	71813.958	1/2	a
4010.987(3)	4011.001	75823.909	3/2	79834.910	3/2	a
4020.568(2)	4020.560	75823.909	3/2	79844.469	5/2	
4037.185(3)	4037.182	61819.779	3/2	65856.960	1/2	a
4057.767(4)*	4057.474	75823.909	3/2	79881.383	3/2	
4057.767(4)*	4057.864	75823.909	3/2	79881.773	1/2	
4065.358(3)	4065.357	79030.992	3/2	74965.635	5/2	a
4090.123(4)	4090.140	79393.205	½	75303.065	1/2	a

σ_{obs} (cm^{-1})	σ_{cal} (cm^{-1})	Even Level E_e (cm^{-1})	J_e	Odd Level E_o (cm^{-1})	J_o	hfs done
4092.841(3)	4092.832	79395.897	3/2	75303.065	1/2	a
4093.758(3)	4093.751	60896.243	½	64989.994	3/2	a,b
4096.094(5)	4096.105	76903.269	5/2	72807.164	3/2	a
4120.470(4)	4120.487	75714.423	½	79834.910	3/2	a
4125.479(2)	4125.460	75704.140	9/2	79829.600	9/2	
4129.795(3)	4129.773	76106.548	5/2	71976.775	3/2	a
4154.875(3)	4154.870	75704.140	9/2	79859.010	11/2	a
4168.639(2)	4168.640	77555.824	3/2	73387.184	1/2	a,b
4184.900(5)	4184.915	79150.550	7/2	74965.635	5/2	
4191.432(4)	4191.430	68615.734	½	72807.164	3/2	a,b
4203.157(4)	4203.152	67298.328	½	71501.480	1/2	a
4204.558(5)	4204.560	79395.897	3/2	75191.337	5/2	a
4212.952(5)	4212.943	75714.423	½	71501.480	1/2	a,b
4217.761(4)	4217.796	76746.978	3/2	72529.182	5/2	a
4219.321(4)	4219.305	68587.859	5/2	72807.164	3/2	a,b
4227.161(3)	4227.152	79418.489	5/2	75191.337	5/2	a,b
4235.752(4)	4235.759	79285.273	½	75049.514	3/2	a
4241.823(5)	4241.829	73114.807	½	77356.636	3/2	b
4289.548(2)	4289.555	73114.807	½	77404.362	1/2	a,b
4291.972(3)	4291.977	73114.807	½	77406.784	3/2	a,b
4293.256(3)	4293.255	79914.682	5/2	75621.427	3/2	
4303.964(5)	4303.871	76903.269	5/2	81207.14	7/2	
4318.448(4)	4318.470	75511.130	7/2	79829.600	9/2	
4321.827(4)	7321.825	75511.130	7/2	79832.955	7/2	
4322.438(3)*	4322.501	75823.909	3/2	71501.408	1/2	a
4322.438(3)*	4322.445	76136.403	3/2	71813.958	1/2	a
4325.706(4)	4325.696	79947.123	3/2	75621.427	3/2	a
4333.341(3)	4333.339	75511.130	7/2	79844.469	5/2	
4336.547(5)	4336.553	75511.130	7/2	79847.683	7/2	
4343.678(5)	4343.691	79393.205	½	75049.514	3/2	a
4348.414(2)	4348.440	75511.130	7/2	79859.570	9/2	
4368.985(3)	4368.975	79418.489	5/2	75049.514	3/2	a
4374.076(3)	4374.087	76903.269	5/2	72529.182	5/2	a
4396.108(4)	4396.111	77450.709	5/2	73054.598	3/2	a,b
4430.294(4)	4430.262	79395.897	3/2	74965.635	5/2	
4438.871(3)	4438.864	68615.734	½	73054.598	3/2	a,b
4441.036(5)	4441.008	76417.783	½	71976.775	3/2	a
4466.773(3)	4466.739	68587.859	5/2	73054.598	3/2	a
4481.221(4)	4481.213	70151.201	5/2	65669.988	7/2	a,b
4497.877(3)	4497.874	70354.834	3/2	65856.960	1/2	a,b
4504.861(4)	4504.855	68549.743	3/2	73054.598	3/2	
4506.734(4)	4506.725	70151.201	5/2	65644.476	5/2	a,b
4515.636(3)	4515.630	67298.328	½	71813.958	1/2	a,b
4603.829(3)	4603.825	76417.783	½	71813.958	1/2	a,b
4610.807(5)	4610.801	70354.834	3/2	74965.635	5/2	a
4644.065(5)	4644.058	79947.123	3/2	75303.065	1/2	a
4654.349(3)	4654.26	76004.731	7/2	80659.030	5/2	

174

σ_{obs} (cm^{-1})	σ_{cal} (cm^{-1})	Even Level E_e (cm^{-1})	J_e	Odd Level E_o (cm^{-1})	J_o	*hfs* done
4655.713(3)	4655.720	75177.235	5/2	79832.955	7/2	a
4667.242(4)	4667.233	75177.235	5/2	79844.469	5/2	
4678.428(2)	4678.447	67298.328	½	71976.775	3/2	a
4694.676(5)	4694.680	70354.834	3/2	75049.514	3/2	a,b
4710.360(3)	4710.358	70354.834	3/2	65644.476	5/2	a
4720.622(3)	4720.626	79914.682	5/2	75194.056	7/2	a
4755.790(4)	4755.786	79947.123	3/2	75191.337	5/2	b
4770.186(3)	4770.203	76746.978	3/2	71976.775	3/2	
4771.417(5)	4771.450	68615.734	½	73387.184	1/2	
4808.124(5)	4808.107	76417.783	½	81225.890	1/2	
4809.465(3)	4809.457	76417.783	½	81227.240	3/2	
4814.437(4)	4814.434	70151.201	5/2	74965.635	5/2	a,b
4836.507(4)	4836.503	70354.834	3/2	75191.337	5/2	a
4837.432(5)	4837.441	68549.743	3/2	73387.184	1/2	a,b
4841.613(5)	4841.606	71903.736	5/2	67062.130	3/2	a,b
4865.175(3)	4865.168	79914.682	5/2	75049.514	3/2	a
4897.615(5)	4897.609	79947.123	3/2	75049.514	3/2	a
4898.317(4)	4898.313	70151.201	5/2	75049.514	3/2	a
4921.500(4)	4921.527	77450.709	5/2	72529.182	5/2	a,b
4937.421(5)	4937.413	73477.834	½	78415.247	3/2	a,b
4948.236(3)	4948.231	70354.834	3/2	75303.065	1/2	a,b
4949.045(3)	4949.047	79914.682	5/2	74965.635	5/2	a
4953.286(4)	4953.272	73639.300	3/2	78592.572	5/2	
4957.210(4)	4957.120	75704.140	9/2	80661.260	7/2	
4960.726(2)	4960.717	60896.243	½	65856.960	1/2	a,b
5012.426(3)	5012.452	72294.881	3/2	77307.333	5/2	a,b
5025.735(5)	5025.881	73977.715	7/2	79003.596	7/2	
5026.642(3)	5026.642	77555.824	3/2	72529.182	5/2	a
5040.139(3)	5040.136	70151.201	5/2	75191.337	5/2	a,b
5042.860(4)	5042.855	70151.201	5/2	75194.056	7/2	a,b
5064.712(3)	5064.704	72294.881	3/2	77359.585	5/2	a,b
5068.999(2)	5068.987	76136.403	3/2	81205.390	5/2	
5095.151(3)	5095.112	76106.548	5/2	81201.660	7/2	
5111.912(4)	5111.903	72294.881	3/2	77406.784	3/2	a
5113.189(3)	5113.190	75511.130	7/2	80624.320	5/2	
5114.180(2)	5114.176	74587.415	3/2	79701.591	1/2	a
5146.392(5)	5146.387	66355.093	3/2	71501.480	1/2	a,b
5161.212(3)	5161.207	70151.201	5/2	64989.994	3/2	a,b
5212.797(5)	5212.769	76004.731	7/2	81217.500	9/2	
5232.759(2)	5232.751	72294.881	3/2	67062.130	3/2	a,b
5242.355(3)	5242.351	61819.779	3/2	67062.130	3/2	a,b
5244.920(4)	5244.911	70151.201	5/2	64906.290	5/2	a,b
5245.470(4)	5245.498	76746.978	3/2	71501.480	1/2	a
5260.876(3)	5260.863	80882.290	5/2	75621.427	3/2	
5266.601(5)	5266.593	70354.834	3/2	75621.427	3/2	a,b
5308.327(5)	5308.247	75898.893	5/2	81207.140	7/2	
5364.843(2)	5364.840	70354.834	3/2	64989.994	3/2	a

σ_{obs} (cm^{-1})	σ_{cal} (cm^{-1})	Even Level E_e (cm^{-1})	J_e	Odd Level E_o (cm^{-1})	J_o	hfs done
5387.876(3)	5387.850	80690.915	3/2	75303.065	1/2	a
5390.931(4)	5390.880	80693.945	½	75303.065	1/2	a
5403.569(3)*	5403.544	71903.736	5/2	77307.280	7/2	
5403.569(3)*	5403.597	71903.736	5/2	77307.333	5/2	
5409.724(5)	5409.723	71903.736	5/2	77313.459	7/2	a,b
5448.548(5)	5448.544	70354.834	3/2	64906.290	5/2	a,b
5452.372(3)	5452.364	74587.415	3/2	80039.779	3/2	a
5455.868(4)	5455.849	71903.736	5/2	77359.585	5/2	a
5458.873(4)	5458.865	66355.093	3/2	71813.958	1/2	a
5470.233(5)	5470.226	70151.201	5/2	75621.427	3/2	a
5473.947(3)	5473.934	77450.709	5/2	71976.775	3/2	a
5479.410(4)	5479.405	80782.470	3/2	75303.065	1/2	
5482.105(2)	5482.114	80676.170	7/2	75194.056	7/2	
5484.847(2)	5484.833	80676.170	7/2	75191.337	5/2	
5486.045(5)	5486.064	80680.120	5/2	75194.056	7/2	
5502.340(5)	5502.337	78889.521	½	73387.184	1/2	a
5508.836(3)	5508.836	67298.328	½	72807.164	3/2	a,b
5513.017(4)	5512.890	75704.140	9/2	81217.030	11/2	
5578.316(3)	5578.284	80772.340	9/2	75194.056	7/2	
5608.511(3)	5608.506	78415.670	½	72807.164	3/2	a,b
5621.671(4)	5621.682	66355.093	3/2	71976.775	3/2	
5630.602(5)	5630.606	80680.120	5/2	75049.514	3/2	a
5641.433(5)	5641.426	80690.94	3/2	75049.514	3/2	a
5677.823(4)	5677.823	80869.160	7/2	75191.337	5/2	a
5688.634(2)	5688.610	75511.130	7/2	81199.740	9/2	
5690.560(3)	5690.530	75511.130	7/2	81201.660	7/2	
5690.950(5)	5690.953	80882.290	5/2	75191.337	5/2	
5710.527(4)	5710.535	80676.170	7/2	74965.635	5/2	
5714.469(2)	5714.485	80680.120	5/2	74965.635	5/2	a
5725.308(5)	5725.280	80690.915	3/2	74965.635	5/2	
5746.867(3)	5746.822	73477.834	½	79224.656	3/2	a
5756.273(5)	5756.270	67298.328	½	73054.598	3/2	a
5776.104(3)	5776.076	80825.590	½	75049.514	3/2	a
5834.915(4)	5834.923	78889.521	½	73054.598	3/2	
5836.593(4)	5836.589	78891.187	3/2	73054.598	3/2	a
5868.722(5)	5868.772	76746.978	3/2	82615.750	1/2	
5888.743(3)	5888.743	78943.341	5/2	73054.598	3/2	a
5898.091(4)	5898.089	79285.273	½	73387.184	1/2	a
5956.290(5)	5956.306	66020.469	5/2	71976.775	3/2	a
5976.389(4)	5976.394	79030.992	3/2	73054.598	3/2	a

a: hfs in this work., b: hfs in previous work [6].

Table 3.3 Even energy levels of I I involved in the spectral region of 1800-6000 cm^{-1} and their experimentally derived *hfs* A and B constants in mK in comparison with previous literature.

Electronic Configuration	Even Level E_e (cm^{-1})	A_{Exp}	B_{Exp}	A Ref. [21]	B Ref. [21]	A Ref. [22]	B Ref. [22]	A Ref. [23]	B Ref. [23]
$5s^25p^4(^3P_1)$									
6s[1]3/2	61819.779	22.32(38)	14.02(56)	22.57(10)	14.5(1.0)	22.68(24)	14(1)	22.65(17)	14.51(67)
6s[1]1/2	63186.758	-4.15(15)						-3.97(07)	
$5s^25p^4(^3P_0)6s$									
[0]1/2	60896.243	53.55(23)		53.58(05)		53.22(28)		53.77(07)	
$5s^25p^4(^1D_2)6s$									
[2]5/2	68587.859	82.40(41)	72.69(1.85)	82.99(10)	71.76(1.0)	82.95(15)	70(1)	83.19(10)	69.91(50)
[2]3/2	68549.743	60.65(39)	36.9(1.2)	60.47(10)	36.70(1.0)	59.08(85)	36(4)	60.71(07)	36.39(33)
$5s^25p^4(^3P_2)7s$									
[2]5/2	71903.736	30.65(33)	-34.2(1.4)	30.36(0.05)	-33.82(1.0)				
[2]3/2	72294.881	33.78(46)	21.03(61)	33.53(0.1)	-20.82(0.5)				
$5s^25p^4(^3P_1)7s$									
[1]3/2	78891.187	6.41(19)	13.52(55)	6.49(20)	15.37(2.0)				
[1]1/2	79285.273	7.06(83)		6.2(3)		6.80(53)		5.84(20)	
$5s^25p^4(^3P_0)7s$									
[0]1/2	78415.670	13.89(44)		13.55(5)		14.40(56)		13.48(03)	
$5s^25p^4(^3P_2)8s$									
[2]3/2	77555.824	35.88(29)	-22.16(47)	36.07(20)	-22.81(80)	35.85(34)	-26(1)	36.06(33)	-23.35(33)
$5s^25p^4(^3P_1)8s$									
[2]5/2	77450.709	27.42(48)	-34.72(1.8)	27.23(50)	-34.64(50)			27.39(33)	-31.02(33)
$5s^25p^4(^3P_2)9s$									
[2]5/2	79914.682	26.14(43)	-31.6(1.3)					26.35(20)	-29.95(67)
[2]3/2	79947.123	36.96(81)	-23.4(1.5)	36.98(10)	-23.95(1.0)			36.83(33)	-14.6(1.0)
$5s^25p^4(^3P_2)5d$									
[4]9/2	67726.415	13.42(07)	-31.74(35)	13.49(10)	-31.48(2.0)				
[4]7/2	68559.540	17.52(08)	-27.17(37)	17.55(10)	-27.45(4.0)			17.75(17)	-28.89(67)
[3]5/2	66020.469	22.94(32)	4.70(55)	21.59(20)	4.0(4.0)	21.57(15)	6(1)	21.41(07)	5.90(33)

Electronic Configuration	Even Level E_e (cm^{-1})	A_{Exp}	B_{Exp}	A Ref. [21]	B Ref. [21]	A Ref. [22]	B Ref. [22]	A Ref. [23]	B Ref. [23]
[2]5/2	70151.201	15.43(28)	4.87(97)	15.46(10)	4.1(5)			15.84(16)	-3.67(1.6)
[2]3/2	70354.834	21.10(21)	22.55(89)	21.08(10)	22.8(5)	21.46(29)	20(1)	21.35(17)	16.34(1.7)
[1]3/2	66355.093	33.34(26)	10.39(1.15)	32.59(05)	10.96(50)	32.55(27)	8(1)	32.56(07)	9.61(33)
[1]1/2	67298.328	38.22(80)		37.8(20)		37.91(23)		39.33(67)	
[0]1/2	68615.734	94.30(34)		94.46(10)		94.56(23)			
$5s^25p^4(^3P_1)5d$									
[3]7/2	73977.715	-2.22(22)	-0.77(35)	-1.92(10)	1.21(50)				
[3]5/2	75177.235	10.17(17)	-4.59(98)	9.79(10)	-4.2(1.0)				
[2]5/2	75898.893	5.21(36)	13.95(83)	4.33(10)	11.31				
[2]3/2	75823.909	11.57(31)	-3.08(36)	11.49(30)	-3.26(50)				
[1]3/2	74587.415	17.69(28)	0.80(52)	17.47(10)	1.0(1.0)				
[1]1/2	73114.807	28.41(49)		28.86(05)					
$5s^25p^4(^3P_0)5d$									
[2]3/2	73639.300	8.82(49)	-9.6(1.7)	9.01(05)	-9.34(50)				
$5s^25p^4(^1D_2)5d$									
[0]1/2	73477.834	294.50(44)		294.77(02)					
$5s^25p^4(^3P_2)6d$									
[4]9/2	75704.140	14.21(42)	-36.8(1.3)						
[4]7/2	76004.731	15.78(26)	-21.51(64)	16.03(10)	-20.86(1.0)				
[3]7/2	75511.130	12.78(43)	-10.16(71)	12.88(10)	-10.15(1.0)				
[3]5/2	76106.548	7.86(39)	-21.08(95)	7.74(10)	-20.33(1.0)				
[2]5/2	76903.269	12.16(33)	12.12(64)			11.37(45)	7(3)		
[2]3/2	76746.978	-5.76(87)	4.34(89)						
[1]3/2	76136.403	5.37(22)	5.58(37)	4.72(10)	5.28(1.0)				
[1]1/2	76417.783	49.06(37)		48.63(30)		48.73(57)		48.60(33)	
[0]1/2	75714.423	25.30(24)		25.33(40)					
$5s^25p^4(^3P_2)7d$									
[4]9/2	79054.985	14.28(26)	-34.26(88)						
[4]7/2	79150.550	17.65(22)	-27.68(39)						
[3]7/2	78904.061	15.06(17)	-11.27(42)						

Electronic Configuration	Even Level E_e (cm^{-1})	A_{Exp}	B_{Exp}	A Ref. [21]	B Ref. [21]	A Ref. [22]	B Ref. [22]	A Ref. [23]	B Ref. [23]
[3]5/2	78943.341	17.85(24)	-6.47(29)	17.68(10)	-6.20(1.0)				
[2]5/2	79418.489	14.78(56)	4.9(1.2)	15.06(10)	4.3(1.0)	14.34(53)	12(6)	14.84(20)	3.87(67)
[2]3/2	79395.897	4.53(53)	16.09(61)			5.90(55)	13(2)	3.84(33)	21.4(1.0)
[1]3/2	79030.992	21.23(49)	3.87(97)	21.17(10)	5.37(50)	20.48(13)	1(5)		
[1]1/2	78889.521	2.13(87)							
[0]1/2	79393.205	1.88(40)							
$5s^2 5p^4(^3P_2)8d$									
[4]7/2	80869.160	24.95(62)	-9.85(79)						
[1]3/2	80690.940	22.93(26)	1.82(1.4)						
	80693.945	-15.07(39)							
	80680.120	17.45(70)	-6.0(1.4)						
	80825.560	49.63(75)							

Table 3.4 Odd energy levels of I I involved in the spectral region of 1800-6000 cm^{-1} and their experimentally derived *hfs* A and B constants in mK in comparison with previous literature.

Electronic Configuration	E_o (cm^{-1})	A_{Exp}	B_{Exp}	A Ref. [21]	B Ref. [21]	A Ref.[22]	B Ref.[22]	A Ref. [23]	B Ref. [23]
$5s^25p^4(^3P_2)6p$									
[3]7/2	65669.988	19.25(16)	-37.70(76)	19.57(5)	-36.84(50)				
[3]5/2	65644.476	23.93(27)	-22.38(87)	24.03(10)	-22.04(50)				
[2]5/2	64906.290	25.27(31)	-19.45(42)	25.31(10)	-18.86(1.0)	26.73(47)	-16(4)	25.38(33)	-17.7(1.0)
[2]3/2	64989.994	35.24(32)	-23.23(84)	35.38(10)	-23.56(1.0)	35.21(43)	-25(2)	35.36(20)	-23.52(67)
[1]3/2	67062.130	29.23(42)	-0.56(55)	29.13(5)	-0.45(50)	29.38(40)	0(2)	28.92(10)	-0.70(33)
[1]1/2	65856.960	57.72(76)		57.25(5)		57.04(35)		57.34(07)	
$5s^25p^4(^3P_1)6p$									
[2]5/2	72529.182	-6.47(57)	15.99(81)	-5.79(5)	14.19(50)				
[2]3/2	72807.164	-0.59(15)	16.9(1.1)	-0.53(10)	16.14(20)				
[1]3/2	73054.598	2.35(31)	-16.04(93)	2.18(5)	-14.58(50)			2.33(20)	-14.01(67)
[1]1/2	73387.184	-31.4(1.2)		-31.46(5)		-31.57(10)		-31.59(07)	
[0]1/2	71501.480	8.40(52)		8.50(5)					
$5s^25p^4(^3P_0)6p$									
[1]3/2	71976.775	0.37(24)	-0.74(56)						
[1]1/2	71813.958	-6.55(36)		-6.01(10)					
$5s^25p^4(^1D_2)6p$									
[3]7/2	79003.596	50.43(18)	71.25(85)	49.60(10)	70.95(1.0)				
[3]5/2	78592.572	67.38(22)	69.08(87)	67.46(10)	68.48(50)			67.58(07)	68.21(50)
[2]3/2	80039.779	74.38(45)	30.44(61)	75.17(10)	30.55(1.0)	75.18(14)	28(1)	75.48(17)	29.62(50)
[1]3/2	78415.247	60.21(64)	15.18(93)	60.38(10)	15.44(50)	60.77(40)	15(2)	60.47(10)	14.2(1.7)
[1]1/2	79701.591	159.5(1.4)		158.47(20)		159.27(73)			
$5s^25p^4(^3P_2)7p$									
[3]7/2	75194.056	19.34(59)	-35.71(73)	18.91(5)	-35.00(1.0)				
[3]5/2	75191.337	22.75(71)	-19.11(96)	22.75(20)	-19.86(1.0)				
[2]5/2	74965.635	24.85(33)	-25.10(75)	24.73(20)	-23.42(1.0)				
[2]3/2	75049.514	37.82(81)	-23.63(86)	38.0710)	-23.60(1.0)				

Electronic Configuration	E_o (cm^{-1})	A_{Exp}	B_{Exp}	A Ref. [21]	B Ref. [21]	A Ref.[22]	B Ref.[22]	A Ref. [23]	B Ref. [23]
[1]3/2	75621.427	27.85(51)	0.9(52)	27.76(5)	0.41(50)	28.41(15)	0(7)	27.58(17)	-1.23(50)
[1]1/2	75303.065	64.99(52)		65.07(5)				64.68(17)	
$5s^25p^4(^3P_1)7p$									
[0]1/2	81506.800	7.84(46)				7.65(12)		6.47(33)	
[2]5/2	82213.940	-6.04(75)	28.69(98)						
$5s^25p^4(^3P_2)8p$									
[3]7/2	78844.303	19.30(73)	-26.76(93)	18.76(1.0)	-24.5(5.0)				
[3]5/2	78854.747	24.58(16)	-14.38(44)					24.96(17)	-19.95(67)
[2]3/2	78815.440	40.78(35)	-17.13(91)			40.37(72)	-15(4)		
[2]5/2	78732.231	25.80(07)	-25.95(33)						
[1]3/2	79224.656	36.89(77)	4.77(99)	36.56(20)	4.32(2.0)			36.09(17)	5.30(67)
[1]1/2	78780.107	79.56(21)				80.07(35)		79.24(17)	
$5s^25p^4(^3P_2)4f$									
[5]9/2	77362.802	14.74(35)	13.21(78)	14.03(1.0)	0.95(2.0)				
[4]9/2	77306.559	10.81(43)	8.01(75)	10.37(50)	7.89(1.0)				
[3]7/2	77313.459	9.22(27)	8.0(1.1)	8.93(50)	9.0(2.0)				
[3]5/2	77307.333	11.44(76)	-2.3(2.5)	10.7(1.0)	-5.0				
[2]5/2	77359.585	-1.17(86)	20.4(1.3)	-0.3(10)	20.0(1.0)			0.10(17)	21.58(67)
[1]3/2	77406.784	-21.51(04)	-4.53(42)	-21.98(10)	-4.78(10)	-21.50(42)	-4(2)		
[1]1/2	77404.362	-44.18(86)		-43.49(10)					
$5s^25p^4(^3P_2)5f$									
[5]11/2	79859.010	11.84(59)	-42.70(83)						
[4]7/2	79832.955	14.28(47)	-5.34(56)						
[2]3/2	79834.910	9.47(24)	18.36(81)			8.75(18)	18(1)	9.31(33)	16.7(1.7)
[1]3/2	79881.383	-15.41(33)	6.14(55)			-21.74(23)	3(1)		
3/2	81722.9	19.24(66)	-17.01(83)						

Table 3.5 A list of center of gravity wavenumbers of I I in the spectral region from 6000-10000 cm^{-1}. The even and odd energy levels are taken from NIST data base [64]. Here σ_{obs} is the center of gravity wavenumber of the observed spectral lines. The value in the parenthesis represents the uncertainty. σ_{cal} is the wavenumber calculated using the level energies given in the NIST database [64]. Numbers given in the parenthesis correspond to the correction in the third decimal value.

σ_{obs} (cm^{-1})	σ_{cal} (cm^{-1})	Even Level E_e (cm^{-1})	J_e	Odd Level E_o (cm^{-1})	J_o
6006.020(3)	6006.021	79393.205	1/2	73387.184	1/2
6008.735(3)	6008.713	79395.897	3/2	73387.184	1/2
6054.347(4)	6054.344	77555.824	3/2	71501.480	1/2
6082.349(3)	6082.357	78889.521	1/2	72807.164	3/2
6084.031(4)	6084.022	78891.187	3/2	72807.164	3/2
6088.846(3)	6088.855	67298.328	1/2	73387.184	1/2
6165.888(3)	6165.887	60896.243	1/2	67062.130	3/2
6174.095(3)	6174.089	66355.093	3/2	72529.182	5/2
6223.839(8)	6223.828	79030.992	3/2	72807.164	3/2
6230.664(3)	6230.676	79285.273	1/2	73054.834	3/2
6233.758(3)	6233.748	71903.736	5/2	65669.988	7/2
6259.267(4)	6259.261	71903.736	5/2	65644.476	5/2
6331.713(5)	6331.58	75704.140	9/2	82035.73	9/2
6331.713(5)	6331.90	75704.140	9/2	82036.05	11/2
6338.594(3)	6338.607	79393.205	1/2	73054.834	3/2
6341.309(3)	6341.300	79395.897	3/2	73054.834	3/2
6362.009(3)	6362.005	78891.187	3/2	72529.182	5/2
6374.861(4)	6374.879	78904.061	7/2	72529.182	5/2
6377.791(3)	6377.775	68587.859	5/2	74965.635	5/2
6403.840(3)	6403.549	73477.834	1/2	79881.383	3/2
6406.102(4)	6406.095	68559.540	7/2	74965.635	5/2
6415.716(4)	6415.704	73477.834	1/2	67062.130	3/2
6415.716(4)	6415.892	68549.743	3/2	74965.635	5/2
6433.777(8)	6433.779	68615.734	1/2	75049.514	3/2
6437.925(4)	6437.921	72294.881	3/2	65856.960	1/2
6438.919(3)	6438.895	78415.670	1/2	71976.775	3/2
6461.659(3)	6461.654	68587.859	5/2	75049.514	3/2
6478.105(5)	6478.109	79285.273	1/2	72807.164	3/2
6479.254(3)	6479.347	76136.403	3/2	82615.75	1/2
6485.182(4)	6485.225	72294.881	3/2	78780.107	1/2
6499.774(6)	6499.771	68549.743	3/2	75049.514	3/2
6501.816(3)	6501.811	79030.992	3/2	72529.182	5/2
6508.711(3)	6508.713	66020.469	5/2	72529.182	5/2
6514.151(4)	6514.158	66015.023	7/2	72529.182	5/2
6559.879(4)	6559.866	72294.881	3/2	78854.747	5/2
6566.494(9)	6566.49	81760.57	9/2	75194.056	7/2
6577.180(3)	6577.170	73639.300	3/2	67062.130	3/2
6586.034(3)	6586.041	79393.205	1/2	72807.164	3/2

σ_obs (cm⁻¹)	σ_cal (cm⁻¹)	Even Level E_e (cm⁻¹)	J_e	Odd Level E_o (cm⁻¹)	J_o
6588.750(4)	6588.733	79395.897	3/2	72807.164	3/2
6598.819(4)	6598.86	81790.22	7/2	75191.337	5/2
6601.714(4)	6601.712	78415.670	1/2	71813.958	1/2
6611.349(10)	6611.325	79418.489	5/2	72807.164	3/2
6631.807(4)	6631.797	68559.540	7/2	75191.337	5/2
6634.519(5)	6634.516	68559.540	7/2	75194.056	7/2
6641.599(5)	6641.594	68549.743	3/2	75191.337	5/2
6650.415(5)	6650.405	72294.881	3/2	65644.476	5/2
6687.323(6)	6687.331	68615.734	1/2	75303.065	1/2
6699.507(5)	6699.505	66355.093	3/2	73054.834	3/2
6720.087(5)	6720.103	73114.807	1/2	79834.91	3/2
6733.204(3)	6733.197	73795.327	5/2	67062.130	3/2
6753.315(4)	6753.322	68549.743	3/2	75303.065	1/2
6786.694(3)	6786.695	66020.469	5/2	72807.164	3/2
6828.497(6)	6828.495	71903.736	5/2	78732.231	5/2
6866.727(5)	6866.716	79395.897	3/2	72529.182	5/2
6911.687(6)	6911.704	71903.736	5/2	78815.44	3/2
6913.746(3)	6913.742	71903.736	5/2	64989.994	3/2
6914.196(3)	6914.189	78415.670	1/2	71501.480	1/2
6914.439(3)	6914.411	78891.187	3/2	71976.775	3/2
6929.774(4)	6929.775	72294.881	3/2	79224.656	3/2
6940.575(3)	6940.566	71903.736	5/2	78844.303	7/2
6952.481(3)	6952.499	70354.834	3/2	77307.333	5/2
6966.595(6)	6966.565	78943.341	5/2	71976.775	3/2
6997.45(3)	6997.446	71903.736	5/2	64906.290	5/2
7001.800(8)	7001.802	70354.834	3/2	77356.636	3/2
7004.760(3)	7004.751	70354.834	3/2	77359.585	5/2
7005.695(7)	7005.693	68615.734	1/2	75621.427	3/2
7033.579(4)	7033.567	68587.859	5/2	75621.427	3/2
7049.539(3)	7049.528	70354.834	3/2	77404.362	1/2
7051.954(3)	7051.950	70354.834	3/2	77406.784	3/2
7054.246(4)	7054.217	79030.992	3/2	71976.775	3/2
7071.709(4)	7071.684	68549.743	3/2	75621.427	3/2
7077.236(5)	7077.229	78891.187	3/2	71813.958	1/2
7156.108(3)	7156.132	70151.201	5/2	77307.333	5/2
7162.261(3)	7162.258	70151.201	5/2	77313.459	7/2
7208.389(4)	7208.384	70151.201	5/2	77359.585	5/2
7217.042(4)	7217.034	79030.992	3/2	71813.958	1/2
7255.583(5)	7255.583	70151.201	5/2	77406.784	3/2
7257.858(4)	7257.847	73114.807	1/2	65856.960	1/2
7304.892(3)	7304.887	72294.881	3/2	64989.994	3/2
7308.512(4)	7308.498	79285.273	1/2	71976.775	3/2
7388.037(4)	7388.041	78889.521	1/2	71501.480	1/2
7389.716(3)	7389.706	78891.187	3/2	71501.480	1/2
7406.715(3)	7406.710	72294.881	3/2	79701.591	1/2
7416.441(4)	7416.430	79393.205	1/2	71976.775	3/2

σ_{obs} (cm^{-1})	σ_{cal} (cm^{-1})	Even Level E_e (cm^{-1})	J_e	Odd Level E_o (cm^{-1})	J_o
7467.651(4)	7467.641	67726.415	9/2	75194.056	7/2
7471.311(3)	7471.315	79285.273	1/2	71813.958	1/2
7529.521(5)	7529.512	79030.992	3/2	71501.480	1/2
7579.237(3)	7579.247	79393.205	1/2	71813.958	1/2
7581.952(3)	7581.939	79395.897	3/2	71813.958	1/2
7602.968(3)	7602.970	0	3/2	7602.970	1/2
7620.894(6)	7620.874	73477.834	1/2	65856.960	1/2
7685.387(5)	7685.432	81072.615	3/2	73387.184	1/2
7751.187(3)	7751.186	67298.328	1/2	75049.514	3/2
7782.346(3)	7782.340	73639.300	3/2	65856.960	1/2
7783.791(5)	7783.793	79285.273	1/2	71501.480	1/2
7867.536(4)	7867.47	73639.300	3/2	81506.800	1/2
7891.720(5)	7891.725	79393.205	1/2	71501.480	1/2
7894.439(3)	7894.417	79395.897	3/2	71501.480	1/2
8004.744(3)	8004.737	67298.328	1/2	75303.065	1/2
8060.433(7)	8060.413	70354.834	3/2	78415.247	3/2
8115.107(4)	8115.105	75177.235	5/2	67062.130	3/2
8124.823(3)	8124.812	73114.807	1/2	64989.994	3/2
8125.341(4)	8125.339	73795.327	5/2	65669.988	7/2
8150.856(5)	8150.852	73795.327	5/2	65644.476	5/2
8237.741(7)	8237.738	70354.834	3/2	78592.572	5/2
8264.050(6)	8264.046	70151.201	5/2	78415.247	3/2
8265.453(4)	8265.451	81072.615	3/2	72807.164	3/2
8307.713(12)	8307.727	73977.715	7/2	65669.988	7/2
8314.716(3)	8314.723	63186.758	1/2	71501.480	1/2
8333.242(3)	8333.239	73977.715	7/2	65644.476	5/2
8425.243(4)	8425.273	70354.834	3/2	78780.107	1/2
8487.843(4)	8487.840	73477.834	1/2	64989.994	3/2
8499.917(5)	8499.913	70354.834	3/2	78854.747	5/2
8610.545(3)	8610.542	66355.093	3/2	74965.635	5/2
8627.197(4)	8627.200	63186.758	1/2	71813.958	1/2
8649.312(3)	8649.306	73639.300	3/2	64989.994	3/2
8694.426(5)	8694.421	66355.093	3/2	75049.514	3/2
8719.422(9)	8719.421	68587.859	5/2	77307.280	7/2
8719.422(9)	8719.474	68587.859	5/2	77307.333	5/2
8725.622(6)	8725.600	68587.859	5/2	77313.459	7/2
8730.457(3)	8730.455	74587.415	3/2	65856.960	1/2
8733.016(3)	8733.010	73639.300	3/2	64906.290	5/2
8747.016(4)	8747.019	68559.540	7/2	77306.559	9/2
8747.757(5)	8747.740	68559.540	7/2	77307.280	7/2
8747.757(4)	8747.793	68559.540	7/2	77307.333	5/2
8753.928(3)	8753.919	68559.540	7/2	77313.459	7/2
8761.783(3)	8761.779	75823.909	3/2	67062.130	3/2
8771.746(12)	8771.726	68587.859	5/2	77359.585	5/2
8788.633(4)	8788.628	68615.734	1/2	77404.362	1/2
8791.050(3)	8791.050	68615.734	1/2	77406.784	3/2

σ_obs (cm⁻¹)	σ_cal (cm⁻¹)	Even Level E_e (cm⁻¹)	J_e	Odd Level E_o (cm⁻¹)	J_o
8803.264(3)	8803.262	68559.540	7/2	77362.802	9/2
8805.334(3)	8805.333	73795.327	5/2	64989.994	3/2
8806.901(4)	8806.893	68549.743	3/2	77356.636	3/2
8809.854(3)	8809.842	68549.743	3/2	77359.585	5/2
8813.414(3)	8813.409	56092.881	3/2	64906.290	5/2
8836.769(4)	8836.763	75898.893	5/2	67062.130	3/2
8852.394(8)	8852.395	70151.201	5/2	79003.596	7/2
8854.632(3)	8854.619	68549.743	3/2	77404.362	1/2
8857.039(3)	8857.041	68549.743	3/2	77406.784	3/2
8889.041(4)	8889.037	73795.327	5/2	64906.290	5/2
8897.113(4)	8897.113	56092.881	3/2	64989.994	3/2
8942.938(6)	8942.939	74587.415	3/2	65644.476	5/2
8945.172(3)	8945.166	66020.469	5/2	74965.635	5/2
8947.986(3)	8947.972	66355.093	3/2	75303.065	1/2
8950.613(5)	8950.611	66015.023	7/2	74965.635	5/2
9029.048(3)	9029.045	66020.469	5/2	75049.514	3/2
9044.429(4)	9044.418	76106.548	5/2	67062.130	3/2
9071.429(4)	9071.425	73977.715	7/2	64906.29	5/2
9074.282(6)	9074.273	76136.403	3/2	67062.130	3/2
9173.596(3)	9173.587	66020.469	5/2	75194.056	7/2
9176.311(7)	9176.314	66015.023	7/2	75191.337	5/2
9179.034(3)	9179.033	66015.023	7/2	75194.056	7/2
9346.752(11)	9346.757	70354.834	3/2	79701.591	1/2
9355.662(4)	9355.653	76417.783	1/2	67062.130	3/2
9485.324(3)	9485.318	70354.834	3/2	79840.152	5/2
9507.254(6)	9507.247	75177.235	5/2	65669.988	7/2
9526.705(3)	9526.549	70354.834	3/2	79881.383	3/2
9532.765(4)	9532.759	75177.235	5/2	65644.476	5/2
9551.586(6)	9551.595	56092.881	3/2	65644.476	5/2
9571.130(3)	9571.135	81072.615	3/2	71501.480	1/2
9580.148(3)	9580.144	67726.415	9/2	77306.559	9/2
9580.862(5)	9580.865	67726.415	9/2	77307.28	7/2
9597.423(3)	9597.421	74587.415	3/2	64989.994	3/2
9600.966(7)	9600.958	66020.469	5/2	75621.427	3/2
9620.402(3)*	9620.406	63186.758	1/2	72807.164	3/2
9635.711(3)*	9635.713	67726.415	9/2	77362.128	11/2
9636.401(4)*	9636.387	67726.415	9/2	77362.802	9/2
9681.130(4)	9681.125	74587.415	3/2	64906.29	5/2
9681.709(4)	9681.701	61819.779	3/2	71501.480	1/2
9684.892(3)*	9684.848	76746.978	3/2	67062.130	3/2
9684.892(3)*	9684.945	70354.834	3/2	80039.779	3/2
9688.957(3)	9688.951	70151.201	5/2	79840.152	5/2
9696.482(5)	9696.482	70151.201	5/2	79847.683	7/2
9764.085(4)	9764.079	56092.881	3/2	65856.960	1/2
9770.612(3)	9770.616	70354.834	3/2	80125.45	5/2
9799.523(5)	9799 .513	68615.734	1/2	78415.247	3/2

σ_{obs} (cm^{-1})	σ_{cal} (cm^{-1})	Even Level E_e (cm^{-1})	J_e	Odd Level E_o (cm^{-1})	J_o
9827.397(3)	9827.388	68587.859	5/2	78415.247	3/2
9841.145(4)	9841.142	75511.13	7/2	65669.988	7/2
9857.471(3)	9857.463	75714.423	1/2	65856.960	1/2
9865.509(5)	9865.504	68549.743	3/2	78415.247	3/2
9866.656(3)	9866.654	75511.13	7/2	65644.476	5/2
9867.840(4)	9867.840	63186.758	1/2	73054.834	3/2
9994.186(4)	9994.180	61819.779	3/2	71813.958	1/2

Table 3.6 Even energy levels of I I involved in the spectral region of 6000-10000 cm^{-1} and their experimentally derived *hfs* A and B constants in mK in comparison with previous literature.

Energy (cm^{-1})	Configuration	J	Present Work		Literature Data			
			A	B	A-Ref.[21]	B-Ref.[21]	A-Ref.[22]	B-Ref.[22]
56092.881	$5s^25p^4(^3P_2)6s[2]$	3/2	18.09(.11)	-13.40(.33)	17.75(.3)	-13.3(1.0)		
61819.779	$5s^25p^4(^3P_1)6s[1]$	3/2	22.60(.13)	14.16(.37)	22.57(.3)	14.5(1.0)	22.68(.24)	14(1.0)
63186.758	$5s^25p^4(^3P_1)6s[1]$	1/2	-5.35(.20)					
66015.023	$5s^25p^4(^3P_2)5d[3]$	7/2	10.42(.06)	10.89(.30)	10.12(.1)	11.24(1.0)		
66020.469	$5s^25p4(^3P_2)5d[3]$	5/2	21.57(.08)	6.05(.25)	21.59(.2)	4.0(4.0)	21.57(.15)	6(1.0)
66355.093	$5s^25p^4(^3P_2)5d[1]$	3/2	32.96(.06)	9.53(.24)	32.59(.05)	10.96(.5)	32.55(.27)	8(1.0)
67726.415	$5s^25p^4(^3P_2)5d[4]$	9/2	13.39(.07)	-31.86(.85)	13.49(.1)	-31.48(2.0)		
68559.540	$5s^25p^4(^3P_2)5d[4]$	7/2	17.57(.13)	-26.78(.74)	17.55(.1)	-27.45(4.0)		
68587.859	$5s^25p^4(^1D_2)6s[2]$	5/2	82.99(.05)	72.61(.07)	82.99(.1)	71.76(1.0)	82.95(.15)	70(1.0)
68615.734	$5s^25p^4(^3P_2)5d[0]$	1/2	94.42(.04)		94.46(.1)		94.56(.23)	
70151.201	$5s^25p^4(^3P_2)5d[2]$	5/2	14.40(.09)	4.73(.68)	15.46(.1)	4.10(.5)		
70354.834	$5s^25p^4(^3P_2)5d[2]$	3/2	20.96(.05)	20.73(.63)	21.08(.1)	22.80(.5)	21.46(.29)	20(1.0)
71903.736	$5s^25p^4(^3P_2)7s[2]$	5/2	30.62(.09)	-32.53(.33)	30.36(.05)	-33.82(1.0)		
73114.807	$5s^25p^4(^3P_1)5d[1]$	1/2	30.48(.12)		28.86(.05)			
73977.715	$5s^25p^4(^3P_1)5d[3]$	7/2	-1.46(.06)	1.30(.29)	-1.92(.1)	1.21(.5)		
74587.415	$5s^25p^4(^3P_1)5d[1]$	3/2	17.62(.03)	0.79(.90)	17.47(.1)	1.0(1.0)		
75177.235	$5s^25p^4(^3P_1)5d[3]$	5/2	9.95(.03)	-4.32(.75)	9.79(.1)	-4.20(1.0)		
75511.130	$5s^25p^4(^3P_2)6d[3]$	7/2	12.88(.03)	-10.13(.71)	12.88(.1)	-10.15(1.0)		

Energy (cm^{-1})	Configuration	J	Present Work		Literature Data			
			A	B	A-Ref.[21]	B-Ref.[21]	A-Ref.[22]	B-Ref.[22]
75714.423	5s^{2}5p^4(^{3}P$_2$)6d[0]	1/2	25.42(.18)		25.33(.4)			
76106.548	5s^{2}5p^4(^{3}P$_2$)6d[3]	5/2	7.54(.28)	-19.67(.81)	7.74(.1)	-20.33(1.0)		
76136.403	5s^{2}5p^4(^{3}P$_2$)6d[1]	3/2	4.92(.13)	5.98(.69)	4.72(.1)	5.28(1.0)		
76417.783	5s^{2}5p^4(^{3}P$_2$)6d[1]	1/2	48.79(.12)		48.63(.3)		48.73(.57)	
77555.824	5s^{2}5p^4(^{3}P$_2$)8s[2]	3/2	36.49(.32)	-22.08(.77)			35.85(.34)	-26(1.0)
78904.061	5s^{2}5p^4(^{3}P$_2$)7d[3]	7/2	14.49(.20)	-11.25(.65)				
78889.521	5s^{2}5p^4(^{3}P$_2$)7d[1]	1/2	2.66(.23)					
79030.992	5s^{2}5p^4(^{3}P$_2$)7d[1]	3/2	21.25(.14)	5.19(.73)	21.17(.1)	5.37(.5)	20.48(.13)	1(5.0)
79285.273	5s^{2}5p^4(^{3}P$_1$)7s[1]	1/2	7.50(.08)		6.2(.3)		6.8(.53)	
79393.205	5s^{2}5p^4(^{3}P$_2$)7d[0]	1/2	1.32(.17)					
79395.897	5s^{2}5p^4(^{3}P$_2$)7d[2]	3/2	5.06(.33)	13.31(.81)			5.90(.55)	13(2.0)
81072.615	5s^{2}5p^4(^{1}D$_2$)5d[1]	3/2	14.34(.40)	-14.34(.85)				

Table 3.7 Odd energy levels of I I involved in the spectral region of 6000-10000 cm^{-1} and their experimentally derived *hfs* A and B constants in mK in comparison with previous literature.

Energy (cm⁻¹)	configuration	J	Present Work			Literature Data		
			A	B	A-Ref.[21]	B-Ref.[21]	A-Ref.[22]	B-Ref.[22]
64906.29	$5s^25p^4(^3P_2)6p[2]$	5/2	26.32(.24)	-19.96(.73)	25.31(.1)	-18.86(1.0)	26.73(.47)	-16(4.0)
64989.994	$5s^25p^4(^3P_2)6p[2]$	3/2	35.39(.15)	-23.88(.89)	35.38(.1)	-23.56(1.0)	35.21(.43)	-25(2.0)
65644.476	$5s^25p^4(^3P_2)6p[3]$	5/2	26.15(.46)	-22.85(.71)	24.03(.1)	-22.04(.5)		
65669.988	$5s^25p^4(^3P_2)6p[3]$	7/2	19.49(.12)	-38.11(.68)	19.57(.05)	-36.84(.5)		
65856.960	$5s^25p^4(^3P_2)6p[1]$	1/2	57.51(.18)		57.25(.05)		57.04(.35)	
67062.130	$5s^25p^4(^3P_2)6p[1]$	3/2	29.34(.19)	-0.45(.60)	29.13(.05)	-0.45(.5)	29.38(.40)	0(2.0)
71501.480	$5s^25p^4(^3P_1)6p[0]$	1/2	8.22(.26)		8.50(.05)			
71813.958	$5s^25p^4(^3P_0)6p[1]$	1/2	-6.29(.06)		-6.01(.1)			
71976.775	$5s^25p^4(^3P_0)6p[1]$	3/2	0.12(.09)	-0.72(.86)				
72807.164	$5s^25p^4(^3P_1)6p[2]$	3/2	-0.56(.04)	16.09(.33)	-0.53(.1)	16.14(.2)		
73387.184	$5s^25p^4(^3P_1)6p[1]$	1/2	-32.07(.05)		-31.46(.05)		-31.57(.10)	
74965.635	$5s^25p^4(^3P_2)7p[2]$	5/2	24.86(.11)	-23.49(.30)	24.73(.2)	-23.42(1.0)		
75191.337	$5s^25p^4(^3P_2)7p[3]$	5/2	22.37(.14)	-19.92(.69)	22.75(.2)	-19.86(1.0)		
75194.056	$5s^25p^4(^3P_2)7p[3]$	7/2	18.96(.03)	-34.47(.62)	18.91(.05)	-35.00(1.0)		
75303.065	$5s^25p^4(^3P_2)7p[1]$	1/2	65.37(.06)		65.07(.05)			
75621.427	$5s^25p^4(^3P_2)7p[1]$	3/2	27.73(.03)	0.92(.83)	27.76(.05)	0.41(.5)	28.41(.15)	0(7.0)
77306.559	$5s^25p^4(^3P_2)4f[4]$	9/2	10.71(.43)	7.19(.57)	10.37(.5)	7.89(1.0)		
77356.636	$5s^25p^4(^3P_2)4f[2]$	3/2	5.05(.5)	1.94(.91)	3.25(.5)	2.00(1.0)		

189

Energy (cm^{-1})	configuration	J	Present Work		Literature Data			
			A	B	A-Ref.[21]	B-Ref.[21]	A-Ref.[22]	B-Ref.[22]
78415.247	$5s^25p^4(^1D_2)6p[1]$	3/2	60.86(.23)	16.32(.75)	60.38(.1)	15.44(.5)	60.77(.40)	15(2.0)
78732.231	$5s^25p^4(^3P_2)8p[2]$	5/2	26.05(.19)	-26.09(.67)				
78780.107	$5s^25p^4(^3P_2)8p[1]$	1/2	79.55(.24)				80.07(.35)	
78815.44	$5s^25p^4(^3P_2)8p[2]$	3/2	40.40(.13)	-15.93(.65)			40.37(.72)	-15(4.0)
78854.747	$5s^25p^4(^3P_2)8p[3]$	5/2	23.85(.12)	-16.56(.41)				
79701.591	$5s^25p^4(^1D_2)6p[1]$	1/2	158.20(.15)		158.47(.2)		159.27(.73)	
79840.152	$5s^25p^4(^3P_2)5f[2]$	5/2	3.39(.33)	11.67(.79)	3.46(1.0)	12.44(2.0)		
79834.91	$5s^25p^4(^3P_2)5f[2]$	3/2	9.13(.03)	17.81(.74)			8.75(.18)	18(1.0)
79847.683	$5s^25p^4(^3P_2)5f[3]$	7/2	7.47(.09)	9.36(.71)				
79881.383	$5s^25p^4(^3P_1)5f[1]$	3/2	-21.20(.12)	2.56(.47)			-21.74(.23)	3(1.0)
80125.45	$5s^25p^4(^1D_2)6p[2]$	5/2	52.52(.05)	32.06(.83)			52.45(.21)	32(2.0)
82615.75		1/2	4.98(.46)					

Table 3.8 Center of gravity wavenumber list of 240 observed spectral transitions of I I in the near IR and visible spectral region along with their classifications. The even and odd energy levels are taken from NIST data base [64]. Here σ_{obs} is the observed center of gravity wavenumber of the observed spectral lines. The value in the parenthesis represents the uncertainty. σ_{cal} is the wavenumber calculated using the level energies given in the NIST database [64]. The Ref. column indicates the transitions also observed previously [21-23] and NL means: New Line, reported here.

σ_{obs} (cm^{-1})	σ_{cal} (cm^{-1})	Even Level E_e (cm^{-1})	J_e	Odd Level E_o (cm^{-1})	J_o	Ref.	*Hfs* done
10004.719(1)	10004.713	68587.859	5/2	78592.572	5/2	[b]	(a,b)
10034.117(1)	10034.152	75704.140	9/2	65669.988	7/2	[b]	(a)
10042.832(1)	10042.829	68549.743	3/2	78592.572	5/2	[b]	(a,b)
10058.316(1)	10058.308	67298.328	1/2	77356.636	3/2	[b]	(a,b)
10106.039(2)	10106.034	67298.328	1/2	77404.362	1/2	[b]	(a,b)
10108.463(1)	10108.456	67298.328	1/2	77406.784	3/2	[b]	(a,b)
10156.979(1)	10156.996	61819.779	3/2	71976.775	3/2	[b]	(a)
10167.751(1)	10167.735	82144.510	5/2	71976.775	3/2	NL	(a)
10187.248(1)	10187.241	75177.235	5/2	64989.994	3/2	[b]	(a,b)
10200.416(1)	10200.426	63186.758	1/2	73387.184	1/2	[b]	(a)
10227.569(2)	10227.581	68587.859	5/2	78815.440	3/2	NL	(a)
10228.910(3)	10228.905	75898.893	5/2	65669.988	7/2	NL	(a)
10230.337(3)	10230.364	68549.743	3/2	78780.107	1/2	NL	(a)
10254.420(1)	10254.417	75898.893	5/2	65644.476	5/2	NL	(a)
10270.955(1)	10270.945	75177.235	5/2	64906.290	5/2	[b]	(a)
10272.860(6)	10272.830	54633.460	5/2	64906.290	5/2	[b]	(a,b)
10279.448(1)	10279.443	76136.403	3/2	65856.960	1/2	[b]	(a,b)
10295.212(1)	10295.207	68559.540	7/2	78854.747	5/2	NL	(a)
10305.007(8)	10305.004	68549.743	3/2	78854.747	5/2	NL	(a)
10356.544(1)	10356.534	54633.460	5/2	64989.994	3/2	[b]	(a,b)
10360.259(1)	10360.255	76004.731	7/2	65644.476	5/2	[b]	(a,b)
10388.595(2)	10388.579	77450.709	5/2	67062.130	3/2	NL	
10415.743(1)	10415.737	68587.859	5/2	79003.596	7/2	[b]	(a,b)
10436.584(6)	10436.560	76106.548	5/2	65669.988	7/2	[b]	(a)
10462.077(2)	10462.072	76106.548	5/2	65644.476	5/2	NL	(a)
10491.933(1)	10491.927	76136.403	3/2	65644.476	5/2	[b]	(a)
10493.688(3)	10493.694	77555.824	3/2	67062.130	3/2	[b]	(a)
10560.832(3)	10560.823	76417.783	1/2	65856.960	1/2	[b]	(a,b)
10604.849(1)	10604.840	75511.130	7/2	64906.290	5/2	[b]	(a,b)
10605.243(1)	10605.237	60896.243	1/2	71501.480	1/2	[b]	(a)
10636.809(1)	10636.797	68587.859	5/2	79224.656	3/2	[b]	(a,b)
10674.919(3)	10674.913	68549.743	3/2	79224.656	3/2	[b]	(a)
10709.418(2)	10709.403	61819.779	3/2	72529.182	5/2	[b]	(a,b)
10724.435(1)	10724.429	75714.423	1/2	64989.994	3/2	[b]	(a,b)
10833.919(1)	10833.915	75823.909	3/2	64989.994	3/2	[b]	(a)
10889.981(1)	10890.018	76746.978	3/2	65856.960	1/2	[b]	(a)
10908.912(1)	10908.899	75898.893	5/2	64989.994	3/2	NL	(a)
10917.682(2)	10917.619	75823.909	3/2	64906.290	5/2	[b]	(a)

191

σ_{obs} (cm^{-1})	σ_{cal} (cm^{-1})	Even Level E_e (cm^{-1})	J_e	Odd Level E_o (cm^{-1})	J_o	Ref.	*Hfs* done
10917.682(2)	10917.715	60896.243	1/2	71813.958	1/2	[b]	(a)
10952.225(1)	10952.240	66355.093	3/2	77307.333	5/2	[b]	(a,b)
10969.250(1)	10969.249	56092.881	3/2	67062.130	3/2	[b]	(a)
10987.388(1)	10987.385	61819.779	3/2	72807.164	3/2	[b]	(a)
10992.607(2)	10992.603	75898.893	5/2	64906.290	5/2	NL	(a)
11001.551(1)	11001.543	66355.093	3/2	77356.636	3/2	[b]	(a)
11004.522(2)	11004.492	66355.093	3/2	77359.585	5/2	NL	
11011.024(2)	11011.016	54633.460	5/2	65644.476	5/2	[b]	(a)
11036.539(7)	11036.528	54633.460	5/2	65669.988	7/2	[b]	(a)
11049.308(9)	11049.269	66355.093	3/2	77404.362	1/2	NL	(a)
11051.704(2)	11051.691	66355.093	3/2	77406.784	3/2	NL	
11080.517(2)	11080.532	60896.243	1/2	71976.775	3/2	[b]	(a)
11085.869(2)	11085.857	68615.734	1/2	79701.591	1/2	NL	(a)
11098.465(9)	11098.441	76004.731	7/2	64906.290	5/2	NL	
11116.561(1)	11116.554	76106.548	5/2	64989.994	3/2	[b]	(a,b)
11146.415(1)	11146.409	76136.403	3/2	64989.994	3/2	[b]	(a,b)
11151.857(1)	11151.848	68549.743	3/2	79701.591	1/2	[b]	(a,b)
11200.265(1)	11200.258	76106.548	5/2	64906.290	5/2	[b]	(a,b)
11230.140(2)	11230.113	76136.403	3/2	64906.290	5/2	NL	
11234.831(2)	11234.819	61819.779	3/2	73054.598	3/2	[b]	(a)
11258.782(2)	11258.793	76903.269	5/2	65644.476	5/2	[b]	(a)
11259.844(4)	11259.824	68587.859	5/2	79847.683	7/2	[b]	(a)
11265.631(3)	11265.649	68615.734	1/2	79881.383	3/2	NL	(a)
11266.089(2)	11266.039	68615.734	1/2	79881.773	1/2	NL	(a)
11273.419(3)	11273.415	68559.540	7/2	79832.955	7/2	[b]	
11286.828(1)	11286.811	66020.469	5/2	77307.280	7/2	[b]	
11286.828(1)	11286.864	66020.469	5/2	77307.333	5/2	[b]	
11290.403(2)	11290.409	68549.743	3/2	79840.152	5/2	NL	
11291.535(1)	11291.536	66015.023	7/2	77306.559	9/2	[b]	(a)
11292.256(1)	11292.257	66015.023	7/2	77307.280	7/2	[b]	
11292.256(1)	11292.310	66015.023	7/2	77307.333	5/2	[b]	
11292.997(2)	11292.990	66020.469	5/2	77313.459	7/2	NL	(a)
11294.735(3)	11294.726	68549.743	3/2	79844.469	5/2	NL	(a)
11298.438(1)	11298.436	66015.023	7/2	77313.459	7/2	[b]	
11300.013(2)	11300.030	68559.540	7/2	79859.570	9/2	[b]	(a)
11336.174(3)	11336.167	66020.469	5/2	77356.636	3/2	[b]	(a)
11339.127(1)	11339.116	66020.469	5/2	77359.585	5/2	[b,c]	(a,c)
11344.568(2)	11344.562	66015.023	7/2	77359.585	5/2	[b,d]	(a,d)
11386.312(1)	11386.315	66020.469	5/2	77406.784	3/2	[b,c]	(a,c)
11427.794(1)	11427.789	76417.783	1/2	64989.994	3/2	[b,c,d]	(a,b,c,d)
11451.957(4)	11451.920	68587.859	5/2	80039.779	3/2	[b,c,d]	(a,c,d)
11490.071(1)	11490.036	68549.743	3/2	80039.779	3/2	[b,c,d]	(a,b,c,d)
11537.593(1)	11537.591	68587.859	5/2	80125.450	5/2	[c,d]	(a,c,d)
11567.395(1)	11567.405	61819.779	3/2	73387.184	1/2	[c,d]	(a,c,d)
11575.706(1)	11575.707	68549.743	3/2	80125.450	5/2	[c,d]	(a,d)
11698.857(2)	11698.864	77555.824	3/2	65856.960	1/2	[c]	(a,c)
11780.731(6)	11780.721	77450.709	5/2	65669.988	7/2	NL	

σ_{obs} (cm^{-1})	σ_{cal} (cm^{-1})	Even Level E_e (cm^{-1})	J_e	Odd Level E_o (cm^{-1})	J_o	Ref.	*Hfs* done
11910.925(1)	11910.921	60896.243	1/2	72807.164	3/2	NL	(a)
11911.342(2)	11911.348	77555.824	3/2	65644.476	5/2	NL	
11913.260(2)	11913.275	76903.269	5/2	64989.994	3/2	NL	(a)
12103.171(3)	12103.185	67726.415	9/2	79829.600	9/2	[c]	(a)
12116.314(5)	12116.307	63186.758	1/2	75303.065	1/2	[c,d]	(a,d)
12132.560(1)	12132.595	67726.415	9/2	79859.010	11/2	[c]	(a)
12158.364(1)	12158.355	60896.243	1/2	73054.598	3/2	[c,d]	(a,c,d)
12237.485(1)	12237.479	66355.093	3/2	78592.572	5/2	[c,d]	(a,c,d)
12333.790(3)	12333.767	79395.897	3/2	67062.130	3/2	[c,d]	(a,c,d)
12356.381(4)	12356.359	79418.489	5/2	67062.130	3/2	[c,d]	(c,d)
12394.783(4)	12394.778	66020.469	5/2	78415.247	3/2	[c,d]	(a,c,d)
12428.678(2)	12428.670	54633.460	5/2	67062.130	3/2	[c,d]	(a,c,d)
12434.680(3)	12434.669	63186.758	1/2	75621.427	3/2	[c,d]	(a,c,d)
12460.727(4)	12460.715	77450.709	5/2	64989.994	3/2	[c,d]	(d)
12490.938(1)	12490.941	60896.243	1/2	73387.184	1/2	[c,d]	(a,c,d)
12536.576(4)	12536.582	67298.328	1/2	79834.910	3/2	[c,d]	(a,c,d)
12544.432(2)	12544.419	77450.709	5/2	64906.290	5/2	[c,d]	(a,d)
12558.714(1)	12558.710	78415.670	1/2	65856.960	1/2	[c,d]	(a,c,d)
12565.825(1)	12565.830	77555.824	3/2	64989.994	3/2	[c,d]	(a,c,d)
12572.109(1)	12572.103	66020.469	5/2	78592.572	5/2	[c,d]	(a,c,d)
12583.427(3)	12583.445	67298.328	1/2	79881.773	3/2	[c]	(c)
12610.197(3)	12610.156	68615.734	1/2	81225.890	1/2	[c]	(a,c)
12611.489(2)	12611.506	68615.734	1/2	81227.240	3/2	[c]	(c)
12642.173(7)	12642.120	68559.540	7/2	81201.660	7/2	[c,d]	(d)
12658.002(1)	12657.960	68559.540	7/2	81217.500	9/2	[c]	
12717.213(5)	12717.208	66015.023	7/2	78732.231	5/2	[c]	(a)
12741.483(4)	12741.451	67298.328	1/2	80039.779	3/2	[c]	(a,c)
12794.970(1)	12794.971	66020.469	5/2	78815.440	3/2	[c]	(a,c)
12852.562(2)	12852.552	79914.682	5/2	67062.130	3/2	[c,d]	(d)
12869.582(2)	12869.563	66355.093	3/2	79224.656	3/2	[c,d]	(d)
12885.020(2)	12884.993	79947.123	3/2	67062.130	3/2	[c,d]	(a,d)
12957.130(9)	12957.057	68549.743	3/2	81506.800	1/2	[c,d]	(a,c,d)
12983.134(1)	12983.127	66020.469	5/2	79003.596	7/2	NL	(a)
12988.569(6)	12988.573	66015.023	7/2	79003.596	7/2	NL	(a)
13032.556(1)	13032.561	78889.521	1/2	65856.960	1/2	NL	(a)
13145.869(2)	13145.856	61819.779	3/2	74965.635	5/2	NL	(a)
13174.042(2)	13174.030	79030.990	3/2	65856.960	1/2	NL	(a)
13204.201(1)	13204.187	66020.469	5/2	79224.656	3/2	NL	(a)
13229.747(3)	13229.735	61819.779	3/2	75049.514	3/2	NL	(a)
13234.064(1)	13234.073	78904.061	7/2	65669.988	7/2	NL	(a)
13259.573(1)	13259.585	78904.061	7/2	65644.476	5/2	NL	(a)
13273.372(1)	13273.353	78943.341	5/2	65669.988	7/2	NL	(a)
13346.510(1)	13346.498	66355.093	3/2	79701.591	1/2	NL	(a)
13371.586(2)	13371.558	61819.779	3/2	75191.337	5/2	NL	
13385.014(1)	13384.997	79054.985	9/2	65669.988	7/2	NL	(a)
13386.532(4)	13386.516	79030.992	3/2	65644.476	5/2	NL	
13425.681(5)	13425.676	78415.670	1/2	64989.994	3/2	NL	(a)

σ_{obs} (cm^{-1})	σ_{cal} (cm^{-1})	Even Level E_e (cm^{-1})	J_e	Odd Level E_o (cm^{-1})	J_o	Ref.	*Hfs* done
13428.310(1)	13428.313	79285.273	1/2	65856.960	1/2	NL	(a)
13479.812(3)	13479.817	66355.093	3/2	79834.910	3/2	NL	(a)
13483.304(1)	13483.286	61819.779	3/2	75303.065	1/2	NL	(a)
13485.069(1)	13485.059	66355.093	3/2	79840.152	3/2	NL	(a)
13489.382(1)	13489.376	66355.093	3/2	79844.469	5/2	NL	(a)
13506.063(1)	13506.074	79150.550	7/2	65644.476	5/2	NL	
13526.657(2)	13526.290	66355.093	3/2	79881.383	3/2	NL	
13526.657(2)	13526.680	66355.093	3/2	79881.773	1/2	NL	
13684.724(1)	13684.686	66355.093	3/2	80039.779	3/2	NL	(a)
13720.347(1)	13720.340	80782.470	3/2	67062.130	3/2	NL	(a)
13770.362(2)	13770.357	66355.093	3/2	80125.450	5/2	NL	(a)
13774.029(2)	13774.013	79418.489	5/2	65644.476	5/2	NL	(a)
13812.489(2)	13812.486	66020.469	5/2	79832.955	7/2	NL	
13814.546(1)	13814.441	66020.469	5/2	79834.910	3/2	NL	
13814.546(1)	13814.577	66015.023	7/2	79829.600	9/2	NL	
13817.932(2)	13817.932	66015.023	7/2	79832.955	7/2	NL	(a)
13820.184(1)	13820.160	80882.290	5/2	67062.130	3/2	NL	
13824.011(1)	13824.000	66020.469	5/2	79844.469	5/2	NL	(a)
13827.223(2)	13827.214	66020.469	5/2	79847.683	7/2	NL	
13829.447(1)	13829.446	66015.023	7/2	79844.469	5/2	NL	
13832.663(1)	13832.660	66015.023	7/2	79847.683	7/2	NL	
13899.526(1)	13899.527	78889.521	1/2	64989.994	3/2	NL	(a)
13901.199(1)	13901.193	78891.187	3/2	64989.994	3/2	NL	(a)
13918.365(2)	13918.332	67298.328	1/2	81216.660	3/2	NL	(a)
13953.359(1)	13953.347	78943.341	5/2	64989.994	3/2	NL	(a)
13984.911(3)	13984.897	78891.187	3/2	64906.290	5/2	NL	(a)
13997.761(1)	13997.771	78904.061	7/2	64906.290	5/2	NL	(a)
14010.499(1)	14010.485	81072.615	3/2	67062.130	3/2	NL	(a)
14037.068(3)	14037.051	78943.341	5/2	64906.290	5/2	NL	
14041.006(7)	14040.996	79030.990	3/2	64989.994	3/2	NL	(a)
14065.928(2)	14066.007	68549.743	3/2	82615.750	1/2	NL	(a)
14090.183(2)	14090.163	79947.123	3/2	65856.960	1/2	NL	(a)
14104.984(1)	14104.981	66020.469	5/2	80125.450	5/2	NL	(a)
14124.716(1)	14124.700	79030.990	3/2	64906.290	5/2	NL	(a)
14153.281(1)	14153.271	60896.243	1/2	75049.514	3/2	NL	(a)
14244.248(3)	14244.260	79150.550	7/2	64906.290	5/2	NL	
14244.703(3)	14244.694	79914.682	5/2	65669.988	7/2	NL	
14295.290(2)	14295.279	79285.273	1/2	64989.994	3/2	NL	(a)
14302.669(1)	14302.647	79947.123	3/2	65644.476	5/2	NL	
14403.206(4)	14403.211	79393.205	1/2	64989.994	3/2	NL	(a)
14406.834(7)	14406.822	60896.243	1/2	75303.065	1/2	NL	(a)
14428.507(4)	14428.495	79418.489	5/2	64989.994	3/2	NL	
14489.604(4)	14489.607	79395.897	3/2	64906.290	5/2	NL	
14725.194(1)	14725.184	60896.243	1/2	75621.427	3/2	NL	
14833.988(3)	14833.980	80690.940	3/2	65856.960	1/2	NL	(a)
14837.047(1)	14837.010	80693.970	1/2	65856.960	1/2	NL	(a)
14850.306(1)	14850.297	66355.093	3/2	81205.390	5/2	NL	

σ_{obs} (cm^{-1})	σ_{cal} (cm^{-1})	Even Level E_e (cm^{-1})	J_e	Odd Level E_o (cm^{-1})	J_o	Ref.	*Hfs* done
14924.687(3)	14924.688	79914.682	5/2	64989.994	3/2	NL	
15006.188(1)	15006.182	80676.170	7/2	65669.988	7/2	NL	(a)
15008.399(2)	15008.392	79914.682	5/2	64906.290	5/2	NL	
15102.392(2)	15102.352	80772.340	9/2	65669.988	7/2	NL	(a)
15181.243(9)	15181.191	66020.469	5/2	81201.660	7/2	NL	
15184.772(2)	15184.717	66015.023	7/2	81199.740	9/2	NL	
15224.677(3)	15224.684	80869.160	7/2	65644.476	5/2	NL	(a)
15228.472(2)	15228.489	63186.758	1/2	78415.247	3/2	NL	
15237.842(7)	15237.814	80882.290	5/2	65644.476	5/2	NL	
15408.600(2)	15408.599	56092.881	3/2	71501.480	1/2	NL	(a)
16346.151(2)	16346.160	81252.450	5/2	64906.290	5/2	NL	
16436.310(1)	16436.301	56092.881	3/2	72529.182	5/2	NL	(a)
16460.418(4)	16460.393	60896.243	1/2	77356.636	3/2	NL	
16508.133(1)	16508.119	60896.243	1/2	77404.362	1/2	NL	(a)
16510.546(5)	16510.541	60896.243	1/2	77406.784	3/2	NL	(a)
16514.836(1)	16514.833	63186.758	1/2	79701.591	1/2	NL	(a)
16595.480(1)	16595.468	61819.779	3/2	78415.247	3/2	NL	(a)
16714.293(5)	16714.283	56092.881	3/2	72807.164	3/2	NL	
16772.800(2)	16772.793	61819.779	3/2	78592.572	5/2	NL	(a)
16961.727(1)	16961.717	56092.881	3/2	73054.598	3/2	NL	(a)
17294.311(1)	17294.303	56092.881	3/2	73387.184	1/2	NL	(a)
17343.301(1)	17343.315	54633.460	5/2	71976.775	3/2	NL	
17404.888(1)	17404.877	61819.779	3/2	79224.656	3/2	NL	(a)
17881.811(1)	17881.812	61819.779	3/2	79701.591	1/2	NL	
17895.733(7)	17895.722	54633.460	5/2	72529.182	5/2	NL	(a)
18173.713(9)	18173.704	54633.460	5/2	72807.164	3/2	NL	(a)
18421.149(2)	18421.138	54633.460	5/2	73054.598	3/2	NL	(a)
18872.766(2)	18872.754	56092.881	3/2	74965.635	5/2	NL	
18956.642(4)	18956.633	56092.881	3/2	75049.514	3/2	NL	
19098.470(1)	19098.456	56092.881	3/2	75191.337	5/2	NL	(a)
19210.197(2)	19210.184	56092.881	3/2	75303.065	1/2	NL	(a)
19528.562(1)	19528.546	56092.881	3/2	75621.427	3/2	NL	(a)
20332.191(1)	20332.175	54633.460	5/2	74965.635	5/2	NL	(a)
20394.181(3)	20394.161	61819.779	3/2	82213.940	5/2	NL	(a)
20416.065(1)	20416.054	54633.460	5/2	75049.514	3/2	NL	(a)
20557.932(7)	20557.877	54633.460	5/2	75191.337	5/2	NL	(a)
20560.613(1)	20560.596	54633.460	5/2	75194.056	7/2	NL	(a)
20708.576(6)	20708.587	60896.243	1/2	81604.830	1/2	NL	
20826.682(2)	20826.657	60896.243	1/2	81722.900	3/2	NL	
20987.982(1)	20987.967	54633.460	5/2	75621.427	3/2	NL	
21266.726(3)	21266.704	56092.881	3/2	77359.585	5/2	NL	(a)
21313.915(1)	21313.903	56092.881	3/2	77406.784	3/2	NL	(a)
21719.427(2)	21719.507	60896.243	1/2	82615.750	1/2	NL	(a)
22322.379(3)	22322.366	56092.881	3/2	78415.247	3/2	NL	(a)
22499.693(3)	22499.691	56092.881	3/2	78592.572	5/2	NL	(a)
22673.834(3)	22673.820	54633.460	5/2	77307.280	7/2	NL	(a)
22673.834(3)	22673.873	54633.460	5/2	77307.333	5/2	NL	

σ_{obs} (cm^{-1})	σ_{cal} (cm^{-1})	Even Level E_e (cm^{-1})	J_e	Odd Level E_o (cm^{-1})	J_o	Ref.	*Hfs* done
22680.022(6)	22679.999	54633.460	5/2	77313.459	7/2	NL	(a)
22687.206(3)	22687.226	56092.881	3/2	78780.107	1/2	NL	(a)
22761.882(3)	22761.866	56092.881	3/2	78854.747	5/2	NL	
23131.795(2)	23131.775	56092.881	3/2	79224.656	3/2	NL	(a)
23608.732(2)	23608.710	56092.881	3/2	79701.591	1/2	NL	(a)
23747.303(2)	23747.271	56092.881	3/2	79840.152	5/2	NL	
23781.819(3)	23781.787	54633.460	5/2	78415.247	3/2	NL	(a)
24098.795(6)	24098.771	54633.460	5/2	78732.231	5/2	NL	(a)
24181.990(4)	24181.980	54633.460	5/2	78815.440	3/2	NL	(a)
24210.871(1)	24210.843	54633.460	5/2	78844.303	7/2	NL	(a)
24221.322(2)	24221.287	54633.460	5/2	78854.747	5/2	NL	
24370.164(3)	24370.136	54633.460	5/2	79003.596	7/2	NL	(a)
24591.223(2)	24591.196	54633.460	5/2	79224.656	3/2	NL	
24704.896(2)	24704.899	56092.881	3/2	80797.780	3/2	NL	(a)

a: *hfs* in this work.
b: *hfs* in previous work [21].
c: *hfs* in previous work [22].
d: *hfs* in previous work [23].

Table 3.9 Even energy levels of I I involved in the spectral region of 10000-25000 cm^{-1} and their experimentally derived *hfs* A and B constants in mK in comparison with previous literature.

Electronic Configuration	Even Level E_e (cm^{-1})	A_{Exp}	B_{Exp}	A Ref. [21]	B Ref. [21]	A Ref. [22]	B Ref. [22]	A Ref. [23]	B Ref. [23]
$5s^2 5p^4(^3P_2)6s$									
[2]3/2	56092.881	17.97(76)	-13.42(75)	17.75(30)	-13.3(1.0)				
$5s^2 5p^4(^3P_1)$									
6s[2]5/2	54633.460	47.79(73)	-36.02(86)	47.27(10)	-35.54(30)	47.29(33)	-34(4)	47.43(20)	-36.63(67)
6s[1]3/2	61819.779	22.58(61)	13.77(84)	22.57(10)	14.5(1.0)	22.68(24)	14(1)	22.65(17)	14.51(67)
6s[1]1/2	63186.758	-5.54(19)						-3.97(07)	
$5s^2 5p^4(^3P_0)6s$									
[0]1/2	60896.243	53.96(43)		53.58(05)		53.22(28)		53.77(07)	
$5s^2 5p^4(^1D_2)6s$									
[2]5/2	68587.859	82.35(62)	72.87(52)	82.99(10)	71.76(1.0)	82.95(15)	70(1)	83.19(10)	69.91(50)
[2]3/2	68549.743	60.31(22)	36.9(2.4)	60.47(10)	36.70(1.0)	59.08(85)	36(4)	60.71(07)	36.39(33)
$5s^2 5p^4(^3P_1)7s$									
[1]3/2	78891.187	6.94(23)	13.67(47)	6.49(20)	15.37(2.0)				
[1]1/2	79285.273	7.62(78)		6.2(3)		6.80(53)		5.84(20)	
$5s^2 5p^4(^3P_0)7s$									
[0]1/2	78415.670	14.54(08)		13.55(5)		14.40(56)		13.48(03)	
$5s^2 5p^4(^3P_2)8s$									
[2]3/2	77555.824	35.72(33)	-21.8(1.1)	36.07(20)	-22.81(80)	35.85(34)	-26(1)	36.06(33)	-23.35(33)
$5s^2 5p^4(^3P_1)8s$									
[2]5/2	77450.709	26.91(66)	-34.47(02)	27.23(50)	-34.64(50)			27.39(33)	-31.02(33)
$5s^2 5p^4(^3P_2)9s$									
[2]3/2	79947.123	40.69(89)	-23.96(05)	36.98(10)	-23.95(1.0)			36.83(33)	-14.6(1.0)
$5s^2 5p^4(^3P_2)5d$									
[4]9/2	67726.415	13.42(07)	-31.74(35)	13.49(10)	-31.48(2.0)				
[4]7/2	68559.540	17.54(25)	-26.84(97)	17.55(10)	-27.45(4.0)			17.75(17)	-28.89(67)
[3]7/2	66015.023	11.01(82)	11.0(3)	10.12(10)	11.24(1.0)			10.21(17)	6.17(67)
[3]5/2	66020.469	22.06(89)	5.99(69)	21.59(20)	4.0(4.0)	21.57(15)	6(1)	21.41(07)	5.90(33)

Electronic Configuration	Even Level E_e (cm^{-1})	A_{Exp}	B_{Exp}	A Ref. [21]	B Ref. [21]	A Ref. [22]	B Ref. [22]	A Ref. [23]	B Ref. [23]
[1]3/2	66355.093	34.60(74)	12.1(1.0)	32.59(05)	10.96(50)	32.55(27)	8(1)	32.56(07)	9.61(33)
[1]1/2	67298.328	37.04(93)		37.8(20)		37.91(23)		39.33(67)	
[0]1/2	68615.734	94.43(04)		94.46(10)		94.56(23)			
$5s^2 5p^4(^3P_1)5d$									
[3]5/2	75177.235	9.84(10)	-4.0(1.4)	9.79(10)	-4.2(1.0)				
[2]5/2	75898.893	5.04(44)	14.27(25)	4.33(10)	11.31				
[2]3/2	75823.909	11.14(53)	-2.90(42)	11.49(30)	-3.26(50)				
$5s^2 5p^4(^1D_2)5d$									
[1]3/2	81072.615	15.08(97)	-11.81(76)						
[3]5/2	82144.510	7.07(94)	-8.71(98)						
$5s^2 5p^4(^3P_2)6d$									
[4]9/2	75704.140	14.24(75)	-35.6(1.0)						
[4]7/2	76004.731	18.51(74)	-20.85(88)	16.03(10)	-20.86(1.0)				
[3]7/2	75511.130	12.84(50)	-10.14(88)	12.88(10)	-10.15(1.0)				
[3]5/2	76106.548	6.98(21)	-19.35(07)	7.74(10)	-20.33(1.0)				
[2]5/2	76903.269	11.77(30)	12.00(98)			11.37(45)	7(3)		
[2]3/2	76746.978	-7.64(64)	4.50(86)						
[1]3/2	76136.403	5.79(07)	5.60(06)	4.72(10)	5.28(1.0)				
[1]1/2	76417.783	49.36(80)		48.63(30)		48.73(57)		48.60(33)	
[0]1/2	75714.423	25.05(48)		25.33(40)					
$5s^2 5p^4(^3P_2)7d$									
[4]9/2	79054.985	14.31(72)	-34.8(1.0)						
[3]7/2	78904.061	14.88(89)	-11.25(57)						
[3]5/2	78943.341	17.24(04)	-6.32(21)	17.68(10)	-6.20(1.0)				
[2]5/2	79418.489	10.14(25)	7.60(57)	15.06(10)	4.3(1.0)	14.34(53)	12(6)	14.84(20)	3.87(67)
[2]3/2	79395.897	4.33(41)	16.77(65)			5.90(55)	13(2)	3.84(33)	21.4(1.0)
[1]3/2	79030.992	21.53(90)	4.89(68)	21.17(10)	5.37(50)	20.48(13)	1(5)		
[1]1/2	78889.521	1.96(87)							
[0]1/2	79393.205	1.50(82)							

Electronic Configuration	Even Level E_e (cm^{-1})	A_{Exp}	B_{Exp}	A Ref. [21]	B Ref. [21]	A Ref. [22]	B Ref. [22]	A Ref. [23]	B Ref. [23]
$5s^25p^4(^3P_2)8d$									
[4]9/2	80772.340	14.21(62)	-29.05(59)						
[4]7/2	80869.160	25.25(58)	-5.40(88)						
[3]7/2	80676.170	12.94(75)	25.81(73)						
[2]3/2	80782.470	11.87(75)	7.80(84)						
[1]3/2	80690.940	24.82(85)	0.5(1.1)						
[1]1/2	80693.970	-15.07(39)							

Table 3.10 Odd energy levels of I I involved in the spectral region of 10000-25000 cm^{-1} and their experimentally derived *hfs* A and B constants in mK in comparison with previous literature.

Electronic Configuration	E_o (cm^{-1})	A_{Exp}	B_{Exp}	A Ref. [21]	B Ref. [21]	A Ref.[22]	B Ref.[22]	A Ref. [23]	B Ref. [23]
$5s^25p^4(^3P_2)6p$									
[3]7/2	65669.988	19.24(67)	-37.40(83)	19.57(5)	-36.84(50)				
[3]5/2	65644.476	27.87(74)	-22.06(67)	24.03(10)	-22.04(50)				
[2]5/2	64906.290	25.19(59)	-19.36(48)	25.31(10)	-18.86(1.0)	26.73(47)	-16(4)	25.38(33)	-17.7(1.0)
[2]3/2	64989.994	35.29(42)	-25.07(69)	35.38(10)	-23.56(1.0)	35.21(43)	-25(2)	35.36(20)	-23.52(67)
[1]3/2	67062.130	29.43(95)	-0.43(05)	29.13(5)	-0.45(50)	29.38(40)	0(2)	28.92(10)	-0.70(33)
[1]1/2	65856.960	58.73(77)		57.25(5)		57.04(35)		57.34(07)	
$5s^25p^4(^3P_1)6p$									
[2]5/2	72529.182	-6.01(43)	14.29(19)	-5.79(5)	14.19(50)				
[2]3/2	72807.164	-0.51(17)	16.20(38)	-0.53(10)	16.14(20)				
[1]3/2	73054.598	2.19(63)	-16.0(1.0)	2.18(5)	-14.58(50)			2.33(20)	-14.01(67)
[1]1/2	73387.184	-33.0(1.0)		-31.46(5)		-31.57(10)		-31.59(07)	
[0]1/2	71501.480	7.90(38)		8.50(5)					
$5s^25p^4(^3P_0)6p$									
[1]3/2	71976.775	0.18(19)	-0.83(58)						
[1]1/2	71813.958	-6.80(41)		-6.01(10)					
$5s^25p^4(^1D_2)6p$									
[3]7/2	79003.596	49.37(20)	71.0(1.0)	49.60(10)	70.95(1.0)				
[3]5/2	78592.572	67.50(40)	67.0(1.0)	67.46(10)	68.48(50)			67.58(07)	68.21(50)
[2]5/2	80125.450	53.0(1.0)	32.15(19)			52.45(21)	32(2)	52.54(10)	32.92(50)
[2]3/2	80039.779	74.80(41)	30.82(55)	75.17(10)	30.55(1.0)	75.18(14)	28(1)	75.48(17)	29.62(50)
[1]3/2	78415.247	61.31(85)	16.17(13)	60.38(10)	15.44(50)	60.77(40)	15(2)	60.47(10)	14.2(1.7)
[1]1/2	79701.591	158.0(1.0)		158.47(20)		159.27(73)			
$5s^25p^4(^3P_2)7p$									
[3]7/2	75194.056	18.94(09)	-34.59(75)	18.91(5)	-35.00(1.0)				

Electronic Configuration	E_o (cm^{-1})	A_{Exp}	B_{Exp}	A Ref. [21]	B Ref. [21]	A Ref.[22]	B Ref.[22]	A Ref. [23]	B Ref. [23]
[3]5/2	75191.337	22.08(94)	-19.68(24)	22.75(20)	-19.86(1.0)				
[2]5/2	74965.635	24.97(16)	-23.53(16)	24.73(20)	-23.42(1.0)				
[2]3/2	75049.514	37.72(72)	-23.62(87)	38.0710)	-23.60(1.0)				
[1]3/2	75621.427	27.78(62)	1.0(1.0)	27.76(5)	0.41(50)	28.41(15)	0(7)	27.58(17)	-1.23(50)
[1]1/2	75303.065	65.24(74)		65.07(5)				64.68(17)	
$5s^2 5p^4(^3P_1)7p$									
[0]1/2	81506.800	8.64(35)				7.65(12)		6.47(33)	
[1]1/2	82615.750	4.83(77)						4.70(33)	
[2]5/2	82213.940	-6.47(89)	27.0(1.0)						
$5s^2 5p^4(^3P_2)8p$									
[3]7/2	78844.303	18.75(95)	-24.0(1.0)	18.76(1.0)	-24.5(5.0)				
[3]5/2	78854.747	23.51(25)	-16.54(32)					24.96(17)	-19.95(67)
[2]3/2	78815.440	41.02(97)	-16.0(1.0)			40.37(72)	-15(4)		
[2]5/2	78732.231	25.85(05)	-26.31(10)						
[1]3/2	79224.656	36.0(1.0)	5.0(1.0)	36.56(20)	4.32(2.0)			36.09(17)	5.30(67)
[1]1/2	78780.107	79.05(05)				80.07(35)		79.24(17)	
$5s^2 5p^4(^3P_2)4f$									
[4]9/2	77306.559	11.17(36)	7.40(96)	10.37(50)	7.89(1.0)				
[4]7/2	77307.280	13.0(75)	136.79(82)						
[3]7/2	77313.459	10.51(24)	9.62(40)	8.93(50)	9.0(2.0)				
[3]5/2	77307.333	11.17(68)	10.70(49)	10.7(1.0)	-5.0				
[2]5/2	77359.585	-0.77(92)	19.71(87)	-0.3(10)	20.0(1.0)			0.10(17)	21.58(67)
[1]3/2	77406.784	-22.61(05)	-4.77(08)	-21.98(10)	-4.78(10)	-21.50(42)	-4(2)		
[1]1/2	77404.362	-44.0(1.0)		-43.49(10)					
$5s^2 5p^4(^3P_2)5f$									
[5]11/2	79859.010	11.51(70)	-46.16(85)						
[5]9/2	79859.570	15.01(18)	-27.35(52)						
[4]9/2	79829.600	11.07(89)	43.0(1.0)						
[4]7/2	79832.955	15.0(2.0)	-3.93(47)						
[3]7/2	79847.683	7.57(14)	9.40(88)						

Electronic Configuration	E_o (cm^{-1})	A_{Exp}	B_{Exp}	A Ref. [21]	B Ref. [21]	A Ref.[22]	B Ref.[22]	A Ref. [23]	B Ref. [23]
[3]5/2	79844.469	9.98(32)	15.99(32)						
[2]5/2	79840.152	1.73(52)	9.74(98)	3.46(1.0)	12.44(2.0)				
[2]3/2	79834.910	9.11(15)	17.64(74)			8.75(18)	18(1)	9.31(33)	16.7(1.7)
[1]3/2	79881.383	-15.24(27)	6.07(68)			-21.74(23)	3(1)		
$5s^2 5p^4(^3P_2)6f$									
[1]1/2	81225.890	-40.09(51)				-42.32(27)			
$5s^2 5p^4(^3P_2)9p$									
[1]3/2	80797.780	28.42(46)	14.0(1.0)			26.19(59)	1(3)	27.45(17)	-0.63(67)

Table 4.1 Center of gravity wavenumber list of 107 observed spectral transitions of Bi I in the IR to UV spectral region along with their classifications. The even and odd energy levels E_e and E_o are taken from NIST data base [93]. Here σ_{obs} is the center of gravity wavenumber of the observed spectral lines. The value in parentheses represents the uncertainty. σ_{cal} is the wavenumber calculated using the level energies given in the NIST database [93]. The last column indicates whether the *hfs* measurement was carried out in the previous work or present.

σ_{obs} (cm^{-1})	σ_{cal} (cm^{-1})	E_e (cm^{-1})	E_o (cm^{-1})	Classification ($E_e - E_o$)	*Hfs*
2566.310(3)	2566.307	54359.456	51793.149	($^3P_0$)5g[4]7/2-($^3P_0$)5f[3]7/2	
2569.032(2)	2569.031	54359.456	51790.425	($^3P_0$)5g[4]7/2-($^3P_0$)5f[3]5/2	
2624.363(5)	2624.357	47373.477	49997.834	($^3P_0$)8s[0]1/2-($^3P_0$)8p[1]1/2	[a,b]
2787.390(3)	2787.389	43912.374	41124.985	($^3P_0$)6d[2]3/2-($^3P_0$)7p[1]1/2	[a,b]
2975.370(4)	2975.364	45915.883	42940.519	($^3P_1$)7s[1]1/2-($^3P_0$)7p[1]3/2	[a,b]
3143.618(4)	3143.623	51158.494	54302.117	($^3P_0$)7d[2]5/2-($^3P_0$)6f[3]5/2	
3146.477(3)	3146.484	51158.494	54304.978	($^3P_0$)7d[2]5/2-($^3P_0$)6f[3]7/2	
3283.025(7)	3283.027	51019.090	54302.117	($^3P_0$)7d[2]3/2-($^3P_0$)6f[3]5/2	[b]
3284.240(5)	3284.242	53878.830	50594.588	($^3P_0$)8d[2]3/2-($^3P_0$)8p[1]3/2	
3303.308(4)	3303.280	48489.869	51793.149	($^3P_2$)7s[2]5/2-($^3P_0$)5f[3]7/2	[b]
3382.462(5)	3382.463	53977.051	50594.588	($^3P_0$)8d[2]5/2-($^3P_0$)8p[1]3/2	
3740.090(4)	3740.091	44865.076	41124.985	($^3P_1$)7s[1]3/2-($^3P_0$)7p[1]1/2	[a,b]
4081.954(6)	4081.951	45915.883	49997.834	($^3P_1$)7s[1]1/2-($^3P_0$)8p[1]1/2	[a,b]
4432.953(4)	4432.958	47373.477	42940.519	($^3P_0$)8s[0]1/2-($^3P_0$)7p[1]3/2	[b]
4678.713(5)	4678.705	45915.883	50594.588	($^3P_1$)7s[1]1/2-($^3P_0$)8p[1]3/2	[b]
4790.899(3)	4790.898	45915.883	41124.985	($^3P_1$)7s[1]1/2-($^3P_0$)7p[1]1/2	[a,b]
4880.129(5)	4880.126	55474.714	50594.588	($^3P_0$)9d[2]5/2-($^3P_0$)8p[1]3/2	
5549.358(4)	5549.350	48489.869	42940.519	($^3P_2$)7s[2]5/2-($^3P_0$)7p[1]3/2	[a,b]
5777.747(3)	5777.747	44816.841	50594.588	($^3P_0$)6d[2]5/2-($^3P_0$)8p[1]3/2	
6085.456(3)	6085.460	43912.374	49997.834	($^3P_0$)6d[2]3/2-($^3P_0$)8p[1]1/2	[a,b]
6095.068(2)	6095.074	47373.477	53468.551	($^3P_0$)8s[0]1/2-($^3P_0$)9p[1]1/2	
6248.488(2)	6248.492	47373.477	41124.985	($^3P_0$)8s[0]1/2-($^3P_0$)7p[1]1/2	[a,b]
6334.873(6)	6334.872	47373.477	53708.349	($^3P_0$)8s[0]1/2-($^3P_0$)9p[1]3/2	[b]
6520.318(6)	6520.313	47373.477	53893.790	($^3P_0$)8s[0]1/2-($^3P_0$)7p[0]1/2	[b]
6520.392(2)	6520.391	49460.910	42940.519	($^3P_2$)7s[2]3/2-($^3P_0$)7p[1]3/2	[b]
6627.383(4)	6627.374	49460.910	56088.284	($^3P_2$)7s[2]3/2-($^3P_1$)7p[1]3/2	[b]
6682.208(6)	6682.214	43912.374	50594.588	($^3P_0$)6d[2]3/2-($^3P_0$)8p[1]3/2	[b]
6814.845(2)	6814.839	49460.910	56275.749	($^3P_2$)7s[2]3/2-($^3P_1$)7p[1]1/2	[a,b]
6925.350(5)	6925.349	44865.076	51790.425	($^3P_1$)7s[1]3/2-($^3P_0$)5f[3]5/2	[b]
6973.586(2)	6973.584	44816.841	51790.425	($^3P_0$)6d[2]5/2-($^3P_0$)5f[3]5/2	
6976.315(3)	6976.308	44816.841	51793.149	($^3P_0$)6d[2]5/2-($^3P_0$)5f[3]7/2	

σ_{obs} (cm^{-1})	σ_{cal} (cm^{-1})	E_e (cm^{-1})	E_o (cm^{-1})	Classification ($E_e - E_o$)	Hfs
7197.080(3)	7197.073	47373.477	54570.550	$(^3P_0)8s[0]1/2-(^3P_1)7p[2]3/2$	[a,b]
7598.448(8)	7598.415	48489.869	56088.284	$(^3P_2)7s[2]5/2-(^3P_1)7p[1]3/2$	[b]
7792.464(7)	7792.466	45915.883	53708.349	$(^3P_1)7s[1]1/2-(^3P_0)9p[1]3/2$	[b]
7878.050(4)	7878.051	43912.374	51790.425	$(^3P_0)6d[2]3/2-(^3P_0)5f[3]5/2$	
7977.906(2)	7977.907	45915.883	53893.790	$(^3P_1)7s[1]1/2-(^3P_1)7p[0]1/2$	[a,b]
8078.572(5)	8078.571	51019.09	42940.519	$(^3P_0)7d[2]3/2-(^3P_0)7p[1]3/2$	[a,b]
8217.978(3)	8217.975	51158.494	42940.519	$(^3P_0)7d[2]5/2-(^3P_0)7p[1]3/2$	
8335.947(2)	8335.925	49460.910	41124.985	$(^3P_2)7s[2]3/2-(^3P_0)7p[1]1/2$	[a,b]
8536.766(3)	8536.764	32588.221	41124.985	$(^3P_0)7s[0]1/2-(^3P_0)7p[1]1/2$	[a,b]
8654.672(6)	8654.667	45915.883	54570.550	$(^3P_1)7s[1]1/2-(^3P_1)7p[2]3/2$	[a,b]
8714.818(2)	8714.807	47373.477	56088.284	$(^3P_0)8s[0]1/2-(^3P_1)7p[1]3/2$	[b]
8843.269(4)	8843.273	44865.076	53708.349	$(^3P_1)7s[1]3/2-(^3P_0)9p[1]3/2$	
8891.501(4)	8891.508	44816.841	53708.349	$(^3P_0)6d[2]5/2-(^3P_0)9p[1]3/2$	
8902.277(5)	8902.272	47373.477	56275.749	$(^3P_0)8s[0]1/2-(^3P_1)7p[1]1/2$	[a,b]
9028.723(3)	9028.714	44865.076	53893.790	$(^3P_1)7s[1]3/2-(^3P_1)7p[0]1/2$	[a,b]
9315.199(7)	9315.198	52255.717	42940.519	$(^3P_0)9s[0]1/2-(^3P_0)7p[1]3/2$	[b]
9488.130(2)	9488.137	44816.841	54304.978	$(^3P_0)6d[2]5/2-(^3P_0)6f[3]7/2$	
9705.480(2)	9705.474	44865.076	54570.550	$(^3P_1)7s[1]3/2-(^3P_1)7p[2]3/2$	[a,b]
9894.103(4)	9894.105	51019.090	41124.985	$(^3P_0)7d[2]3/2-(^3P_0)7p[1]1/2$	[a,b]
9981.428(6)	9981.416	43912.374	53893.790	$(^3P_0)6d[2]3/2-(^3P_1)7p[0]1/2$	
10172.403(5)	10172.401	45915.883	56088.284	$(^3P_1)7s[1]1/2-(^3P_1)7p[1]3/2$	[a,b]
10352.300(4)	10352.298	32588.221	42940.519	$(^3P_0)7s[0]1/2-(^3P_0)7p[1]3/2$	[a,b]
10359.848(5)	10359.866	45915.883	56275.749	$(^3P_1)7s[1]1/2-(^3P_1)7p[1]1/2$	[b]
10389.734(3)	10389.743	43912.374	54302.117	$(^3P_0)6d[2]3/2-(^3P_0)6f[3]5/2$	
10700.758(3)	10700.757	44865.076	55565.833	$(^3P_1)7s[1]3/2-(^3P_1)7p[2]5/2$	[a,b]
10807.211(4)	10807.227	44865.076	55672.303	$(^3P_1)7s[1]3/2-(^3P_0)7f[3]5/2$	
10853.660(4)	10853.652	44816.841	55670.493	$(^3P_0)6d[2]5/2-(^3P_0)7f[3]7/2$	
10927.310(5)	10927.307	32588.221	21660.914	$(^3P_0)7s[0]1/2-6p^3\,^2P_{1/2}$	[a,b]
10938.312(2)	10938.311	53878.830	42940.519	$(^3P_0)8d[2]3/2-(^3P_0)7p[1]3/2$	
11130.729(2)	11130.732	52255.717	41124.985	$(^3P_0)9s[0]1/2-(^3P_0)7p[1]1/2$	[a,b]
11223.205(4)	11223.208	44865.076	56088.284	$(^3P_1)7s[1]3/2-(^3P_1)7p[1]3/2$	[b]
11410.672(2)	11410.673	44865.076	56275.749	$(^3P_1)7s[1]3/2-(^3P_1)7p[1]1/2$	[a,b]
11419.038(5)	11419.039	11419.039	0	$6p^3\,^2D_{3/2}-6p^3\,^4S_{3/2}$	
11620.109(3)	11620.118	54560.637	42940.519	$(^3P_0)10s[0]1/2-(^3P_0)7p[1]3/2$	
11652.033(4)	11652.036	44816.841	33164.805	$(^3P_0)6d[2]5/2-6p^3\,^2P_{3/2}$	[a,b]
11700.271(4)	11700.271	44865.076	33164.805	$(^3P_1)7s[1]3/2-6p^3\,^2P_{3/2}$	[a,b]
11759.907(7)	11759.929	43912.374	55672.303	$(^3P_0)6d[2]3/2-(^3P_0)7f[3]5/2$	

σ_{obs} (cm^{-1})	σ_{cal} (cm^{-1})	E_e (cm^{-1})	E_o (cm^{-1})	Classification ($E_e - E_o$)	Hfs
12175.910(3)	12175.910	43912.374	56088.284	($^3P_0$)6d[2]3/2-($^3P_1$)7p[1]3/2	[a,b]
12484.781(3)	12484.782	55425.301	42940.519	($^3P_0$)9d[2]3/2-($^3P_0$)7p[1]3/2	
12534.202(6)	12534.195	55474.714	42940.519	($^3P_0$)9d[2]5/2-($^3P_0$)7p[1]3/2	
12578.711(4)	12578.739	43912.374	56491.113	($^3P_0$)6d[2]3/2-($^3P_0$)8f[3]5/2	
12751.060(6)	12751.078	45915.883	33164.805	($^3P_1$)7s[1]1/2-6p^3 $^2P_{3/2}$	[a,b]
12753.841(5)	12753.845	53878.830	41124.985	($^3P_0$)8d[2]3/2-($^3P_0$)7p[1]1/2	[b]
12884.002(7)	12884.009	55824.528	42940.519	($^3P_0$)11s[0]1/2-($^3P_0$)7p[1]3/2	
13418.957(8)	13418.929	56359.448	42940.519	($^3P_0$)10d[2]5/2-($^3P_0$)7p[1]3/2	
13435.633(8)	13435.652	54560.637	41124.985	($^3P_0$)10s[0]1/2-($^3P_0$)7p[1]1/2	[a,b]
14208.677(4)	14208.672	47373.477	33164.805	($^3P_0$)8s[0]1/2-6p^3 $^2P_{3/2}$	
14300.319(4)	14300.316	55425.301	41124.985	($^3P_0$)9d[2]3/2-($^3P_0$)7p[1]1/2	[a,b]
15205.993(7)	15204.990	56329.975	41124.985	($^3P_0$)10d[2]3/2-($^3P_0$)7p[1]1/2	[b]
15325.061(5)	15325.064	48489.869	33164.805	($^3P_2$)7s[2]5/2-6p^3 $^2P_{3/2}$	[b]
16296.121(4)	16296.105	49460.910	33164.805	($^3P_2$)7s[2]3/2-6p^3 $^2P_{3/2}$	[a,b]
17409.611(2)	17409.613	32588.221	49997.834	($^3P_0$)7s[0]1/2-($^3P_0$)8p[1]1/2	[b]
17854.288(3)	17854.285	51019.090	33164.805	($^3P_0$)7d[2]3/2-6p^3 $^2P_{3/2}$	[b]
18006.366(5)	18006.367	32588.221	50594.588	($^3P_0$)7s[0]1/2-($^3P_0$)8p[1]3/2	[a,b]
21120.116(5)	21120.128	32588.221	53708.349	($^3P_0$)7s[0]1/2-($^3P_0$)9p[1]3/2	[a,b]
21169.201(4)	21169.182	32588.221	11419.039	($^3P_0$)7s[0]1/2-6p^3 $^2D_{3/2}$	[a,b]
22251.461(8)	22251.460	43912.374	21660.914	($^3P_0$)6d[2]3/2-6p^3 $^2P_{1/2}$	[a,b]
23204.152(3)	23204.162	44865.076	21660.914	($^3P_1$)7s[1]3/2-6p^3 $^2P_{1/2}$	[a,b]
24254.985(3)	24254.969	45915.883	21660.914	($^3P_1$)7s[1]1/2-6p^3 $^2P_{1/2}$	[a,b]
25712.568(5)	25712.563	47373.477	21660.914	($^3P_0$)8s[0]1/2-6p^3 $^2P_{1/2}$	[a,b]
27799.995(5)	27799.996	49460.910	21660.914	($^3P_2$)7s[2]3/2-6p^3 $^2P_{1/2}$	[a,b]
28474.894(3)	28474.873	43912.374	15437.501	($^3P_0$)6d[2]3/2-6p^3 $^2D_{5/2}$	[a,b]
29427.603(7)	29427.575	44865.076	15437.501	($^3P_1$)7s[1]3/2-6p^3 $^2D_{5/2}$	[a,b]
32493.347(3)	32493.335	43912.374	11419.039	($^3P_0$)6d[2]3/2-6p^3 $^2D_{3/2}$	[a,b]
32588.210(4)	32588.221	32588.221	0	($^3P_0$)7s[0]1/2-6p^3 $^4S_{3/2}$	[a,b]
33052.382(5)	33052.368	48489.869	15437.501	($^3P_2$)7s[2]5/2-6p^3 $^2D_{5/2}$	[a,b]
33397.801(8)	33397.802	44816.841	11419.039	($^3P_0$)6d[2]5/2-6p^3 $^2D_{3/2}$	[a,b]
33446.034(9)	33446.037	44865.076	11419.039	($^3P_1$)7s[1]3/2-6p^3 $^2D_{3/2}$	[a,b]
34023.412(8)	34023.409	49460.910	15437.501	($^3P_2$)7s[2]3/2-6p^3 $^2D_{5/2}$	[a,b]
34496.851(3)	34496.844	45915.883	11419.039	($^3P_1$)7s[1]1/2-6p^3 $^2D_{3/2}$	[a,b]
35581.598(6)	35581.589	51019.090	15437.501	($^3P_0$)7d[2]3/2-6p^3 $^2D_{5/2}$	[a,b]
35720.926(8)	35720.993	51158.494	15437.501	($^3P_0$)7d[2]5/2-6p^3 $^2D_{5/2}$	[a,b]
35954.440(4)	35954.438	47373.477	11419.039	($^3P_0$)8s[0]1/2-6p^3 $^2D_{3/2}$	[a,b]
37070.837(5)	37070.830	48489.869	11419.039	($^3P_2$)7s[2]5/2-6p^3 $^2D_{3/2}$	[a,b]

σ_{obs} (cm^{-1})	σ_{cal} (cm^{-1})	E_e (cm^{-1})	E_o (cm^{-1})	Classification ($E_e - E_o$)	Hfs
38041.881(4)	38041.871	49460.910	11419.039	($^3P_2$)7s[2]3/2-6p$^{3\,2}$D$_{3/2}$	[a,b]
39600.054(5)	39600.051	51019.190	11419.039	($^3P_0$)7d[2]3/2-6p$^{3\,2}$D$_{3/2}$	

a: Hfs observed previously [32,79,80,81,82,83,86,87,35,37,89,38,66].

b: Hfs studied in this work.

Table 4.2 Even energy levels of Bi I and their experimentally derived *hfs* A and B constants in mK in comparison with previous literature.

E_e (cm^{-1})	Configuration	J	This Work A(mK)	B(mK)	Previous Work A(mK)	B(mK)	Ref
32588.221	6p^2(^{3}P$_0$)7s[0]	1/2	164.13(39)*		164.66(23)		[38]
					164.171(34)		[89]
					163.6(3)		[35]
					163.76(6)		[84]
45915.883	6p^2(^{3}P$_1$)7s[1]	1/2	-144.04(40)		-144.17(26)		[38]
					-143.72(10)		[89]
					-144.1(1)		[35]
44865.076	6p^2(^{3}P$_1$)7s[1]	3/2	-2.19(20)	-22.46(31)	-1.62(25)		[38]
					-2.02(8)	-21.58(91)	[89]
					-2.26(5)	0(3)	[82]
					3.17(13)		[85]
					-2.03(5)	-24.65(30)	[83]
49460.910	6p^2(^{3}P$_2$)7s[2]	3/2	94.03(21)	-2.07(85)	93.88(25)		[38]
					94.42(2)	-3.96(33)	[89]
					94.33(71)	-3.08(66)	[37]
					94.419(17)	-4.42(15)	[86]
48489.869	6p^2(^{3}P$_2$)7s[2]	5/2	124.29(35)	-4.22(59)	123.81(37)	-4(10)	[89]
					124.16(10)	-2.6(3)	[82]
					123.999(17)	-4.60(17)	[86]
47373.477	6p^2(^{3}P$_0$)8s[0]	1/2	34.05(14)		33.88(9)		[89]
					34.68(5)		[82]
52255.717	6p^2(^{3}P$_0$)9s[0]	1/2	20.15(42)		19.65(20)		[89]
43912.374	6p^2(^{3}P$_0$)6d[2]	3/2	4.61(30)	1.56(39)	3.82(76)		[38]
					4.34(2)	1.83(17)	[89]
					4.25(5)	0(3)	[82]
					4.27(2)	1.93(13)	[85]
					4.28(9)	1.17(23)	[83]
44816.841	6p^2(^{3}P$_0$)6d[2]	5/2	0.72(16)	0.28(45)	0.46(3)	0(3)	[82]
51019.090	6p^2(^{3}P$_0$)7d[2]	3/2	11.85(53)	0.87(71)	11.25(6)	0	[89]
					11.11(10)	0	[82]
51158.494	6p^2(^{3}P$_0$)7d[2]	5/2	0.83(10)	0.00(57)	0.51(5)	0(3)	[82]
53878.830	6p^2(^{3}P$_0$)8d[2]	3/2	-1.02(10)	-1.00(60)			
55425.301	6p^2(^{3}P$_0$)9d[2]	3/2	-1.37(15)	-0.83(44)	0.7(10)		[38]

E_e (cm^{-1})	Configuration	J	This Work A(mK)	B(mK)	Previous Work A(mK)	B(mK)	Ref
56329.975	6p^2(^{3}P$_0$)10d[2]	3/2	-11.34(13)	-2.00(52)			

*The numbers in parentheses denote the uncertainty on the level of one standard deviation in the units of the last digit of the value, e.g., 164.13(39) denotes 164.13±0.39.

Table 4.3 Odd energy levels of Bi I and their experimentally derived *hfs A* and *B* constants in mK in comparison with previous literature.

E_e (cm^{-1})	Configuration	J	This Work A(mK)	B(mK)	Previous Work A(mK)	B(mK)	Ref
0	6p^3 ^{4}S	3/2	-15.41(27)*	-10.43(60)	-14.76(27)	-10.8(27)	[89]
					-14.91(3)	-10.16(6)	[66]
					-14.909(1)	-10.12(1)	[79]
11419.039	6p^3 ^{2}D	3/2	-41.36(28)	-21.72(52)	-40.95(4)	-20.03(40)	[89]
					-41.0(2)	-22.6(20)	[35]
					-41.1(2)	-20.0 (20)	[80]
					-40.92(4)	-20.58(33)	[66]
15437.501	6p^3 ^{2}D	5/2	83.24(23)	2.36(50)	83.69(27)	1.9(55)	[89]
					83.48(187)	0.77(37)	[83]
21660.914	6p^3 ^{2}P	1/2	375.13(29)		375.68(44)		[89]
					375.9(2)		[35]
					376.0(6)		[80]
33164.805	6p^3 ^{2}P	3/2	16.89(42)	36.29(65)	16.27(4)	34.20(46)	[89]
					16.267(43)	34.20(43)	[37]
41124.985	6p^2(^{3}P$_0$)7p[1]	1/2	27.47(15)		27.7(15)		[38]
					27.49(8)		[89]
42940.519	6p^2(^{3}P$_0$)7p[1]	3/2	2.36(74)	-2.20(12)	2.49(42)		[38]
					2.35(13)	0	[89]
53893.790	6p^2(^{3}P$_1$)7p[0]	1/2	-118.75(10)		-118.88(13)		[89]
56275.749	6p^2(^{3}P$_1$)7p[1]	1/2	-59.67(10)		-59.93(31)		[89]

E_e (cm^{-1})	Configuration	J	This Work A(mK)	This Work B(mK)	Previous Work A(mK)	Previous Work B(mK)	Ref
56088.284	6p^2(^{3}P$_1$)7p[1]	3/2	-0.36(13)		-0.33(72)		[38]
54570.550	6p^2(^{3}P$_1$)7p[2]	3/2	-20.96(10)	-9.82(54)	-21.03(5)	-9.86(88)	[89]
55565.833	6p^2(^{3}P$_1$)7p[2]	5/2	-33.86(10)	-23.02(61)	-33.77(2)	-22.95(77)	[89]
49997.834	6p^2(^{3}P$_0$)8p[1]	1/2	9.81(17)		9.42(7)		[89]
50594.588	6p^2(^{3}P$_0$)8p[1]	3/2	1.12(31)	-3.23(55)			
53708.349	6p^2(^{3}P$_0$)9p[1]	3/2	-1.36(10)	-4.70(15)			
51790.425	6p^2(^{3}P$_0$)5f[3]	5/2	0.40(5)	-1.48 (32)			
54302.117	6p^2(^{3}P$_0$)6f[3]	5/2	0.33(10)	-1.73(40)			

*The numbers in parentheses denote the uncertainty on the level of one standard deviation in the units of the last digit of the value, e.g., -15.41(27) denotes -15.41±0.27.

Table 5.1 The experimental parameters are for I II, spectral range, resolution, number of scans and optics has been used in data acquisition. All the data have been recorded under cooling condition. Optical filters used from 450 nm − 800 nm were band pass filters with 50 nm band width.

Spectral range	Resolution (cm^{-1})	No. of scans	1+K	Beam splitter	Detector
9000-15000 cm^{-1}	0.008	132	0.999999983	CaF$_2$	Si diode
	0.01	28	0.999999917	CaF$_2$	S diode
11000-24000 cm^{-1}	0.04	356	-	QrUV	
800 nm	0.008	20	0.999999952	QrVis	
775 nm	0.012	78	0.999999981	QrUV	
	0.018	34	0.999999924	QrUV	
750 nm	0.01	84	0.999999969	QrUV	
725 nm	0.008	6	0.999999926	QrUV	
	0.01	66	0.999999981	QrUV	
	0.018	34	0.999999848	QrUV	
700 nm	0.018	48	0.999999934	QrVis	
	0.02	20	0.999999963	QrUV	
675 nm	0.01	30	0.999999825	QrVis	
	0.02	42	0.999999944	QrVis	
650 nm	0.01	36	0.999999985	QrVis	
	0.02	38	1.000000051	QrVis	
625 nm	0.02	42	1.000000165	QrVis	PMT
	0.02	34	0.999999969	QrVis	
600 nm	0.01	70	0.999999840	QrUV	
	0.012	128	0.999999922	QrUV	
	0.02	32	0.999999968	QrUV	
575 nm	0.02	10	0.999999935	QrVis	
	0.08	24	0.999999948	QrVis	
550 nm	0.01	40	0.999999914	QrUV	
	0.018	72	0.999999885	QrUV	
	0.018	100	0.999999974	QrVis	
525 nm	0.02	32	0.999999944	QrVis	
	0.04	48	0.999999928	QrVis	
500 nm	0.018	32	1.000000086	QrUV	
	0.02	118	0.999999905	QrUV	
	0.02	44	0.999999988	QrUV	
475 nm	0.018	72	0.999999959	QrUV	
	0.02	24	0.999999823	QrUV	
450 nm	0.02	192	0.999999982	QrUV	
425 nm	0.02	52	1.000000141	QrUV	

Table 5.2 Center of gravity wavenumber list of 141 observed spectral transitions of I II along with energy levels and configurations were given. The Even and Odd energy levels their electronic configurations are taken from NIST database [117]. Here σ_{obs} is center of gravity wavenumber of the observed spectral lines. The values in the parenthesis represent the uncertainty. Unclassified lines were indicated by *. A magnetic dipole (M1) transition indicated by $. Both the levels are belongs to even parity.

Wave number σ_{obs} (cm^{-1})	Even Level (cm^{-1})	Even configuration	Odd Level (cm^{-1})	Odd configuration	variance
12818.7090(14)*					
12923.503(7)	110006.71	$(^2D^0)6p\ ^3D_1$	97083.30	$(^2D^0)5d\ ^3D_2$	0.093
13041.5936(19)	112419.04	$(^2D^0)6p\ ^3F_3$	99377.47	$(^2D^0)5d\ ^3F_4$	0.0236
13054.7613(17)	99219.61	$(^4S^0)6p\ ^5P_1$	86164.86	$(^4S^0)5d\ ^5D_2$	0.0113
13162.3085(7)	99327.14	$(^4S^0)6p\ ^5P_2$	86164.86	$(^4S^0)5d\ ^5D_2$	0.0285
13599.214(3)	99327.14	$(^4S^0)6p\ ^5P_2$	85727.98	$(^4S^0)5d\ ^5D_3$	0.054
13835.495(4)	99219.61	$(^4S^0)6p\ ^5P_1$	85384.15	$(^4S^0)5d\ ^5D_0$	0.035
14366.3935(9)	100402.68	$(^4S^0)6p\ ^5P_3$	86036.32	$(^4S^0)5d\ ^5D_4$	0.0335
14484.3017(15)	99327.14	$(^4S^0)6p\ ^5P_2$	84842.87	$(^4S^0)6s\ ^3S_1$	0.0317
14674.761(4)	100402.68	$(^4S^0)6p\ ^5P_3$	85727.98	$(^4S^0)5d\ ^5D_3$	0.061
14997.461(5)	99219.61	$(^4S^0)6p\ ^5P_1$	84222.19	$5s5p^5\ ^3P_1$	0.041
16315.435(3)	110006.71	$(^2D^0)6p\ ^3D_1$	93691.35	$(^2D^0)6s\ ^3D_2$	0.075
16510.540(6)	125524.56	$(^4S^0)4f\ ^3F_2$	142035.14	$(^4S^0)6g\ ^3G_3$	-0.04
16801.361(3)	101644.21	$(^4S^0)6p\ ^3P_1$	84842.87	$(^4S^0)6s\ ^3S_1$	0.021
17311.7793(5)	99219.61	$(^4S^0)6p\ ^5P_1$	81907.83	$5s5p^5\ ^3P_2$	-0.0007
17354.2556(14)	112179.49	$(^2D^0)6p\ ^3D_2$	94825.33	$(^2D^0)6s\ ^3D_1$	0.0956
17419.3512(17)	99327.14	$(^4S^0)6p\ ^5P_2$	81907.83	$5s5p^5\ ^3P_2$	0.0412
17422.0512(10)	101644.21	$(^4S^0)6p\ ^3P_1$	84222.19	$5s5p^5\ ^3P_1$	0.0312
17506.6533(12)	114157.21	$(^2D^0)6p\ ^1F_3$	96650.55	$(^2D^0)6s\ ^3D_3$	-0.0067
17532.712(3)	115708.45	$(^2D^0)6p'\ ^3P_2$	98175.75	$(^2D^0)5d\ ^3D_3$	0.012
17567.0182(19)	115267.82	$(^2D^0)6p\ ^3D_3$	97700.81	$(^2D^0)6s\ ^1D_2$	0.0082
17606.7710(10)	111298.09	$(^2D^0)6p\ ^3F_2$	93691.35	$(^2D^0)6s\ ^3D_2$	0.031
17770.6735(6)	102613.52	$(^4S^0)6p\ ^3P_2$	84842.87	$(^4S^0)6s\ ^3S_1$	0.0235
17851.124(4)	125477.08	$(^4S^0)4f\ ^3F_4$	107625.89	$(^2D^0)5d\ ^3G_3$	-0.066
17856.903(3)	113812.79	$(^2D^0)6p\ ^1P_1$	95955.85	$5s5p^5\ ^1P_1$	-0.037
17874.136(4)	110006.71	$(^2D^0)6p\ ^3D_1$	92132.61	$(^4S^0)5d\ ^3D_1$	0.036
18007.664(5)	115708.45	$(^2D^0)6p\ ^3P_2$	97700.81	$(^2D^0)6s\ ^1D_2$	0.024
18024.701(7)	125222.20	$(^2P^0)6p\ ^3D_2$	143246.49	$(^2P^0)7s\ ^3P_1$	0.411
18104.206(5)	128563.14	$(^2P^0)6p\ ^3S_1$	110458.93	$(^2P^0)6s\ ^3P_2$	-0.004
18161.2105(8)	103004.04	$(^4S^0)6p\ ^3P_0$	84842.87	$(^4S^0)6s\ ^3S_1$	0.0405
18186.9444(11)	99219.61	$(^4S^0)6p\ ^5P_1$	81032.70	$(^4S^0)6s\ ^5S_2$	0.0344
18196.637(5)	115353.94	$(^2D^0)6p\ ^3F_4$	133550.54	$(^2D^0)7s\ ^3D_3$	0.037
18198.500(4)	112419.04	$(^2D^0)6p\ ^3F_3$	130617.58	$(^2D^0)7s\ ^3D_2$	-0.04
18204.906(3)	100402.68	$(^4S^0)6p\ ^5P_3$	118607.56	$(^4S^0)7s\ ^5S_2$	0.026
18294.4830(7)	99327.14	$(^4S^0)6p\ ^5P_2$	81032.70	$(^4S^0)6s\ ^5S_2$	0.043
18384.037(3)	116084.84	$(^2D^0)6p\ ^3P_1$	97700.81	$(^2D^0)6s\ ^1D_2$	0.007
18391.3681(6)	102613.52	$(^4S^0)6p\ ^3P_2$	84222.19	$5s5p^5\ ^3P_1$	0.0381

Wave number σ_{obs} (cm^{-1})	Even Level (cm^{-1})	Even configuration	Odd Level (cm^{-1})	Odd configuration	variance
18488.1563(18)	112179.49	$(^2D^0)6p\ ^3D_2$	93691.35	$(^2D^0)6s\ ^3D_2$	0.0163
18494.8733(9)	100402.68	$(^4S^0)6p\ ^5P_3$	81907.83	$5s5p^5\ ^3P_2$	0.0233
18617.2861(12)	115267.82	$(^2D^0)6p\ ^3D_3$	96650.55	$(^2D^0)6s\ ^3D_3$	0.0161
18679.958(5)	114635.82	$(^2D^0)6p\ ^3P_0$	95955.85	$5s5p^5\ ^1P_1$	-0.012
18703.3746(12)	115353.94	$(^2D^0)6p\ ^3F_4$	96650.55	$(^2D^0)6s\ ^3D_3$	-0.0154
18727.7302(7)	112419.04	$(^2D^0)6p\ ^3F_3$	93691.35	$(^2D^0)6s\ ^3D_2$	0.0402
18769.210(2)	115267.82	$(^2D^0)6p\ ^3D_3$	134037.06	$(^2D^0)7s\ ^1D_2$	-0.03
18781.9040(18)	103004.04	$(^4S^0)6p\ ^3P_0$	84222.19	$5s5p^5\ ^3P_1$	0.054
18903.060(3)	125006.38	$(^2P^0)6p\ ^3P_0$	106103.28	$(^2P^0)6s\ ^3P_1$	-0.04
18972.3805(15)	129431.27	$(^2P^0)6p\ ^3D_3$	110458.93	$(^2P^0)6s\ ^3P_2$	0.0405
18987.463(6)	113812.79	$(^2D^0)6p\ ^1P_1$	94825.33	$(^2D^0)6s\ ^3D_1$	0.003
19057.9289(6)	115708.45	$(^2D^0)6p\ ^3P_2$	96650.55	$(^2D^0)6s\ ^3D_3$	0.0289
19118.9078(16)	125222.20	$(^2P^0)6p\ ^3D_2$	106103.28	$(^2P^0)6s\ ^3P_1$	-0.0122
19165.4754(8)	111298.09	$(^2D^0)6p\ ^3F_2$	92132.61	$(^4S^0)5d\ ^3D_1$	-0.0046
19173.5357(14)	112179.49	$(^2D^0)6p\ ^3D_2$	93005.95	$(^4S^0)5d\ ^3D_3$	-0.0043
19262.2620(12)	141080.89	$(^4S^0)6f\ ^5F_3$	121818.65	$(^4S^0)6d\ ^5D_2$	0.022
19262.8603(15)	141088.90	$(^4S^0)6f\ ^5F_5$	121826.09	$(^4S^0)6d\ ^5D_4$	0.0503
19267.6114(5)	128563.14	$(^2P^0)6p\ ^3S_1$	109295.45	$(^2D^0)5d\ ^3S_1$	-0.0786
19280.455(2)	99327.14	$(^4S^0)6p\ ^5P_2$	118607.56	$(^4S^0)7s\ ^5S_2$	0.035
19294.823(2)	141073.17	$(^4S^0)6f\ ^5F_4$	121778.34	$(^4S^0)6d\ ^5D_3$	-0.007
19313.861(3)	129772.76	$(^2P^0)6p\ ^3P_2$	110458.93	$(^2P^0)6s\ ^3P_2$	0.031
19317.131(8)	111298.09	$(^2D^0)6p\ ^3F_2$	130615.21	$(^2D^0)7s\ ^3D_1$	0.011
19370.0336(4)	100402.68	$(^4S^0)6p\ ^5P_3$	81032.70	$(^4S^0)6s\ ^5S_2$	0.0536
19388.002(3)	99219.61	$(^4S^0)6p\ ^5P_1$	118607.56	$(^4S^0)7s\ ^5S_2$	0.052
19413.1140(16)	112419.04	$(^2D^0)6p\ ^3F_3$	93005.95	$(^4S^0)5d\ ^3D_3$	0.024
19421.266(5)	125524.56	$(^4S^0)4f\ ^3F_2$	106103.28	$(^2P^0)6s\ ^3P_1$	-0.014
19465.843(3)	134363.21	$(^2P^0)6p\ ^1S_0$	114897.43	$(^2D^0)5d\ ^1P_1$	0.063
19483.089(4)	131444.69	$(^2P^0)6p\ ^1D_2$	111961.58	$(^2P^0)6s\ ^1P_1$	-0.021
19508.471(4)	110006.71	$(^2D^0)6p\ ^3D_1$	90498.31	$(^4S^0)5d\ ^3D_2$	0.071
19736.3883(10)	101644.21	$(^4S^0)6p\ ^3P_1$	81907.83	$5s5p^5\ ^3P_2$	0.0083
19749.9404(17)	124950.92	$(^4S^0)7p\ ^5P_1$	105200.97	$(^2P^0)6s\ ^3P_0$	-0.0096
19810.5242(8)	114635.82	$(^2D^0)6p\ ^3P_0$	94825.33	$(^2D^0)6s\ ^3D_1$	0.0342
19879.901(6)	114157.21	$(^2D^0)6p\ ^1F_3$	134037.06	$(^2D^0)7s\ ^1D_2$	0.051
19961.0567(10)	125162.00	$(^2P^0)6p\ ^3P_1$	105200.97	$(^2P^0)6s\ ^3P_0$	0.0267
20025.588(5)	128563.14	$(^2P^0)6p\ ^3S_1$	108537.50	$(^2D^0)5d\ ^1D_2$	-0.052
20046.8610(11)	112179.49	$(^2D^0)6p\ ^3D_2$	92132.61	$(^4S^0)5d\ ^3D_1$	-0.019
20121.451(3)	113812.79	$(^2D^0)6p\ ^1P_1$	93691.35	$(^2D^0)6s\ ^3D_2$	0.011
20132.619(3)	126235.91	$(^4S^0)7p\ ^3P_1$	106103.28	$(^2P^0)6s\ ^3P_1$	-0.011
20224.330(4)	113812.79	$(^2D^0)6p\ ^1P_1$	134037.06	$(^2D^0)7s\ ^1D_2$	0.06
20300.827(3)	126404.16	$(^4S^0)7p\ ^3P_2$	106103.28	$(^2P^0)6s\ ^3P_1$	-0.053
20465.880(3)	114157.21	$(^2D^0)6p\ ^1F_3$	93691.35	$(^2D^0)6s\ ^3D_2$	0.02
20547.151(2)	124742.50	$(^4S^0)4f\ ^5F_5$	145289.63	$(^4S^0)7g\ ^5G_6$	0.021
20611.510(5)	101644.21	$(^4S^0)6p\ ^3P_1$	81032.70	$(^4S^0)6s\ ^5S_2$	0
20675.978(3)	125222.20	$(^2P^0)6p\ ^3D_2$	104546.19	$(^2D^0)5d\ ^3D_1$	-0.032
20705.7130(18)	102613.52	$(^4S^0)6p\ ^3P_2$	81907.83	$5s5p^5\ ^3P_2$	0.023

Wave number σ_{obs} (cm^{-1})	Even Level (cm^{-1})	Even configuration	Odd Level (cm^{-1})	Odd configuration	variance
20799.809(2)	111298.09	$(^2D^0)6p\ ^3F_2$	90498.31	$(^4S^0)5d\ ^3D_2$	0.029
20883.136(4)	115708.45	$(^2D^0)6p\ ^3P_2$	94825.33	$(^2D^0)6s\ ^3D_1$	0.016
20893.743(3)	129431.27	$(^2P^0)6p\ ^3D_3$	108537.50	$(^2D^0)5d\ ^1D_2$	-0.027
20978.362(4)	125524.56	$(^4S^0)4f\ ^3F_2$	104546.19	$(^2D^0)5d\ ^3D_1$	-0.008
20985.7781(19)	131444.69	$(^2P^0)6p\ ^1D_2$	110458.93	$(^2P^0)6s\ ^3P_2$	0.0181
21078.6025(19)	127181.99	$(^4S^0)7p\ ^3P_0$	106103.28	$(^2P^0)6s\ ^3P_1$	-0.1075
21131.506(3)	112419.04	$(^2D^0)6p\ ^3F_3$	133550.54	$(^2D^0)7s\ ^3D_3$	0.006
21134.110(5)	101644.21	$(^4S^0)6p\ ^3P_1$	122778.31	$(^2D^0)5d\ ^3F_2$	0.01
21151.237(6)	114157.21	$(^2D^0)6p\ ^1F_3$	93005.95	$(^4S^0)5d\ ^3D_3$	-0.023
21219.074(4)	115353.94	$(^2D^0)6p\ ^3F_4$	136573.00	$(^4S^0)5g\ ^5G_5$	0.014
21371.038(3)	112179.49	$(^2D^0)6p\ ^3D_2$	133550.54	$(^2D^0)7s\ ^3D_3$	-0.012
21375.6996(4)	100402.68	$(^4S^0)6p\ ^5P_3$	121778.34	$(^4S^0)6d\ ^5D_3$	0.0396
21379.5204(11)	115353.94	$(^2D^0)6p\ ^3F_4$	136733.42	$(^2D^0)6d\ 8_4$	0.0404
21381.9857(10)	119082.78	$(^2D^0)6p\ ^1D_2$	97700.81	$(^2D^0)6s\ ^1D_2$	0.0157
21415.9904(17)	100402.68	$(^4S^0)6p\ ^5P_3$	121818.65	$(^4S^0)6d\ ^5D_2$	0.0204
21423.4528(5)	100402.68	$(^4S^0)6p\ ^5P_3$	121826.09	$(^4S^0)6d\ ^5D_4$	0.0428
21465.615(3)	115267.82	$(^2D^0)6p\ ^3D_3$	136733.42	$(^2D^0)6d\ 8_4$	0.015
21536.4860(8)	112419.04	$(^2D^0)6p\ ^3F_3$	133955.51	$(^2D^0)6d\ 2_3$	0.016
21541.8247(11)*					
21576.4971(17)	115267.82	$(^2D^0)6p\ ^3D_3$	93691.35	$(^2D^0)6s\ ^3D_2$	0.0271
21580.8577(7)	102613.52	$(^4S^0)6p\ ^3P_2$	81032.70	$(^4S^0)6s\ ^5S_2$	0.0377
21630.2757(9)*					
21680.1711(10)	113812.79	$(^2D^0)6p\ ^1P_1$	92132.61	$(^4S^0)5d\ ^3D_1$	-0.0089
21734.1506(16)*					
21776.059(2)	112179.49	$(^2D^0)6p\ ^3D_2$	133955.51	$(^2D^0)6d\ 2_3$	0.039
21844.3963(14)	112179.49	$(^2D^0)6p\ ^3D_2$	134023.88	$(^2D^0)6d\ 3_3$	0.0063
21856.154(6)	99219.61	$(^4S^0)6p\ ^5P_1$	121075.75	$(^2P^0)5d\ ^3D_1$	0.014
21868.483(2)	99327.14	$(^4S^0)6p\ ^5P_2$	121195.57	$(^2P^0)5d\ ^3F_3$	0.053
21920.772(3)	112419.04	$(^2D^0)6p\ ^3F_3$	90498.31	$(^4S^0)5d\ ^3D_2$	0.042
21999.510(2)	119082.78	$(^2D^0)6p\ ^1D_2$	97083.30	$(^2D^0)5d\ ^3D_2$	0.03
22001.7208(10)	111298.09	$(^2D^0)6p\ ^3F_2$	133299.80	$(^2D^0)6d\ 1_2$	0.0108
22017.138(2)	115708.45	$(^2D^0)6p\ ^3P_2$	93691.35	$(^2D^0)6s\ ^3D_2$	0.038
22083.449(3)	112419.04	$(^2D^0)6p\ ^3F_3$	134502.39	$(^4S^0)7d\ ^5D_4$	0.099
22272.7071(16)	110006.71	$(^2D^0)6p\ ^3D_1$	87734.06	$(^4S^0)5d\ ^5D_1$	0.0571
22334.969(5)	103004.04	$(^4S^0)6p\ ^3P_0$	125339.01	$(^4S^0)6d\ ^3D_1$	-0.001
22347.9613(12)	115353.94	$(^2D^0)6p\ ^3F_4$	93005.95	$(^4S^0)5d\ ^3D_3$	-0.0287
22393.5250(12)	116084.84	$(^2D^0)6p\ ^3P_1$	93691.35	$(^2D^0)6s\ ^3D_2$	0.035
22401.6395(16)	134363.21	$(^2P^0)6p\ ^1S_0$	111961.58	$(^2P^0)6s\ ^1P_1$	0.0095
22414.372(2)$^\$$	29501.30	$5p^4\ ^1S_0$	7087.00	$5s^25p^4\ ^3P_1$	0.072
22422.922(5)	114157.21	$(^2D^0)6p\ ^1F_3$	136580.12	$(^4S^0)5g\ ^5G_4$	0.012
22432.245(3)	119082.78	$(^2D^0)6p\ ^1D_2$	96650.55	$(^2D^0)6s\ ^3D_3$	0.015
22451.2500(17)	99327.14	$(^4S^0)6p\ ^5P_2$	121778.34	$(^4S^0)6d\ ^5D_3$	0.05
22482.120(2)	99219.61	$(^4S^0)6p\ ^5P_1$	121701.69	$(^4S^0)6d\ ^5D_0$	0.04
22491.543(3)	99327.14	$(^4S^0)6p\ ^5P_2$	121818.65	$(^4S^0)6d\ ^5D_2$	0.033
22503.233(3)	114635.82	$(^2D^0)6p\ ^3P_0$	92132.61	$(^4S^0)5d\ ^3D_1$	0.023

213

Wave number σ_{obs} (cm^{-1})	Even Level (cm^{-1})	Even configuration	Odd Level (cm^{-1})	Odd configuration	variance
22576.254(3)	114157.21	($^2D^0$)6p $^1F_3$	136733.42	($^2D^0$)6d 8_4	0.044
22599.083(2)	99219.61	($^4S^0$)6p $^5P_1$	121818.65	($^4S^0$)6d $^5D_2$	0.043
22657.453(3)	111298.09	($^2D^0$)6p $^3F_2$	133955.51	($^2D^0$)6d 2_3	0.033
22674.819(2)	102613.52	($^4S^0$)6p $^3P_2$	125288.29	($^4S^0$)6d $^3D_3$	0.049
22702.5122(16)	115708.45	($^2D^0$)6p $^3P_2$	93005.95	($^4S^0$)5d $^3D_3$	0.0122
22725.850(4)	111298.09	($^2D^0$)6p $^3F_2$	134023.88	($^2D^0$)6d 3_3	0.06
22780.670(4)	112179.49	($^2D^0$)6p $^3D_2$	134960.14	($^4S^0$)7d $^3D_2$	0.02
22844.781(2)*					
23024.011(4)	99219.61	($^4S^0$)6p $^5P_1$	122243.58	($^4S^0$)6d $^5D_1$	0.041
23126.908(3)	119082.78	($^2D^0$)6p $^1D_2$	95955.85	5s5p^5 $^1P_1$	-0.022
23165.938(4)	112419.04	($^2D^0$)6p $^3F_3$	135584.94	($^4S^0$)7d $^3D_3$	0.038
23293.072(5)	110006.71	($^2D^0$)6p $^3D_1$	133299.80	($^2D^0$)6d 1_2	-0.018
23658.878(3)	114157.21	($^2D^0$)6p $^1F_3$	90498.31	($^4S^0$)5d $^3D_2$	-0.022
23952.230(3)	116084.84	($^2D^0$)6p $^3P_1$	92132.61	($^4S^0$)5d $^3D_1$	0

Table 5.3 Experimentally derived *hfs* constants A and B values for 29 **Even parity** energy levels of I II in mK. The energy level and their electronic configurations are taken from NIST database [117].

Even Level (cm^{-1})	Configuration	J	A(mK)	B(mK)	A$_{ref}$ (mK)[29]	B$_{ref}$ (mK)[29]
7087.00	$5s^25p^4\,^3P_1$	1	-20.8(0.1)	17.9(0.4)		
29501.30	$5s^25p^4\,^1S_0$	0	0	0		
99219.61	$(^4S^0)6p\,^5P_1$	1	-6.8(0.6)	3.4(1.0)		
99327.14	$(^4S^0)6p\,^5P_2$	2	11.1(1.1)	3.1(1.3)	10.87	4.6
100402.68	$(^4S^0)6p\,^5P_3$	3	3.9(0.5)	-10.0(0.9)	4.54	-11
101644.21	$(^4S^0)6p\,^3P_1$	1	15.1(0.3)	4.4(0.1)		
102613.52	$(^4S^0)6p\,^3P_2$	2	-4.5(0.2)	6.2(0.2)		
103004.04	$(^4S^0)6p\,^3P_0$	0	0	0		
110006.71	$(^2D^0)6p\,^3D_1$	1	18.2(1.9)	-21.9(2.9)		
111298.09	$(^2D^0)6p\,^3F_2$	2	44.7(2.1)	-32.0(0.7)		
112179.49	$(^2D^0)6p\,^3D_2$	2	10.8(0.4)	-9.8(1.8)		
112419.04	$(^2D^0)6p\,^3F_3$	3	27.0(1.6)	-38.3(2.9)		
113812.79	$(^2D^0)6p\,^1P_1$	1	107.9(0.9)	19.6(1.6)		
114157.21	$(^2D^0)6p\,^1F_3$	3	71.7(2.1)	-6.3(1.2)		
114635.82	$(^2D^0)6p\,^3P_0$	0	0	0		
115267.82	$(^2D^0)6p\,^3D_3$	3	60.1(0.1)	16.0(1.7)		
115353.94	$(^2D^0)6p\,^3F_4$	4	55.9(1.1)	-9.5(3.9)	55	-7.3
115708.45	$(^2D^0)6p\,^3P_2$	2	76.3(1.0)	-16.0(0.2)		
116084.84	$(^2D^0)6p\,^3P_1$	1	45.4(0.1)	-9.0(0.3)		
119082.78	$(^2D^0)6p\,^1D_2$	2	87.9(0.2)	19.6(0.2)		
124950.92	$(^4S^0)7p\,^5P_1$	1	-20.3(0.2)	-1.5(0.3)		
125006.38	$(^2P^0)6p\,^3P_0$	0	0	0		
125162.00	$(^2P^0)6p\,^3P_1$	1	-21.0(0.1)	1.7(0.6)		
125222.20	$(^2P^0)6p\,^3D_2$	2	39.9(0.2)	-13.4(1.2)		
126235.91	$(^4S^0)7p\,^3P_1$	1	-1.8(0.8)	15.2(1.0)		
126404.16	$(^4S^0)7p\,^3P_2$	2	14.7(1.4)	-27.8(2.0)		
127181.90	$(^4S^0)7p\,^3P_0$	0	0	0		
129772.76	$(^2P^0)6p\,^3P_2$	2	37.1(0.2)	12.0(0.4)		
134363.21	$(^2P^0)6p\,^1S_0$	0	0	0		

215

Table 5.4 Experimentally derived *hfs* constants A and B values for 32 **Odd parity** energy levels of I II in mK. The energy level and their electronic configurations are taken from NIST database [117].

Odd Level (cm^{-1})	Configuration	J	A(mK)	B(mK)	A$_{ref}$ (mK)[29]	B$_{ref}$ (mK)[29]
81032.70	$(^4S^0)6s\ ^5S_2^0$	2	88.4(2.0)	5.9(0.8)	92.41	4.6
81907.83	$5s5p^5\ ^3P_2^0$	2	156.1(0.4)	23.0(2.6)	159.2	29.3(1.5)
84222.19	$5s5p^5\ ^3P_1^0$	1	19.2(2.1)	-8.3(0.2)	22	
84842.87	$(^4S^0)6s\ ^3S_1^0$	1	-7.8(1.8)	-6.5(0.5)		
85384.15	$(^4S^0)5d\ ^5D_0^0$	0	0	0		
85727.98	$(^4S^0)5d\ ^5D_3^0$	3	0.4(0.9)	0.4(1.5)		
86036.32	$(^4S^0)5d\ ^5D_4^0$	4	-1.7(0.5)	-4.8(1.0)		
86164.86	$(^4S^0)5d\ ^5D_2^0$	2	14.0(0.7)	3.9(0.2)		
87734.06	$(^4S^0)5d\ ^5D_1^0$	1	38.2(0.5)	-21.4(1.1)		
90498.31	$(^4S^0)5d\ ^3D_2^0$	2	15.3(0.7)	-5.1(0.9)		
92132.61	$(^4S^0)5d\ ^3D_1^0$	1	26.8(0.7)	-7.1(3.1)		
93005.95	$(^4S^0)5d\ ^3D_3^0$	3	2.7(0.4)	-14.0(1.0)	0	-7.3
93691.35	$(^2D^0)6s\ ^3D_2^0$	2	63.0(0.8)	-55.3(2.8)		
94825.33	$(^2D^0)6s\ ^3D_1^0$	1	42.3(0.1)	-7.0(1.0)		
95955.85	$5s5p^5\ ^1P_1^0$	1	176.6(0.6)	7.9(1.0)	176	9.9
96650.55	$(^2D^0)6s\ ^3D_3^0$	3	94.2(1.3)	7.3(0.5)		
97083.30	$(^2D^0)5d\ ^3D_2^0$	2	62.7(0.3)	29.5(2.0)		
97700.81	$(^2D^0)6s\ ^1D_2^0$	2	70.3(0.3)	15.1(0.6)		
99377.47	$(^2D^0)5d\ ^3F_4^0$	4	42.7(0.5)	22.7(1.3)		
105200.97	$(^2P^0)6s\ ^3P_0^0$	0	0	0		
106103.28	$(^2P^0)6s\ ^3P_1^0$	1	175.8(1.9)	15.4(1.5)		
110458.93	$(^2P^0)6s\ ^3P_2^0$	2	54.4(0.7)	-4.0(0.8)		
111961.58	$(^2P^0)6s\ ^1P_1^0$	1	26.9(0.1)	-0.2(0.3)		
114897.43	$(^2D^0)5d\ ^1P_1^0$	1	35.3(0.1)	-8.8(0.3)		
121701.69	$(^4S^0)6d\ ^5D_0^0$	0	0	0		
125339.01	$(^4S^0)6d\ ^3D_1^0$	1	34.2(0.4)	-4.2(1.0)		
133550.54	$(^2D^0)7s\ ^3D_3^0$	3	65.0(0.4)	-8.4(0.2)		
136580.12	$(^4S^0)5g\ ^5G_4^0$	4	11.6(1.2)	63.1(1.5)		
133299.80	$(^2D^0)6d\ 1_2^0$	2	27.6(0.1)	12.5(1.1)		
133955.51	$(^2D^0)6d\ 2_3^0$	3	19.9(0.3)	-13.3(2.2)		
134023.88	$(^2D^0)6d\ 3_3^0$	3	18.5(0.5)	-21.2(1.2)		
136733.42	$(^2D^0)6d\ 8_4^0$	4	34.5(1.1)	22.2(0.9)		

Table 5.5 Spectral transitions of I II and I I involved in blended line at 20611 cm^{-1} with their energy levels were given. *Hfs* constants A and B values were used to generate calculated profile. Here $\sigma_{cal} = |E_e - E_o|$.

	σ_{cal}(cm^{-1})	Even Level E_e (cm^{-1})	A (mK)	B (mK)	Odd Level E_o (cm^{-1})	A (mK)	B (mK)
I II	20611.51	101644.21 (J=1)	15.14	4.38	81032.70 (J=2)	88.42	5.91
I I	20611.37	61819.78 (J=1.5)	22.35	20.21	82431.15 (J=1.5)	10.82	-12.04

Table 5.6 Center of gravity wavenumber list of 46 observed spectral transitions of Bi II in the spectral region from visible to UV, along with their classifications. The energy level values and their classifications are taken from NIST data base [117]. Here σ_{obs} is the observed center of gravity wavenumber of the observed spectral lines. The value in the parenthesis represents the uncertainty. Here '*' represents the magnetic dipole transition.

σ_{obs} (cm^{-1})	σ_{cal} (cm^{-1})	E_e (cm^{-1})	E_o (cm^{-1})	Classification	*Hfs*
13325.476(4)*	13325.401	13325.401	0	6p^2 ^{3}P$_1$ - 6p^2 ^{3}P$_0$	a
14681.000(3)	14681.971	84280.446	69598.475	6p7p (1/2,1/2)1 - 6p7s (1/2,1/2)1	a
15146.579(6)	15146.555	84280.446	69133.891	6p7p (1/2,1/2)1 - 6p7s (1/2,1/2)0	a
17431.886(6)	17432.053	105270.947	122703.833	6p7p (3/2,1/2)1 − 6p11d (1/2,3/2)1	a
17480.309(5)	17480.302	87078.777	69598.475	6p7p (1/2,1/2)0 - 6p7s (1/2,1/2)1	a
17495.748(4)	17495.685	126653.813	109158.128	6p5f (3/2,5/2)4 - 6p7d (1/2,5/2)3	a
17527.481(5)	17527.493	125536.550	108009.057	6p5f (3/2,7/2)4 - 6p6d (3/2,5/2)3	-
17626.890(3)	17626.267	125753.623	108126.733	(1/2,1/2)1 - 6p7d (1/2,3/2)1	-
17678.046(4)	17678.044	106449.487	88771.443	6p5f (1/2,5/2)2 - 6p7s (3/2,1/2)2	a
18044.558(4)	18044.539	88566.685	106611.224	6p7p (1/2,3/2)1 - 6p6d (3/2,5/2)1	-
18172.472(6)	18172.472	126299.205	108126.733	6p5f (3/2,5/2)2 - 6p7d (1/2,3/2)1	-
18208.631(7)	18208.648	112650.875	94442.227	6p7p (3/2,3/2)0 - 6s6p^3 ^{3}D$_1$	a
18520.605(6)	18520.609	108406.284	89885.675	6p7p (3/2,3/2)1 - 6p7s (3/2,1/2)1	a
18644.755(4)	18644.756	126653.813	108009.057	6p5f (3/2,5/2)4 - 6p6d (3/2,5/2)3	a
18668.792(4)	18668.791	108280.653	126949.444	6p7p (3/2,3/2)3 - 6p7d (3/2,3/2)3	-
18968.229(3)	18968.21	88566.685	69598.475	6p7p (1/2,3/2)1 - 6p7s (1/2,1/2)1	a
19002.806(3)	19002.844	108888.519	89885.675	6p8p (1/2,3/2)2 - 6p7s (3/2,1/2)1	a
19057.508(5)	19057.51	127184.243	108126.733	6p5f (3/2,7/2)2 - 6p7d (1/2,3/2)1	-

σ_{obs} (cm^{-1})	σ_{cal} (cm^{-1})	E_e (cm^{-1})	E_o (cm^{-1})	Classification	*Hfs*
19191.008(3)	19191.003	88789.478	69598.475	6p7p (1/2,3/2)2 - 6p7s (1/2,1/2)1	a
19219.619(7)	19219.579	88789.478	108009.057	6p7p (1/2,3/2)2 - 6p6d (3/2,5/2)3	-
19219.619(4)	19219.786	109105.461	89885.675	6p8p (1/2,3/2)1 - 6p7s (3/2,1/2)1	-
19432.796(5)	19432.794	88566.685	69133.891	6p7p (1/2,3/2)1 - 6p7s (1/2,1/2)0	a
19509.240(3)	19509.21	108280.653	88771.443	6p7p (3/2,3/2)3 - 6p7s (3/2,1/2)2	a
19634.871(4)	19634.841	108406.284	88771.443	6p7p (3/2,3/2)1 - 6p7s (3/2,1/2)2	a
20020.313(5)	20020.312	109905.987	89885.675	6p7p (3/2,3/2)2 - 6p7s (3/2,1/2)1	a
20117.077(4)	20117.076	108888.519	88771.443	6p8p (1/2,3/2)2 - 6p7s (3/2,1/2)2	a
21134.541(5)	21134.544	109905.987	88771.443	6p7p (3/2,3/2)2 - 6p7s (3/2,1/2)2	a
21246.775(5)	21246.751	84280.446	105527.197	6p7p (1/2,1/2)1 - 6p7d (1/2,3/2)2	a
22765.205(3)	22765.200	112650.875	89885.675	6p7p (3/2,3/2)0 - 6p7s (3/2,1/2)1	a
23240.107(4)	23240.1	105289.732	82049.632	6p5f (1/2,7/2)3 - 6p6d (1/2,5/2)2	a
23401.421(3)	23401.413	105451.045	82049.632	6p5f (1/2,5/2)3 - 6p6d (1/2,5/2)2	-
23470.808(3)	23470.809	105728.060	82257.251	6p5f (1/2,7/2)4 - 6p6d (1/2,5/2)3	a
23650.330(5)	23650.308	126653.813	103003.505	6p5f (3/2,5/2)4 - 6p6d (3/2,3/2)3	-
23775.980(4)	23775.974	126107.642	102331.668	6p5f (3/2,7/2)3 - 6p6d (3/2,3/2)2	a
24508.468(4)	24508.461	105085.532	80577.071	6p7p (3/2,1/2)2 - 6p6d (1/2,3/2)1	a
25823.853(5)	25823.894	88789.478	114613.372	6p7p (1/2,3/2)2 - 6p9s (1/2,1/2)1	a
25872.400(4)	25872.416	106449.487	80577.071	6p5f (1/2,5/2)2 - 6p6d (1/2,3/2)1	a
26012.424(6)	26012.416	88566.685	114579.101	6p7p (1/2,3/2)1 - 6p9s (1/2,1/2)0	a
26359.925(4)	26359.904	105451.045	79091.141	6p5f (1/2,5/2)3 - 6p6d (1/2,3/2)2	a
26880.171(5)	26880.169	127062.615	100182.446	6p5f (3/2,5/2)1 - 6p6d (3/2,3/2)0	a
33883.619(5)	33883.615	116140.866	82257.251	6p6f (1/2,7/2)4 - 6p6d (1/2,5/2)3	a
34041.348(4)	34041.348	116090.980	82049.632	6p6f (1/2,7/2)3 - 6p6d (1/2,5/2)2	a
35637.300(6)	35637.317	116214.383	80577.071	6p6f (1/2,5/2)2 - 6p6d (1/2,3/2)1	a
36845.432(4)	36845.415	115936.556	79091.141	6p6f (1/2,5/2)3 - 6p6d (1/2,3/2)2	-

a: *Hfs* observed in this work.

Table 5.7 Even energy levels of Bi II and their experimentally derived *hfs* A and B constants in mK in comparison with previous literature.

Even Levels (cm⁻¹)	Designation	J	A This	B work	A [ref]	B [ref]	[ref]
0	$6p^2\,^3P$	0	0	0			
13325.401	$6p^2\,^3P$	1	-82.7(5)	-15.2(14)	-82.9(1)	-16.5(10)	[110]
					-82.5(7)	-15.5(35)	[111]
84280.446	6p7p (1/2,1/2)	1	271.02(5)	2.96(16)	270.7(6)	-0.6(18)	[107]
					269.25(5)	1(2)	[42]
87078.777	6p7p (1/2,1/2)	0	0	0			
88566.685	6p7p (1/2,3/2)	1	-102.16(6)	-3.67(12)	-102.5(3)	-0.2(3)	[107]
					-102.10(5)	-1(1)	[42]
88789.478	6p7p (1/2,3/2)	2	123.95(8)	-10.67(18)	123.6(3)	-6.2(21)	[107]
					123.35(10)	-12(2)	[42]
105085.532	6p7p (3/2,1/2)	2	-14.54(6)	-20.01(13)	-13.6(3)	-20(8)	[42]
105270.947	6p7p (3/2,1/2)	1	13.58(9)	-10.84(25)	17.4(10)	-2.1(21)	[107]
					13.3(8)	-10(10)	[42]
105289.732	6p5f (1/2,7/2)	3	-31.15(3)	-8.34(10)	-28.8(2)	-8(4)	[42]
105451.045	6p5f (1/2,5/2)	3	56.83(5)	9.34(9)	56.9(4)	5(5)	[42]
105728.060	6p5f (1/2,7/2)	4	59.84(3)	-2.73(6)	59.1(3)	-6(5)	[42]
106449.487	6p5f (1/2,5/2)	2	-23.45(5)	-12.31(22)	-21.0(8)	-12.9(83)	[107]
					-23.25(20)	-13(5)	[42]
108280.653	6p7p (3/2,3/2)	3	10.51(6)	-34.00(18)	11.3(4)	-16.1(21)	[107]
					10.4(2)	-40(10)	[42]
108406.284	6p7p (3/2,3/2)	1	-14.26(4)	4.51(11)	-13.7(4)	8(5)	[42]
108888.519	6p8p (1/2,3/2)	2	101.99(4)	6.76(23)	101.8(12)	1.1(35)	[107]
					101.4(4)	6(5)	[42]
109905.987	6p7p (3/2,3/2)	2	37.05(5)	-10.31(18)	37.2(6)	-12.7(26)	[107]
					37.05(10)	-8(3)	[42]

112650.875	6p7p (3/2,3/2)	0	0	0			
116090.980	6p6f (1/2,7/2)	3	-58.64(8)	24.02(13)	-57.75(10)	25(3)	[42]
116140.866	6p6f (1/2,7/2)	4	59.71(6)	47.03(19)	59.5(5)	40(20)	[42]
116214.383	6p6f (1/2,5/2)	2	-79.39(4)	-2.57(10)	-78.0(2)	-2(8)	[42]
126107.642	6p5f (3/2,7/2)	3	-2.57(6)	31.35(14)	-11(3) -2.5(5)	27(5) -	[109] [42]
126653.813	6p5f (3/2,5/2)	4	11.93(5)	-36.27(19)	12.60(15)	-36(5)	[42]
127062.615	6p5f (3/2,5/2)	1	-18.85(5)	4.2(2)	-18.55(15)	-4(2)	[42]

Table 5.8 Odd energy levels of Bi II and their experimentally derived *hfs* A and B constants in mK in comparison with previous literature.

Odd Levels	Designation	J	A This	B work	A [ref]	B [ref]	Ref
69133.891	6p7s (1/2,1/2)	0	0	0			
69598.475	6p7s (1/2,1/2)	1	391.93(3)	3.24(19)	391.1(1)	2.8(6)	[110]
					392.1(7)	0.6(11)	[111]
					390.7(1)	3(1)	[42]
79091.141	6p6d (1/2,3/2)	2	120.74(4)	3.00(14)	119.5(5)	0(5)	[42]
80577.071	6p6d (1/2,3/2)	1	-176.30(2)	-5.26(12)	-174.1(2)	-5(2)	[42]
82049.632	6p6d (1/2,5/2)	2	91.95(7)	12.67(13)	90.75(20)	10(2)	[42]
82257.251	6p6d (1/2,5/2)	3	85.69(5)	2.9(2)	84.0(2)	0(4)	[42]
88771.443	6p7s (3/2,1/2)	2	107.04(3)	-38.05(20)	106.0(1)	-38(1)	[110]
					107.8(3)	-	[111]
					106.2(2)	34.5(29)	[42]
						-38(3)	
89885.675	6p7s (3/2,1/2)	1	-61.09(4)	-22.10(14)	-60.6(1)	-21(1)	[110]
					-61.4(8)	-	[111]
					-60.6(1)	25.9(30)	[42]
						22(2)	
94442.227	6s6p^3 ^{3}D	1	-303.88(6)	-6.80(13)	-305(1)	-50(4)	[110]
					-307.9(5)	-23(10)	[42]
100182.446	6p6d (3/2,3/2)	0	0	0			
102331.668	6p6d (3/2,3/2)	2	103.47(5)	7.34(13)	100.3(5)	8(5)	[42]
105527.197	6p7d (1/2,3/2)	2	116.81(5)	5.33(11)	116.2(2)	5(3)	[42]
108009.057	6p6d (3/2,5/2)	3	56.41(4)	-24.68(14)	56.3(4)	-25(10)	[42]
109158.128	6p7d (1/2,5/2)	3	184.79(5)	11.77(12)	170(6)	10(10)	[109]
114579.101	6p9s (1/2,1/2)	0	0	0			

| 114613.372 | 6p9s (1/2,1/2) | 1 | 218.15(9) | -19.51(15) | 2108.15(10) | 18(1) | [42] |
| 122703.833 | (1/2,3/2) | 1 | -80.49(6) | 3.4(4) | -80(8) | | [116] |